DEVELOPMENT AND APPLICATION OF A GENERALIZED PHYSIOLOGICALLY-BASED TOXICOKINETIC MODEL FOR ENVIRONMENTAL RISK ASSESSMENT

BY ALAN F. SASSO

A dissertation submitted to the

Graduate School—New Brunswick

Rutgers, The State University of New Jersey

in partial fulfillment of the requirements

for the degree of

Doctor of Philosophy

Graduate Program in Chemical and Biochemical Engineering

Written under the direction of

Dr. Panos Georgopoulos

and

Dr. Sastry Isukapalli

and approved by

_____

_____

_____

_____

_____

New Brunswick, New Jersey

January, 2010

ABSTRACT OF THE DISSERTATION

DEVELOPMENT AND APPLICATION OF A GENERALIZED PHYSIOLOGICALLY-BASED TOXICOKINETIC MODEL FOR ENVIRONMENTAL RISK ASSESSMENT

by Alan F. Sasso

Dissertation Director: Dr. Panos Georgopoulos

Co-advisor: Dr. Sastry Isukapalli

This thesis presents the development, evaluation, and application of a generalized toxicokinetic model for mixtures of chemicals. Humans are exposed to mixtures of chemicals that are found together in multiple exposure media (soil, food, and air), and at levels that have been shown to cause adverse effects due to toxic interactions. Although several physiologically based toxicokinetic (PBTK) models exist for different environmental chemicals, using them in assessing risks to co-occurring contaminants is often impractical.

This is especially true for the case of toxic metals, where half-lives in the human body span days (e.g. arsenic), months (e.g. methylmercury), and decades (e.g. lead,

cadmium). Several differences in the formulation of these models exist with respect to (a) physiological structure (e.g. body tissue volumes and blood flow ratios), (b) general modeling assumptions (e.g. for transport and transformation of the chemicals within the body), and (c) exposure-relevant parameters. Since assumptions made for one metal or metal compound can be incompatible with the assumptions made for another metal, current formulations are inadequate for use in assessing health risks from mixtures of toxic metals. Further complications arise when assessing risks of both metals and nonmetals, which also interact at the toxicokinetic and toxicodynamic levels. The issues of consistent representation of physiology and chemical interactions across different classes of chemicals such as mixtures of metals and mixtures of metals and organics are addressed through the development of a Generalized Toxicokinetic Model for Mixtures of chemicals (GTMM).

The GTMM resolves inconsistencies by standardizing the physiology across all models, and by allowing simulations of different models to be done simultaneously. It has been implemented as a set of modules in Matlab and as a user-oriented graphical interface in Matlab-Simulink. The GTMM has been evaluated with multiple existing PBTK models for individual chemicals, and the results demonstrate that the GTMM produces identical results as the original published formulations. Subsequently, the GTMM has been applied to different problems relevant to population risk assessment.

Preface

Physiologically-based toxicokinetic models serve as the link between environmental exposure and toxicological response. As these models have grown more complex over the years, it has become apparent that toxic effects are not dependent solely on the contaminant levels of inhaled air or ingested food and water. Inter-individual variabilities in physiology, biochemistry, and genetic factors have significant impacts on absorption, distribution, metabolism, excretion and toxicity. For this reason, there have been increased applications of "whole-body" physiologically-based toxicokinetic (WBPBTK) models to reduce model uncertainties and better characterize inter-individual variabilities [264]. Concurrently, PBTK models of mixtures which incorporate chemical interactions of metabolism and toxic effects are developed since humans are exposed to multiple environmental contaminants and drugs simultaneously [106, 222].

Unfortunately, such modeling efforts have not been applied to the vast field of toxic metal compounds, and there are no PBTK models for mixtures of metals. Very recent developments in the field of molecular biomarkers have discovered additive and synergistic toxic interactions between metals such as arsenic, lead, and cadmium [393]. The cited reference also notes that exposure to metal mixtures may lead to new toxic effects that are not seen in single component exposures. In addition to metal-metal interactions, altered drug and chemical metabolism due to toxic metal exposures is also

possible [260]. Within this thesis is a further review of chemical interactions involving toxic and essential metals, and environmental contaminants. There is a very specific need for an interactive toxicokinetic model of mixtures of both metal and nonmetal compounds.

Since toxic metals have widely varying half-lives in different compartments, the existing toxicokinetic models differ in basic mechanistic assumptions. Additionally, some of these models were developed over 15 years ago, before the advent of the WBPBTK approach. And finally, current platforms for constructing and implementing PBTK models are not modular enough to allow for incorporation of the highly complex metabolic and transport mechanisms that are needed for each of the individual metals.

To address these needs, a generalized toxicokinetic model for mixtures (GTMM) was developed. This framework **1)** improved on existing models for toxic metals by updating them using the current knowledgebase of whole-body physiology and inter-individual variability, **2)** simulates all metals and nonmetals consistently and simultaneously in a single human or animal, **3)** is modular enough to allow the incorporation of complex models of exposure, parameter optimization, metabolism, transport, and toxicological response. Through the application of the GTMM to case-studies requiring flexible toxicokinetic frameworks, various aspects of the system are demonstrated and evaluated.

The following page contains an illustrated outline of the thesis. Not all thesis sections are included, since it is an outline of the major concepts and applications. The generalized toxicokinetic model was central to many applications of PBTK models presented in this thesis.

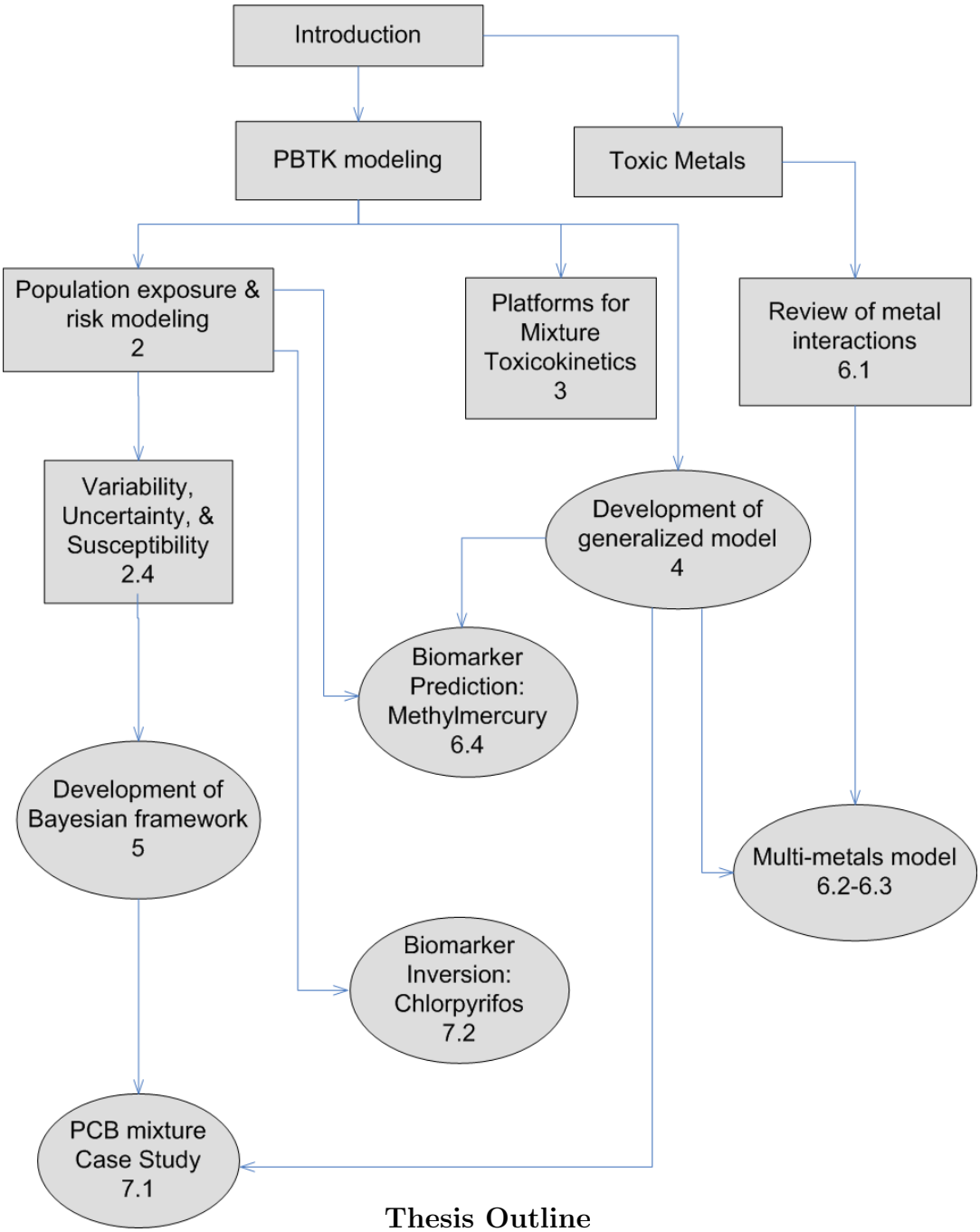

Thesis Outline

Acknowledgements

I would like to thank my thesis advisor Dr. Panos Georgopoulos for his guidance, and for providing me the opportunity to join and participate in such an integrative and interdisciplinary laboratory. I would also like to thank my co-advisor Dr. Sastry Isukapalli. Without his guidance and his faith in me as a graduate student, much of the work presented in this thesis would not have been possible.

I would like to acknowledge the help I have recieved from outside of our research group. I am very grateful to Dr. Kannan Krishnan, who introduced me to very interesting real-world problems and data involving mixture toxicokinetics, and providing valuable insight on the science as a whole. The entire Bayesian PCB mixtures case study would not be a part of this thesis had it not been for him. I would also like to acknowledge Dr. Amit Roy for his very thoughtful comments on my thesis draft. His outside knowledge from industry was extremely valuable in helping me to standardize much of the conflicting language and nomenclature that is common to this interdisciplinary science.

I would like to acknowledge the funding sources which supported me throughout my graduate student career. A special thanks to Dr. Henrik Pedersen for granting me the NIH Biotechnology Fellowship, which provided me with support for my first two years and a summer internship at Bristol-Myers Squibb. Support for this thesis

has been provided primarily by the USEPA-funded Environmental Bioinformatics and Computational Toxicology Center (ebCTC) and the USEPA funded Center for Exposure and Risk Modeling (CERM). Additional support has been provided by the NIEHS sponsored UMDNJ Center for Environmental Exposures and Disease.

Table of Contents

Abstract ii

Preface iv

Acknowledgements vii

List of Tables xiv

List of Figures xvi

1 Background and importance 1

1.1 Short history of pharmacokinetics and toxicokinetics 2

1.2 Basic principles of pharmacokinetic modeling 3

1.3 The need for a generalized PBTK model for toxic metal compounds . . 5

2 Overview of Integrated Exposure and Risk Modeling 11

2.1 Background 11

2.2 Exposure framework 12

2.3 Dose response 13

2.3.1 Toxicodynamic models 13

2.3.2 Inter-species extrapolation 15

2.4 Uncertainty and natural variability 17

2.4.1 Overview . . . 17

2.4.2 Physiology and susceptibility . . . 18

3 Current methods and platforms for mixture toxicokinetics . . . 20

3.1 Exposure Related Dose Estimating Model . . . 20

3.1.1 Population limitations . . . 21

3.1.2 Unresolved model inconsistencies . . . 21

3.1.3 Physiological limitations . . . 22

3.2 Steady-state model reduction . . . 23

3.2.1 Rationale . . . 23

3.2.2 Model equations . . . 24

3.2.3 Evaluation . . . 26

3.2.4 Results and conclusions . . . 28

4 Development of a Generalized PBTK Modeling Framework . . . 35

4.1 Overview . . . 35

4.2 PBTK equations . . . 38

4.2.1 Compartment mass balances . . . 38

4.2.2 Circulatory recycle mass balances . . . 40

4.2.3 Metabolism . . . 42

4.3 Computational implementation . . . 45

5 Development of a Bayesian framework for the generalized model . . . 50

5.1 Theory . . . 50

5.2 Markov-Chain Monte Carlo Methods . . . 56

5.2.1 Metropolis and Metropolis-Hasting Algorithm 57
5.2.2 Adaptive Metropolis 58
5.2.3 Delayed Rejection 60
5.3 Evaluation of four sampling methods 61
5.4 Alternatives to Bayesian Analysis 71
5.4.1 Maximum Likelihood 71
5.4.2 Artificial Neural Networks 72

6 Applications of the generalized model to toxic metals 75
6.1 Overview of general toxicology of metals 75
6.1.1 Role of essential elements in metal toxicity 75
6.1.2 Molecular biomarkers and dose-response models 77
6.1.3 Neurotoxicity risk 77
6.2 Toxicology and PBTK implementation of specific metals 79
6.2.1 Cadmium 79
6.2.2 Arsenic 85
6.2.3 Lead 91
6.2.4 Chromium 98
6.2.5 Mercury 103
6.3 Demonstration of simulations with multiple metals and nonmetals . . . 109
6.4 Population case study of methylmercury exposure 117
6.4.1 Sample demographics 117
6.4.2 Population exposure model 118
6.4.3 Toxicokinetic assumptions 119

6.4.4 Results 121

7 Applications of the generalized model to mixtures of nonmetals . . 123

7.1 Bayesian Analysis of a PCB mixture using a lipid-based model 123

7.1.1 Background 123

7.1.2 Methods 124

7.1.3 Results 141

7.1.4 Discussion 155

7.2 Application of toxicokinetic models to biomarker inversion 156

7.2.1 Background 156

7.2.2 Methods for Exposure Reconstruction from Population Biomonitoring Studies 158

7.2.3 Major Factors Influencing Exposure Reconstruction 161

7.2.4 Toxicokinetic model for chlorpyrifos exposure 167

7.2.5 Case Study 1: Chlorpyrifos dose reconstruction from available NHEXAS-MD data 167

7.2.6 Preliminary analysis of the linked PK-biomarker approach using forward modeling 171

7.2.7 Computational Inversion Techniques used for Evaluation 173

7.2.8 Results for Case Study 1 174

7.2.9 Case Study 2: Chlorpyrifos dose reconstruction from a "synthetically-augmented" NHEXAS-MD data 178

7.2.10 Results for Case Study 2 180

7.2.11 Discussion and Conclusion 184

8 Discussion and Conclusions 189

Appendix A. Toxic metals in dust 193

Appendix B. Complete PCB evaluation runs 202

Vita 238

List of Tables

1.1 Selected interactions between metals and CYP450 enzymes 8

1.2 Pharmacokinetic models for metals and metalloids 10

2.1 Selected modeling tools for population physiology 19

3.1 Notation used for steady-state parameters. 25

3.2 Parameters used in the rat PBTK model for a complex mixture 27

3.3 Predictions by the steady-state algorithm of liver concentration 30

3.4 Predictions by the steady-state algorithm of metabolic rate 30

5.1 Posterior distributions of population parameters and modeling errors . . 69

6.1 PBTK model parameters for cadmium 81

6.2 Tissue/blood equilibrium partition coefficients for arsenic species 88

6.3 Kinetic parameters for the arsenic PBTK model 89

6.4 PBTK model parameters for lead in humans 94

6.5 PBTK model parameters for chromium in humans 101

6.6 PBTK model parameters for methylmercury 107

7.1 Lipid content of rat tissues [123, 296] 126

7.2 Physiological values for a standard 225-g rat (adapted from [123]) 126

7.3 Basal CYP1A/2B parameters (adapted from [11, 324]): 136

7.4 Population-level parameters to be estimated by Bayesian analysis 139

7.5 Posterior distributions of population metabolic parameters 142

7.6 Posterior distributions of consolidated basal metabolic parameters . . . 144

7.7 Ranges of exposure parameters used in augmenting NHEXAS-MD . . . 181

7.8 Comparison of NHEXAS and NHANES datasets 187

7.9 Inter-individual genetic variability for transport and transformation . . 188

A.1 Mean lead concentration in house dust (mg/kg). 194

A.1 (Continued) 195

A.2 Mean cadmium concentration in house dust 196

A.3 Paired indoor and outdoor metal concentrations 197

A.4 Metal composition of household dust sampled in the U.K. 198

A.5 Literature summary of studies of microenvironmental levels of metals . . 199

A.5 (Continued) 200

A.5 (Continued) 201

List of Figures

1.1 PBPK model of chloroform for inhalation and dermal absorption 4

1.2 Toxicokinetic model structures of four metals 9

2.1 Schematic of an exposure modeling system 13

2.2 "Critical window" concept in fetal risk assessment 15

3.1 Estimates using the steady-state and full PBTK models for VOCs . . . 29

3.2 Impact of inhibitors on the liver concentration of toluene 31

3.3 Impact of inhibition on toluene concentration in the rat liver 32

3.4 Liver concentration and extraction ratio for xylene and toluene exposure 33

4.1 A schematic of the generalized PBTK modeling framework 37

4.2 Schematic of diffusion-limited sub-compartments 38

4.3 Simulink block diagram depicting the generalized PBTK template . . . 47

4.4 Simulink block diagram depicting tissue mass balance 48

4.5 Prototype user interface for the generalized Simulink PBTK model . . . 48

4.6 Flow chart of Matlab and Simulink model hierarchy 49

5.1 Schematic of a hierarchical Bayesian framework 52

5.2 Model/data scatter of synthetic data 63

5.3 MCMC chains of four different sampling methods 67

5.4 Markov-chains and actual values of population parameter **μka** 68

5.5 Posterior distributions for **Vm** and **ka** 69

5.6 A single neuron of an artificial neural network 73

5.7 A three-layer artificial neural network 73

5.8 An artificial neural network learning algorithm 74

6.1 Toxicokinetic model structure for cadmium 82

6.2 Comparisons of PBTK model results and data for cadmium 84

6.3 Toxicokinetic model structure for arsenic 87

6.4 Comparisons of PBTK model results and data for urinary arsenic 90

6.5 Toxicokinetic model structures for lead 93

6.6 Bone volumes as a function of age 95

6.7 Comparisons of PBTK model results and data for short term blood lead 96

6.8 Comparisons of PBTK model results and data for long term blood lead 97

6.9 PBTK model for chromium in humans 100

6.10 Predictions of Cr^{III}concentrations and urinary rates 102

6.11 Schematic of maternal and fetal PBTK models for methylmercury . . . 104

6.12 Comparisons of PBTK model results and data methylmercury 108

6.13 Illustration of metal timescales 110

6.14 Effect of inhibition on toluene liver concentration 111

6.15 Effect of noncompetitive inhibition on benzene liver concentration . . . 114

6.16 Effect of varying inhibition assumptions on benzene liver concentration . 115

6.17 Effect of hypothetical metabolic disruption 116

6.18 Schematic diagram of population methylmercury intake methodology . . 120

6.19 Percentiles of methylmercury biomarker predictions 122

7.1 The effects of four dosing scenarios on PCB levels 128

7.2 Inter-individual variability in PCB data 130

7.3 Schematic of the induction model 136

7.4 Schematic of a hierarchical Bayesian framework 137

7.5 Posterior distributions of population metabolic and induction parameters 143

7.6 Posterior distribution of population metabolic parameter 144

7.7 Model predictions for PCBs in total plasma lipid at 5 μg/kg exposure. . 146

7.8 Model predictions for PCBs in total lipid at 500 μg/kg exposure. 147

7.9 Model predictions for PCB concentrations for selected evaluation data. . 149

7.10 Scatterplot of PBTK model predictions vs. measured data 150

7.11 Predicted metabolic clearance of PCB 118 151

7.12 Predicted metabolic clearance of PCB 138 152

7.13 Measured PCB concentration order within rats 154

7.14 Exposure time-scale contribution to biomarkers 164

7.15 Contribution of prior exposures to observed biomarker levels 165

7.16 Predicted versus actual biomarkers for the NHEXAS-MD population . . 172

7.17 Comparison of predicted doses using creatinine/liquid-based concentrations175

7.18 CDFs of dietary CPF uptakes for the NHEXAS-MD population 176

7.19 PDFs of dietary CPF uptakes for the NHEXAS-MD population 177

7.20 CDFs of dietary CPF uptakes for the synthetic population 183

B.1 Model predictions for PCB concentrations at 5 μg/kg exposure 203

B.2 Model predictions for PCB concentrations at 50 μg/kg exposure 204

B.3 Model predictions for PCB concentrations at 500 μg/kg exposure . . . 205

B.4 Model predictions for PCB concentrations at 5 μg/kg exposure 206

B.5 Model predictions for PCB concentrations at 50 μg/kg exposure 207

B.6 Model predictions for PCB concentrations at 500 μg/kg exposure 208

Chapter 1

Background and importance

Every day, human beings are exposed to low doses of hazardous materials from their environment. Outdoor and indoor air contains a variety of contaminants from automobiles, industrial emissions, building materials and stoves. Drinking water contains disinfectant byproducts and metals, and food contains mixtures of pesticides, polychlorinated biphenyls (PCBs), and metals. These chemicals, along with pharmaceuticals, alcohol, and smoking byproducts, accumulate in the body and remain for varying periods of time. Environmental and toxicological risk assessment aims to quantify the likelihood of adverse effects due to chemical exposure, while taking into account a wide variety of factors other than just air, water, or food quality. Demographics, lifestyle, and genetic factors all contribute to the potentially harmful outcomes of exposure. Within the field of toxicological risk assessment lies toxicokinetics, which involves the modeling and prediction of chemical concentrations in human tissues. Toxicokinetics provides the modeling link between environmental exposure and toxic effects.

1.1 Short history of pharmacokinetics and toxicokinetics

For hundreds of years, animals have been used to predict human responses to both chemical medicines and poisons. Recorded systematic study of the subject began in the nineteenth century, and one commonly known application was the use of canary birds to alert miners of air toxics [60]. Later, attention became focused on the reasons why animals and humans experience health effects from chemicals. It was generally known that chemicals enter the body from different routes, and exert their effects on specific target organs (i.e. brain, liver, or kidneys). An accurate characterization of the lethality or benefit of doses would require knowledge of where the chemicals are in the body, and how long they spend in target organs. Mathematical approaches to analyze the time course of foreign chemicals in the body began in the 1930's, and were limited to very simple models due to the lack of available tools [160]. Experiments and analysis by Bischoff and Dedrick in the 1960's illustrated that these mathematical approaches could be successfully applied to real world problems [41].

These methods have since matured and are applied in the fields of environmental and occupational health, and pharmaceutical drug development. The U.S. Environmental Protection Agency (USEPA) and Centers for Disease Control and Prevention (CDC) use toxicokinetic modeling to assess risk for both existing and emerging contaminants, and to interpret exposure biomarker data for the U.S. population. Meanwhile the pharmaceutical industry routinely employs pharmacokinetic modeling to characterize exposure, and risk-benefit of pharmaceutical drugs. Pharmacokinetics (analogous to toxicokinetics) is is the description of the absorption, distribution, metabolism, and

elimination of xenobiotics by biological organisms. The U.S. Food and Drug Administration (USFDA) also considers pharmacokinetics to be an important factor of drug design, since it relates directly to drug toxicity and efficacy. Toxicokinetic and pharmacokinetic models are used by multiple regulatory agencies to help guide public policy and health decisions [113, 145]. There exists a comprehensive text on additional applications of PBPK models by Reddy et. al. (2005) [307].

1.2 Basic principles of pharmacokinetic modeling

Physiologically based toxicokinetic (PBTK) and pharmacokinetic (PBPK) models are the mathematical descriptions of absorption, distribution, metabolism, and excretion (ADME) of xenobiotics in humans or animals. These models are used to estimate the levels of chemicals in the body tissues and fluids such as blood, hair, and urine. Fundamentally, the models consist of mass balances on different compartments in a human or animal body. These compartments may represent specific organs, or multiple tissues lumped together. Physiologically-based pharmacokinetics/toxicokinetics aims to incorporate physically realistic restrictions and biological knowledge on the systems of equations. PBTK models can include many different organs and describe mass balances as differential equations. Figure 1.1 illustrates a flow-limited PBPK model for chloroform, incorporating exposure routes by inhalation and dermal absorption. The blood leaving all compartments recycles through a central compartment, typically the lung or a compartment representing the blood.

For a simple constant-volume, perfusion-limited compartment with no metabolism or excretion, the concentration C (mass/volume) of chemical i in compartment j can be represented as a function of inlet arterial concentration C^{art}, compartment volume V,

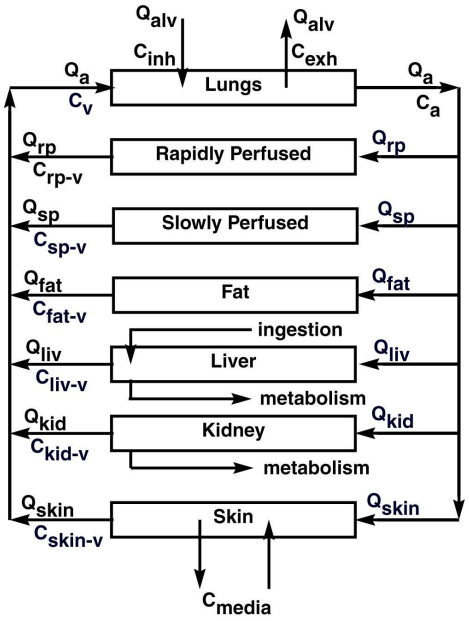

Figure 1.1: PBPK model of chloroform for inhalation and dermal absorption exposure routes (adapted from Roy et al. (1996) [319])

compartment blood flow rate Q (volume/time), and equilibrium tissue:blood partition coefficient P:

$$V_j \frac{dC_{i,j}}{dt} = Q_j \left(C_{i,j}^{\text{art}} - \frac{C_{i,j}}{P_{i,j}} \right) \tag{1.1}$$

In practice, the differential equations are expressed in terms of mass rather than concentration since compartment volumes may change with time. Mass balance equations for compartments become more complex with the addition of metabolic or transport terms, and with the discretization of the compartment space. More detailed equations are presented in Section 4.2.

For a wide variety of chemicals, there already exist databases of values for partition coefficients for humans and animals [294–297]. Therefore models developed in rats can be scaled to humans (interspecies scaling) by using human values for physiology and biochemical parameters for metabolism and excretion. PBTK models could also be used to predict internal tissue concentrations for humans under extreme exposure conditions

where data are unavailable (dose extrapolation), such as chronic low-dose exposures or acute high-dose exposures. Interspecies scaling and dose extrapolation have been highly effective in the development and application of PBTK models [10, 159]. For these reasons, physiologically based pharmacokinetic models for a wide variety of drugs and toxics are published each year for application to human risk assessment [113, 145].

1.3 The need for a generalized PBTK model for toxic metal compounds

Each of these models have their own sets of assumptions, and usually focus on a narrow set of target tissues (i.e. tissues that may experience toxic effects). The lumping of various tissue groups is done to reduce the number of parameters to specify (such as the partition coefficient or any metabolic parameters of each tissue), and to reduce the number of equations. Tissues with high blood flow rates per unit volume are considered "rapidly perfused", and those with lower perfusion rates are "slowly perfused". Non-target tissues are lumped accordingly, and these two groups are each assigned a single partition coefficient, volume, blood flow rate, and set of metabolic parameters. Lumping tissues has been effective in speeding up model development, improving computational efficiency, and maintaining overall parsimony. PBPK models containing large numbers of lumped parameters are capable of predicting the fate of xenobiotics in human or animal models.

However, improper application of lumping for population risk assessments can lead to unnatural probability distributions being used to represent physiology of lumped groups. In cases where the brain, kidneys, and gastrointestinal organs are lumped into the "rapidly perfused" group, approximately 25% of the total cardiac output might be treated as a single random variable, as opposed to the sum of multiple random variables.

Countless other anomalies arise when applying lumped models to varying populations. For example, the blood-brain barrier selectively blocks the entry of certain chemicals into the brain, which is approximately 2% of whole-body tissue volume for the average adult, but 10% for infants and young children [196]. Incorporating the brain into a rapidly-perfused group while it may be unavailable for chemical accumulation creates modeling error. Assumptions that are suitable for modeling a single standard human may cause a significant and unnecessary propagation of uncertainty and error when applied at the population level.

Modeling mixtures of diverse chemicals simultaneously and consistently is sometimes difficult due to these conflicting assumptions. Toxic metals and metalloids present unique modeling challenges which make incorporating them into models for complex mixtures infeasible. The half-lives of key toxic metals in humans span days (e.g. arsenic and chromium), months (e.g. methylmercury), and decades (e.g. lead and cadmium). Model formulations for each metal differ greatly to account for the varying toxic endpoints and distribution mechanisms in the body, further making integration with other models difficult. Humans are exposed to multiple toxic metals such as lead, cadmium, and arsenic concurrently, at levels that have been shown to cause adverse effects due to toxic interactions among these metals [393]. However, toxicokinetic simulations of exposures to these chemicals are often performed in isolation due to the lack of a consistent modeling framework.

Despite differences between PBTK models for metals and metalloids (Figure 1.2), many similarities exist in fundamental toxicokinetics. The Divalent Metal Transporter 1 (DMT1) is a common gastrointestinal absorption pathway for metals in divalent form (such as lead and cadmium) [49, 50, 151]. Metallothionein (a metal binding

protein) plays an important role in overall absorption, distribution, elimination and toxicity of most toxic and essential metals [274]. Metabolism of metal and metalloid compounds is limited to redox reactions, methylation/demethylation, and protein conjugation [279]. Elimination of absorbed dose occurs primarily by renal excretion [28]. Many of the toxic effects are attributable to "molecular mimicry", in which toxic elements transport to target cells due to their similarities to essential elements [26, 51]. The result of these similarities are toxicokinetic and toxicodynamic interactions among toxic and essential metals, a topic that has already been extensively reviewed [51, 78, 164, 210, 242, 243, 289, 332, 364, 393]. Interactions between arsenic and cadmium in the kidneys [57, 94, 193, 271, 273], and lead and cadmium in the liver and kidneys [286, 326, 327] have already been observed in humans and animals.

Toxic metals also impact the toxicokinetics of additional classes of chemicals due to accumulation in the liver and kidneys, and long half-lives. The hepatic and renal toxicities caused by metals effect cytochrome P450 (CYP450) enzymes, which metabolize other xenobiotics [260, 328]. Chemicals of interest to the regulatory community such as pesticides, polychlorinated biphenyls (PCBs), polycyclic aromatic hydrocarbons (PAHs), and volatile organic compounds (VOCs) could therefore be affected by metals. If there were no metal/metal interactions, a framework would still be necessary to link metal toxicokinetics, CYP450 dose responses, and the subsequent effect on the toxicokinetics of nonmetals. Since many PCBs, pesticides, and organic pollutants also induce or inhibit CYP450 enzymes, additional metabolic interactions may occur. Table 1.1 outlines some of the CYP450 enzymes that may be affected by toxic metals, along with the classes of substrates metabolized by those enzymes. The final row

cites a complex interaction in which exposure to metals had a direct impact on the induction of CYP1A enzymes caused by PAHs and tetrachlorodibenzo-p-dioxin (TCDD).

Table 1.1: Selected interactions between metals and CYP450 enzymes

Metals	CYP450 effects	Potential substrates†	Reference
Cadmium	Induced 2A6	Carbamates, drugs	[328]
	Induced 2E1	Halogenated aliphates, triazines, organophosphates, VOCs, drugs	[328]
	Induced 2C9	Drugs, organophosphates, triazines	[328]
Lead	Inhibited 2A6	Drugs	[325]
	Inhibited 1A2 (rats)	Arylamines, organophosphates, triazines, VOCs, PCBs, drugs	[103]
Arsenic	Induced 1A1 (rats)	PAHs, VOCs, PCBs, triazines	[7, 334]
Metal mixtures	Altered 1A1/2 induction by PAHs/TCDD (rats)	PAHs, VOCs, PCBs, triazines, organophosphates, drugs	[245, 246, 386, 387]

†Substrate/P450 relationships from [69, 189, 307, 322].

Additional reviews on interactions between metals, environmental toxins, and drugs are outlined in [260, 328].

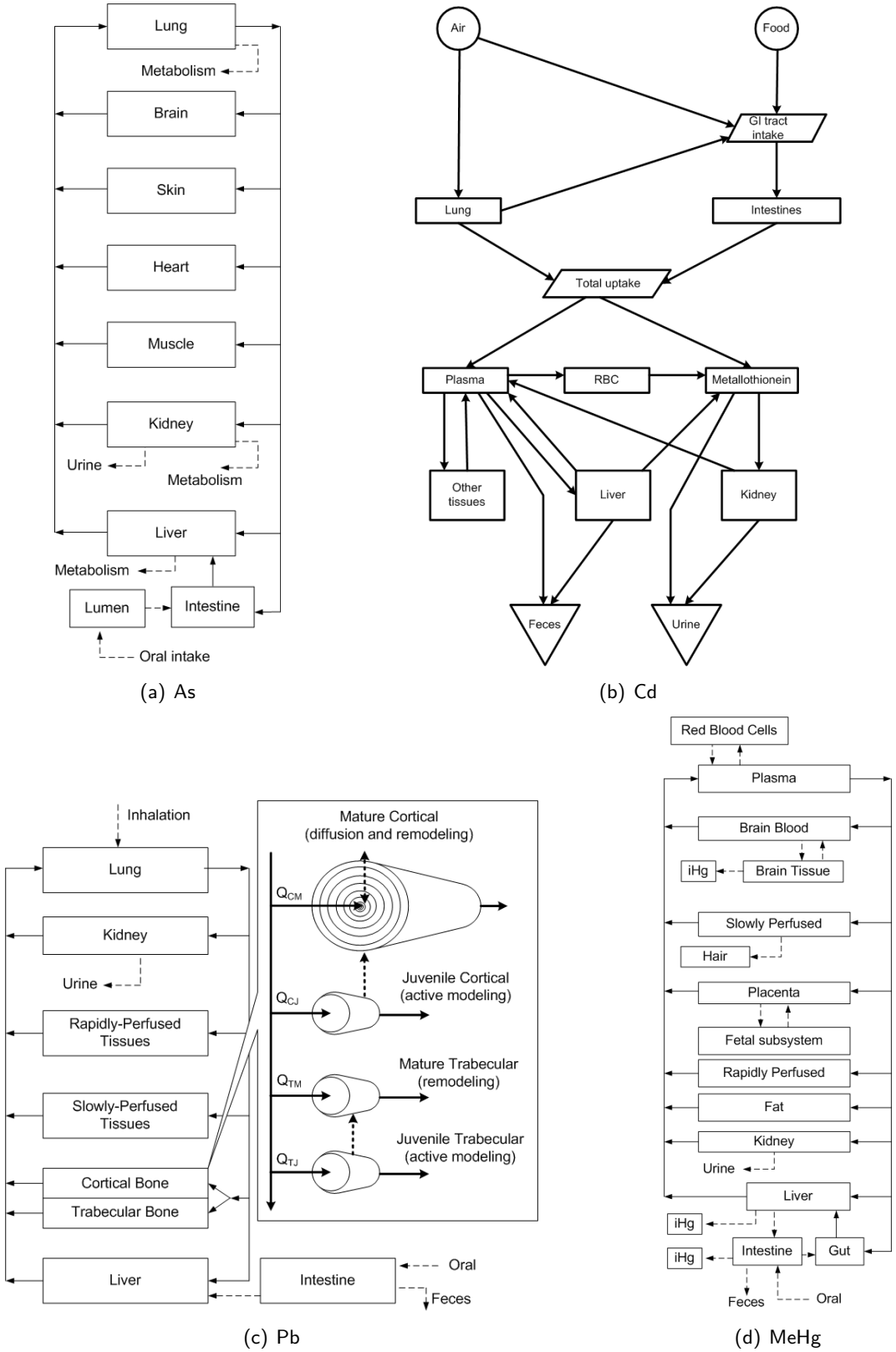

(a) As (b) Cd

(c) Pb (d) MeHg

Figure 1.2: Toxicokinetic model structures for arsenic (As) [120], cadmium (Cd) [272], lead (Pb) [280], and methylmercury (MeHg) [338].

Table 1.2: Pharmacokinetic models for metals and metalloids

Metal	Model Reference	Comments
Arsenic	Mann et al. (1996) [247]	Diffusion-limited PBPK
	Yu (1999) [414]	Flow-limited PBPK
	El-Masri/Kenyon (2008) [120]	Flow-limited PBPK
Cadmium	Nordberg et al. (1979) [272]	Linear biokinetic
	Choudhury et al. (2001) [77], Diamond et al. (2003) [109]	Based on Nordberg et al. (1979), but with differential equations, and linkage of iron status with intestinal absorption.
Chromium	Tossavainen et al. (1980) [377]	Linear biokinetic; one compartment
	O'Flaherty et al. (2001) [281]	Flow-limited PBPK with bone absorption
Mercury	Cember (1969) [70]	Biokinetic (elemental mercury & inorganic mercury)
	Smith et al. (1996) [341]	Biokinetic (methylmercury & inorganic mercury)
	Jonsson et al. (1999) [208]	Biokinetic (elemental mercury & inorganic mercury only)
	Clewell et al. (1999) [84] , Shipp et al. (2000) [338]	Flow-limited PBPK (methylmercury & inorganic mercury); human pregnancy components
	Byczkowski et al. (2001) [59]	Based on Clewell et al. (1999), modified to include lactational transfer of methylmercury to infants
	Young et al. (2001) [412]	Flow-limited PBPK (methylmercury & inorganic mercury); no red blood cell compartment
	Leggett et al. (2001) [228]	Biokinetic/inhalation & deposition model of elemental mercury
	Carrier et al. (2001) [66]	Flow-limited PBPK (methylmercury & inorganic mercury); no red blood cell compartment
	Pierrehumbert et al. (2002) [291]	Biokinetic model (elemental & inorganic mercury only)
Lead	Rabinowitz (1976) [305]	Biokinetic model
	Bert (1989) [39]	Biokinetic model
	Leggett (1993) [227, 298]	Biokinetic model developed by the International Commission for Radiation Protection (ICRP) for application to children and adults
	USEPA (1998) [190, 257, 417]	Integrated Exposure Uptake Biokinetic Model (IEUBK); exposure and biomarker model for children
	O'Flaherty (2000) [277–280]	Flow-limited PBPK; non-linear binding to red blood cells; diffusion into bone
Manganese	Nong et al. (2009) [267–269, 361–363]	Hybrid toxic/essential metal model

Chapter 2

Overview of Integrated Exposure and Risk Modeling

2.1 Background

In the typical daily life of a person in the average home, the characterization of the most important routes for exposure to various chemicals are already well known. For example, the major pathway of exposure to heavy metals (aside from cigarette smoke) is by dietary ingestion [321]. However, other pathways such as inhalation, dermal exposure and non-dietary ingestion are also contributing factors. Contaminated soils from hazardous waste sites could migrate into the home and cause elevated levels of toxins in household dusts [391]. Forest fires, building construction and demolition, and indoor household renovations may also cause contamination. In an extreme case, the collapse of the World Trade Center caused significant increases of non-typical dust particles throughout a wide area [359, 408]. When these situations arise, the risks due to all exposure pathways must be re-assessed. PBTK models become part of a larger framework, and utilize complex, time-varying human exposure data or model outputs to produce estimates of the amount of chemical inhaled, consumed, or contacted with skin. As a result, the generalized PBTK model was required to be adaptive enough for incorporation into multi-media, multi-pathway human exposure modeling systems (illustrated in Figure 2.1).

2.2 Exposure framework

A PBPK model becomes a key component in estimating risk when incorporated into exposure modeling systems. From a standpoint of the PBPK model, exposure models create the boundary and initial conditions for the systems of equations. Models for ground water, drinking water, air quality, along with national survey data, can all be used to estimate the toxicant concentrations for micro-environments (outdoors, indoors, buildings, etc.) and ingested food or water. In addition to environmental concentrations, human activities have a significant impact on exposure and absorbed dose.

The Consolidated Human Activities Database (CHAD) [250], is a database of survey results concerning activities that different people do throughout their day. CHAD, together with demographic, dietary, and food residue databases are used to create time-activity-exposure diaries for individuals in a population. Each person's diary contains information on what the individual does during the day. It dictates the microenvironment the individual is in, and the activity he or she is doing. Therefore, time, location, exposure concentrations, and activity are all incorporated into the model. Human activity is important since it impacts not only how somebody is exposed (i.e. drinking water, showering, eating), but it also influences important physiological parameters such as ventilation rate and cardiac output. Each activity has an assigned metabolic equivalent of task (MET), which is empirically correlated with cardiac output, ventilation rate, and lung dosimetry parameters. Other useful databases such as the National Human Exposure Assessment Survey (NHEXAS) [335], and the National Health and Nutrition Examination Survey (NHANES) [52] are useful in providing data on food intakes, and typical values of chemical residues on foods.

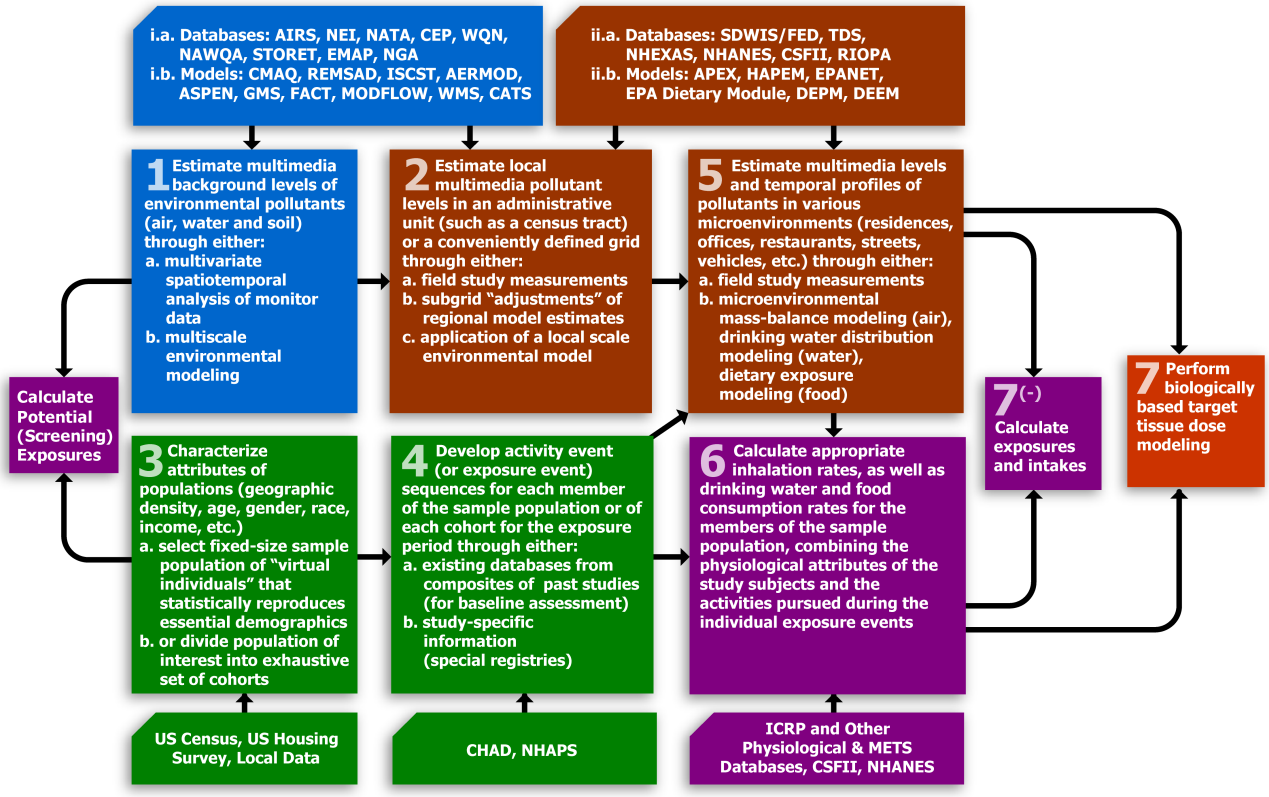

Figure 2.1: Schematic of a source-to-dose population based modeling framework (adapted from Georgopoulos et al. (2008) [156])

2.3 Dose response

2.3.1 Toxicodynamic models

Combined exposure and PBTK models only predict the concentration of chemicals in human tissues. The next step in chemical risk assessment is the use of this information to determine the likelihood of adverse effects. The correlation of dose to effect has always been the main concern of toxicokinetic modeling, and as technology progresses, it becomes possible to analyze toxic effects with a greater degree of accuracy. It is now possible to measure the effects of chronic low doses on animal or human target tissues via molecular biomarkers. While toxicokinetic models predict the time course of chemical concentrations in tissues, toxicodynamic dose-response models use those

results to predict adverse effects. Biologically-based dose-response (BBDR) models attempt to predict adverse effects mechanistically and with minimal simplifications of the system [12, 108]. However, due to lack of data, most other dose response models use an empirical model to estimate effect.

For chronic exposure studies, the steady-state tissue burden is usually of concern. The risk of tumors or organ dysfunction (including neurotoxicity) is a function of the concentration-time course of toxicant in the organ. For acute exposure studies where the half-life of the chemical is not excessively long, the area under the concentration vs time curve for specified organs is generally the most relevant measure of concern. This value represents the cumulative exposure experienced by the organ. In general, the concentration of toxicant, and length of time it remains in a certain tissue, is a key indicator of the likelihood of adverse effects [143].

In-utero risk assessment requires both maternal and fetal PBTK and dose-response models. Depending on the placental barrier and chemical, the concentration in fetal blood may or may not run parallel to concentration in maternal blood. Some chemicals may only exert their toxicity during certain stages of development. There is a limited time frame in which the fetus is susceptible to certain toxic endpoints, illustrated by Figure 2.2. For example, once the palate has been completely formed, a chemical can no longer cause a cleft palate [90]. Similarly, there is a window of time in which the fetal blood-brain barrier has not yet developed, in which the fetus is more susceptible to neurotoxins. Being able to estimate the specific time in which a pregnant mother is being exposed is extremely important, and highlights the advantages of a time-concentration-activity modeling approach.

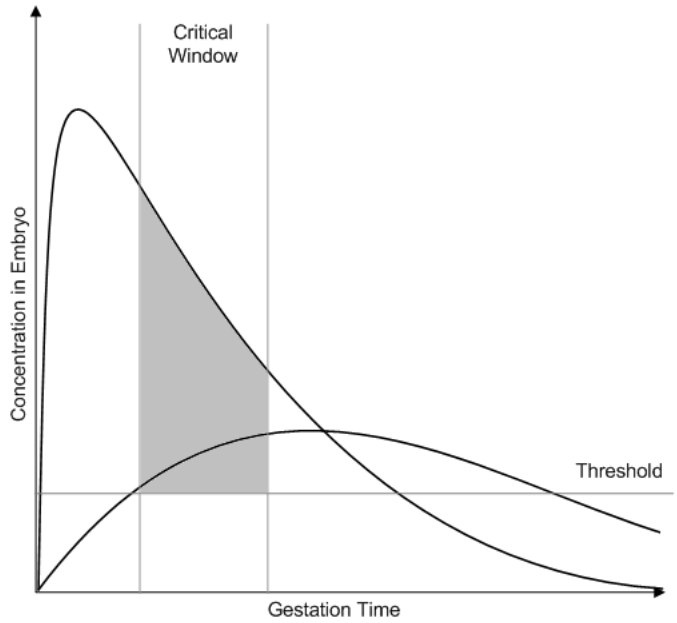

Figure 2.2: "Critical window" concept in fetal risk assessment (adapted from Corley et al. (2003) [90] and Young et al. (1997) [411]). The curves represent concentration in fetal sub-compartments, the horizontal line represents the concentration threshold, and the vertical lines represent the gestational age range of susceptibility to developmental problems.

2.3.2 Inter-species extrapolation

PBPK modeling is heavily dependent on animal and human data to formulate accurate parameter values. At the same time, PBPK models can use pharmacokinetic and toxicity data from animals to derive the safe exposure limits for humans. In general, animal experiments serve as a source for the reduction of parameter uncertainty, and as a method to predict potential adverse effects (such as birth defects or cancer) in humans.

Metabolic and transport parameters can be determined by experiments in animals, and these values can sometimes be extrapolated to the human models. Many internal processes are mechanisms for water homoeostasis and heat regulation, therefore

parameter values have been observed to be proportional to body surface area (or approximately (body weight)$^{0.75}$) [5, 60]. The actual value of the exponent varies, and interspecies scaling remains a primary source of uncertainty. It has become common practice in PBPK modeling to scale most human metabolic and excretory parameters (regardless of their derivation) to (body weight)$^{0.75}$ [307]. Partition coefficients between human blood and tissues are usually different from animals, and are either available from literature, or adjusted to fit data.

Parameters obtained from animal experiments are used as the starting point for the human model. After scaling up, model simulations are compared to human data. Time-course data on the tissue burdens of humans exposed to highly toxic chemicals are virtually nonexistent. However autopsy data, data from epidemiological events, in-vitro tissue experiments, and controlled human studies in which biomarkers are monitored can be used to improve on various aspects of the human model. Curve-fitting or trial-and-error techniques are sufficient for the simple cases, while more complex optimization techniques may be necessary for others.

While many chemical interactions at the pharmacokinetic level are negligible or nonexistent, the toxicity of a chemical mixture may be different than if each chemical were acting alone. This would effect values such as the lowest observed effect level (LOAEL) and the no observed effect level (NOAEL), which are exposure concentrations (usually inhaled) characterizing thresholds that should not be exceeded.

When these "OEL's" are known for animals, they can be extrapolated to humans using PBPK models [107]. The belief is that an adverse effect is directly related to both the concentration of toxin in the target tissue, and the amount of time the chemical spends in the tissue. If an inhaled concentration of X ppm causes the kidney

concentration to reach Y μg/L in a mouse (leading to an adverse health effect in the mouse), human PBPK simulations should determine the inhaled concentration (which is probably not equal to X ppm) that causes the kidney concentration to reach Y μg/L in the human. In general, the important metrics are both the maximum concentration Y μg/L, and the area under the time-concentration curve, for blood or a specific tissue. This scale-up method has previously been used [149, 150, 154]. Similar approaches may be done in scaling fetal risk from animals to humans [149, 180].

2.4 Uncertainty and natural variability

2.4.1 Overview

Uncertainty and sensitivity analysis aid in testing the limits and applicability of PBTK models. PBTK models are essentially stochastic in nature, due to inter-individual variation (population variability), dynamic intra-individual variation (fluctuations), and model uncertainties. The assessment of uncertainty and variability of PBTK model assumptions and parameters is a topic that has been extensively discussed [84, 86, 200, 299].

Uncertainty primarily exists due to incomplete or imprecise knowledge of exact parameter values and model definition. Uncertainty could be reduced through the collection of additional human and animal data, and by making models more complex and mechanistic. In the assessment of risk at the population level, uncertainty goes beyond just the parameter values, but extends also to human behavior. Lifestyle implications such as type of food consumed, personal hygiene, exercise, type of home, and occupation are all variables that contribute to uncertainty. Reduction of this type of uncertainty involves use of census or survey data. On the other hand, inter-individual variability

occurs naturally in PBPK models, and cannot be reduced. No two individuals are ever the same, and significant differences will exist in body weight, organ volumes, blood flow rates, and metabolic pathways [114].

Inter-individual variability can significantly effect model solutions, therefore its accurate assessment has become routine for toxicokinetic model development and analysis. Monte Carlo simulations are typically adequate for these assessments. For the random sampling Monte Carlo procedure, values are drawn from the distributions of each uncertain model parameter. The model is then run using this set of parameters, and the process is repeated for a given number of iterations.The distributions of the output parameters are useful in observing the impacts that parameter uncertainty and natural variability have on the model outcomes. The sensitivity of the model outputs to the input values are tested by observing the magnitude of variable responses, and how they deviate from arbitrary or normal values [200]. Accurate characterization of uncertainties and variabilities of input parameters are therefore very important for simulation results and analysis.

2.4.2 Physiology and susceptibility

For toxic metals, special considerations are needed for populations at high risk for metal toxicity, such as infants and young children [182, 285], and women [383, 384]. A number of databases, scaling methods, and empirical relationships exist for estimating human physiology which account for age and gender differences. Table 2.1 outlines selected methods for whole-body PBTK parameter estimation. Methods defining whole-body organ physiology as a continuous function of age are useful for performing long-term simulations for an individual. PK-Pop and P3M are discontinuous with respect to age, but provide more realistic inter-individual variability than regression equations.

Table 2.1: Selected modeling tools for population physiology

Method	Variables	Notes	Reference
Age regression	Age, gender	Polynomials as a function of age	[173, 299]
PostNatal	Age, gender, BW	Polynomials as a function of body weight	[238, 239, 413]
P3M	Age, gender, BW, BH, race	Empirical formulas; age, race, BH neglected for some tissues; discontinuities	[300]
PK-Pop	Age, gender, BW, BH, race	Body-height formula with age, gender, race variation; discontinuities	[117, 397, 398]
Literature Database	N/A	Discrete database of records; includes elderly and health impaired	[370]

The P3M physiological parameter database [300] implemented a wide variety of different published empirical and allometric formulas to estimate parameters for the NHANES III dataset. However, individuals of identical age, gender, body weight, body height would produce identical physiology. The PK-Pop algorithm [398], a module developed within the PK-SIM software [397], scales adult organ parameters by body height. Additional random variation is included to prevent individuals of similar size from being assigned identical parameters. The probability distributions are age, gender, and race dependent [398]. The PK-Pop algorithm performs similarly to P3M when applied to the NHANES III dataset [398], and both software may be used to create physiology databases accessible by the Matlab-Simulink environment. PK-Pop, P3M, and age-polynomial functions have been implemented in the current work. For the generalized PBTK model, the PK-Pop methodology is used to predict a majority of the organ parameters, while the PostNatal equations are used for the remainder.

Chapter 3

Current methods and platforms for mixture toxicokinetics

While there are currently numerous platforms for predicting toxicokinetics for chemicals in humans (e.g. PK-SIM [117, 397, 398], SimCYP [203], and PostNatal [238, 239, 413]), they were primarily developed for applications to pharmaceuticals. This chapter instead overviews two methods which were recently developed for the specific aim of simulating mixtures of environmental contaminants in humans.

3.1 Exposure Related Dose Estimating Model

The Exposure Related Dose Estimating Model (ERDEM) is a modeling platform developed by the USEPA for the PBTK modeling of multiple environmental contaminants [42]. It is a generalized framework containing compartments for arterial/venous blood, brain, carcass, closed chamber, skin, fat, intestine, kidney, liver, rapidly/slowly perfused tissues, spleen, stomach, and lung. The GI tract may optionally include stomach wall/lumen, duodenum, lower small intestine, and colon with lymph pool and portal blood. The lung may be optionally modeled as a full "breathing lung" containing alveoli, lower/upper dead space, lung tissue, and pulmonary capillaries. While the platform does have advantages (maintains physiological constancy for modeling mixtures, a graphical user interface (GUI), automatically generates detailed simulation reports),

it contains some aspects that are disadvantageous for population mixture models.

3.1.1 Population limitations

The platform currently allows for the formulation of a PBPK model only for one individual. There is no direct way to incorporate uncertainties, probability distributions on parameters, or to model population exposures without editing the underlying code written in ACSL (Advanced Continuous Simulation Language). All models developed in the GUI may be exported into ACSL for changes (with an ACSL license), but models altered in ACSL cannot be imported back and fourth between the GUI with ease. ACSL is no longer a language supported by the software developer (AEGIS), and the modeling capabilities of the language are limited.

3.1.2 Unresolved model inconsistencies

The GUI front-end allows for the definition of model data sets (MDSs). These are data sets which define an individual and physiological modeling assumptions, the exposure chemicals and scenarios, and toxicokinetics. While few basic MDS's are imported along with the installation of ERDEM, there is no online repository of MDS's used or developed by the EPA or other developers (both final and beta versions).

The MDS concept is a powerful tool, (since MDSs store PBPK modeling parameters, exposure scenarios, and datasets), but has not yet been effectively implemented (i.e. through extensive public MDS releases). Some complex models developed by the USEPA in ERDEM have required customizations in the ACSL environment (due to assumptions that are unavailable in the GUI), and are essentially ACSL codes controlled by ERDEM command-line functions. These advanced implementations of ERDEM by

USEPA have only been performed for internal purposes and have not been made publicly available. This may be due to incompatibility issues between models available in the GUI, ACSL-only models, and models developed in previous ERDEM versions.

Due to the differences in model assumptions and structure across different MDS's, there is no clear method as to how to integrate multiple models together into a consistent framework. To do this, it seems that either: a) The models are run separately from each other, with alterations to either the GUI front-end or the ACSL code to ensure that the organ volumes and flow rates are consistent across models (as is seen in [365]), or b) A "meta" model data set is formulated in the GUI or ACSL, in which all chemicals are defined and the PBPK structure is general enough to model them all. Note that method (a) cannot model interactions, while method (b) could become unnecessarily time consuming if the GUI is used. ERDEM does have the ability to model multiple different chemicals and metabolites. However, importing multiple existing (and separate) MDSs into a single MDS capable of modeling interactions is no easy task.

3.1.3 Physiological limitations

Additional limitations of ERDEM make the modeling environment especially difficult to simulate toxic metals. It is not currently possible to implement diffusion-limited PBTK models, despite the fact that many metals and non-metals require the diffusion assumption in all tissues. Red blood cells (RBC) are not explicitly defined in ERDEM, (however it may be possible to manipulate plasma protein binding equations to simulate RBC binding). As a result, it is only possible to develop a few of the flow-limited models for metals in the ERDEM GUI. The O'Flaherty model for lead [280] could be developed, but without the complex bone kinetics. Methylmercury (MeHg) could be

modeled, but without the developing fetus. A diffusion-limited RBC compartment, and a hair compartment are required for the MeHg model, and workarounds might not be possible. Modeling arsenic would be possible for the Yu formulation [414], but not for the more complex El-Masri/Kenyon formulation [120]. It is not possible to model cadmium in ERDEM.

While ERDEM has many useful features and very detailed models of the lung, GI-tract, and liver (including enzyme depletion/re-generation and metabolic interactions), the platform is still young and rapidly evolving. It is still possible to use the framework to construct a generalized MDS capable of modeling mixtures of VOCs and pesticides simultaneously (which has been the primary purpose of ERDEM). Current issues with model compatibility, difficulties in incorporating ERDEM models into pre-existing exposure frameworks, and the inability to model all toxic metals lead to the conclusion that the ERDEM framework is insufficient for the generalized/multi-metal PBTK model.

3.2 Steady-state model reduction

3.2.1 Rationale

Simplifications to the system of differential equations for PBTK models can be made under certain circumstances, reducing the number of parameters and equations. If exposure is constant for a long enough period of time, a quasi steady-state of chemical concentration may be reached in the body. In such a scenario, all differential equations are set to zero, and algebraic solutions for individual chemicals can be derived [74].

Significant uncertainties exist in determining the exposure-time profiles large human populations, and quantitatively characterizing all interactions of complex mixtures is

practically impossible. The need to know the daily or weekly fluctuations of chemical concentrations in all tissues becomes less important in the presence of these uncertainties, and the average quasi-steady-state values are adequate when estimating lifetime risk from chronic exposures. Additionally, many risk assessments consider only "worst-case" scenarios (i.e. continuous lifetime exposure) despite the unrealistic assumptions, in order to obtain a preliminary analysis of risk and prioritize research needs. For these reasons, simplifying assumptions regarding internal dose profiles and metabolic interactions are sometimes appropriate.

3.2.2 Model equations

The general steady-state equations for inhalation modeling for a single chemical case are well established (e.g., see [43, 74]). At steady-state, all PBTK derivative equations are set to zero and all tissues with no clearance (via metabolism or excretion) have equal inlet and outlet concentrations. For many organic chemicals, the liver (metabolism) and lung (gas exchange) become the only compartments explicitly required to solve the resulting system of algebraic equations. The starting equations for deriving the steady-state algorithm are outlined in [74]:

$$Q_{\mathrm{P}}C_{\mathrm{I},i} + Q_{\mathrm{L}}C_{\mathrm{L},i} = \frac{Q_{\mathrm{P}}C_{\mathrm{A},i}}{P_{\mathrm{B},i}} + Q_{\mathrm{L}}C_{\mathrm{A},i} \tag{3.1}$$

$$Q_{\mathrm{L}}C_{\mathrm{A},i} = Q_{\mathrm{L}}C_{\mathrm{L},i} + R_{\mathrm{met},i} \tag{3.2}$$

Notations for variables are found on the following page in Table 3.1. Assuming that only competitive inhibition occurs during metabolism, and that the competitive inhibition constants for each chemical i inhibiting chemical $j \neq i$ is equal to the Michaelis affinity constant for i, it has been shown that the following steady-state solution for

PBTK mixtures can be derived [202]:

$$\begin{aligned} A_i + x_i &= B_i x_i/(1+X) && (3.3)\\ x_i &= \frac{A_i(1+X)}{B_i-(1+X)} && (3.4)\\ X &= \sum \frac{A_i(1+X)}{B_i-(1+X)} \quad \text{by summing Eq 3.4} && (3.5) \end{aligned}$$

where

$$x_i = \frac{C_{\mathrm{L},i}}{K_{\mathrm{m},i}}; \quad B_i = \frac{V_{\mathrm{max},i}}{\beta_i K_{\mathrm{m},i}}; \quad A_i = \frac{\alpha_i C_{\mathrm{I},i}}{K_{\mathrm{m},i}\beta_i}, \text{ and } X = \sum \frac{C_{\mathrm{L},j}}{K_{\mathrm{m},j}} \tag{3.6}$$

and

$$\begin{aligned} \alpha_i &= Q_{\mathrm{P}} \Big/ \left(1 + \frac{Q_{\mathrm{P}}}{Q_{\mathrm{L}} P_{\mathrm{B},i}}\right)\\ \beta_i &= -Q_{\mathrm{L}} + Q_{\mathrm{L}} \Big/ \left(1 + \frac{Q_{\mathrm{P}}}{Q_{\mathrm{L}} P_{\mathrm{B},i}}\right) \end{aligned} \tag{3.7}$$

Table 3.1: Notation used for steady-state parameters.

Symbol	Description
Q_{P}	Inhalation rate
Q_{L}	Blood flow rate to liver
$C_{\mathrm{I},i}$	Inhalation concentration
$C_{\mathrm{L},i}$	Concentration in liver venous blood
$C_{\mathrm{A},i}$	Concentration in arterial blood
$P_{\mathrm{B},i}$	Blood:air partition coefficient
$V_{\mathrm{max},i}$	Maximal velocity of metabolism
$K_{\mathrm{m},i}$	Michaelis affinity constant
α_i	Derived (Equation 3.7)
β_i	Derived (Equation 3.7)
x_i	Derived (Equation 3.6)
A_i	Derived (Equation 3.6)
B_i	Derived (Equation 3.6)
X	Derived (Equation 3.6)

Equation 3.5 can be used iteratively to compute the value of X, by starting with an initial guess. The final value of X can be substituted into 3.4 in order to obtain concentrations of individual chemicals in the liver. The concentration in arterial blood is assumed to be $Q_{\mathrm{P}} C_{\mathrm{A},i}/P_{\mathrm{B},i}$.

The major assumption in this algorithm is that all interactions are assumed to be competitive, and the competitive inhibition constant K_{i} for each interaction was assumed equal to the inhibitor's K_{m}. This assumption was considered reasonable, since the K_{i} values are typically found to be within the order of magnitude as the K_{m} values in-vivo. Additionally, there are significant uncertainties for the values $V_{\max}$, K_{m}, and K_{i} under complex mixture conditions. Experimentally determining the actual in-vivo inhibition constants for high order mixtures is impractical.

3.2.3 Evaluation

Since the PBTK model structures, metabolic equations, and parameters for volatile organic compounds (VOCs) are typically very similar, VOCs are a convenient case-study for illustrating and evaluating these algorithms as applied to mixtures. The rationale for modeling the pharmacokinetics of multi-VOC exposure, and extrapolating complex mixture effects from binary mixture data has been previously discussed [172]. Individuals are exposed to multiple VOCs in everyday environments, and VOC mixtures have been observed in air and biomarker samples by general population studies [82, 233]. In addition, these chemicals may interact at the metabolic level via CYP2E1 metabolism [357].

Since the half-lives of these chemicals are on the order of 10-24 hours, it can be shown that a quasi-steady state in blood concentration is possible for chronic daily exposure [181]. Assuming a steady state allows for the use of steady state algorithms, which require less physiological and physiochemical parameters than full-blown PBPK models. This becomes particularly important for mixtures, since the number of parameters and equations increases with each additional chemical.

The steady-state liver blood concentration was obtained with the physiological algorithm and compared with the simulations of the full PBPK models for rats written in the Matlab framework. The simulation consisted of inhalation exposure of a complex mixture, ranging in concentration from very low (0.2 mg/m^3 air) to very high (200 mg/m^3 air). The mixture consisted of benzene, toluene, ethylbenzene, m-xylene, o-xylene (BTEX), trichloroethylene, tetrachloroethylene, styrene, vinyl chloride, carbon tetrachloride, and chloroform. The rat PBPK model parameters used in this study are outlined in Table 3.2. Parameters for BTEX, trichloroethylene, tetrachloroethylene, and styrene were obtained from [171]. Model parameters for vinyl chloride, carbon tetrachloride, and chloroform were obtained from [85], [105], and [313], respectively.

The model consisted of four tissue compartments interconnected with systemic circulation: fat, liver, slowly perfused (SP), and richly perfused (RP). The tissue uptake of toluene was described as a perfusion-limited process and metabolic clearance was described in the liver. The simulations of liver blood concentration were obtained after 5 days of continuous inhalation exposure, to ensure the attainment of steady-state.

Table 3.2: Parameters used in the rat PBTK model for the complex mixture case

	TOL	BNZ	XYL*	EBZ	CHL	PERC	TCE	CCl4	VCL	STY
Blood:air PC	18	15	46	42.7	19.3	18.9	21.9	4.52	2.4	40
Vmax†	3.44	2.11	6.49	6.39	6.8	0.19	11	0.99	4	3.6
KM (mg/L)	0.13	0.01	0.45	1.07	0.25	0.3	0.25	0.25	0.1	0.36
Fat:blood PC	57	33	40	36	20	122	25	79	10	40
SP:blood PC	1.54	1	0.91	0.61	0.68	1.06	0.46	1.01	0.4	0.91
RP:blood PC	4.64	1.13	1.98	1.41	1	3.72	1.24	3.14	0.7	1.98
Liver:blood PC	4.64	1.13	1.98	1.96	1	3.72	1.24	3.14	0.7	1.98
Inhalation‡	15									
Liver flow‡	3.75									

*Parameters for m- and o-xylene
†Units of mg/h/kg$^{0.75}$ body-weight
‡Units of L/h/kg$^{0.7}$ body-weight

3.2.4 Results and conclusions

Figure 3.1 shows a comparison of arterial and liver blood concentrations estimated by the steady-state algorithm with those of a full PBTK model for the case of the most complex mixture (11 VOCs) at two different doses. Four chemicals are shown in the figure. Tables 3.3 and 3.4 show the liver blood concentrations and rates of metabolism for additional exposure scenarios (inhalation of 50 ppm of each VOC for binary, ternary, and higher order mixtures). In all cases, the results were compared with the corresponding PBTK model results and showed negligible difference between the PBTK and the steady-state algorithm. Simulation results were essentially identical.

Tables 3.3 and 3.4 show the effect of different BTEX mixture combinations on liver blood concentration and metabolic rate. While mixture content has a significant impact on predictions of steady-state levels, the non-linearity of metabolic interactions is apparent at high exposure due to saturation. Figure 3.2 illustrates the effect of 50 ppm inhibitor concentrations (of varying composition) on liver blood concentration of toluene (from 1 ppm to 500 ppm exposure), and figure 3.3 illustrates the effect of inhibitors on toluene arterial blood concentration. In both cases, it is possible that simply computing mixture effects as a net summation of observed binary or tertiary interactions may lead to unrealistic conclusions.

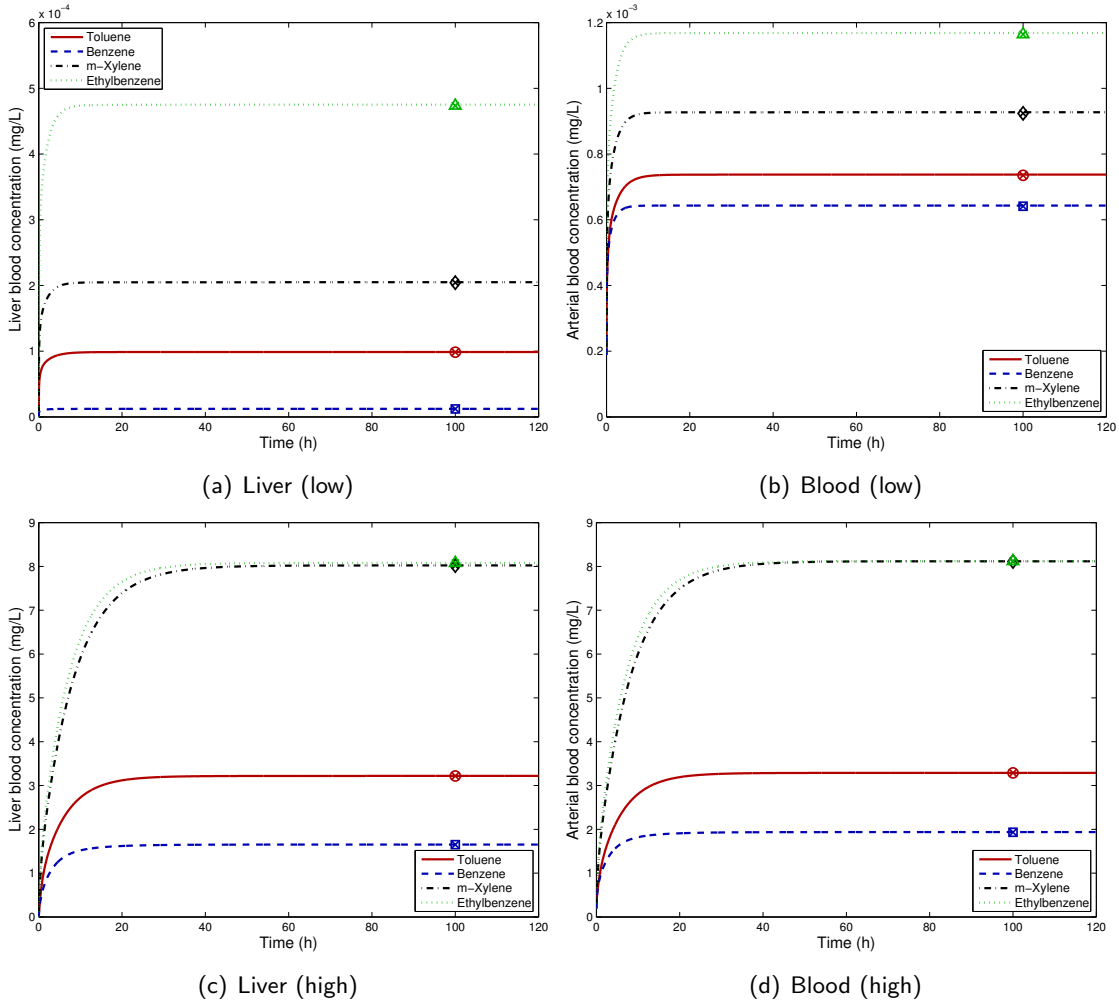

(a) Liver (low) (b) Blood (low)

(c) Liver (high) (d) Blood (high)

Figure 3.1: Comparison of estimates of arterial and liver blood concentrations from the steady-state algorithm with those from a full PBTK model for a complex mixture of VOCs (a total of 11 VOCs) in a rat. Lines represent predictions by the PBTK model with continuous exposure, and colored shapes at t=100 hours correspond to predictions by the steady-state algorithm. The top panel corresponds to exposures of 0.2 mg/m^{3}of each VOC, and the bottom panel corresponds to exposures of 200 mg/m^{3}of each VOC.

Table 3.3: Predictions by the steady-state algorithm of liver blood concentrations under varying BTEX exposures, for inhalation of 50 ppm of each VOC.

Scenario	Liver concentrations (mg/L)			
	Toluene	m-xylene	Benzene	Ethylbenzene
BT	2.27	-	0.54	-
TX	0.89	2.22	-	-
BX	-	5.78	0.48	-
TEX	1.37	3.54	-	5.44
TBX	2.55	7.11	0.74	-
BTEX	2.64	7.38	0.81	8.16

Table 3.4: Predictions by the steady-state algorithm of metabolic rate under varying BTEX exposures, for inhalation of 50 ppm of each VOC.

Scenario	Rate of metabolism(mg/h)			
	Toluene	m-xylene	Benzene	Ethylbenzene
BT	0.27	-	0.51	-
TX	0.60	0.82	-	-
BX	-	0.44	0.53	-
TEX	0.48	0.68	-	0.43
TBX	0.20	0.30	0.46	-
BTEX	0.18	0.28	0.44	0.13

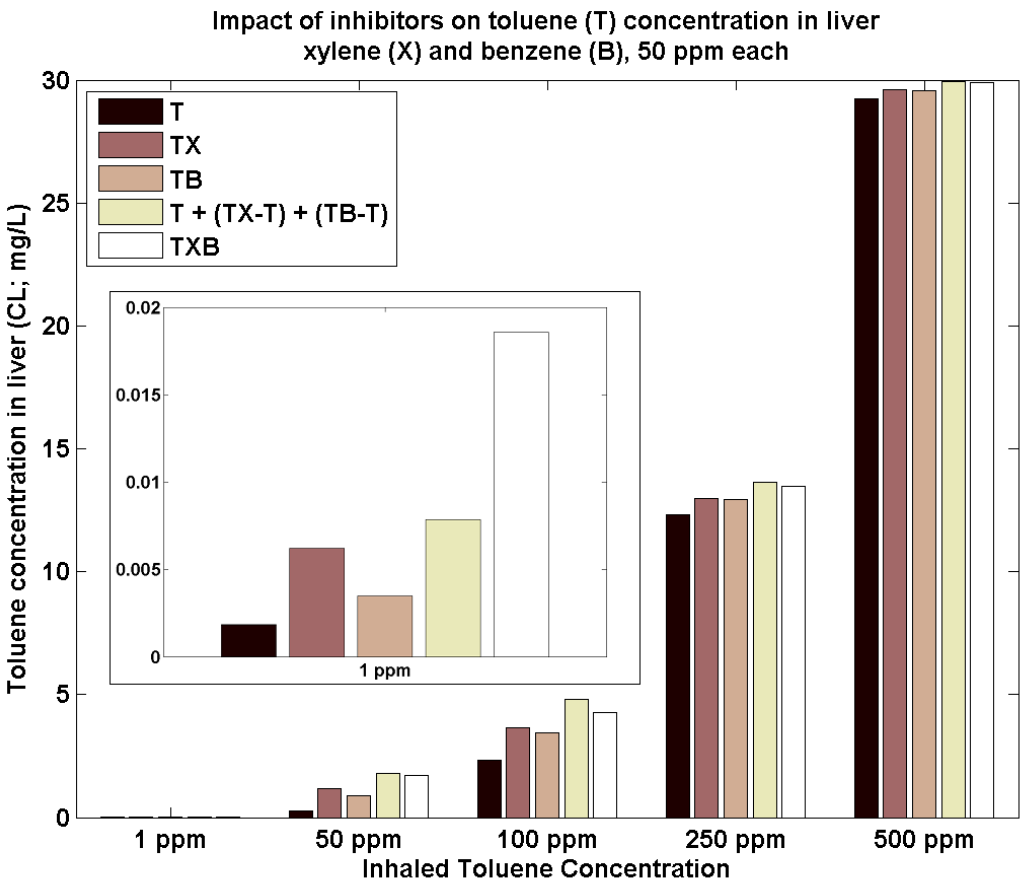

Figure 3.2: Impact of addition of successive inhibitors on the liver concentration of toluene. Different combinations of benzene and xylene, each at 50 ppm inhalation concentrations are studied. For low toluene concentrations, the impact of the inhibitors is pronounced, and the total mixture effects are not adequately captured by binary interactions. For higher concentrations of toluene, the impact of inhibitors is not as significant.

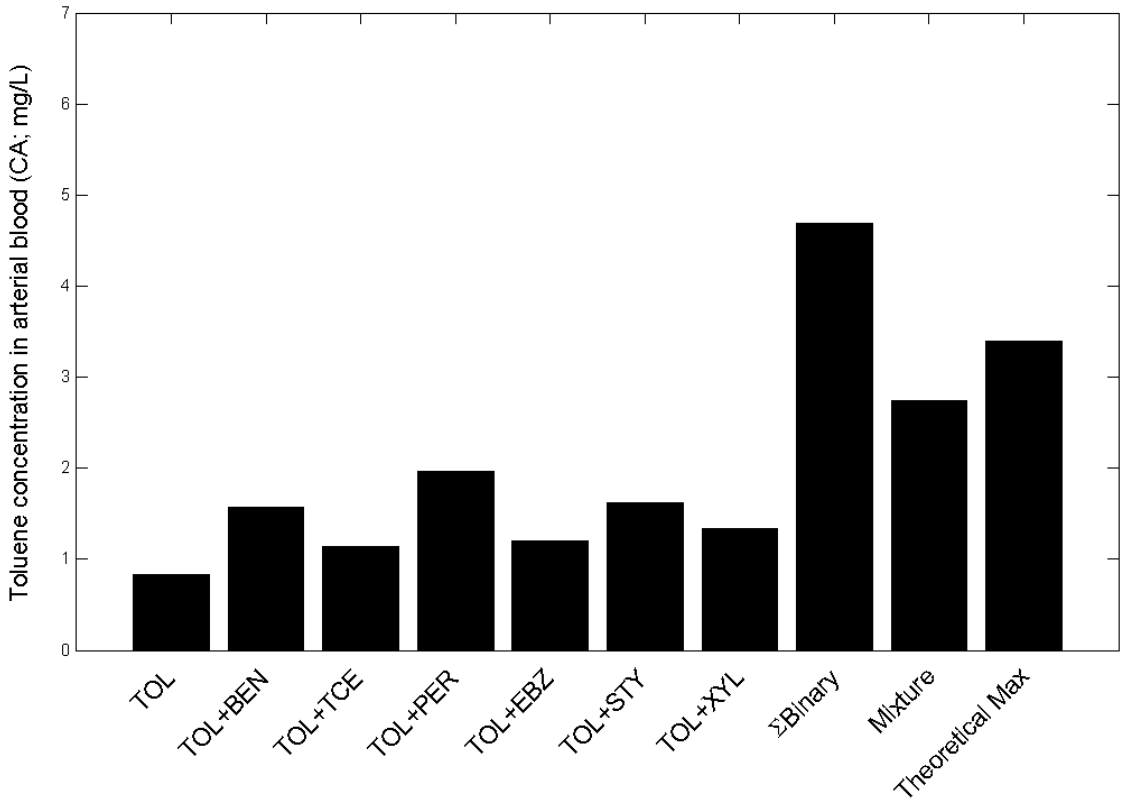

Figure 3.3: Impact of competitive inhibition on toluene (TOL) concentration in the rat liver by binary mixtures, and by a complex mixture of multiple inhibitors. Inhaled concentration of 50 ppm was assumed for toluene and inhibitors. The theoretical maximum was estimated by assuming no metabolism in the liver. The sum of effects from binary interactions does not adequately capture the overall inhibition by the components of the complex mixture, and is in fact significantly higher than the theoretical maximum.

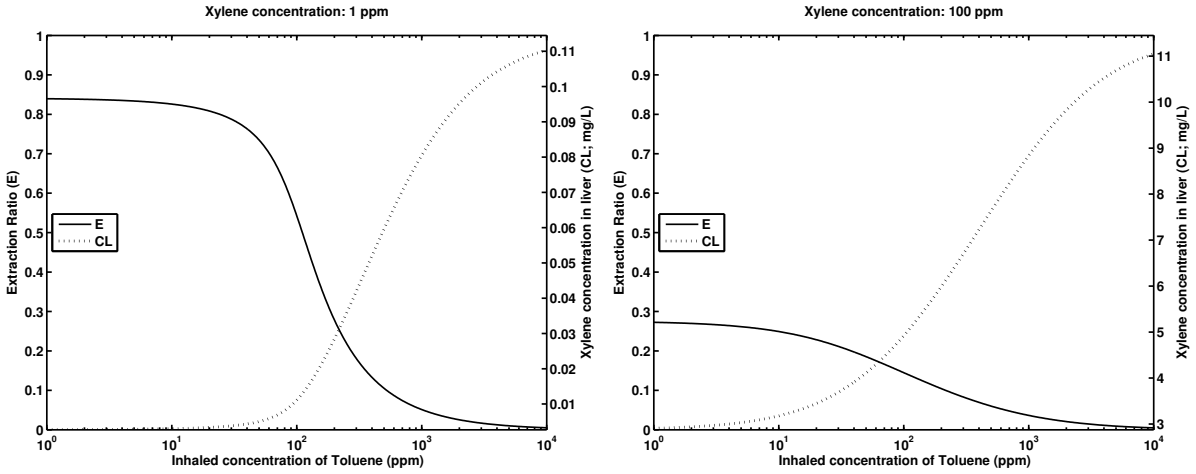

(a) 1 ppm xylene

(b) 100 ppm xylene

Figure 3.4: Liver concentration and extraction ratio under continuous inhalation exposure to xylene and toluene. Predictions were made using the steady-state algorithm with human parameters. Figures show the effects of toluene exposure on xylene liver concentration and extraction ratio for the 1 ppm (left) and 100 ppm (right) xylene exposure. Extraction ratio is the fraction of chemical entering the liver that metabolizes.

Steady-state models require fewer physiological and biochemical parameters and can be implemented in simple spreadsheet software, making preliminary risk analysis of large complex mixtures faster and more concise. Certain analysis requiring many discrete model predictions over large spans of exposure concentrations (such as those in Figure 3.4) would require solving systems of differential equations hundreds of thousands (if not millions) of times. The primary goal of these steady-state algorithms is to rapidly analyse "worst-case" scenarios of continuous long-term exposures. However when more precise analysis is required (i.e. realistic unsteady-state exposures or alternative metabolic interaction assumptions), full PBTK models are necessary.

Chapter 4

Development of a Generalized PBTK Modeling Framework

4.1 Overview

Models for different chemicals have alternative lumping arrangements or compartment perfusion assumptions. However, they can be considered subsets of the same generalized model outlined in Figure 4.1. Blood flow rates and volumes of compartments which are common to different models are equal, regardless of chemical. Parameters of lumped compartments (e.g. slowly perfused and rapidly perfused) vary by chemical, but are constrained to be consistent with the sum of remaining whole body parameters. As stated earlier, software can be used to estimate physiological values for a majority of the tissue groups outlined in Figure 4.1 (e.g. PK-SIM [117, 397, 398], P3M [300], SimCYP [203], and PostNatal [238, 239, 413]).

Deriving lumped parameter PBTK models from the generalized framework reduces an artificial source of inter model variation, maintains the structure of the original models, and usually will not require estimation of additional parameters. Variation may arise when estimating PBTK parameters of different models (the "inverse problem"), while using inconsistent or contradictory physiological assumptions. Variation may also arise when estimating tissue and biomarker levels ("forward problem"), if

multiple PBTK models are run simultaneously for individuals while overlooking major inconsistencies.

In probabilistic applications, distributions describing organ physiology are defined for the generalized model. The relationships between the generalized model and chemical-specific PBTK sub-models are deterministic. This property is useful when applying sensitivity analysis methods to integrated exposure/PBPK models for multiple contaminants, and when simulating mixtures consistently from source-to-dose in "virtual" individuals of a population. PBTK models in the literature often include components specific to a transport process, absorption route, or physiological condition. Some examples include distributed-parameter models for diffusion into skin [319] and bone [280], maternal/fetal models for pregnancy [90], and kidney sub-compartments for renal transport processes [91]. Despite discretization of compartments, total tissue volumes and blood flow rates remain consistent with the whole-body model.

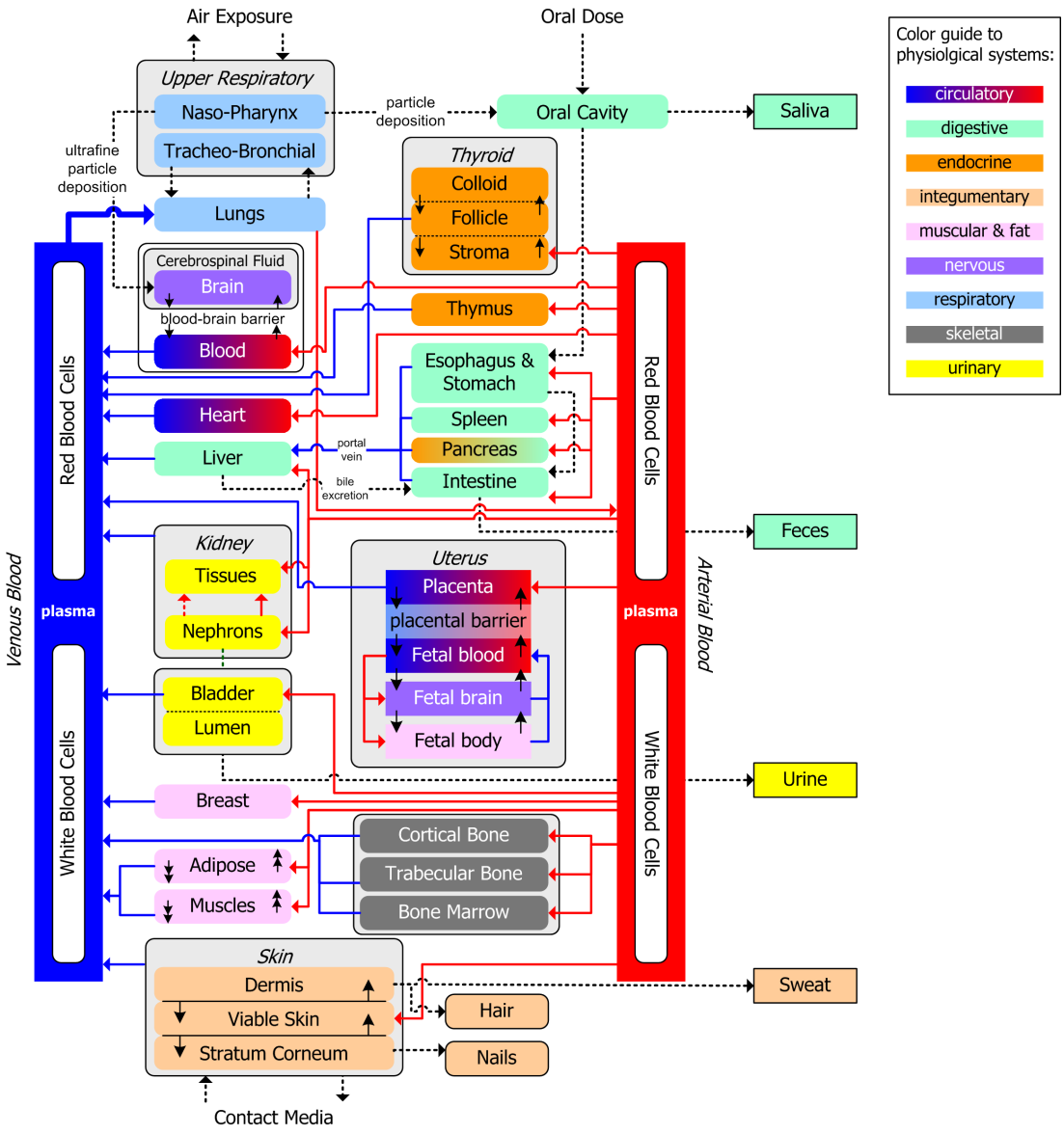

Figure 4.1: A schematic depiction of major compartments considered in the generalized PBTK modeling framework and the interactions among compartments. All PBTK models involving mixtures of metals and organics are defined to be subsets of the same whole-body physiology. While the models may contain structural differences, volumes and blood flow rates to common compartments are be identical, and parameters for lumped tissue groups are be consistent with the remaining whole-body tissues.

4.2 PBTK equations

4.2.1 Compartment mass balances

Compartments that are perfusion-limited assume that rapid diffusion occurs for a chemical between the blood and tissue, causing blood flow rate to be the limiting transport step. Diffusion-limited compartments assume diffusion to be the rate-limiting step. Since diffusion is a function of both the chemical and tissue properties, the incorporation of perfusion- or diffusion-limited compartments vary by the PBTK model.

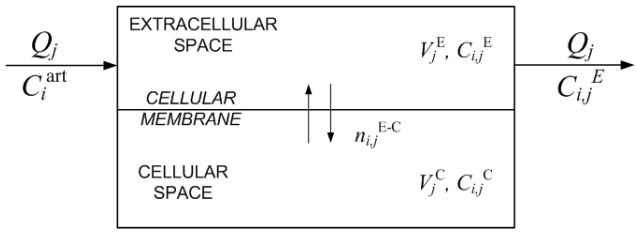

Figure 4.2: Schematic of diffusion-limited sub-compartments and transport processes.

The diffusion-limited assumption divides compartments into extra-cellular blood and internal tissue/cellular regions described by [159]:

$$\begin{aligned} \frac{dA_{i,j}^{E}}{dt} &= Q_j(C_{i,j}^{art} - C_{i,j}^{E}) - n_{i,j}^{E\text{-}C} \\ \frac{dA_{i,j}^{C}}{dt} &= n_{i,j}^{E\text{-}C} + R_{i,j} + T_{i,j} \\ n_{i,j}^{E\text{-}C} &= PA_{i,j}\left(C_{i,j}^{E} - \frac{C_{i,j}^{C}}{P_{i,j}}\right) \end{aligned} \tag{4.1}$$

Where: subscripts i and j denote chemical and compartment index, respectively; A amount of chemical in tissue (mass); C chemical concentration (mass/L); Q compartment blood flow rate (L/min); P chemical tissue:blood partition coefficient; R net reaction rate (mass/min); T net transport rate via additional processes (mass/min);

$n_{i,j}^{\text{E-C}}$ the permeation rate of chemical into the tissue (mass /min); PA the permeability-area coefficient (L/min); superscripts **E** and **C** denote extracellular and cellular space, respectively; superscripts **art** and **ven** denotes the arterial blood venous blood, respectively.

Metabolism typically occurs in the cellular space, and the venous blood concentration leaving the tissue is equal to the extracellular concentration. The diffusion equation for compartmental flux $n_{i,j}^{\text{E-C}}$ may have alternate forms (i.e. carrier-mediated transport [159]). Concentration is calculated by dividing mass by the volume of the tissue (or tissue sub-compartment).

In cases where rapid steady-state is assumed in extracellular blood, a diffusion-limited compartment simplifies to [307]:

$$\begin{aligned} \frac{dA_{i,j}}{dt} &= n_{i,j}^{\text{E-C}} + R_{i,j} + T_{i,j} \\ n_{i,j}^{\text{E-C}} &= PA_{i,j}\left(C_{i,j}^{\text{art}} - \frac{C_{i,j}}{P_{i,j}}\right) \\ C_{i,j}^{\text{ven}} &= C_{i,j}^{\text{art}} - \frac{n_{i,j}^{\text{E-C}}}{Q_{i,j}} \end{aligned} \tag{4.2}$$

At the limit $PA_{i,j} = Q_{i,j}$ (high permeation rate), the diffusion-limited equations simplify to the perfusion-limited case. Perfusion limited (or "flow-limited") compartments are modeled as well-mixed systems within a single volume (similar to continuous stirred tank reactors), and may be expressed as [307]:

$$\begin{aligned} \frac{dA_{i,j}}{dt} &= Q_j\left(C_{i,j}^{\text{art}} - \frac{C_{i,j}}{P_{i,j}}\right) + R_{i,j} + T_{i,j} \\ C_{i,j}^{\text{ven}} &= \frac{C_{i,j}}{P_{i,j}} \end{aligned} \tag{4.3}$$

4.2.2 Circulatory recycle mass balances

Equations for the recycling of venous blood streams throughout the body depend on chemical properties. A toxin may re-circulate unchanged (with the arterial blood concentration equal to the total mass flow in venous blood, divided by total cardiac output). A central compartment may be used to account for additional reactions or transport that occurs in the blood (such as binding to red blood cells, exhalation/inhalation of chemical in the lungs, or intravenous dosage).

For chemicals which may be inhaled and eliminated from the blood via exhalation (which is a common assumption for many volatile organic compounds), the re-circulation equations are [307]:

$$\frac{dA_{i,bl}}{dt} = Qc(C_i^{\text{mix}} - C_i^{\text{art}}) + Qp(C_i^{\text{inh}} - C_i^{\text{alv}}) \tag{4.4}$$

$A_{i,bl}$ is the amount of chemical i in the blood compartment; Qc is total cardiac output; C_i^{mix} is concentration in mixed venous blood (calculated by summing the mass flows of outlet streams from all tissues emptying into the venous blood, and dividing by total cardiac output); Qp is pulmonary air-exchange rate (usually set equal to the inhalation rate); C_i^{inh} is the inhaled air concentration; C_i^{alv} is the alveolar air concentration exhaled from lung, and is assumed to equilibrate with the arterial blood concentration with a blood:air partition coefficient Pb_i ($C_i^{\text{alv}} = C_i^{\text{art}}/Pb_i$).

$$C_i^{\text{art}} = \frac{C_i^{\text{mix}}\ Qc + C_i^{\text{inh}}}{Qc + Qp/Pb_i} \tag{4.5}$$

The concentration of chemical measured in the exhaled breath is usually corrected to account for 30% deadspace in the lung, and is therefore assumed to be a mixture of alveolar air (70%) and the inhaled air (30%) concentrations.

While toxic metals are not eliminated from the blood by exhalation, many instead bind to (or diffuse into) red blood cells. Such chemicals are transported into tissues by concentration gradients in the plasma as opposed to the whole blood, and chemicals within the red blood cells are sequestered. The central recycle compartments are used to calculate absorbed dose from the lung, and any binding to red blood cells (or blood proteins).

If the relationship between chemical concentration in the blood and plasma is assumed to be linear (typically for free-diffusion), the following partitioning coefficient equation describes the relationship between whole blood, plasma, and red blood cell concentrations [187]:

$$P_{i,\text{wbl/pl}} = P_{i,\text{rbc/wbl}}\ Hc + (1 - Hc) \tag{4.6}$$

Where $P_{i,\text{wbl/pl}}$ is the partition ratio of chemical i between whole blood (wbl) and plasma (pl); $P_{i,\text{rbc/wbl}}$ is the partition ratio of chemical i between red blood cells (rbc) and plasma; Hc is the hematocrit (ratio of red blood cell volume to whole blood volume)

To convert a tissue/whole-blood partition coefficient to a tissue/plasma partition coefficient, it is multiplied by whole-blood/plasma partition coefficient (equation 4.6).

For the case where a chemical exhibits saturable binding to the red blood cells, the relationship between red blood cell and plasma concentration follows a Langmuir-type isotherm [159, 187] :

$$C_{i,\text{rbc}} = C_{i,\text{pl}} \left(\frac{a_i}{b_i + C_{i,\text{pl}}} \right) \tag{4.7}$$

Where a_i is the binding coefficient (mass/L), and b_i is the dissociation constant (mass/L).

4.2.3 Metabolism

Metabolism may occur in any tissue in the body, and metabolic networks can become infinitely complex. PBTK models simplify these processes into lumped reaction constants, and only those metabolites that are relevant for biomarker predictions or risk assessment are typically modeled. Minor pathways and unstable metabolites or intermediates are neglected.

Non-saturable reaction rates in PBPK models are usually described as first or second order equations:

$$R_{i,j} = k_{cl} C_{i,j} \tag{4.8}$$

$$R_{i,j} = k_1 C_{i,j}\ V_j \tag{4.9}$$

$$R_{i,j} = k_2 (C_{i,j} V_j)\ (C_{n,j} V_j) \tag{4.10}$$

Where k_{cl} is intrinsic clearance (L/h); k_1 is a first order rate constant (h^{-1}); k_2 is a second order rate constant ($h^{-1}mass^{-1}$); $C_{n,j}$ is the concentration of species n (usually an enzyme) in tissue j (mass/L). First order reactions typically describe a degradation-type process the reactant undergoes, such as demethylation or reduction. Second order reactions occur when an additional reactant, typically an enzyme or antioxidant, is involved.

In each tissue, a network of first-order reactions may be represented by [142]:

$$
\begin{aligned}
\frac{dy_1}{dt} &= \left(-\sum_{j=1}^{N}{}' k_{j1}\right)\ y_1 \ +\ k_{12}\ y_2 \ +\ \cdots +\ k_{1N}\ y_N \\
\frac{dy_2}{dt} &= k_{21}\ y_1 \ +\ \left(-\sum_{j=1}^{N}{}'\ k_{j2}\right)\ y_2 \ +\ \cdots +\ k_{2N}\ y_N \\
&\ . \\
&\ . \\
\frac{dy_N}{dt} &= k_{21}\ y_1 \ +\ k_{12}\ y_2 \ +\ \cdots +\ \left(-\sum_{j=1}^{N}{}'\ k_{jN}\right)\ y_N
\end{aligned}
\tag{4.11}
$$

Where k_{AB} is the first-order rate constant for the reaction $B \rightarrow A$ (h^{-1}); y_n is the amount of species n (mass); N is the total number of chemical species.

The following simplification in notation has been made:

$$
-\sum_{j=1}^{N}{}'\ k_{ji} = -\sum_{\substack{j=1 \\ j\neq i}}^{N}\ k_{ji}
$$

The reaction network of the system of equations 4.11 can be represented in matrix form [142]:

$$
\frac{d\mathbf{y}}{dt} = \mathbf{K}\ \mathbf{y} \tag{4.12}
$$

$$
\mathbf{y} = \begin{pmatrix} y_1 \\ y_2 \\ \vdots \\ y_N \end{pmatrix} \qquad \mathbf{K} = \begin{pmatrix} -\sum{}' k_{j1} & k_{12} & \dots & k_{1N} \\ k_{21} & -\sum{}' k_{j2} & \dots & k_{2N} \\ \vdots & \vdots & & \vdots \\ k_{N1} & k_{N2} & \dots & -\sum{}' k_{jN} \end{pmatrix} \tag{4.13}
$$

Where $\mathbf{K}$ is the matrix of net first order rate constants, and $\mathbf{y}$ is the vector of chemical amounts. Such a formulation is convenient for the Matlab environment. The

reaction networks for typical PBTK models are not large enough to be computationally expensive (as long as the matrix networks are restricted to only those species undergoing transformation).

Saturable reactions occur when a reactant is utilizing a limited number of enzyme sites to undergo transformation. These are usually described by Michaelis-Menten kinetics [159]:

$$R_{i,j} = C_{i,j} \frac{\mathrm{Vm}_{i,j}}{C_{i,j} + \mathrm{Km}_{i,j}} \tag{4.14}$$

Where $\mathrm{Vm}_{i,j}$ is the maximum reaction velocity (mass/hr), and $\mathrm{Km}_{i,j}$ is the Michaelis constant (mass/L). When different species of reactant compete for a finite number of the same enzyme sites, metabolism may be mutually inhibited [222]. For a given tissue, the rate of metabolism of component i in the presence of an inhibitor k is given by the following relationship. (Note that for simplicity, tissue j notation was omitted).

$$R_i = \frac{\mathrm{Vm}_i C_i}{C_i + \mathrm{Km}_i \left(1 + \dfrac{C_k}{\mathrm{I}_{k,i}}\right)} \tag{4.15}$$

Where C_i is the concentration of reacting species i (mass/L); C_k is the concentration of inhibitor species k (mass/L); $\mathrm{I}_{k,i}$ is the inhibition constant for k inhibiting metabolism of i (mass/L). Extrapolating this to more complex mixtures, where metabolism is occurring in the presence of multiple inhibitors,

$$R_i = \frac{\mathrm{Vm}_i C_i}{C_i + \mathrm{Km}_i \left(1 + \displaystyle\sum_{m \neq i}^{N} \frac{C_m}{\mathrm{I}_{m,i}}\right)} \tag{4.16}$$

While competitive inhibition reduces metabolism by increasing Km_i, noncompetitive inhibition results in a reduction of Vm_i via the noncompetitive inhibition constant I^{nc} (mass/L). The metabolic rate in the presence of multiple noncompetitive inhibitors may be defined as:

$$R_i = \frac{C_i \ \mathrm{Vm}_i \left(1 + \sum_{m \neq i}^{N} \frac{C_m}{\mathrm{I}^{\mathrm{nc}}_{m,i}}\right)^{-1}}{C_i + \mathrm{Km}_i} \tag{4.17}$$

If including both noncompetitive and competitive inhibition in a model, the rate of reaction becomes:

$$R_i = \frac{C_i \ \mathrm{Vm}_i \left(1 + \sum_{m \neq i}^{N} \frac{C_m}{\mathrm{I}^{\mathrm{nc}}_{m,i}}\right)^{-1}}{C_i + \mathrm{Km}_i \left(1 + \sum_{m \neq i}^{N} \frac{C_m}{\mathrm{I}_{m,i}}\right)} \tag{4.18}$$

It should be noted that while N represents the total number of chemicals in the PBTK model, not every chemical may cause inhibition. Inhibition constants for chemicals not causing inhibition (either competitive or noncompetitive) may be set to infinity.

4.3 Computational implementation

The Matlab-Simulink programming environment has previously been reviewed as a useful tool for PBPK applications [116], and tutorials exist for model development and good coding practices [201]. PBTK models include graphical and dynamic elements, which lend themselves well to Simulink. Models in Simulink can be constructed graphically, and linked together within a hierarchical framework. Tools are also available for modeling complex metabolic networks, such as the commercial SIMBIOLOGY toolbox [249], and open-source Systems Biology Toolbox [331]. Additionally, the PBTK models in Simulink may be embedded within Matlab functions defining exposure scenarios for the simulation (i.e. exposure routes and durations, physiological characteristics of the individual, and activities). This allows for integration into a source-to-dose modeling

framework.

A generalized PBTK modeling template was created in Simulink to sufficiently account for major tissues, and absorption and excretion mechanisms (Figure 4.3). All tissue groups and exposure pathways are defined as "enabled subsystems" in Simulink, allowing any of them to be neglected (disabled) for some PBTK models. Within each tissue is an additional diffusion-limited "deep tissue" compartment, which may be enabled and included in the model (Figure 4.4). All disabled tissue groups are lumped into rapidly or slowly perfused groups accordingly. A user interface (UI) was constructed in order to be able to efficiently make changes to model assumptions (Figure 4.5). The template served as the basis for the PBTK models for lead, cadmium, chromium, arsenic, and methylmercury. Models for the individual metals could then be pooled into the same workspace, allowing for simultaneous exposure and dose simulations with the ability to model interactions. Model hierarchy is illustrated in Figure 4.6.

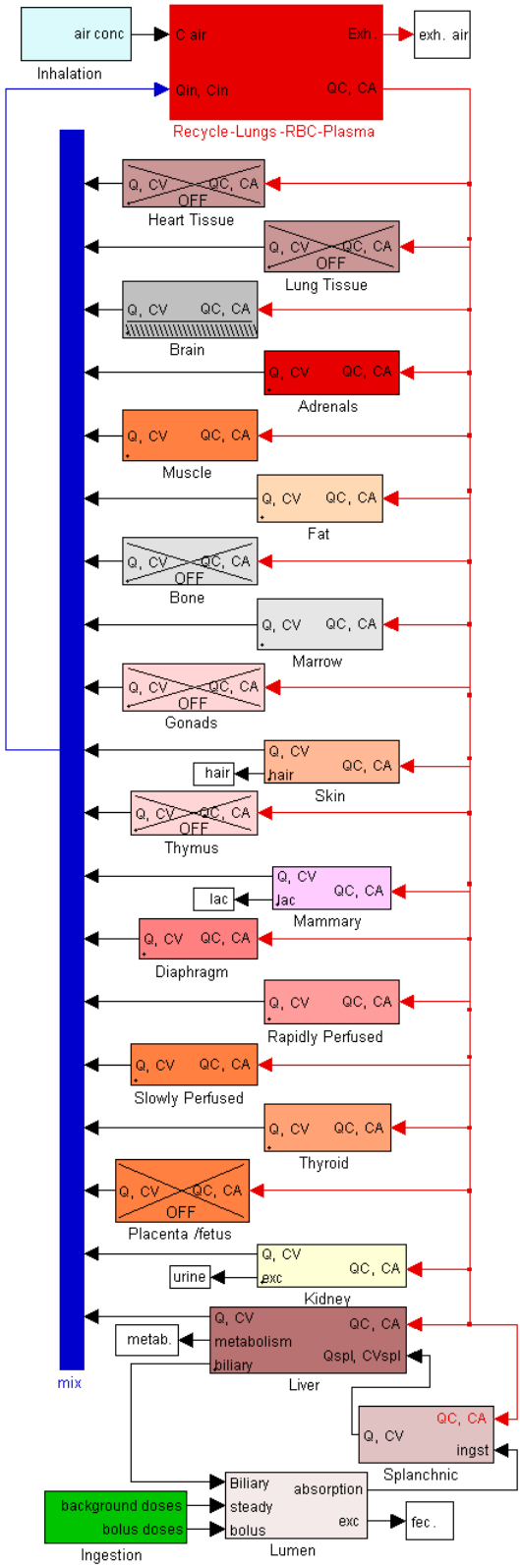

Figure 4.3: Simulink block diagram depicting the generalized PBTK template. Disabled tissues are crossed-out and are incorporated into lumped groups. Hatch-marks indicate diffusion-limitation is enabled. Red blood cells, plasma, fetal system, and splanchnic organs have been condensed into subsystems for simplicity.

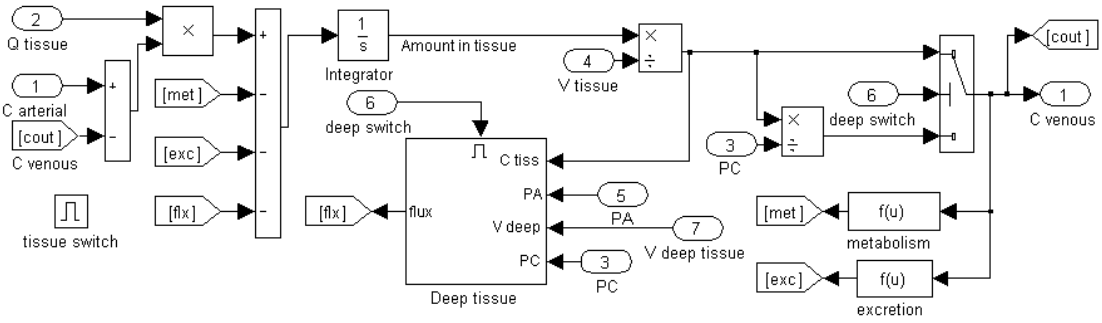

Figure 4.4: Simulink block diagram depicting the mass balance within a tissue compartment. Ovals denote input ports, tapered flags represent "go-to" and "from" ports (which reduce the number of lines and connectors), and the linked algebraic and integrator blocks define the differential mass balance equation.

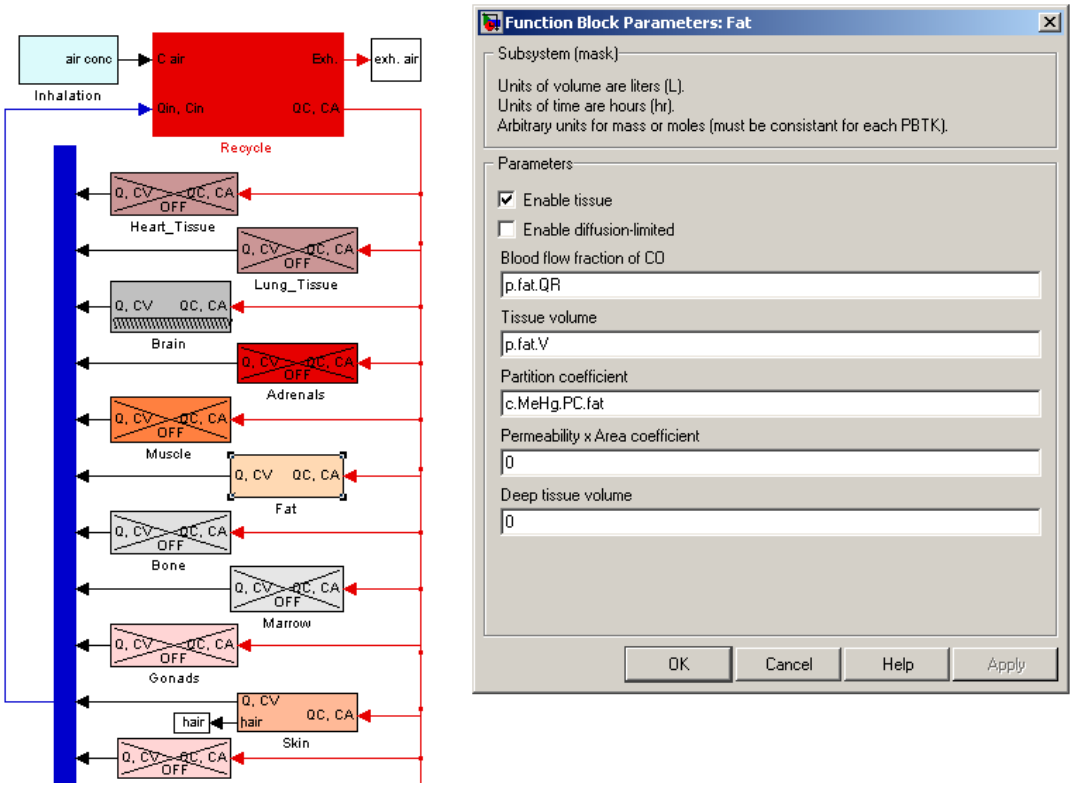

Figure 4.5: Prototype user interface for the generalized Simulink PBTK model. Clicking on a tissue allows input of parameters and a variety of options. Some organ systems may have additional inputs for metabolism and excretion.

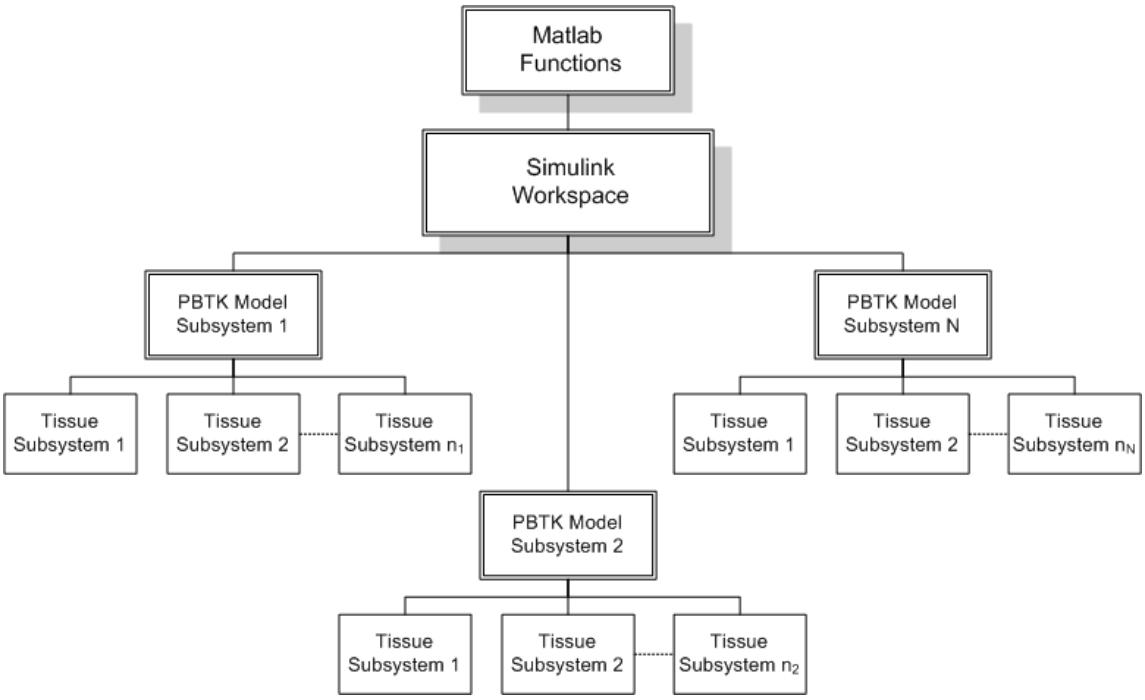

Figure 4.6: Flow chart of Matlab and Simulink model hierarchy. A Simulink workspace may be used to model **N** PBTK models simultaneously, with the ability to incorporate interactions. The PBTK models consist of $\mathbf{n}_i$ tissue subsystems with varying configuration. The Simulink workspace is invoked by Matlab functions that may interface with other models for exposure, dose response, or parameter optimization.

Chapter 5

Development of a Bayesian framework for the generalized model

5.1 Theory

Physiologically-based toxicokinetic models contain parameters for physiology (organ volumes and blood flow rates, inhalation rate, cardiac output), and pharmacology (tissue:blood partition coefficients, parameters for absorption, metabolism, and excretion). For chemical mixtures, the number of parameters increases further. Significant challenges are faced when simultaneously estimating large numbers of PBTK parameters with relatively limited data.

Over the past decade, the Bayesian approach to parameter estimation has become a highly used optimization technique [209]. This is partially due to the fact that PBTK parameters can be interpreted as being both random and hierarchical. Individuals are members of a sub-population (i.e. males, females, young, old), and sub-populations are subsets of a general population (i.e. humans living in the U.S.). At each level in the hierarchy, parameters may lie within a specified range and distribution. When optimizing PBTK parameters to obtain the best model/data fit, the probability that the parameters are realistic given the population being modeled should therefore be incorporated. Bayesian methods also require the statistical inclusion of prior information

and knowledge at each hierarchical level.

Bayes' rule provides a statistical model for relating a set of parameters (θ) with data (y). The joint probability distribution $p(\theta, y)$ may be decomposed into a prior distribution $p(\theta)$ and a sampling distribution $p(y|\theta)$[153]:

$$p(\theta, y) = p(\theta) \times p(y|\theta) \tag{5.1}$$

The purpose is to find the values for the parameter set θ which will yield a high probability given data y. This conditional probability $p(\theta|y)$ may be expanded using Bayes' rule:

$$\begin{aligned} p(\theta|y) &= p(\theta, y)/p(y) \\ &= p(y|\theta) \times p(\theta)/p(y) \\ &\propto p(y|\theta) \times p(\theta) \end{aligned} \tag{5.2}$$

The final relationship omits the value $p(y)$, since it is a constant representing the total probability of y over all values of θ, which is not efficient to directly estimate for most applications.

A hierarchical PBTK modeling framework consists of multiple parameters describing each random variable (Figure 5.1). A random PBTK variable Ψ_{ik} (individual i, parameter k) can be considered the realization of a population probability distribution defined by mean μ_k and variance Σ_k^2. Population parameters μ_k and Σ_k may be considered random variables with additional hyperparameters if they are to be estimated by Bayesian analysis, or they may be considerd constants if the priors are well-informed. Each variable Ψ_{ik} at the individual level, and each variable μ_k and Σ_k at the population level have an inherent probability which is used to calculate the total prior $p(\theta)$.

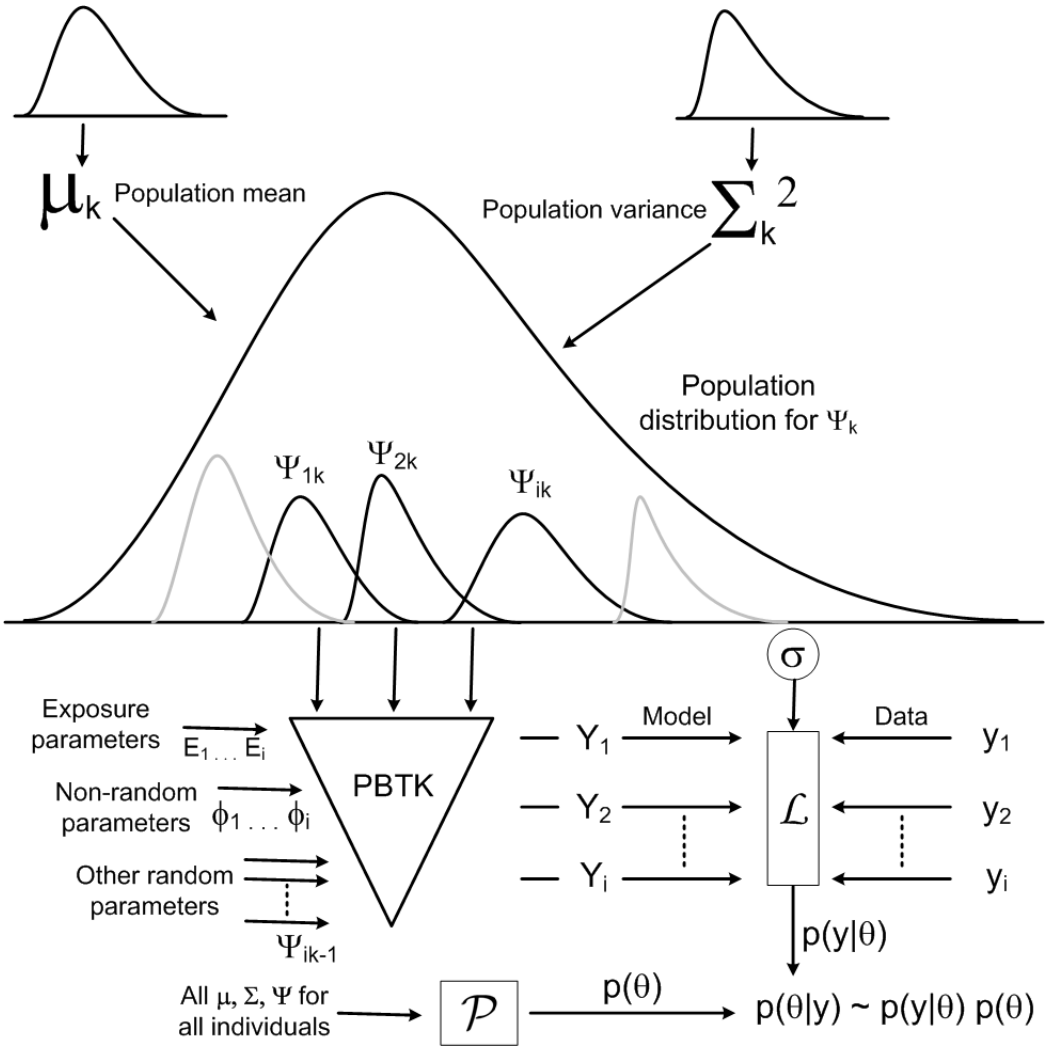

Figure 5.1: Schematic of a hierarchical Bayesian framework (adapted from [170]). Each random parameter Ψ_{ik} is assumed to be derived from a population distribution defined by μ_k and Σ_k. Random and non-random parameters are used as inputs to the PBTK model to predict $\mathbf{Y}$. The likelihood function calculates the probability of an adequate model prediction of data $\mathbf{y}$ given the set of random parameters. The prior function calculates the probability of all random parameter values given the current set of assumptions of their distributions. The posterior probability is proportional to the product of the likelihood and prior.

PBTK models predict $\mathbf{Y}$ using the set of random variables Ψ, the set of non-random variables ϕ (i.e. gender and body weight), and the set of exposure variables E (i.e. inhalation concentration and exposure duration).

A likelihood is calculated assuming that each measured data observation j for individual i (y_{ij}) deviates from the corresponding model prediction (Y_{ij}) by an error relationship. If the error model is lognormal (which is commonly used when modeling exponentially-decaying concentrations), then:

$$\begin{aligned} \log y_{ij} &= \log Y_{ij} + N_{\mathrm{rnd}}(\mu = 0, \sigma) \\ &= \log(f(t_{ij}, E_i, \Psi_{i\,\cdot}, \phi_i)) + N_{\mathrm{rnd}}(\mu = 0, \sigma) \end{aligned} \tag{5.3}$$

Where N_{rnd} is a normal random variable. The function $f(t_{ij}, E_i, \Psi_{i\,\cdot}, \phi_i)$ represents the PBTK model as a function of t_{ij} (the point in time for data j and individual i), E_i (exposure parameters for individual i), $\Psi_{i\,\cdot}$ (all random parameters for individual i), and ϕ_i (the set of non-random PBTK parameters for individual i). The error between the log-transformed data and model prediction is assumed to be a normal random variable with mean 0 and standard deviation σ. The parameter σ represents model misspecification error, intraindividual variation, and other causes of deviations between the model and data. It may be held to a known constant, or considered an unknown random variable. Datasets with more than one metric (i.e. separate blood and urinary samples), may require multiple σ values.

The resulting total likelihood over all data and individuals is represented by $p(y|\theta)$, and the posterior probability is proportional to the product of $p(y|\theta)$ and $p(\theta)$. A formal derivation illustrates the practical relationships between model parameters and measured data, and is outlined by [37] but expanded here with additional intermediate

steps.

Substituting Ψ, μ, Σ, and σ into Equation 5.3 yields the basis for the posterior calculation $p(\theta, |y)$:

$$p(\Psi, \mu, \Sigma, \sigma, |y) \quad \propto \quad p(y|\Psi, \mu, \Sigma, \sigma) \times p(\Psi, \mu, \Sigma, \sigma) \tag{5.4}$$

The likelihood term of Equation 5.4 is a conditional probability which may be decomposed into [153]:

$$p(y|\Psi, \mu, \Sigma, \sigma) \quad = \quad p(\mu, \Sigma, y|\Psi, \sigma)/p(\mu, \Sigma|\Psi, \sigma) \tag{5.5}$$

If y is conditionally independent of μ and Σ given Ψ and σ, then the following relationship is true:

$$p(\mu, \Sigma, y|\Psi, \sigma) \quad = \quad p(y|\Psi, \sigma)p(\mu, \Sigma|\Psi, \sigma) \tag{5.6}$$

This conditional independence is a valid assumption in the hierarchical model, since y will depend solely on the direct PBTK model inputs and model/data error (Equation 7.7), and not the population parameters [37].

Substituting Equation 5.6 into Equation 5.5 yields a simplified definition of the likelihood:

$$p(y|\Psi, \mu, \Sigma, \sigma) \quad = \quad p(y|\Psi, \sigma) \tag{5.7}$$

The error variance may be considered independent of other model parameters, leading to decomposition of the prior probability function:

$$p(\Psi, \mu, \Sigma, \sigma) \quad = \quad p(\Psi, \mu, \Sigma)p(\sigma) \tag{5.8}$$

The joint probability term in Equation 5.8 can be factored to [153]:

$$p(\Psi, \mu, \Sigma) \quad = \quad p(\Psi|\mu, \Sigma)p(\mu, \Sigma) \tag{5.9}$$

Substituting this expression into Equation 5.8 and assuming μ and Σ are independent, the resulting form of the prior probability is [37]:

$$\begin{aligned} p(\Psi, \mu, \Sigma, \sigma) &= p(\Psi|\mu, \Sigma)p(\mu, \Sigma)p(\sigma) \\ &= p(\Psi|\mu, \Sigma)p(\mu)p(\Sigma)p(\sigma) \end{aligned} \tag{5.10}$$

The posterior probability is the product of the likelihood and prior defined by Equations 5.7 and 5.10, respectively:

$$p(\Psi, \mu, \Sigma, \sigma, |y) \propto p(y|\Psi, \sigma)p(\Psi|\mu, \Sigma)p(\mu)p(\Sigma)p(\sigma) \tag{5.11}$$

Extending the model to I individuals, each having n_i data observations and K random PBTK variables, the posterior becomes the product over all probabilities:

$$p(\theta|y) \propto \prod_{i=1}^{I}\prod_{j=1}^{n_i} p(y_{ij}|\Psi_i\cdot, \sigma)\prod_{i=1}^{I}\prod_{k=1}^{K} p(\Psi_{ik}|\mu_k, \Sigma_k)\prod_{k=1}^{K} p(\mu_k)\prod_{k=1}^{K} p(\Sigma_k)p(\sigma) \tag{5.12}$$

The likelihood function implements the PBTK model for each individual i, predicting a time profile of biomarkers, corresponding to n_i observed data points.

$$\begin{aligned} \prod_{i=1}^{I}\prod_{j=1}^{n_i} p(y_{ij}|\Psi_i\cdot, \sigma) &= \prod_{i=1}^{I}\prod_{j=1}^{n_i} N_{\text{pdf}}(log(y_{ij}), log(Y_{ij}), \sigma) \\ &= \prod_{i=1}^{I}\prod_{j=1}^{n_i} N_{\text{p}df}(log(y_{ij}), log(f(t_{ij}, E_i, \Psi_i\cdot, \phi_i)), \sigma) \end{aligned} \tag{5.13}$$

Where $N_{\text{p}df}(log(y_{ij}), log(Y_{ij}), \sigma)$ is the normal probability density function calculated at $log(y_{ij})$ (log transformed data point), assuming a mean of $log(Y_{ij})$ (log transformed PBTK prediction) and standard deviation σ (the model/data error term). This is equivalent to $N_{\text{p}df}(log(y_{ij}) - log(Y_{ij}), 0, \sigma)$, or $N_{\text{p}df}(log(y_{ij}/Y_{ij}), 0, \sigma)$.

The form of the prior probabilities for the Ψ_{ik}'s (i.e. normal or lognormal), and population parameters μ_k and Σ_k depend on prior knowledge of each parameter. μ_k's and Σ_k's which are known to a high degree of certainty may be considered constants.

Unknown μ_k's may be considered random variables, with a probability distribution based on prior knowledge (i.e. uniform distribution with upper/lower bounds, or normal distribution with either low or high uncertainty around the mean). Unknown Σ_k's have typically been assigned a wide inverse gamma distribution with a shape parameter equal to one (or as high as three), and a scale parameter equal to the prior assumption for Σ_k [37]. The specification of an inverse gamma distribution for Σ_k was previously done out of convenience, so that a closed form of the posterior could be derived (since an inverse gamma is the conjugate prior of a normal distribution) [166]. While this specification is not always necessary due to the use of brute-force Markov-Chain Monte Carlo techniques (to be discussed in the following section), it is required for the Gibbs sampling method [153]. The inverse gamma description of variance priors has been adopted in many PBTK studies, perhaps to maintain uniformity.

5.2 Markov-Chain Monte Carlo Methods

The probability distribution defined by Equation 5.12 is too complex to be directly computed. To obtain the distribution and summary statistics of each parameter requires brute-force sampling of the multi-dimensional parameter space. Iterative numerical techniques, particularly Markov-Chain Monte-Carlo (MCMC), provide the fundamentals for the estimation of $p(\theta|y)$.

The goal is draw many samples from the posterior distribution of each parameter, without prior knowledge of where the sampling should be taking place. Sampling outside the target posterior parameter distribution leads to zero posterior probability, due to low likelihood (inadequate model/data fit), or low prior probabilities (unrealistic

parameter values). The regions where parameter values yield non-zero posterior probability must be estimated, and heavily sampled to obtain the range and shape of the full parameter space.

MCMC is a class of methods based on iteratively sampling the parameters from a "proposal" or transitional distribution until convergence to the unique "stationary" or target distribution. At each iteration t, parameter values θ^t take a step to θ^{t+1} based on the proposal distribution ($T_t(\theta^{t+1}|\theta^t)$).

The Markov Chain is the set of parameters from θ^0 to θ^t. At each iteration, parameter draws depends only on the previous value. Upon convergence to the stationary distribution, values of θ^t will have "forgotten" the initial starting value θ^0, which likely lies outside the final distribution.

Various MCMC algorithms are available which set different rules for the proposal distributions and sampling methods. Sampling algorithm efficiency is important, since at each iteration t, the PBTK model must be solved for I individuals using the updated parameter set θ^t. To properly explore the parameter space of the posterior distribution, thousands of well-placed samples are needed. Thousands of additional "burn-in" samples are usually required to allow the Markov-Chain to converge, since initial parameter guesses may lie outside the target distribution. Repeatedly solving a complex dynamic system tens (or hundreds) of thousands of times becomes a significant computational burden.

5.2.1 Metropolis and Metropolis-Hasting Algorithm

Sampling methods based on the Metropolis algorithm have been widely used to estimate posterior distributions, since they require that the posterior probability be calculated

only to a proportionality ($p(y)$ therefore does not need to be calculated). A multi-variate normal distribution (centered around the current iteration value θ^t, with covariance C) is used to draw a candidate value for θ^{t+1} (θ). The Metropolis algorithm uses a symmetric jumping distribution $J(\theta^t|\theta^{t-1})$ to explore the parameter space.

The rule to accept the new value is based on the ratio r of the new posterior probability to the probability at the previous step.

$$r = \frac{p(\theta|y)}{p(\theta^t|y)} \tag{5.14}$$

The new parameter set θ is accepted or rejected according to the following rule:

$$\theta^{t+1} = \begin{cases} \theta \text{ with probability } min(r,1) \\ \\ \theta^t \text{ otherwise} \end{cases} \tag{5.15}$$

The Metropolis-Hastings algorithm is a generalization of the Metropolis algorithm to allow for asymmetric jumping distributions. The ratio r is redefined as:

$$r = \frac{p(\theta|y)/J(\theta|\theta^{t-1})}{p(\theta^{t-1}|y)/J(\theta^{t-1}|\theta)} \tag{5.16}$$

5.2.2 Adaptive Metropolis

Sampling efficiency for the Metropolis algorithms depend strongly on the jumping distribution. Ideally the jumping distribution should be similar to the posterior distribution, as this would allow for the posterior probability space to be efficiently explored.

If the jumping distribution is too wide, acceptance rates are low due to parameters frequently leaving the posterior distribution. If the jumping distribution is too narrow, acceptance rates are high and the Markov-Chain would explore the parameter space too slowly (leading to "snaking" or poor "mixing" of the chain). This has a disadvantage since it would require many more iterations (and costly model evaluations) to achieve

convergence. For models of moderately high dimensionality, the optimal acceptance ratio (samples accepted/total samples) is 0.23 [153]. However this optimal ratio decreases to between 0.1 and 0.15 for very high dimensional models [311].

If the jumping distribution is multivariate normal, the covariance matrix C strongly effects the behavior of the Markov-Chain. This parameter can be iteratively tuned to obtain an optimal acceptance rate. The covariance may be set to a constant at the beginning of the MCMC simulation (after preliminary runs have determined a suitable matrix C). However, prior knowledge about the range and variance of the posterior values is needed to make a sufficient assumption about C.

Adaptive Metropolis methods allow for on-the-fly adjustment of C, based on the behavior of the Markov-Chain as it nears convergence.

The covariance matrix at iteration t (C_t) is updated according to the following rule [167]:

$$C_t = \begin{cases} C_0;\ t \leq t_0 \\ \\ s_d^2 cov(X_0, \ldots, X_{t-1}) + s_d^2 \epsilon I_d;\ t > t_0 \end{cases} \tag{5.17}$$

The scaling factor s_d is usually set to $2.4\sqrt{d}$ for efficiency purposes (where d is the number of dimensions) [153]. The value of ϵ is an arbitrarily small number (> 0) to prevent a singularity in the algorithm, and I_d is the identity matrix. Variable X_i represents the entire parameter set at iteration i (i.e. a vector of values for all random variables). The iteration t_0 defines the "burn-in" time, before which the chain will not adapt. The portion of the chain before t_0 is not used in the adaptation calculation of the covariance. In practice, the MCMC chain will not adapt at each step beyond t_0, but every few hundred iterations. Since adaptation of the chain occurs based on previous chain positions, the sampling method is no longer considered Markovian (or

"memory-less"). However it has been shown that the Adaptive Metropolis method converges to the target distribution [167]. The method is considered robust and has been incorporated into a number of MCMC software programs (such as WinBUGS).

5.2.3 Delayed Rejection

In problems where the proposal distribution poorly represents the posterior, off-line tuning of the proposal becomes a manual, iterative process [165]. Delayed rejection Metropolis sampling is a method in which alternative proposal functions may be implemented automatically during an MCMC simulation. When a proposed move to θ_1 is rejected, a "second-stage" move is proposed, using an alternate proposal distribution function. Third- and fourth-stage proposals may also be made upon further rejections.

The ratio r calculated for the rule in Equation 5.15 may be defined [165]:

$$r_1(\theta^t, \theta_1) = \frac{p(\theta_1|y)q_1(\theta_1, \theta^t)}{p(\theta^t|y)q_1(\theta^t, \theta)} \tag{5.18}$$

The variable q_1 represents the proposal distribution for the first stage, which was used to generate θ_1. This is analogous to Equation 5.16, with a generalized proposal distribution $q_i(\theta_1, \theta^t, \cdot)$ which may change at stage i. If the proposed move to θ_1 is rejected, a move to θ_2 is proposed using a second-stage proposal distribution ($q_2(\theta^t, \theta_1, \theta_2)$), rather than immediately reverting to θ^t. Parameter θ_2 is accepted according to the rule outlined in Equation 5.15, but with the following definition of r:

$$r_2(\theta^t, \theta_1, \theta_2) = \frac{p(\theta_2|y)q_1(\theta_2, \theta_1)q_2(\theta_2, \theta_1, \theta^t)(1 - r_1(\theta_2, \theta_1))}{p(\theta^t|y)q_2(\theta^t, \theta_1, \theta_2)(1 - r_1(\theta^t, \theta_1))} \tag{5.19}$$

The proposal q_2 may be dependent on the current value θ^t, and/or the rejected value θ_1. This can allow for a number of different combinations of first and second stage proposals. Wide variances for first proposal step could be followed by smaller variances for

the second step (which could help explore the distribution space efficiently). Alternatively, higher stage proposals may vary in dimension. The first proposal step may be "global", updating all parameters, while the second step may be "local", only updating selected variables.

Equation 5.19 can be extended to further stages, with the ith stage ratio r_i being defined as:

$$r_i(\theta^t, \theta_1^*, \ldots, \theta_i^*) = \frac{p(\theta_i^*|y)q_1(\theta_i, \theta_{i-1})q_2(\theta_i, \theta_{i-1}, \theta_{i-2} \ldots q_i(\theta_i, \theta_{i-1}, \theta^t)}{p(\theta^t)q_1(\theta^t, \theta_1)q_2(\theta^t, \theta_1, \theta_2) \ldots q_i(\theta^t, \theta_1, \ldots, \theta_i)} \frac{(1 - r_1(\theta_i, \theta_{i-1}))(1 - r_2(\theta_i^*, \theta_{i-1}^*, \theta_{i-2}^*)) \ldots (1 - r_{i-1}(\theta_i^*, \ldots, \theta_1^*))}{(1 - r_1(\theta^t, \theta_1^*))(1 - r_2(\theta^t, \theta_1^*, \theta_2^*)) \ldots (1 - r_{i-1}(\theta^t, \theta_1^*, \ldots, \theta_{i-1}^*))} \tag{5.20}$$

Each time a proposed move is rejected, a higher stage move is proposed. This continues either until a move is accepted, or the final stage move is rejected.

Both the Delayed-Rejection and Adaptive-Metropolis methods may be implemented simultaneously [168]. If the proposal functions at each stage are multivariate Gaussian, the covariance matrices can be tuned to achieve a desirable acceptance rate. This can be advantageous for PBTK model parameter optimization, since

5.3 Evaluation of four sampling methods

To evaluate the convergence performance of the four different sampling methods - Metropolis-Hasting (MH), Adaptive Metropolis (AM), Delayed Rejection (DR), and Delayed Rejection Adaptive Metropolis (DRAM) - synthetic data were generated for a small population of humans using a generic PBTK model.

The PBTK model consisted of intestinal lumen, gut, liver, fat, lungs, slowly-perfused and rapidly-perfused tissues. Equilibrium partition coefficients were arbitrarily chosen to be reasonable values for drugs or contaminants in humans (i.e. between 1 and 15). It was assumed that the chemical is only eliminated via metabolism in the liver. The

PBTK model and Bayesian framework were constructed in Matlab.

A hierarchical model was constructed, assuming that the Michaelis constant **Vm** (mole/min/kg$^{0.75}$), intestinal absorption constant **ka** (1/min/kg$^{0.75}$), and liver/blood partition coefficient **PL** were random variables. The Michaelis and absorption constants were normalized by BW$^{0.75}$.

Seven individuals were generated by selecting subjects from the NHANES-III database, and using body weight and body height to generate physiological parameters (organ volumes and blood flow rates) via the PKpop algorithm [398]. A small population size was chosen to simulate small-scale exposure and drug pharmacokinetics studies. Probability distribution for **Vm** was assumed to be lognormal with a population mean of 0.124 (μmol/min/kg$^{0.75}$) and log-scale standard deviation of 0.3; **ka** was assumed lognormal with mean 1.7x10^{-4} (1/min/kg$^{0.75}$) and log-scale standard deviation of 0.17; **PL** was assumed lognormal with mean 15.5 and log-scale standard deviation of 0.25. For each of the 7 individuals, PBTK parameters were randomly generated from these population distributions.

A single dose of 500 μg chemical (of molecular weight 75) is modeled using the PBTK model for each of the 7 virtual individuals. 15 data points at varying time intervals were generated using the PBTK model. Model predictions were scattered to simulate model/data error, assuming the log of each data point **d** would have an error that is normally distributed (with mean 0 and standard deviation 0.2) around the log of the corresponding model prediction **y**:

$$\log(d) = \log(y) + N(0, 0.2) \tag{5.21}$$

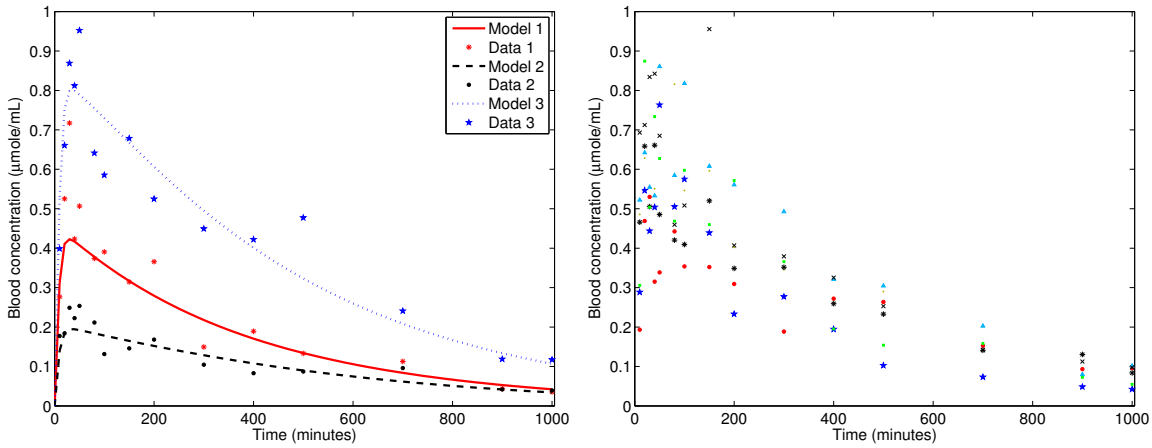

(a) Example model/data scatter

(b) Full synthetic dataset

Figure 5.2: Illustration of model predictions and synthetic data used for the MCMC analysis. (a): Three example curves showing the typical model/data error scatter between PBTK model predictions and synthetic data points. Data point colors correspond to the colored lines representing model predictions. (b): The full synthetic dataset used for the parameter optimization

In performing the MCMC analysis on the data, it was assumed that the population distributions for **ka** and **Vm** were unknown (except for the fact that the distribution was likely lognormal). The model/data error σ was also assumed to be unknown. The population distribution of **PL** was assumed to be known.

The unknowns for the analysis were totaled 26 parameters: population mean and standard deviation for **Vm** (μ**Vm** and Σ**Vm**, respectively); population mean and standard deviation for **ka** (μ**ka** and Σ**ka**, respectively); the values of **Vm, ka** and **PL** for each of the seven individual in the study; and lognormal model/data error term σ.

For the MCMC analysis, it was assumed that there was no prior information on μ**Vm** or μ**ka**, and therefore a non-informative uniform prior was used for these parameters. The variances (Σ^2) for **Vm** and **ka** were assumed to be inverse-gamma with a shape parameter of 1 (indicating large uncertainty), and a scale parameter of natural log(5) (indicating that **Vm** and **ka** are initially assumed to vary by a factor of 5 in the population) [37]. Since it was assumed that the population distribution for **PL** was well known, an informative lognormal prior (mean 15.5 and log-scale standard deviation of 0.25) was used.

A single MCMC chain was run for each of the four sampling methods. MCMC analysis was performed in the log-space, to bring all parameters to the same order of magnitude, and reduce correlations [153]. Each method was initiated with the same set of initial guesses. A multi-variate Gaussian proposal distribution was used, with an initial covariance matrix being the identity matrix multiplied by a positive scale factor. The scale factor was poorly tuned (too small), leading to poor chain mixing and inefficient sampling.

For the two adaptive methods (AM and DRAM), the chains had a "burn-in" of

15000 iterations (meaning that re-scaling of the sampling covariance matrix could not occur until after 15000 iterations). Preliminary runs had shown that 15000 iterations were sufficient in bringing parameters to near the convergence values. For both AM and DRAM, the covariance matrix (and thus the poorly tuned proposal distribution) was allowed to adapt every 500 iterations (after burn-in).

For the DR and DRAM methods, four proposal functions were used. If the first proposed Metropolis step is rejected, an additional move is proposed (using an alternate proposal function). The method was allowed to try 3 additional moves after the first rejection before making a final rejection and starting over again (from the original proposal function). All four proposal distributions were normal (with means of zero), but with different proposal variances. The proposal distributions were ordered so that the first move would be bold (large variances), and each successive try would be scaled down by a factor. The fourth proposal would be the poorly-tuned distribution. After automatic adaptation of the covariance matrix, the DRAM method will retain the same scale-down factors, but with a different proposal distribution. While the acceptance rates of the DR and DRAM methods should still be very high (by the fourth try, moves will likely be accepted due to the small proposal variance), the chains should mix better since many of the bold moves (the first 1 or 2) may also be accepted.

For all parameters, the adaptive methods (AM and DRAM) converged by about 20,000 iterations. Non-adaptive methods exhibited poor mixing and did not converge, as illustrated in Figures 5.3 and 5.4. The acceptance rate for AM was about 23%, which is optimal for the dimensionality of the current problem. For MH, the acceptance rate was about 70%, which is abnormally high and inefficient. The acceptance rate for DR was 34%, and for DRAM was 43%. Despite the relative high acceptance rate, the

DRAM chain showed significantly better sampling and efficiency than the DR and AM chains. This is due to the fact that there was a mix of both large and small "jumps" made by the random walk. Since many of the bold proposed moves were also accepted in addition to the small/inefficient ones, chain mixing improved. The adaptive aspect of the sampling method ensured that acceptance rates would not become excessively large.

Table 5.1 and Figure 5.5 illustrate the difference between the actual and estimated population distributions of **Vm** and **ka** using DRAM sampling. The estimations are sufficiently close, with slight biases due to the sparsity of the data and the model/data error.

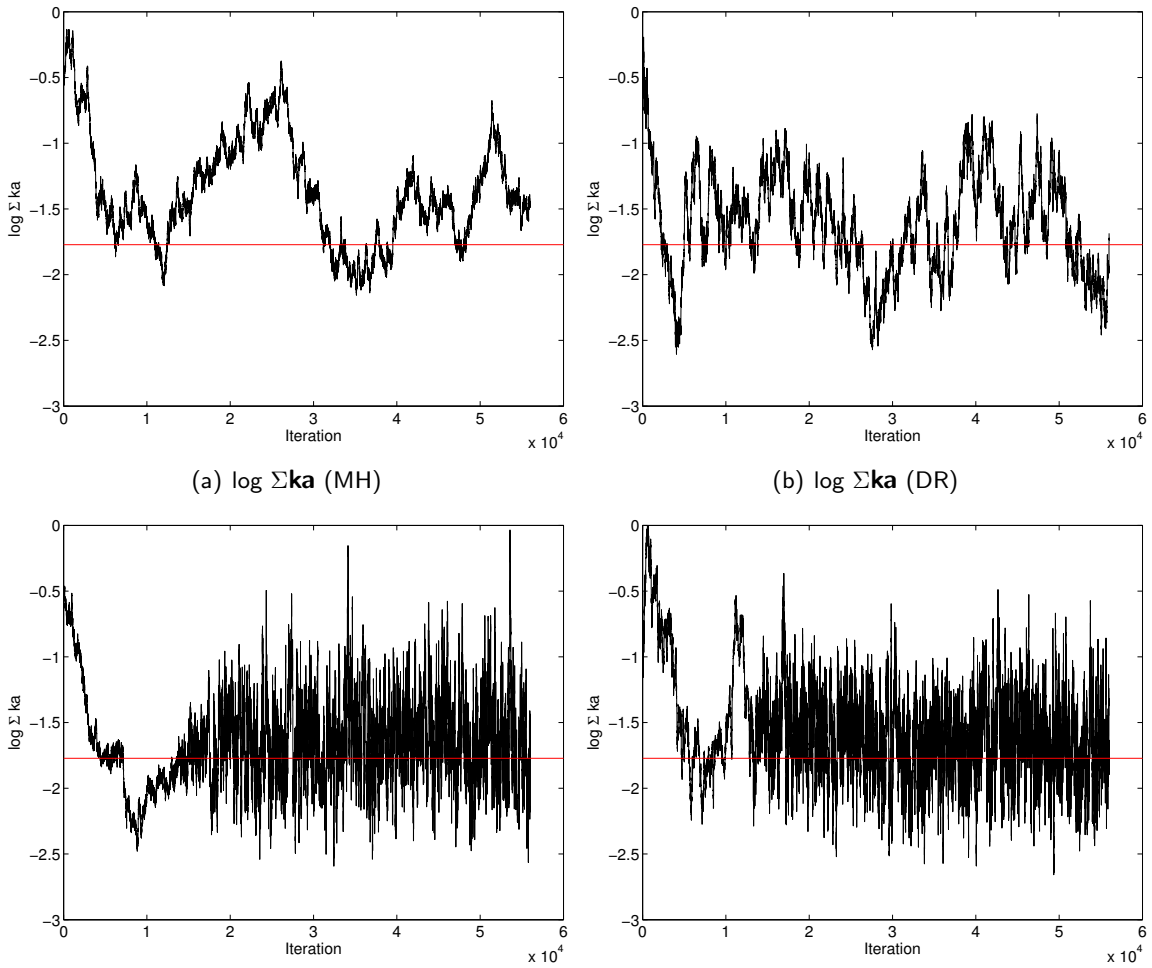

(a) log Σ**ka** (MH)

(b) log Σ**ka** (DR)

(c) log Σ**ka** (AM)

(d) log Σ**ka** (DRAM)

Figure 5.3: Markov-chains of the log(Σ) for absorption constant **ka**. Red lines indicate the actual values used to generate the synthetic data. Population standard deviations were the parameters taking the longest to converge. This is due to the fact that they are highly correlated with other parameters, they strongly influence the prior probabilities of individual-level parameters, and they themselves have weak/poorly tuned prior assumptions. The non-adaptive Metropolis Hasting (MH) failed to converge, since the poorly tuned proposal function failed to explore the posterior parameter space. While the non-adaptive Delayed Rejection (DR) method performed better than MH, only the two adaptive methods (AM and DRAM) managed to converge.

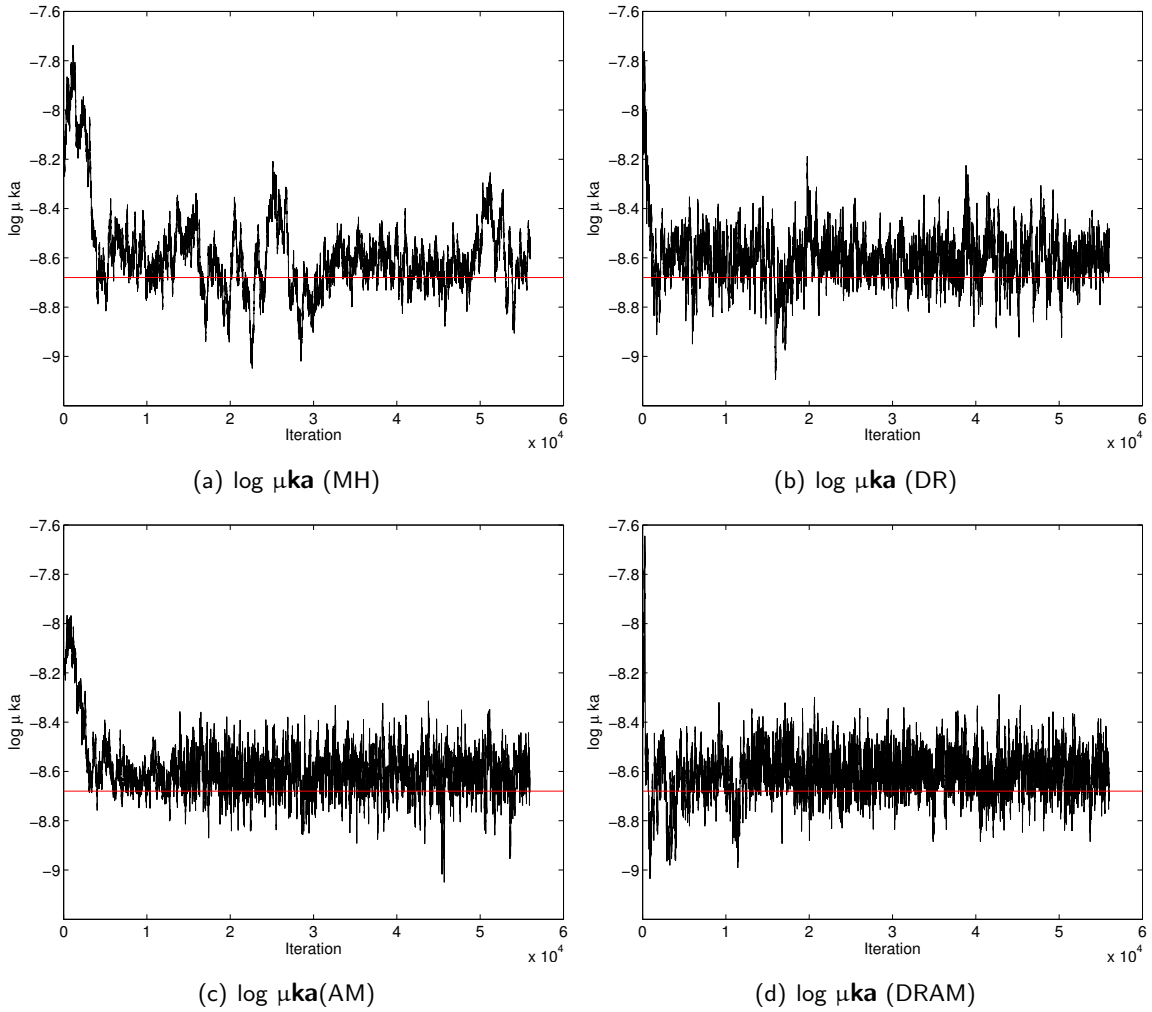

(a) log μ**ka** (MH)

(b) log μ**ka** (DR)

(c) log μ**ka**(AM)

(d) log μ**ka** (DRAM)

Figure 5.4: Markov-chains of the log(μ) for absorption constant **ka**. Red lines indicate the actual values used to generate the synthetic data. Population means converged sooner than population standard deviations. Non-adaptive Metropolis Hasting (MH) has come close to convergence, however the chain exhibits poor mixing (inefficient sampling due to acceptance rate being too high). The MH chain also shows the effects of correlation with the non-converged Σ**ka**. The Delayed-Rejection chains (DR and DRAM) more rapidly approach the convergence region due to the bolder proposal variances.

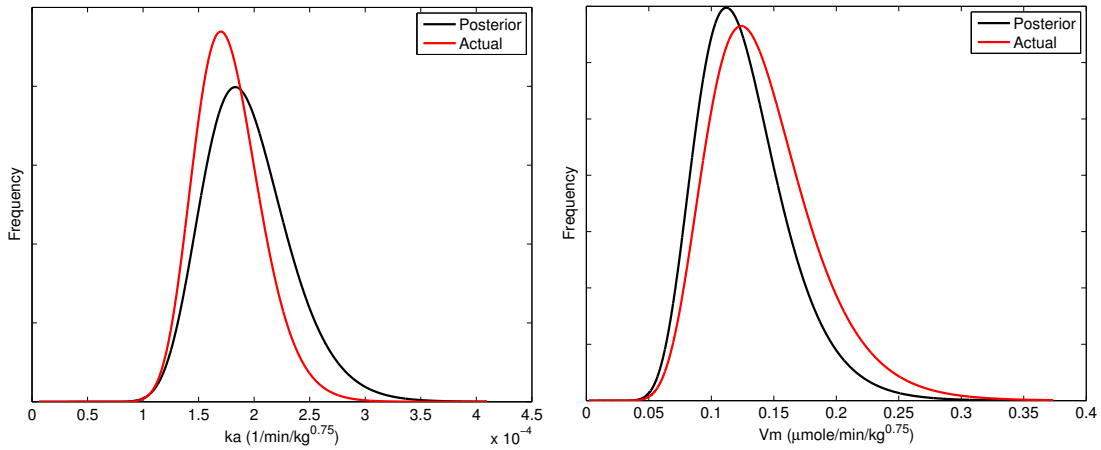

(a) Absorption constant (b) Michaelis constant

Figure 5.5: Actual population distributions for **Vm** and **ka**, compared to the posterior distributions estimated by MCMC analysis (with DRAM sampling) of the synthetic data. A slight bias exists in the posterior distributions due to the sparsity of the data and model/data error. The prior distributions were non-informative uniform (not shown).

Table 5.1: Posterior distributions of population parameters and modeling errors

Parameter	Unknowns	Posterior	Actual	Uncertainty CV†
Michaelis constant	μ**Vm**	0.112	0.124	0.17
(μmol/min/kg$^{0.75}$)	Σ**Vm**	0.29	0.30	0.44
Absorption constant	μ**ka**	1.8x10^{-4}	1.7x10^{-4}	0.08
(1/min/kg$^{0.75}$)	Σ**ka**	0.20	0.17	0.33
Model/data error	σ	0.21	0.20	0.08

*Median value of converged chain;†Coefficient of variance of chain

One main advantage that DRAM has is that it requires less tuning and re-adjustment than the other methods. Markov chains typically need slightly larger proposal distributions in the beginning, as the initial guesses approach the convergence region. Once the values are close to convergence, the proposal variances need to be smaller (since large "jumps" will land back outside the region and be rejected). A simple DR or DRAM method using just 2 or 3 proposal functions (where each proposed move is successively

smaller than the previous) will do this automatically. When the values are far from convergence, the initial bold moves are advantageous. When they are close to convergence, bold moves are rejected, and smaller moves are attempted. One disadvantage in this example was that it was computationally more expensive (by about a factor of 3) due to the additional proposed moves made after rejection per iteration. This extra computational cost is a direct function of the number of "trys" allowed for the DRAM method, which could be tuned for each individual problem. To reduce computational cost, DR or DRAM can be used in the burn-in step to search the parameter space and find the convergence region, after which AM is used (with an optimized covariance matrix calculated from the end of the burn-in chain).

5.4 Alternatives to Bayesian Analysis

5.4.1 Maximum Likelihood

Maximum likelihood is a method in which an objective function is used to iteratively improve (or optimize) PBTK parameters. This has been applied to problems of both PBTK parameter and inverse exposure optimizations [157, 318]. The objective function is the likelihood function defined by:

$$L(\varepsilon_1, ..., \varepsilon_n, \sigma_1, ..., \sigma_n) = \left(\frac{1}{\sqrt{2\pi}}\right) \exp\left(-\sum_{i=1}^{n} \frac{\varepsilon_i^2}{2\sigma_i^2}\right) \prod_{i=1}^{n} \left(\frac{1}{\sigma_i}\right) \quad (5.22)$$

Where $\varepsilon_i = z_i - \mu_i$; z_i is the ith observed data point; μ_i is the model prediction corresponding to the ith data point; n is number of observations; σ_i is the standard deviation of ε_i.

The standard deviation of the ε_i's serve a similar purpose as the model/data error parameter used in Bayesian analyses, since they represent the error model. Since the actual standard deviation representing the scatter of data that should occur around the model at each time point cannot be known (in fact, there may only be one measurement available at each time point), an error model estimating the variance of ε_i is required [157, 318]:

$$s_i^2 = \omega^2 \mu_i^{\gamma} \quad (5.23)$$

Where s_i is the estimate for σ_i; ω is a proportionality constant; and γ is the heteroscedastic constant.

If the dependent variable has not been transformed into the log scale, assuming $\gamma = 2$ implies that the variance is proportional to the magnitude of the model prediction. This is analogous to the lognormal error assumption used for the Bayesian analysis error model. The scatter of data points would be wider at high measurements, and narrower

at low measurements. A γ of 1 implies the opposite (that data points are expected to fall within an absolute range, regardless of magnitude).

The value of ω can be derived by taking the derivative of the likelihood function (to determine the value that maximizes likelihood), and is defined as [157, 318]:

$$\omega^2 = \frac{1}{n}\sum_{i=1}^{n}\frac{(z_i-\mu_i)^2}{\mu_i^{\gamma}} \tag{5.24}$$

While the maximum likelihood estimation (MLE) and Bayesian methods should theoretically produce the same result for the case of non-informative, non hierarchical priors, MLE cannot explicitly account for prior knowledge of parameter distributions. However, a number of alternative optimization methods may be used maximize the MLE objective function, as opposed to Bayesian analysis (where MCMC is the only viable option). This is advantageous when other optimization techniques are simpler to implement and less computationally intensive, and if prior knowledge is very limited.

5.4.2 Artificial Neural Networks

An alternative method of using animal data to predict xenobiotic behavior in humans is through the use of artificial neural networks (ANN's). ANN's have been previously shown to be able to predict dose responses by recognizing patterns in animal or human data [4, 104, 177]. These predictions have even been accurate enough to warrant further study for direct clinical applications [152, 404].

Artificial neural networks attempt to mimic the learning process of the brain. Each neuron (Figure 5.6) contains weighted inputs. The neuron calculates a weighted sum from the inputs (the "activation function"), which is then transformed using an arbitrary "transformation function" (typically the sigmoid function) [4]. The resulting value is the neuron output. In a neural network, the outputs of one layer of neurons become

inputs to the next layer of neurons (Figure 5.7). The purpose of the entire net is to take a set of inputs, and transform them to a final output using the layers of neurons. For applications in pharmacokinetics, the final outputs may be xenobiotic half life, elimination rate, or even adverse effect. The inputs to the input layer could be body weight, animal species, age, gender, and any other parameter believed to significantly effect the output.

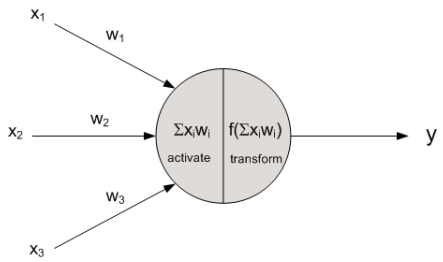

Figure 5.6: A single neuron of an artificial neural network (adapted from Agatonovic-Kustrin and Beresford (2000) [4])

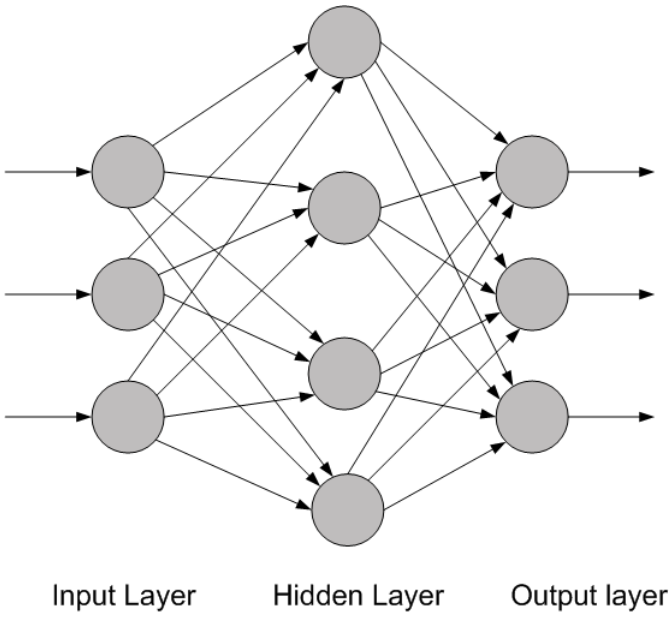

Figure 5.7: A three-layer artificial neural network (adapted from Hashemi and Young (2003) [177])

In order for the network to work correctly, all of the weights need to be optimized

by a learning algorithm. Figure 5.8 illustrates a learning algorithm, in which the network is iteratively fed inputs which already have known outputs (i.e. data) [4]. The weights are continuously optimized until the error is satisfactory, but before the net is "over-trained" (which can reduce its applicability to diverse data sets). In one study by Hashemi and Young (2003) [177], a neural network was able to predict methylmercury half-life in human data sets, even though the network was trained only using animal data sets.

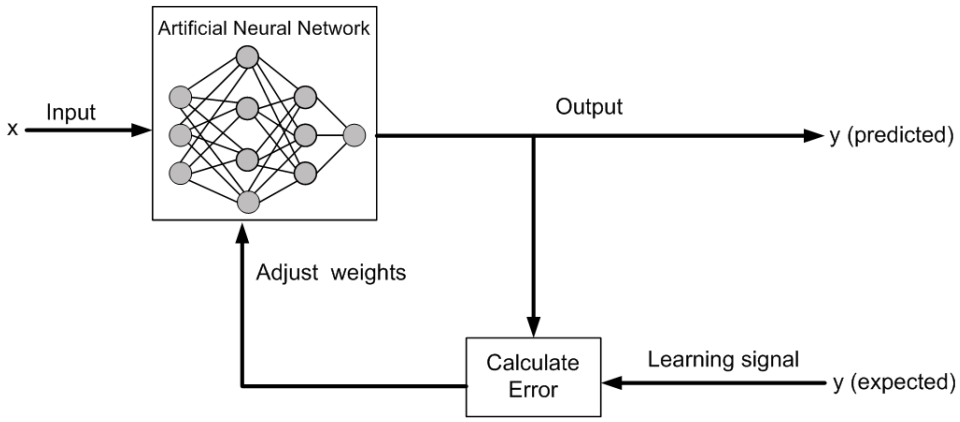

Figure 5.8: A neural network learning algorithm (adapted from Agatonovic-Kustrin and Beresford (2000) [4])

As the methylmercury neural network study noted, the choice of inputs (and even the format of the input data) could significantly effect the performance of the net [177]. Formulating these problems can become difficult due to the vast number of candidate parameters to base the result on. Additionally, relationships become purely based on pattern recognition rather than physiological or biochemical models, leading to potentially misleading results.

Chapter 6

Applications of the generalized model to toxic metals

6.1 Overview of general toxicology of metals

6.1.1 Role of essential elements in metal toxicity

Toxic metals such as lead, arsenic, mercury, and cadmium serve no essential biological functions in humans [164]. However, one aspect of their toxicity is their apparent similarity to essential metals, and their ability to "mimic" them to gain entry into target cells and tissues [51]. This leads to significant interactions between toxic and essential metals [78, 164], and between the toxic metals themselves [21, 242]. Nutritional status of individuals or a population becomes a significant source of uncertainty and variability for metals risk assessment [13, 289].

There is significant inhibition of lead and cadmium intestinal absorption by iron since iron, lead, and cadmium absorption are regulated by the DMT1 transporter [315]. Cadmium and zinc are known to have significant interactions in many human tissues due to the metal-binding protein metallothionein [48, 54, 211]. Selenium can potentially alter both arsenic and methylmercury toxicity [75, 164, 219, 351]. Furthermore, the presence of selenium in metal-binding proteins lead to a variety of interactions among selenium, methylmercury, inorganic mercury, arsenic, and cadmium [146].

The need for PBTK models of essential metals, as well as the need for better characterization of toxic metal bioavailability and toxic/essential metal interactions, has been discussed previously [61]. Low essential element status generally leads to higher toxic metal absorption. Iron deficiency may cause increased absorption of lead, cadmium, and manganese, while low zinc or calcium may effect lead and cadmium. Chronically malnourished individuals may experience extended periods or cycles of high toxic metal absorption. Healthy individuals, while still maintaining a lower average toxic metal bioavailability, may still experience temporal fluctuations of increased metal absorption due to homeostasis or illness [198]. The consequence of neglecting these variabilities may be the under prediction of dose given input exposure models for the "forward problem", or overestimation of exposures given biomarker data for the "inverse problem".

Metal contaminants may also interfere with essential element absorption [332], creating a toxic feedback loop. Iron deficiency and anemia are potential toxic endpoints of lead exposure, since iron deficiency causes increased lead uptake, and iron absorption may decline once lead levels reach a threshold [224]. Even humans receiving only mild acute lead exposure have been shown to have decreased iron levels [390], and there are similar findings for humans exposed to manganese [93]. This highlights an additional area of toxicokinetic interactions, and the potential for modeling susceptibilities in the population. PBTK models for manganese (which is both an essential element and a toxic metal) are currently under development [267–269, 361–363], which could potentially lead to a more broad treatment of essential element pharmacokinetics. Other nutrients such as antioxidants, Vitamins A/C/E, magnesium, phosphorous, riboflavin, and methionine are also known to impact toxic metal susceptibility [210, 385]

6.1.2 Molecular biomarkers and dose-response models

Molecular biomarkers for the toxic effects of metals in humans are becoming reliable enough to detect toxic interactions (particularly for renal effects) [393]. Ultimately, PBTK models for metal mixtures should be linked with biologically-based dose-response models for toxic effects. However, BBDR modeling is currently not as extensively developed as PBTK modeling [108, 218], and there are very few models that can be classified as purely BBDR (with parameters having direct biological correspondence, and minimal empirical components [87]). Empirical and mechanistically-based dose-response models linking pharmacokinetics with pharmacodynamics that exist for some metals include methylmercury neurodevelopment response [128, 129], renal tubular dysfunction from cadmium exposure [148, 353], and inorganic arsenic carcinogenicity [87].

6.1.3 Neurotoxicity risk

In addition to their association with cancer and organ dysfunction risk, metals such as arsenic, mercury, lead, and manganese are neurotoxins [314, 420]. Particularly vulnerable to this adverse effect are children, who exhibit high gastrointestinal absorption of metals, and high hand-to-mouth activity (which increases the chance for non-dietary ingestion) [205]. The rapid bone growth of children also plays a role in toxicity. A large percentage of the body burden for lead is in the bone, and mineral-exchange causes lead to diffuse back to the blood for years after exposure [277, 278]. Children's bones have a much higher growth rate than those of adults, and will more readily absorb lead.

Children are also vulnerable to neurotoxins since their central nervous systems (CNS) are still developing [285]. Similarly, the developing CNS of a fetus is susceptible to damage by maternal exposure to neurotoxins. There are a number of PBPK

models for pregnancy that can be applied to this problem [90]. Additionally, metal interactions may occur at both the placental barrier [99, 211, 223], and the blood-brain barrier [317]. A unified model approach for multiple metals simulating blood-brain barrier and placental-fetal barrier transport would aid in developmental risk assessment studies.

6.2 Toxicology and PBTK implementation of specific metals

There are some differences between the major sources of toxic metal exposure, and between the prevalent toxic outcomes. As a result, many of the toxicokinetic models were developed by separate institutions and government agencies, each focusing on different exposure pathways and tissue doses. The toxicokinetics and toxicodynamics of each of the major toxic metals are outlined below. A comparison of biomarker predictions by the GTMM with data was then performed using the same case studies used to validate the original models. For these simulations, physiological parameters for the GTMM were set to the values which were used in the original case studies in the PBTK model literature. This was done to ensure that the models had in fact been reproduced.

6.2.1 Cadmium

The general population is exposed to cadmium by dietary ingestion of foods with high cadmium content (various vegetable and grain products, and marine shellfish), and by inhalation of cigarette smoke [16]. The high content of cadmium in various edible and tobacco crops is due to the fact that cadmium is readily absorbed by plants in contaminated soil [342]. At low chronic doses, cadmium can cause a wide range of toxicological effects in humans. Kidney damage is the primary health concern, however toxic effects in the liver, altered enzyme levels, oxidative stress, cancer, and hypertension have been observed in both humans and animals [270, 328].

The toxicokinetic model for cadmium (Figure 6.1) is relatively simple, however it is sufficient for predicting both short-term and long-term blood concentrations, and

long-term kidney and liver burdens. Due to the half-life of cadmium in humans (approximately 20 years [206]), typical PBTK formulations cannot be applied. Rather than being transported into tissues by diffusion or blood/tissue equilibrium processes, cadmium is carried throughout the body by the metal-binding protein metallothionein. Cadmium absorbed from the lung or intestinal tract will either become bound to albumin in the plasma or metallothionein. Albumin-bound Cd is absorbed in the liver, the red blood cells and other tissues such as muscle and bone. Metallothionein-bound Cd is readily absorbed by the kidneys, where it will accumulate and slowly be excreted in the urine. Cadmium bound in red blood cells accounts for most of the cadmium detected in blood, and albumin-bound or metallothionein-bound cadmium in plasma is typically undetectable [158]. As erythrocytes degrade, red blood cell cadmium binds to metallothionein and is cleared from the plasma by the kidney (where it will accumulate). Absorbed cadmium will initially accumulate in the liver, where it will slowly transport to the kidneys via metallothionein kinetics [206]. Liver also serves as a source of the long-term elevated cadmium levels detected in blood, as some cadmium is transported back to the plasma and red blood cells.

Cadmium does not pass through the blood-brain barrier nor the placental barrier. Humans are born essentially free of cadmium, despite detectable levels in maternal blood and the placenta [140]. The blood-brain barrier protection against cadmium accumulation is reflected in the toxicokinetic model by neglecting brain tissue volume in the "other tissues" compartment, which consists of the sums of various organ systems (such as fat, muscle, and bone). As a result, brain tissue does not accumulate any cadmium in the model.

Due to the long half-life of cadmium in humans, toxicokinetic model evaluation is

made by comparing model predictions to population biomarker and autopsy studies. The PBTK model for cadmium was originally evaluated using short-term data in occupationally exposed humans, as well as long-term population data [217]. Improvements were later made to account for observed gender differences in gastrointestinal absorption [77], and the model has been shown to perform adequately for long-term population exposures [9]. Updated model parameters are listed in Table 6.1. Selected model/data comparisons are illustrated in Figure 6.2.

Table 6.1: PBTK model parameters for cadmium, adapted from Choudhury et al. (2001) [77]

Constant	Value	Definition
k1	0.1 (cigarette), 0.7 (dust)	Fraction swallowed after deposition and clearance from nasopharyngeal/tracheobronchial compartments
k2	0.4 (cigarette), 0.13 (dust)	Fraction of inhaled dust/smoke deposited in alveolar compartment
k3	0.05/day	Rate constant for absorption by system from lung
k4	0.1× k3	Rate constant for clearance to the G.I. tract from respiratory system
k5	0.05 (men), 0.10 (women)	Fraction absorbed to GI tract and systemic circulation
k6	0.05/day	Rate constant for absorption to system from G.I.
k7	0.25	Fraction of cadmium absorbed by system that is up taken to blood-3 compartment
k8	1 μg/day	Maximum rate that can be up taken to blood-3 compartment
k9	0.44	Fraction transferred from blood-1 to other tissues
k10	$1.4\text{x}10^{-4}$/day	Rate constant for transfer from other tissues to blood-1
k11	0.27	Fraction transferred from blood-1 to feces
k12	0.25	Fraction transferred from blood-1 to liver
kx*	0.04	Fraction transferred from blood-1 to blood-2
k13	$3.0\text{x}10^{-5}$/day	Rate constant for transfer from liver to blood-1
k14	$1.6\text{x}10^{-4}$/day	Rate constant for transfer from liver to blood-3
k15	$5.0\text{x}10^{-5}$/day	Rate constant for transfer from liver to feces
k16†	0.012/day	Rate constant for transfer from blood-2 to blood-3
k17‡	0.95	Fraction transferred from blood-3 to kidneys
k18	$1\text{x}10^{-5}$/day	Rate constant for transfer from kidney to blood-1
k19⊕	$1.4\text{x}10^{-4}$/day	Rate constant for transfer of cadmium from kidney tubules to urine
k21	$1.1\text{x}10^{-6}$/day	Factor for increased transfer to urine after age 30

* kx = (1-k9-k11-k12)

† From red blood cell decay (83 day half-life)

‡ Decreases from age 30 to 80 by 33%. Fraction transferred from blood-3 to urine is (1-k17)

⊕ Increases from age 30 by k21

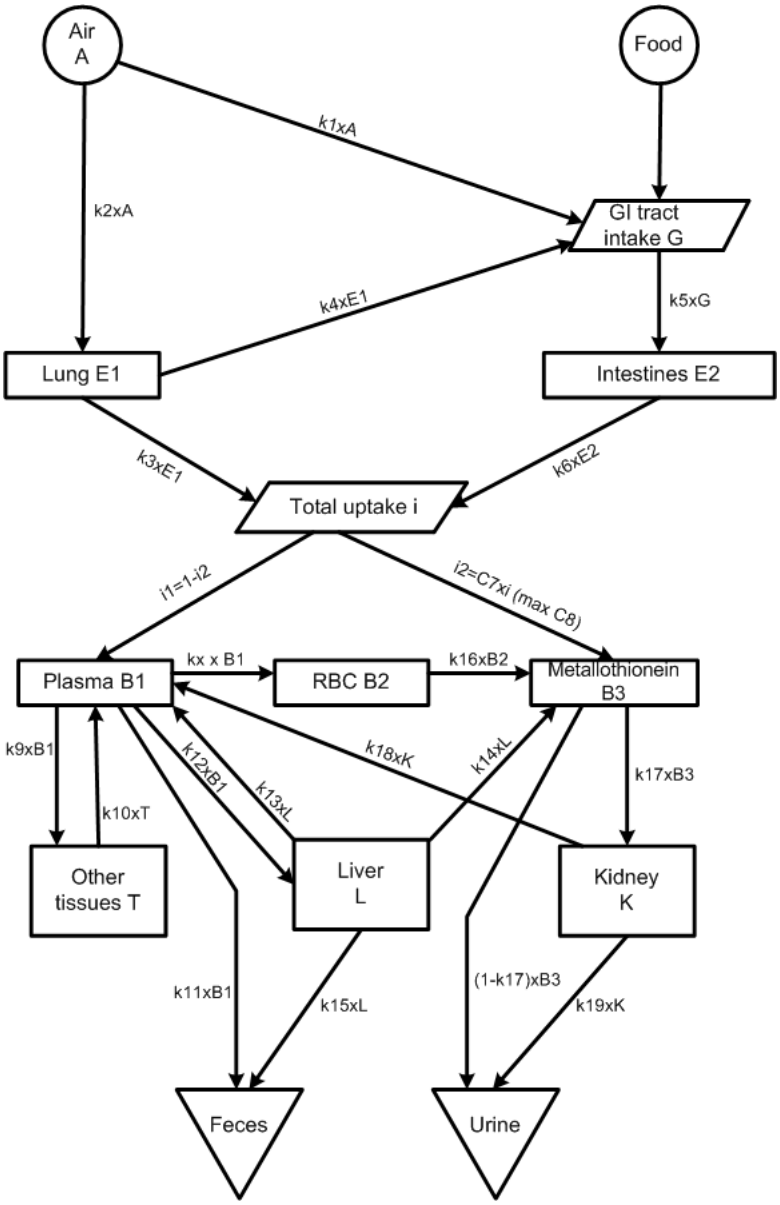

Figure 6.1: Toxicokinetic model structure for cadmium (Cd) [272]. The cadmium biokinetic model neglects blood perfusion, and assumes transport occurs via albumen, erythrocytes, and metallothionein binding.

In order to assess model performance, model/data comparisons similar to published applications of the original formulations were reproduced [77, 109]. Figure 6.2a shows predictions of NHANES III urinary data. NHANES III data for urinary levels contained only individuals who were nonsmokers, and were not occupationally exposed to cadmium, as reported by [77]. Figure 6.2b shows comparisons with autopsy data for kidney cadmium levels. Autopsy data from [240] (UK) and [35] (Quebec) contains both smokers and nonsmokers, and both sexes. Data from and [141] (Sweden) contains nonsmokers only, and both sexes. Data from [35] represents concentration in whole kidney, while all other data and model predictions represent concentration in kidney cortex. Each data point represents a mean value of a binned age group. For both sets of simulations, estimates for age and gender dependent dietary cadmium intakes and absorption fractions were obtained from [77]. The model assumed 5% cadmium absorption for males, and 10% for females. Model predictions are for standard reference humans, using a growth algorithm to predict organ weights [277].

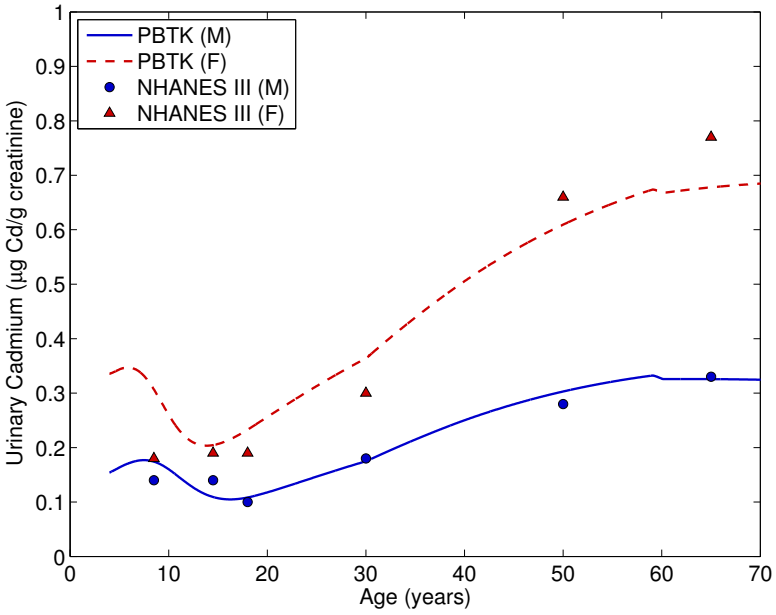

(a) Urinary cadmium (µg Cd/g creatinine)

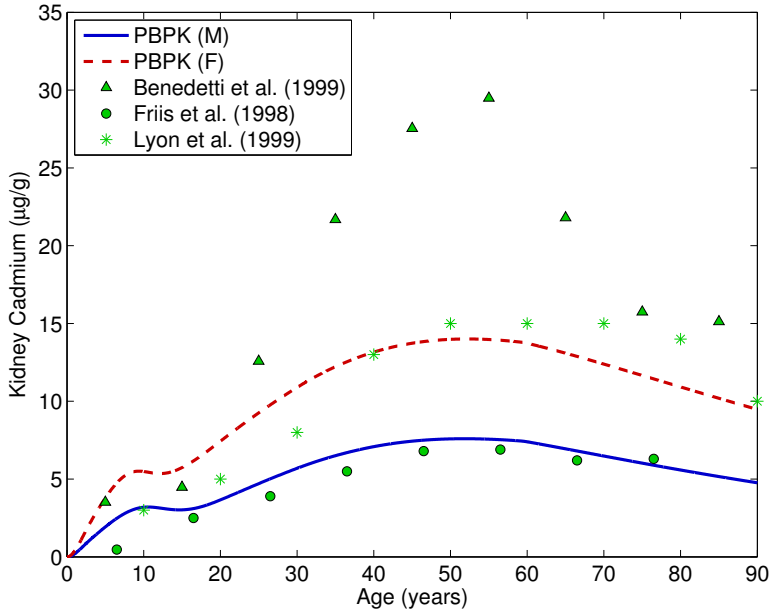

(b) Kidney cadmium (µg/g)

Figure 6.2: Comparisons of PBTK model results and measured data for the GTMM implementation for cadmium.

6.2.2 Arsenic

Arsenic is a known human carcinogen (bladder, lung, and skin), and cancer is the primary health concern for arsenic exposure in the US. An additional toxic endpoint is immune system disruption, and one study in rats has shown that immunological response due to arsenic exposure could increase susceptibility to the H1N1 influenza virus [220]. Individuals living in areas with naturally high levels of arsenic in soil and groundwater may experience chronic arsenic exposure. Arsenic exists in a variety of forms, each exhibiting different toxicological behavior in humans. Inorganic species arsenate (As^{V}) and arsenite (As^{III}) exist naturally in soil and drinking water. Arsenic levels naturally vary by geographic region, but may exist in high levels near mining and smelting communities, or agricultural areas where arsenic pesticides (which are now banned) have been used in the past [18].

Organic species such as monomethylarsenic acid $MMA^{V}$and dimethylarsenic acid DMA^{V}exist in the environment, and are also products of inorganic arsenic metabolism in humans. Arsenobetaine and arsenocholine are additional organic arsenicals which accumulate in fish and shellfish, and contribute to arsenic levels detected in urine. While this "fish arsenic" is considered to be non toxic, the extent to which the species break down to other arsenicals or effect humans is not fully known [253].

The PBTK models of arsenic (Yu [414, 415], Mann [247], El-Masri/Kenyon [120]) include at least four main arsenic species: As^{V}, As^{III}, $MMA^{V}$and DMA^{V}. There is still uncertainty in the metabolic pathways and toxic mechanisms of each arsenical [367]. The El-Masri/Kenyon is the most comprehensive (Figure 6.3), and will be a future component in the biologically based dose response (BBDR) model of arsenic toxicity being developed by the USEPA [87]. Major metabolic steps are **(1)** reduction of $As^{V}$to As^{III};

(2) methylation of $As^{III}$to MMA^{V}; **(3)** methylation of $As^{III}$to DMA^{V}; **(4)** reduction of $MMA^{V}$to MMA^{III}; **(5)** methylation of $MMA^{III}$to DMA^{V}; and **(6)** reduction of $DMA^{V}$to DMA^{III}.

It is also assumed that 90% of ingested $As^{V}$is reduced to As^{III}in the gut. Oxidation occurs to a small extent for all species, however demethylation does not occur. Noncompetitive inhibition occurs for the methylation steps **2** and **5**, since these reactions are catalyzed by arsenic (+3) methyltransferase (AS3MT). In this model, step **2** is inhibited by MMA^{III}concentration in the liver, while step **5** is inhibited by As^{III}. Urinary excretion of organic and inorganic arsenic is currently the only mechanism for elimination in the model, as it is the primary biomarker for arsenic exposure. PBTK parameters are listed in Tables 6.2 and 6.3. Arsenic is also known to be excreted in hair, fingernails, and breast milk, and is capable of crossing the placental barrier and the blood brain barrier [18], however these are currently neglected in the El-Masri/Kenyon formulation.

Significant interindividual variability exists for arsenic metabolism and susceptibility. Genetic polymorphisms of AS3MT and Glutathione S-transferase theta 1 (GSTT1) have been linked to altered DMA, MMA, and inorganic arsenic biomarker levels and toxicological endpoints [114, 330, 368]. Arsenic also interacts with the essential element selenium. Selenium deficiency may decrease methylation, and increase the likelihood for skin lesions [195]. Adequate selenium status may have an anticarcinogenic effect, and may also increase biliary excretion of arsenic [419]. However, excessive selenium exposure has been shown to inhibit arsenic methylation, and increase retention of inorganic arsenic in rat hepatocytes [351, 392]. The relatively nontoxic “fish arsenic” has been shown to effect blood selenium levels in humans [253].

Arsenic has a shorter half-life than methylmercury, cadmium, and lead, therefore toxicokinetic model evaluations are performed using short timescale exposure studies. The generalized formulation adequately reproduced the model evaluations by the original authors [120]. A model and data comparison is illustrated in Figures 6.4(a-f). In separate studies, human volunteers ingested varying forms and doses of arsenic, and urinary biomarkers were collected [55, 56].

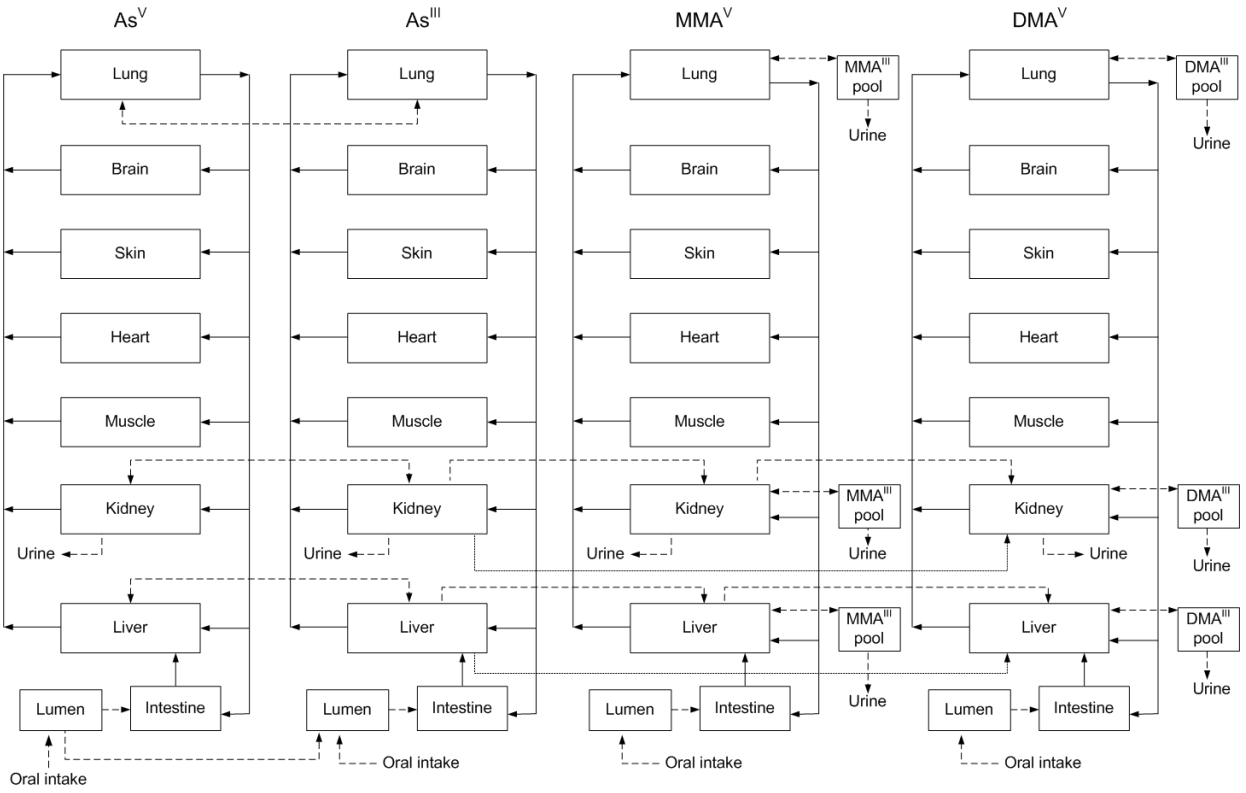

Figure 6.3: Toxicokinetic model structure for arsenic (As) [120] Arsenic species As^V, As^{III}, $MMA^V$and DMA^Vcirculate in the body. $MMA^{III}$and $DMA^{III}$are assumed to be either excreted or oxidized upon formation.

Table 6.2: Tissue/blood equilibrium partition coefficients for arsenic species, adapted from El-Masri & Kenyon (2007) [120].

Tissue	As^{V}	As^{III}	MMA^{V}	DMA^{V}
Small Intestine	2.7	8.3	2.2	2.1
Skin	7.9	7.4	2.61	2.4
Brain	2.4	2.4	2.2	3.3
Muscle	7.9	7.4	2.61	2.4
Kidney	8.3	11.7	4.4	3.8
Liver	15.8	16.5	3.3	3.3
Lung	2.1	6.7	1.3	1.3
Heart Muscle	7.9	7.4	2.61	2.4

Table 6.3: Kinetic parameters for the arsenic PBTK model, adapted from El-Masri & Kenyon (2007) [120]

Parameter	Value	Units
Oral absorption		
As^{V}	0.003	min^{-1}
As^{III}	0.004	min^{-1}
MMA^{V}	0.007	min^{-1}
DMA^{V}	0.007	min^{-1}
Urinary excretion		
$As^{V}$and As^{III}	0.07	min^{-1}
$MMA^{V}$and MMA^{III}	0.3	min^{-1}
$DMA^{V}$and DMA^{III}	0.13	min^{-1}
Reduction		
$As^{V}\rightarrow As^{III}$	0.003	min^{-1}
$MMA^{V}\rightarrow MMA^{III}$	0.008	min^{-1}
$DMA^{V}\rightarrow DMA^{III}$	0.004	min^{-1}
Oxidation		
$As^{III}\rightarrow As^{V}$	0.25	unitless
$MMA^{III}\rightarrow MMA^{V}$	0.63	unitless
$DMA^{III}\rightarrow DMA^{V}$	0.65	unitless
Methylation		
Vmax ($As^{III}\rightarrow MMA^{V}$)	$5.3x10^{-7}$	mole/min
Km ($As^{III}\rightarrow MMA^{V}$)	$3x10^{-6}$	mole/L
Vmax ($As^{III}\rightarrow DMA^{V}$)	$2x10^{-6}$	mole/min
Km ($As^{III}\rightarrow DMA^{V}$)	$3x10^{-6}$	mole/L
Vmax ($MMA^{III}\rightarrow DMA^{V}$)	$6.6x10^{-7}$	mole/min
Km ($MMA^{III}\rightarrow DMA^{V}$)	$3x10^{-6}$	mole/L
Ki*	$4x10^{-5}$	mole/L

*Noncompetitive inhibition for MMA^{III} inhibiting As^{III} methylation, and As^{III} inhibiting MMA^{III} methylation

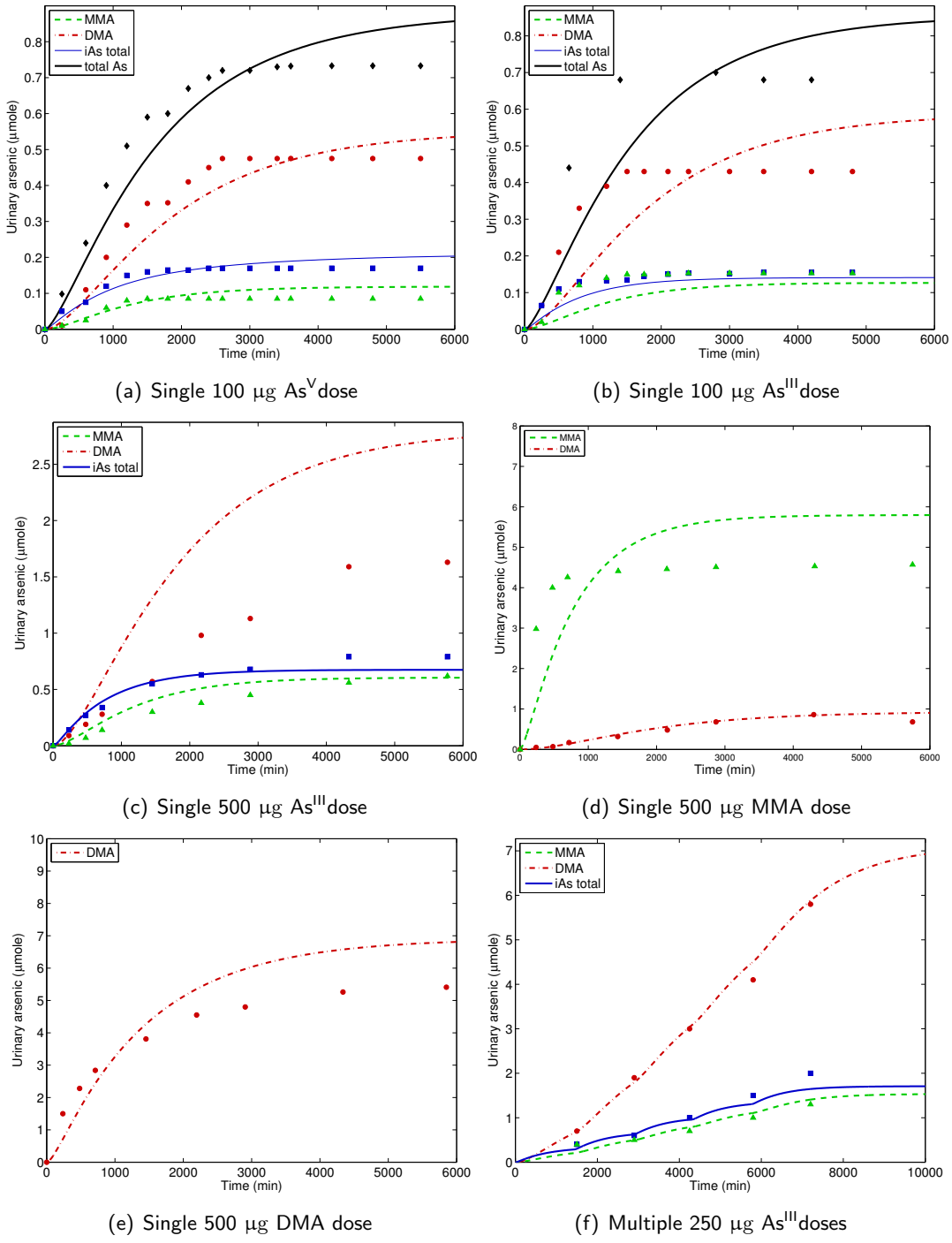

(a) Single 100 µg As^{V}dose

(b) Single 100 µg As^{III}dose

(c) Single 500 µg As^{III}dose

(d) Single 500 µg MMA dose

(e) Single 500 µg DMA dose

(f) Multiple 250 µg As^{III}doses

Figure 6.4: Comparisons of PBTK model results and data for cumulative arsenic in urine using the GTMM implementation for arsenic. Each pane represents experimental data and model predictions for a single individual. (♦ total As, ■ iAs, ▲ MMA, ●DMA)

6.2.3 Lead

The general population is exposed to lead from ingestion of contaminated food and water, and inhalation of cigarette smoke. Children are a particularly vulnerable sub-population due to the likelihood for non-dietary ingestion of soil, dust, and lead paint chips [17]. Children are also more susceptible to neurotoxic effects of lead during development (such as lowered IQ). Lead readily passes through the placental barrier, leading to increased blood lead levels in children born to exposed mothers [17]. In addition to neurotoxicity, anemia [224], low birth weight [17], nephrotoxicity [243], and the metabolic disruptions (Table 1.1) are potential toxic effects.

Once lead is absorbed into systemic circulation, it binds to red blood cells and reaches a non-linear equilibrium with lead in plasma. Lead in plasma serves as the driving force for lead transport into the various soft and bone tissues [277]. Lead is cleared from plasma by excretion into urine, and uptake into bone. Approximately 95% of the lead body burden in humans is in bone, which serves as a long-term reservoir for replenishment of blood lead in humans [17]. Bone lead has been shown to be mobilized during pregnancy, leading to higher levels in maternal blood, and fetal skeleton [138]. Throughout the life-span, bone formation and loss effect the rates of lead bone diffusion.

The O'Flaherty PBTK model for lead [280] accounts for diffusion into several bone compartments to simulate the long time-scales of lead kinetics in bone. It is assumed cortical bone accounts for of 80% of the skeleton in the human body, while the other 20% is trabecular bone [276]. Cortical and trabecular bone are further sub-divided into juvenile and mature. In juvenile bone, a process known as modeling takes place, where elements are rapidly absorbed. In mature bone, remodeling takes place, where elements are slowly transported into bone via mineral exchanges. The modeling and

remodeling rates are a function of the bone formation rates of trabecular and cortical bone. Juvenile bone turns over to mature bone as humans grow, and thus the lead contained in juvenile bone is carried over (Figure 6.5).

For all trabecular bone, and for juvenile cortical bone, transport modeled as diffusion-limited, with diffusion coefficients being functions of their respective bone formation rates. For mature cortical bone, diffusion of lead is modeled as occurring across 8 cylindrical shells in the radial direction. The mature cortical bone compartment is essentially a distributed-parameter model, with the partial differential equation (in cylindrical coordinates) for diffusion discretized into 8 layers in the radial direction. Lead is absorbed from plasma into in the canalicule region of cortical bone, which is the interface between plasma and the diffusion-region of bone. The published model code for the bone model (both the bone growth equations and transport equations) is available in O'Flaherty (2000) [280].

Short and long term exposure studies were originally used to evaluate model performance, in addition to blood lead/skeletal lead ratios observed in autopsies of exposed individuals [277]. To assess short timescale performance of the generalized model, data from a volunteer tracer lead exposure study was reproduced [305], similar to the original model evaluation. The reported age, gender, body weight, exposure duration, and tracer lead absorption rate for each individual were used as inputs to the PBTK model. Short term results are shown in Figures 6.7(a-d). To evaluate long timescale performance, the generalized PBTK model was linked with the O'Flaherty childhood lead exposure model using the same parameters as those used in the author's analysis of data from the Cincinnati Prospective Lead Study [47]. Results are shown in Figures 6.8(a-d).

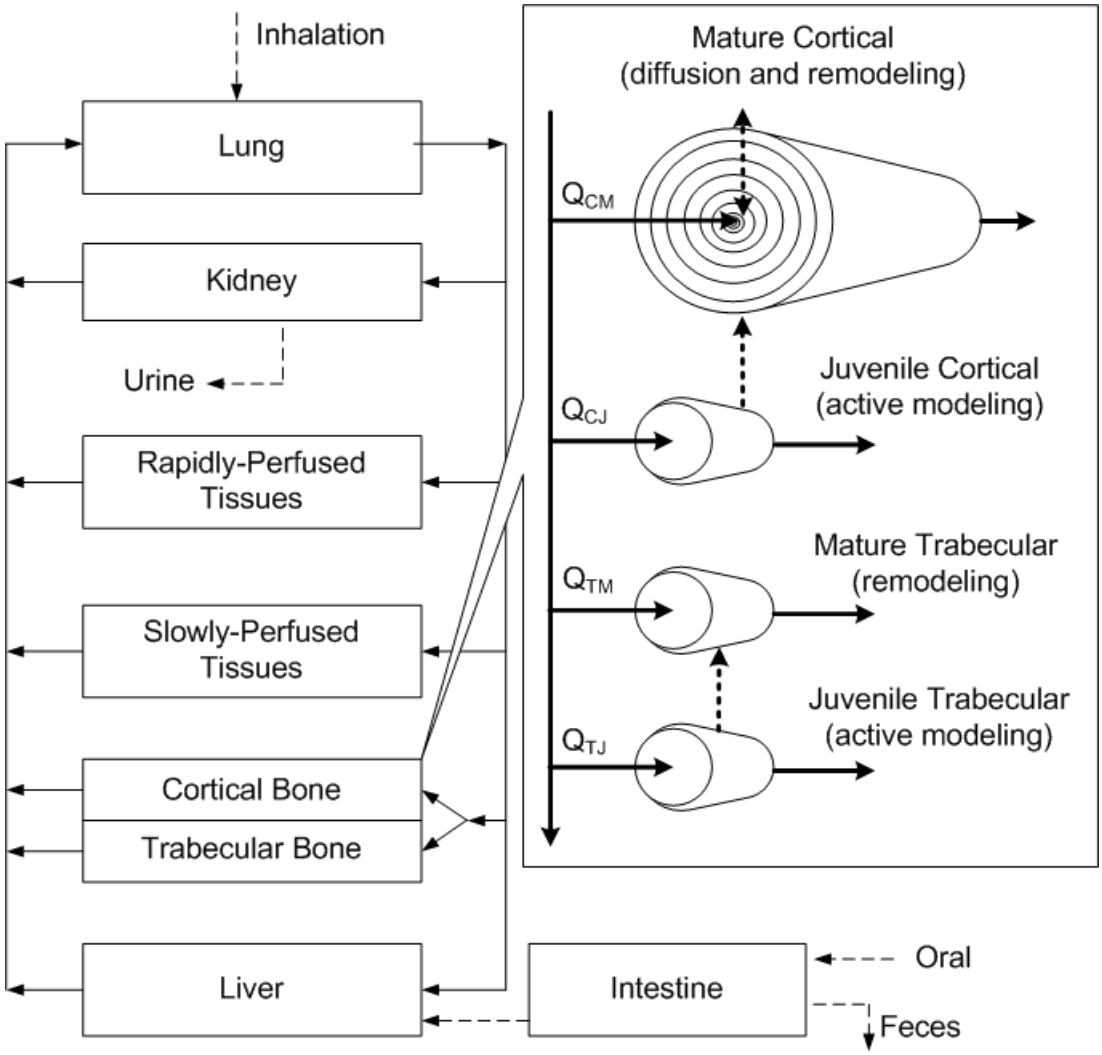

Figure 6.5: Toxicokinetic model structures for lead (Pb) [280]. The lead toxicokinetic model contains a complex multi-compartment bone transport model.

Table 6.4: PBTK model parameters for lead in humans, adapted from O'Flaherty (1995) [278]

Parameter	Value	Notes
Partition coefficients		
Liver/plasma	50	
Kidney/plasma	50	
Rapidly perfused/plasma	50	
Poorly perfused/plasma	2	
Kinetic parameters		
Plasma/bone clearance	15000	Fractional clearance of lead from plasma into forming bone (L plasma cleared/L bone formed)
RBC bind capacity	2.7	Maximum capacity of sites in red blood cells to bind lead (mg/L of RBC volume)
RBC bind saturation	0.0075	Half-saturation concentration of lead for binding by sites in red blood cells (mg/L of RBC volume)
RBC unbound linear	1.2	Linear parameter for unbound lead in red blood cells
Fractional GI absorption	variable	Function of age and gender
Fractional lung absorption	0.5	
Urinary clearance	variable	Function of glomerular filtration rate
Bone parameters		
D Diffusion constant	$5e^{-7}$	Diffusion within bone (cm/day/$0.5e^{-4}$ cm)
R Permeability constant	$5e^{-7}$	Diffusion from bone to canalicule (cm/day/$0.5e^{-4}$ cm)
P Permeability constant	0.02	Diffusion from canalicule to bone (cm/day/$0.5e^{-4}$ cm)

Additional model parameters and equations are provided in O'Flaherty (2000) [280]

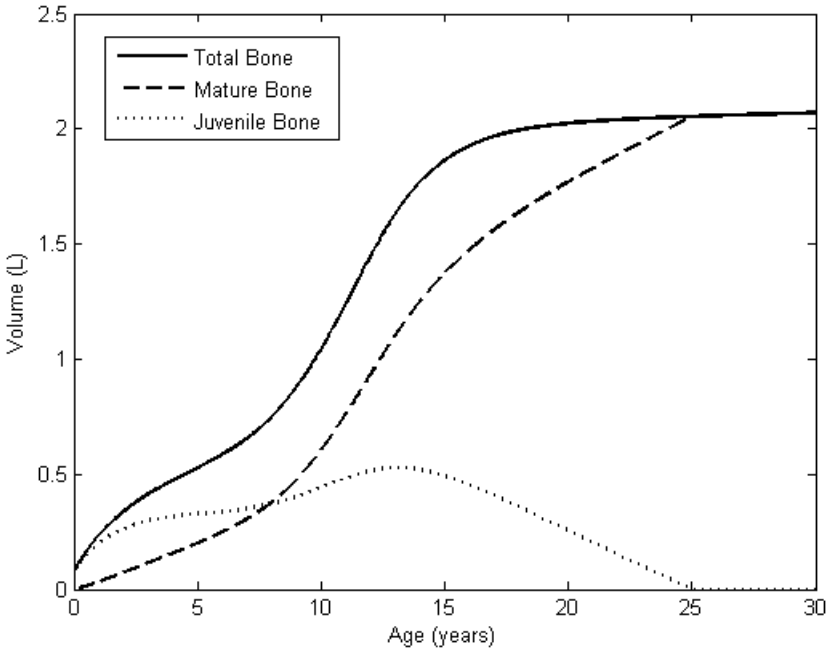

Figure 6.6: Volumes of total, mature, and juvenile bone as a function of age. The percentage of total bone that is juvenile decreases from 100% at birth to 0% at young adulthood [278]. By adulthood, all bone is mature. Lead toxicokinetics differ within each type of bone compartment, and therefore bone growth is an important element in the model.

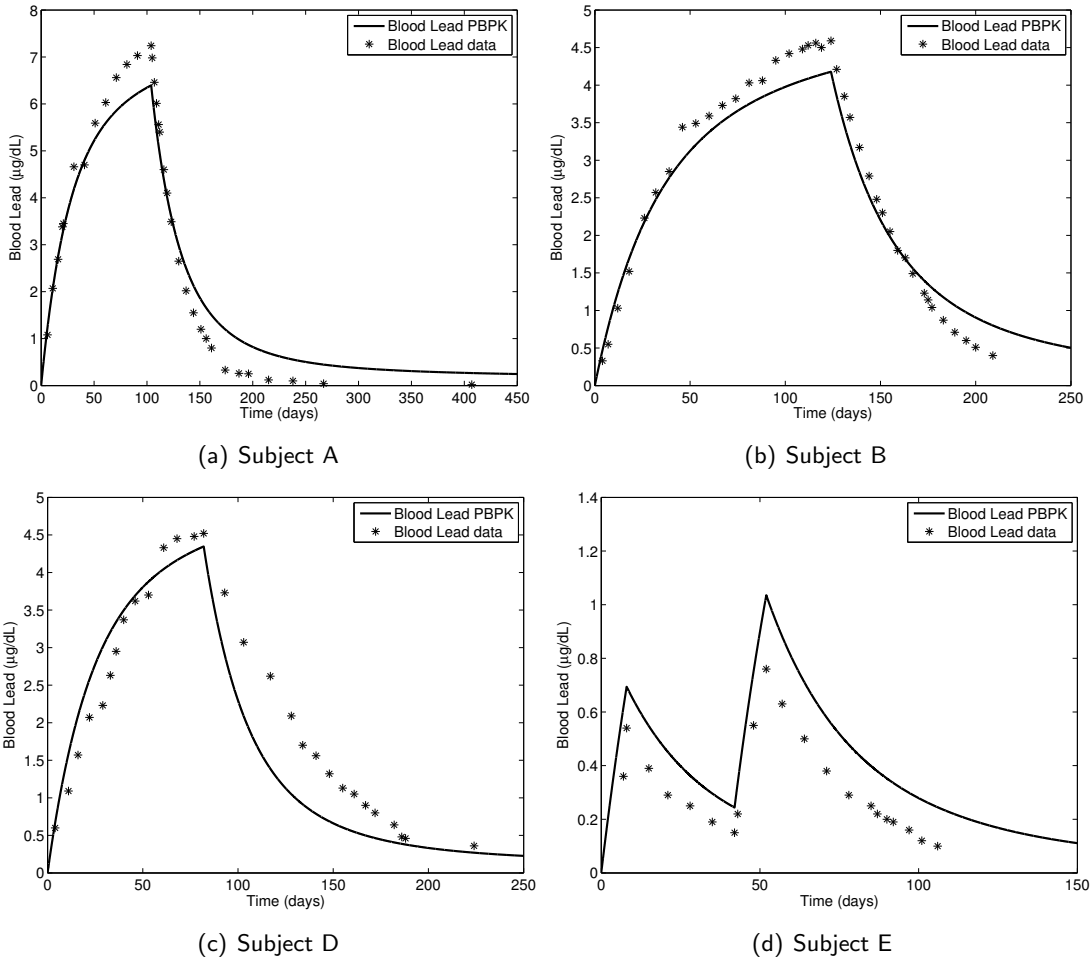

(a) Subject A

(b) Subject B

(c) Subject D

(d) Subject E

Figure 6.7: Comparisons of short term lead PBTK model results and data from [305] using the GTMM implementation for lead.

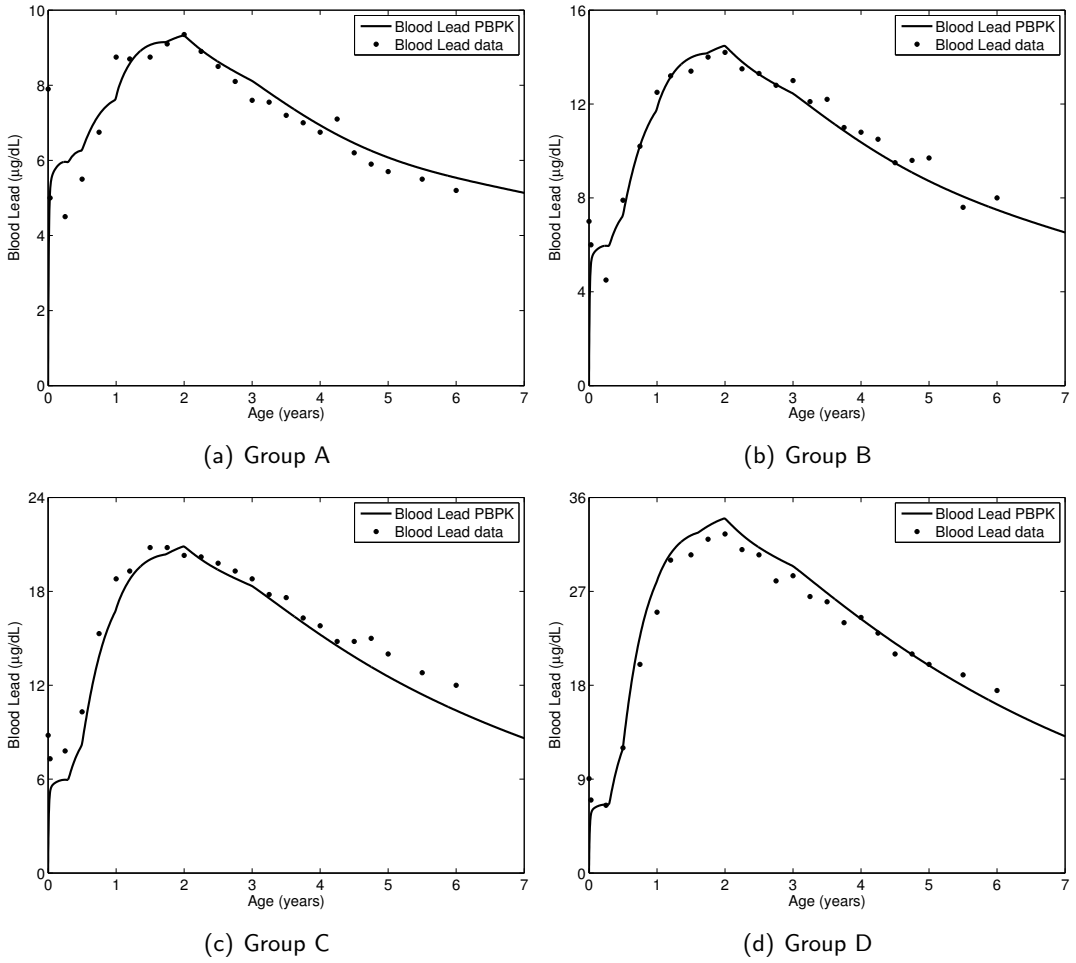

(a) Group A

(b) Group B

(c) Group C

(d) Group D

Figure 6.8: Comparisons of long term lead PBTK model result and data for four subgroups of children from the Cincinnati Prospective Lead Study [47] using the GTMM.

6.2.4 Chromium

Hexavalent chromium (Cr^{VI}) is a toxic metal that can lead to a variety of health effects in humans, while ingested trivalent chromium (Cr^{III}) is widely considered to be an essential nutrient. Inhaled Cr^{VI}or Cr^{III}can lead to respiratory effects (both chronic and acute), and inhaled Cr^{VI}has been known to cause lung cancer [19]. As with other toxic metals, renal and hepatic effects are possible [33], as are toxic interactions with other metals [21].

Humans are exposed to Cr^{VI}through multiple pathways (inhalation, ingestion, and dermal contact). Chromium (primarily Cr^{III}) is released into the environment by industry (electroplating, textile production) and state utilities (power plants and waste disposal) [19]. Occupational exposure can occur from welding fumes and other sources within metal-related industries (i.e. chromate or stainless steel production), and exposure for some occupational groups can be two orders of magnitude greater than the general population [19]. Chromium has been detected at numerous hazardous waste sites in the presence of other metals as a mixture, and therefore individuals living at these sites risk exposure [21].

Potential synergistic interaction for oxidative stress between chromate and arsenite (leading to DNA damage) has been observed in-vitro [352]. The wood preservative chromated copper arsenate (CCA) contains a mixture of Cr^{VI}, As^{V}, and copper. Environmental and health risks related to the production and disposal of CCA-treated wood, as well as potential multiroute exposures for the general population from wood dusts, is currently receiving much attention from the scientific community [31, 76, 118, 185, 186, 214, 215, 329, 347, 396, 403, 418].

The chromium PBTK model is an adaptation of the O'Flaherty model for lead (and

was formulated by the same author) [281]. However, chromium is modeled as diffusion-limited in all tissues, and contains a less complex bone model. Two bone compartments (cortical and trabecular) are used, rather than 4 compartments and cylindrical shells.

While the model is diffusion-limited, it is assumed there is rapid equilibrium in the blood compartment, thereby reducing the number of differential equations. The following describes the mass balance of chromium in compartment j.

$$\frac{dA_j}{dt} = \mathrm{Kd}(C_{\mathrm{art}} - C_j) \pm \mathrm{RED}_j \tag{6.1}$$

Where C_{art} is chromium concentration in arterial plasma (mg/L), C_j is chromium concentration in tissue, RED_j is the reduction rate of $\mathrm{Cr^{VI}}$(mg/day), and Kd is the tissue diffusion clearance (L/day).

The concentration of chromium in venous blood leaving tissue j ($C_{j,\mathrm{ven}}$) (and re-circulating in the body) is calculated from the overall mass balance of chromium in the plasma perfusing the tissue, incorporating tissue plasma flow rate Q_j :

$$C_{j,\mathrm{ven}} = C_{\mathrm{art}} - \frac{\mathrm{Kd}(C_{\mathrm{art}} - C_j)}{Q_j} \tag{6.2}$$

The rate of urinary excretion is assumed to be saturable, since the body retains chromium as an essential metal.

$$\mathrm{Excr} = C_{\mathrm{A}}\left(\mathrm{cl} - \frac{\mathrm{vm}}{C_{\mathrm{A}} + \mathrm{km}}\right) \tag{6.3}$$

Where cl is the clearance parameter (L/h), vm (mg/day) and km (mg/L) are saturation constants. At low background levels (i.e. plasma concentration of 0.05-0.15 μg/L), clearance is around 2 L/day. Clearance increases sharply above plasma concentrations around 1 μg/L [281].

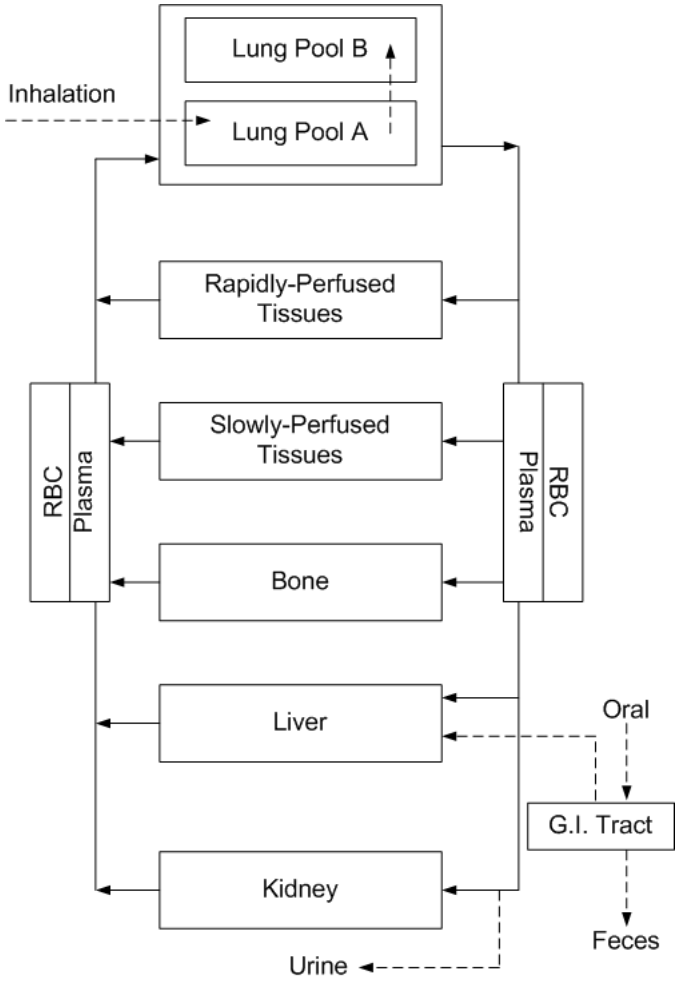

Figure 6.9: PBTK model for chromium in humans, based on the formulation of O'Flaherty [281]. Chromium can diffuse into and bind inside red blood cells. All tissues are modeled as diffusion-limited. Diffusion constants for trabecular and cortical bone are functions of their respective bone formation rates. Renal excretion is assumed to be saturable.

Table 6.5: PBTK model parameters for chromium in humans, adapted from O'Flaherty (1995) [278]

Parameter	Value	Notes
Diffusion		
KRBC3	12	Clearance of diffusible Cr^{III}between plasma/RBC (L/day)
Kd3	3	Diffusion clearance between plasma and all tissues for Cr^{III}
Kd6	30	Diffusion clearance between plasma and all tissues for Cr^{VI}
CR3	5	Fractional deposition of Cr^{III}into forming bone
CR6	15	Fractional deposition of Cr^{VI}into forming bone
Kinetics		
KREDKL	500	Reduction of $Cr^{VI}$to Cr^{III}in liver and kidney (day^{-1})
KREDBP	0.2	Reduction of $Cr^{VI}$to Cr^{III}in plasma (day^{-1})
KREDRC	7	Reduction of $Cr^{VI}$to Cr^{III}in RBCs (day^{-1})
KREDGI	100	Reduction of $Cr^{VI}$to Cr^{III}in GI tract (day^{-1})
KREDO	5	Reduction of $Cr^{VI}$to Cr^{III}in all other tissues (day^{-1})
KGI3	0.25	Absorption of Cr^{III}in GI tract (day^{-1})
KGI6	2.5	Absorption of Cr^{VI}in GI tract (day^{-1})
KFX	14	Transport of Cr from GI tract (day^{-1})
KLOSS3B	0.023	Turnover of $Cr^{III}$from bound diffusible RBC form (day^{-1})
cl	12	Clearance for saturable urinary excretion (L/day)
vm	0.18/0.008†	(mg/day)
km	0.015/0.0008†	(mg/L)

Additional model parameters and equations are provided in O'Flaherty (2001) [281]
†Two sets of parameters were required to fit the different datasets

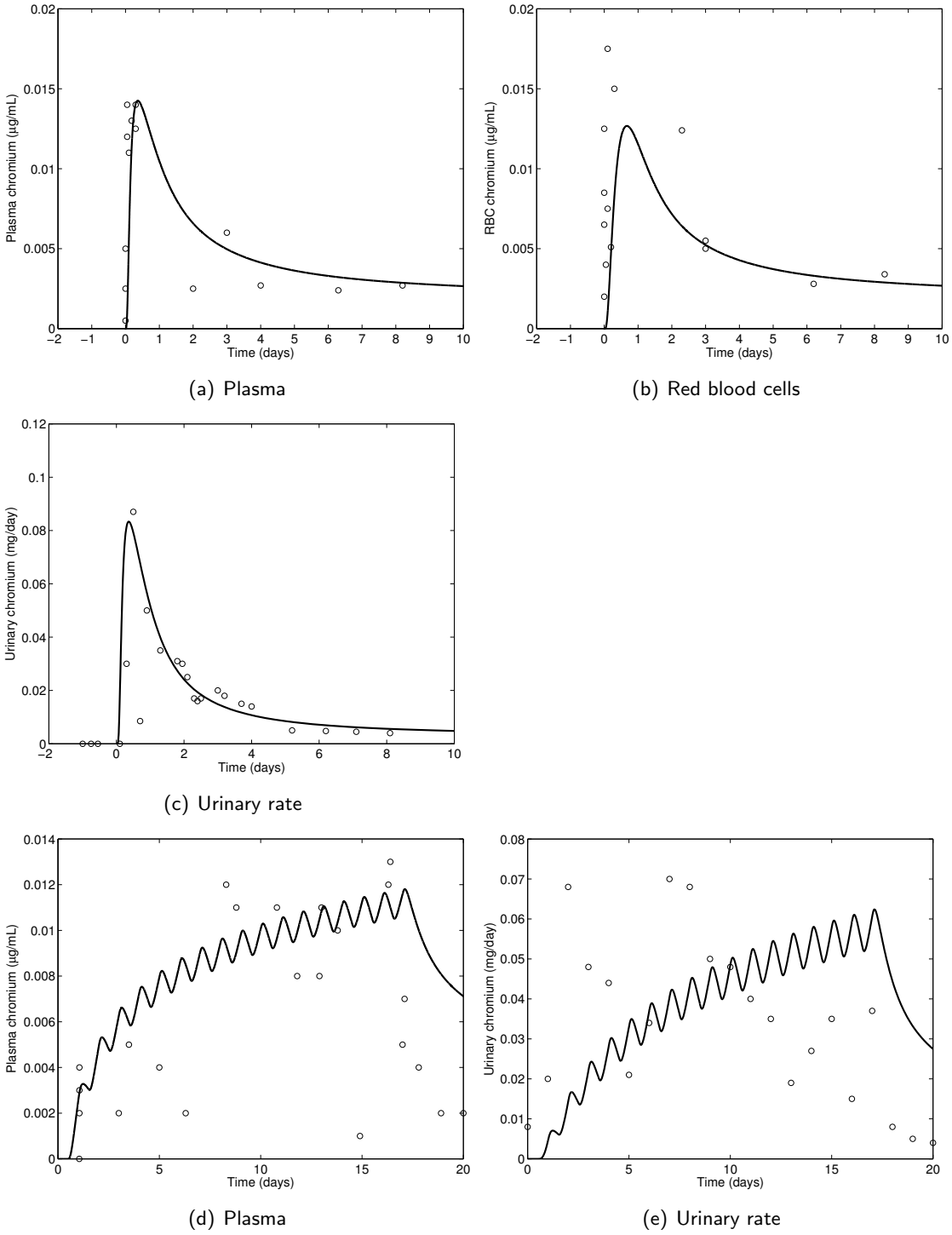

(a) Plasma

(b) Red blood cells

(c) Urinary rate

(d) Plasma

(e) Urinary rate

Figure 6.10: Predictions of Cr^{III}concentrations and urinary rates for a volunteer study using the GTMM for chromium. Results are for a male volunteer after a single 2.5 mg oral dose of Cr^{VI}(top three), and after multiple oral doses (about 4 mg/day) of Cr^{VI}(bottom two). Predictions are of red blood cell and plasma concentrations, and rate of urinary excretion.

6.2.5 Mercury

The general population is typically exposed to mercury in the form of methylmercury (MeHg), due to the natural methylation of inorganic mercury in the environment. Methylmercury enters and accumulates in the food chain from both natural and man-made sources. High levels of methylmercury are found in ocean and freshwater fish which are consumed by humans.

Methylmercury is a neurotoxin that can pass through the blood-brain barrier and the placental barrier. Blood methylmercury levels in infants are may be higher than the maternal blood, due to the toxicokinetics of MeHg transport across the placenta (Figure 6.12). Pregnant women and women of childbearing age are typically the subject of exposure and biomonitoring studies, due to the developmental neurotoxicity risk to fetuses exposed to methylmercury in-utero. This is reflected in the PBTK model for methylmercury [338], which focuses on women, and includes a dynamic fetal subsystem for pregnancy.

The PBTK model assumes upwards of 90% of ingested MeHg is absorbed into systemic circulation. Enterohepatic recirculation between the liver and intestines is accounted for. The red blood cells, brain tissue, and placenta are modeled as diffusion-limited compartments, with the remaining compartments considered plasma flow-limited. Unlike the other metals, methylmercury is not significantly excreted in the urine, but rather the hair, feces, and breast milk (which becomes a pathway for neonatal exposure). Methylmercury is also converted to inorganic mercury throughout the body (particularly in the intestine, where conversion to inorganic mercury is followed by excretion to feces). Relative to other toxic metals, absorption of methylmercury is high and not

influenced by essential element status. It has been suggested that selenium may be central to interactions between methylmercury, inorganic mercury, and arsenic [146, 219]. While selenium has been shown to protect against methylmercury neurotoxicity in animal models, human epidemiological studies have been inconclusive [75].

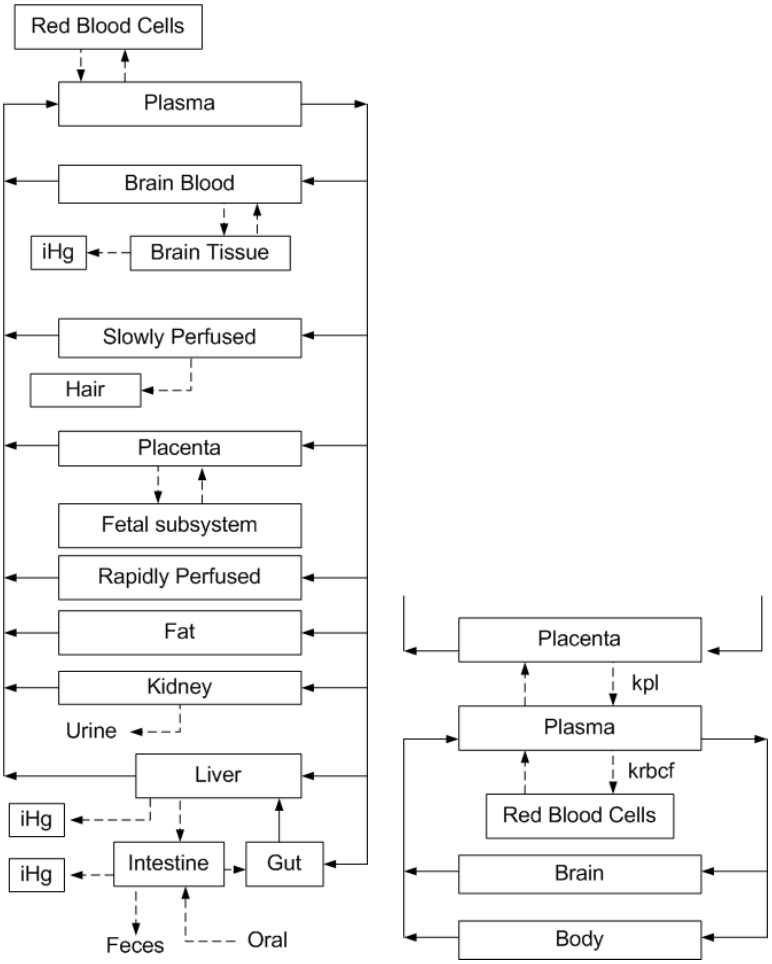

Figure 6.11: Schematic depiction of the maternal PBTK model of methylmercury (a), and the linked fetal PBTK model (b). Diffusion of methylmercury occurs across the placental barrier. The fetal subsystem contains a separate circulatory system. Physiological parameters for the maternal body, placenta, and fetal body are a function of gestational age.

Since the PBTK model is plasma-based, it is necessary to define most of the partition coefficients in terms of tissue/plasma equilibrium instead of tissue/blood equilibrium. The conversion of a tissue/blood partition coefficient ($P_{\text{tissue/blood}}$) to a tissue/plasma partition coefficient ($P_{\text{tissue/plasma}}$) is:

$$P_{\text{tissue/plasma}} = P_{\text{tissue/blood}}(P_{\text{rbc/plasma}}\text{HMT} + (1 - \text{HMT})) \tag{6.4}$$

Where $P_{\text{rbc/plasma}}$ is the red blood cell/plasma partition coefficient, and HMT is the hematocrit (the ratio of total red blood cell volume to whole blood volume).

The mass balance on the maternal placenta is defined as:

$$\frac{d(C_{\text{p}}V_{\text{p}})}{dt} = Q_{\text{p}}\left(C_{\text{mA}} - \frac{C_{\text{p}}}{P_{\text{p/mpl}}}\right) - J_{\text{p-fepl}} \tag{6.5}$$

Where C_{p} and C_{mA} are methylmercury concentrations in the placenta and maternal arterial plasma, respectively (mass/L); $J_{\text{p-fepl}}$ is placenta-fetal plasma diffusion rate (mass/h); Q_{p} is plasma flow rate to placenta (L/h); V_{p} is placenta volume (L); and $P_{\text{p/mpl}}$ is placenta/maternal plasma equilibrium partition coefficient for methylmercury.

The placenta-fetal plasma diffusion rate is defined:

$$J_{\text{p-fepl}} = k_{\text{p}}\left(C_{\text{p}} - \frac{C_{\text{fepl}}}{P_{\text{fepl/p}}}\right)$$

Where C_{fepl} is methylmercury concentration in fetal arterial plasma (mass/L); $P_{\text{fepl/p}}$ is the fetal plasma/placenta partition coefficient for methylmercury; k_{p} is the diffusion constant for placenta (L/h).

The mass balance on the fetal plasma is defined :

$$\frac{d(C_{\text{fepl}}V_{\text{fepl}})}{dt} = Q_{\text{fe}}(C_{\text{feV}} - C_{\text{fepl}}) + J_{\text{p-fepl}} - J_{\text{ferbc-fepl}} \tag{6.6}$$

C_{feV} Concentration in fetal venous plasma (the mixture of all tissue venous streams, mass/L); Q_{fe} fetal cardiac output (L/h); V_{fepl} fetal plasma volume (L); $J_{\text{ferbc-fepl}}$ fetal

red blood cell/fetal plasma diffusion rate (defined below, mass/h).

$$J_{\text{ferbc-fepl}} = k_{\text{rbcf}} \left(C_{\text{fepl}} - \frac{C_{\text{ferbc}}}{P_{\text{ferbc/fepl}}} \right)$$

Where k_{rbcf} diffusion constant for fetal red blood cells (L/h); C_{ferbc} concentration in fetal red blood cells (mass/L); $P_{\text{ferbc/fepl}}$ fetal red blood cell/fetal plasma partition coefficient. The mass balance on fetal red blood cells is simply $J_{\text{ferbc-fepl}}$.

The mass balance on the hair compartment is defined as:

$$\frac{d(C_{\text{hair}} V_{\text{hair}})}{dt} = k_{\text{h}}(C_{\text{V}} P_{\text{hair/plasma}} - C_{\text{hair}}) \tag{6.7}$$

Where k_{h} is the hair excretion rate (L/h); C_{V} is the methylmercury concentration in venous plasma (mass/L); C_{hair} is concentration in hair (mass/L); V_{hair} is the volume of hair (L); and $P_{\text{hair/plasma}}$ is the hair/plasma partition coefficient. The density of human hair (1.324 mg/mL) is used to convert the concentration of methylmercury in hair from mass/L to parts per million [338]. The rate of methylmercury excretion into hair is subtracted from the slowly perfused tissue mass balance.

In order to assess model performance, simulations previously done by the original authors were reproduced [338]. Figure 6.12a show simulations for a male consuming approximately 3 μg/kg/day MeHg for 96 days, with data from [188]. Figure 6.12b shows simulations for a pregnant woman and fetus during the methylmercury poisoning outbreak in Iraq [24]. Hair and blood data for the mother/infant pair are from [8]. It was assumed the mother (51 kg) consumed 42 μg/kg/day MeHg for 108 days, which began shortly after the start of pregnancy.

Table 6.6: PBTK model parameters for methylmercury, adapted from Shipp et. al. (2000) [338]

Parameter	Mean	CV	Notes
Partition coefficients			
Brain/blood	3.0	0.30	
Brain blood/plasma	1.0	0.30	
Fat/blood	0.15	0.30	
Fetal plasma/placenta	2.0	0.30	
Gut/blood	1.0	0.70	
Hair/blood	248.66	0.70	
Kidney/blood	4.0	0.30	
Liver/blood	5.0	0.30	
Placenta/blood	2.0	0.30	
RBC/plasma	12.0	0.30	
Fetal RBC/plasma	14.0	0.30	
Rapidly perfused/blood	1.0	0.30	
Slowly perfused/blood	2.0	0.30	
Kinetic parameters			
iHg to brain	$5.0\text{x}10^{-5}$	0	iHg from kidneys to brain, L/h/kg$^{0.75}$
Loss of iHg from brain	0.001	0	iHg from brain to kidneys, L/h/kg$^{0.75}$
Brain MeHg to iHg	$1.2\text{x}10^{-5}$	0.30	De-methylation of MeHg, h^{-1}
Biliary clearance of MeHg	0.0001	0.30	MeHg from liver to intestine, L/h/kg$^{0.75}$
Brain/brain plasma MeHg diffusion	0.01	0.30	Blood-brain barrier transport, L/h/kg$^{0.75}$
Intestinal MeHg to iHg	0.0001	0.30	De-methylation of MeHg, L/h/kg$^{0.75}$
Fecal excretion of MeHg	0.0002	0.36	From intestine, L/h/kg$^{0.75}$
Excretion of MeHg into hair	$7.0\text{x}10^{-6}$	0.25	(see text for details), L/h/kg$^{0.75}$
Liver MeHg to iHg	$1.0\text{x}10^{-5}$	0.30	L/h/kg$^{0.75}$
RBC/plasma MeHg diffusion	1.5	0.30	L/h/kg$^{0.75}$
Intestinal reabsorption of MeHg	0.005	0.30	From intestine to gut, L/h/kg$^{0.75}$
Fetal kinetic parameters			
Placenta/fetal MeHg diffusion	1.0	0.50	L/h
Fetal RBC/plasma diffusion	100.0	0.50	(see text for details), L/h/kg$^{0.75}$

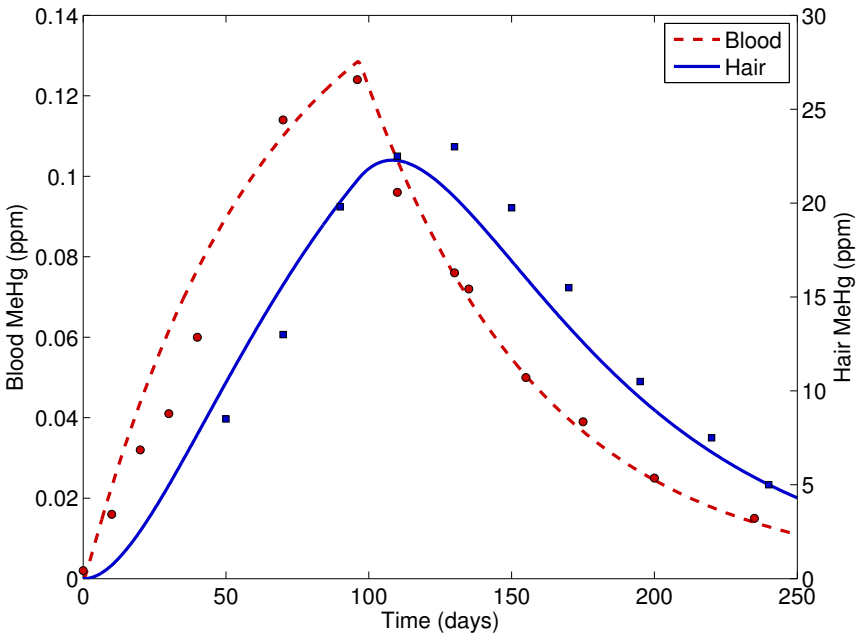

(a) Dietary MeHg study (male)

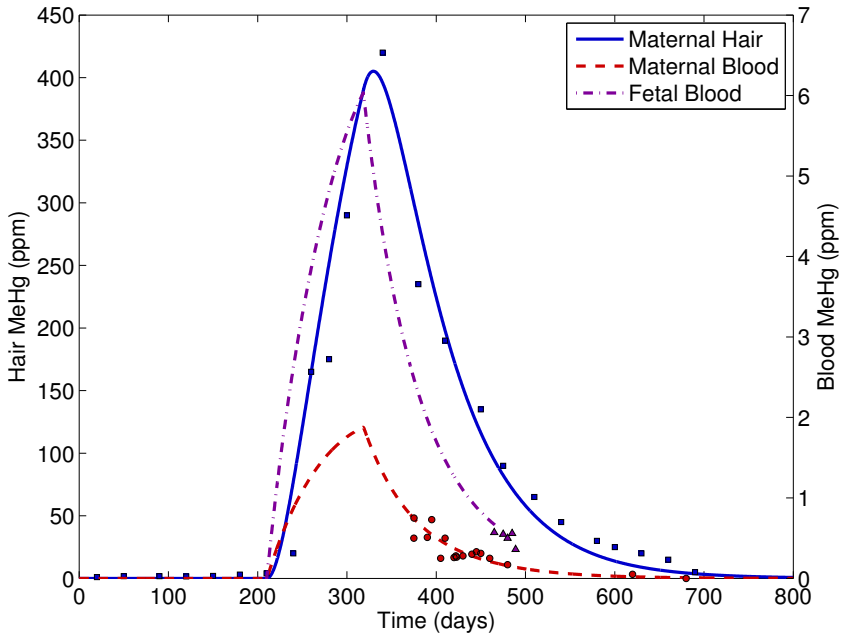

(b) Iraqi MeHg poisoning (pregnant female)

Figure 6.12: Comparisons of PBTK model results and data for hair and blood methylmercury (MeHg) concentrations using the GTMM of methylmercury. (■ hair, ●blood, ▲ fetal blood)

6.3 Demonstration of simulations with multiple metals and nonmetals

Simulations were performed using the GTMM in which multiple metals and nonmetals were modeled simultaneously, with interactions. This was done to test the computational efficiency and demonstrate applications of the framework.

Figure 6.13 demonstrates the use of PBTK models to simulate periodic dietary exposure to arsenic (100 μg/day), lead (45 μg/day), cadmium (20 μg/day), and methylmercury (20 μg/day). The timescales of each metal vary depending on the tissue. Organic metabolites of arsenic may have a slightly longer half-life than the parent inorganic forms. Cadmium and lead have similar half-lives in their respective sink compartments (liver and kidneys for cadmium, bone for lead), and have a similar absorption percentage (5-10% for healthy adults). Lead in systemic circulation is lower due to absorption into bone, and the half-life in blood and organs is significantly shorter than in bone. Methylmercury exhibits a long half-life and high absorption percentage (90-100%). Model predictions were performed simultaneously in the same standard reference male. While interactions were not included, incorporating them is computationally easy to implement since all models are contained within the same Simulink workspace.

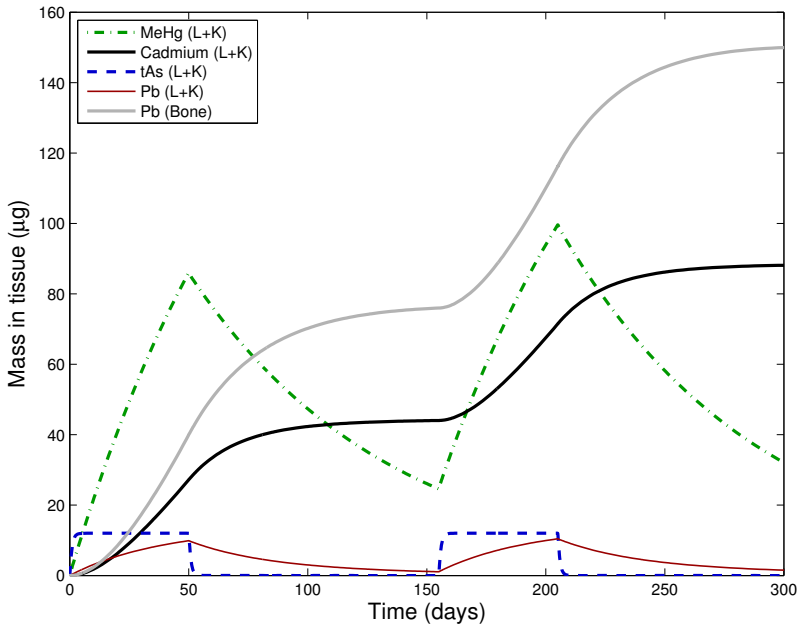

Figure 6.13: Illustration of metal timescales in the liver and kidneys (L+K) for cycles of 50 days exposure, and 100 days non exposure to a mixture of methylmercury (MeHg), lead (Pb), cadmium (Cd), and inorganic arsenic (iAs). Bone lead is included, and total arsenic (tAs) is shown.

Toxic metal exposure could inhibit and disrupt metabolic enzymes that metabolize a variety of drugs and chemicals [260]. Figure 6.14 illustrates the effects of adding a noncompetitive inhibition assumption to a PBTK model of a metal and toluene. Noncompetitive inhibition occurs if the presence of one chemical reduces the amount of active enzyme, by either interfering with enzyme structure or concentration. This effectively reduces the maximum rate of reaction.

The following noncompetitive inhibition relationship was assumed:

$$\begin{aligned} \mathrm{R}_{\mathrm{TOL}} &= C_{\mathrm{TOL}} \frac{\mathrm{Vm}^{*}_{\mathrm{TOL}}}{C_{\mathrm{TOL}} + \mathrm{Km}_{\mathrm{TOL}}} \\ \mathrm{Vm}^{*}_{\mathrm{TOL}} &= \frac{\mathrm{Vm}_{\mathrm{TOL}}}{1 + C_{\mathrm{met}}/\mathrm{Ki}_{\text{met-TOL}}} \end{aligned}$$

Where $\mathrm{R}_{\mathrm{TOL}}$ is the rate of toluene metabolism (mass/hr); $\mathrm{Vm}^{*}_{\mathrm{TOL}}$ the apparent

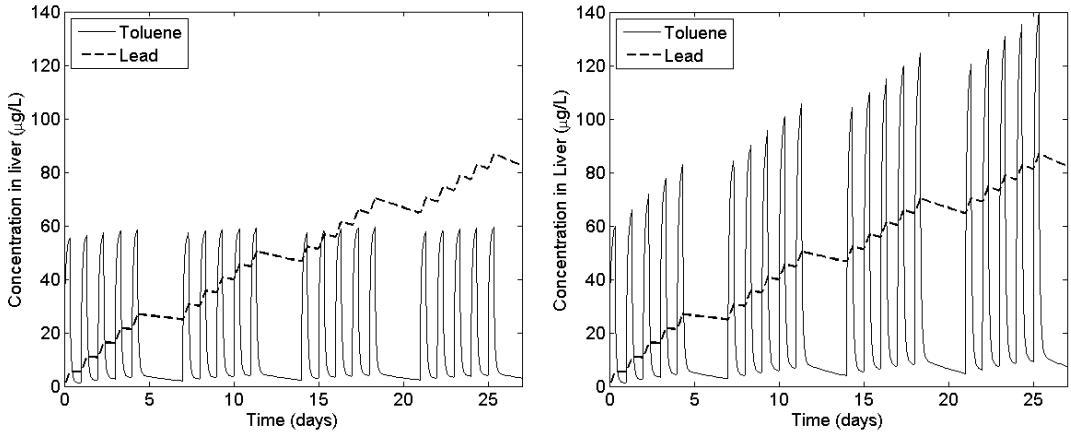

(a) No interaction (b) Noncompetitive inhibition

Figure 6.14: Hypothetical effect of inhibition due to metal exposure on toluene liver concentration. A simulated 8 hours/day, 5 days/week inhaled occupational exposure to 150 μg/m^{3}metal and 5 ppm toluene was modeled. Despite having a very short half-life due to elimination in exhaled air, disruption of metabolism increases the daily peak systemic levels of toluene, and may lead to a higher quasi steady-state over time.

maximum reaction velocity of toluene (mass/hr); $\mathrm{Vm_{TOL}}$ the uninhibited maximum reaction velocity of toluene (mass/hr); $\mathrm{Km_{TOL}}$ the Michaelis-Menten constant for toluene (mass/L); $\mathrm{Ki_{met\text{-}TOL}}$ the noncompetitive inhibition constant for metal acting on toluene enzyme (mass/L); C_{TOL} and C_{met} are the concentrations in the liver of toluene and metal, respectively.

In the current example, $\mathrm{Ki_{met\text{-}TOL}}$ was set to 50% of $\mathrm{Km_{TOL}}$. This was an arbitrary assumption in order to illustrate the example, and is not an actual estimate of the potency of metals on CYP450 enzymes. A simple occupational exposure scenario was simulated, where an individual is exposed via inhalation to 150 μg/m^{3}metal and 5 ppm toluene. The PBTK model for lead was used to represent metal due to its relatively long half life. In reality, occupational lead exposure would be much lower (the OSHA 8-hour permissible exposure (PEL) limit is 50 μg/m^3), and the prediction of lead in the liver is really to represent any one or combination of metals. The metal accumulation

in liver causes higher peak toluene liver levels, and eventually a higher average quasi steady state.

A more complex simulation is illustrated in Figure 6.15, and involves a mixture of methylmercury, cadmium, lead, arsenic (and metabolites), toluene, and benzene. In this case, there might be noncompetitive inhibition by metals on the aromatic compounds, and competitive inhibition between aromatics. As more metals accumulate in the liver, the maximum rate of reaction is reduced, causing higher accumulation of benzene and toluene. As benzene and toluene concentrations increase, so does the effect of competitive inhibition between these two chemicals, further reducing the rate of metabolism.

The metabolism of toluene with the inclusion of both noncompetitive and competitive inhibition is defined as:

$$\mathrm{R_{TOL}} = C_{\mathrm{TOL}} \frac{\mathrm{Vm^{*}_{TOL}}}{C_{\mathrm{TOL}} + \mathrm{Km^{*}_{TOL}}} \quad \text{where} \tag{6.8}$$

$$\mathrm{Km^{*}_{TOL}} = \mathrm{Km_{TOL}} \left(1 + \frac{C_{\mathrm{BNZ}}}{\mathrm{Ki_{BNZ\text{-}TOL}}}\right) \text{ and } \mathrm{Vm^{*}_{TOL}} = \frac{\mathrm{Vm_{TOL}}}{1 + C_{\mathrm{met}}/\mathrm{Ki_{met\text{-}TOL}}}$$

Similarly, the metabolism of benzene is defined as:

$$\mathrm{R_{BNZ}} = C_{\mathrm{BNZ}} \frac{\mathrm{Vm^{*}_{BNZ}}}{C_{\mathrm{BNZ}} + \mathrm{Km^{*}_{BNZ}}} \quad \text{where} \tag{6.9}$$

$$\mathrm{Km^{*}_{BNZ}} = \mathrm{Km_{BNZ}} \left(1 + \frac{C_{\mathrm{TOL}}}{\mathrm{Ki_{TOL\text{-}BNZ}}}\right) \text{ and } \mathrm{Vm^{*}_{BNZ}} = \frac{\mathrm{Vm_{BNZ}}}{1 + C_{\mathrm{met}}/\mathrm{Ki_{met\text{-}BNZ}}}$$

Where subscripts BNZ, TOL, and met denote benzene, toluene, and metals, respectively; variable C denotes concentration (mass/L); R rate of reaction (mass/time); Vm the uninhibited maximum reaction velocity (mass/hr); $\mathrm{Vm^{*}}$ the apparent maximum reaction velocity (mass/hr); Km the Michaelis-Menten constant (mass/L); Km the apparent Michaelis-Menten constant (mass/L); $\mathrm{Ki_{TOL\text{-}BNZ}}$ (toluene inhibiting benzene)

and $\mathrm{Ki}_{\text{BNZ-TOL}}$ (benzene inhibiting toluene) denotes competitive inhibition constants (mass/L); $\mathrm{Ki}_{\text{met-TOL}}$ and $\mathrm{Ki}_{\text{met-BNZ}}$ the noncompetitive inhibition constant for metal acting on toluene and benzene metabolism, respectively (mass/L); and C_{met} is the sum of lead, arsenic (and metabolites), and cadmium concentrations in the liver. While methylmercury was included in the model, it was assumed it did not contribute to inhibition. For simplicity, it was assumed $\mathrm{Ki}_{\text{met-TOL}} = \mathrm{Ki}_{\text{met-BNZ}}$. The unknown noncompetitive inhibition constant was defined as a factor of the Michaelis constant for benzene (which was 0.1 mg/L), and varied over a range of values. Parameters for the PBTK models of benzene and toluene (partition coefficients, metabolic constants, and competitive inhibition constants) were obtained from Haddad et. al. (2001) [173].

Continuous dietary exposure to 29 μg/day cadmium, 60 μg/day methylmercury, 70 μg/day lead, and 100 μg/day inorganic arsenic was assumed for 500 days (the approximate steady state). Metal intakes were cut to 30% of these values beyond day 500, in order to observe the dynamic effects. Due to the long timescale of cadmium, the cadmium PBTK model was first run for an individual from birth to age 30, using age-dependent intake rates of Choudhury et. al. (2001) [77]. The levels of cadmium in all tissues at age 30 were then used as the initial condition for the short-term simulations. The 29 μg/day cadmium intake rate at age 30 (from Choudhury et. al. (2001) [77]) was also continued to maintain the quasi-steady state. Continuous exposure to 20 ppm toluene and 10 ppm benzene continued for the entire span of the simulation, and was not reduced at day 500.

Figure 6.15(a) shows predicted concentrations in the liver of cadmium, lead, total arsenic, methylmercury, benzene, and toluene for the base-case (no competitive or noncompetitive inhibition). While methylmercury was included in the model, it was

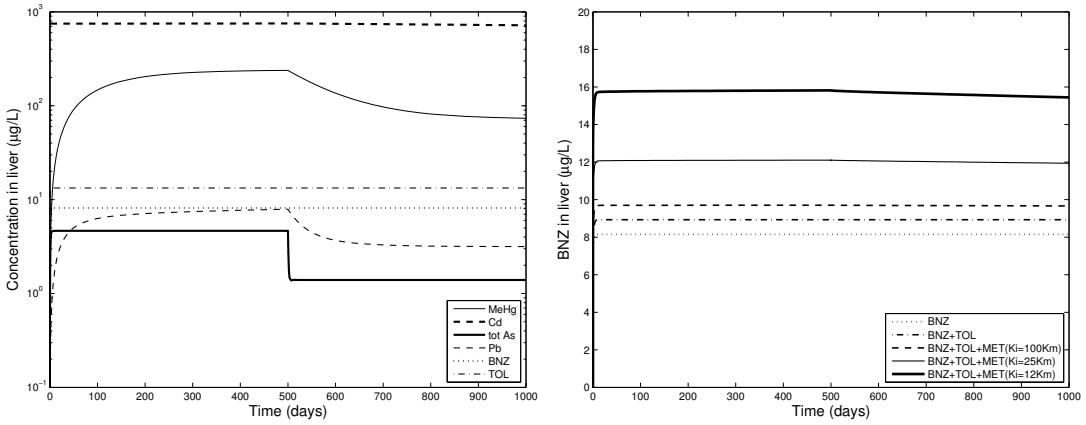

(a) Metal and VOC liver concentrations (b) Benzene liver concentrations

Figure 6.15: Effect of noncompetitive inhibition assumption of cadmium (Cd), lead (Pb), and total arsenic (tot As) on benzene (BNZ) liver concentration, with competitive inhibition by toluene (TOL). Metal intakes were reduced to 30% of the original intakes at day 500.

assumed it did not contribute to inhibition. Figure 6.15b shows predicted liver benzene concentration for the base-case scenario, and different interaction scenarios. The effect of competitive inhibition between toluene and benzene, and the additional effects of noncompetitive inhibition due to the sum of lead, cadmium, and arsenic are shown. Depending on the assumed noncompetitive inhibition constant, there could be significant increases in the steady-state level of benzene. Due to cadmium having both the highest liver concentration and the longest half-life, there is negligible dynamic change in benzene concentration over the course of 500 days when metal exposure is reduced.

Figures 6.16(a-b) illustrate the effect of incremental changes in the noncompetitive inhibition constant on benzene concentration in liver, both with and without concurrent toluene exposure. As the noncompetitive inhibition constant is reduced (which reduces maximum reaction velocity), benzene liver concentration increases. Competative inhibition with toluene compounds the effects of noncompetitive inhibition.

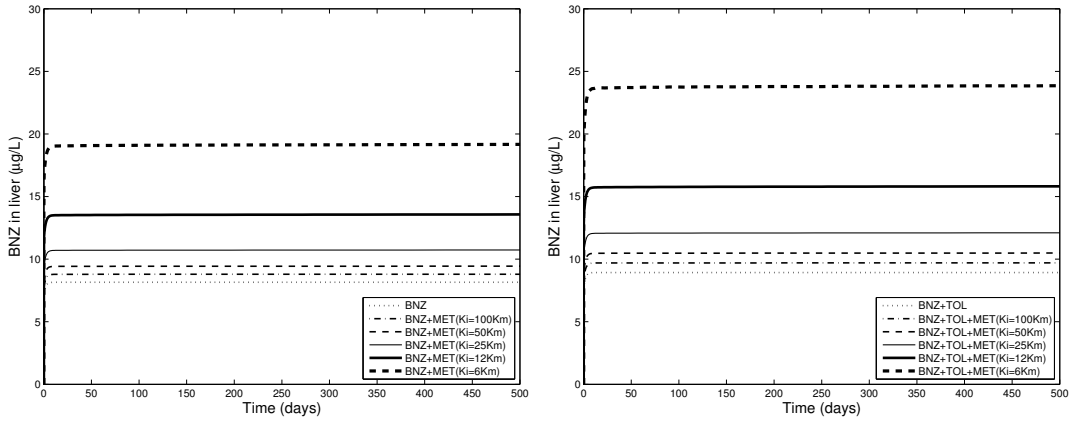

(a) Liver benzene (without toluene) (b) Liver benzene (with toluene)

Figure 6.16: Effect of varying inhibition assumptions on benzene liver concentration. Noncompetitive inhibition constants were varied by factors of two between 6 and 100 times the benzene Michaelis constant.

An alternative interaction scenario was performed, assuming metabolic interaction was due to a toxic response, rather than a direct inhibtion. To model a hypothetical effect of toxic metals on metabolic rate, a linear tissue exposure-response model with a short time-lag was used to relate liver metal concentration with a fraction decrease in maximum velocity. The contribution of each metal to the toxic response was arbitrary since such a model does not exist. However, parameters were selected to give metals with low liver concentrations higher weights in order for each metal to have an approximately equal toxic effect. Continuous dietary exposure to 15 µg/day cadmium (0.2 µg/kg/day over lifetime), 40 µg/day methylmercury, 70 µg/day lead, and 100 µg/day inorganic arsenic was assumed for 500 days (the approximate steady state). Metal intakes were increased by 40% of these values beyond day 500, in order to observe the dynamic effects. Continuous exposure to 20 ppm toluene and 10 ppm benzene continued for the entire span of the simulation, and was not reduced at day 500. Figure 6.17 (a) shows predicted concentrations in the liver of cadmium, lead, total arsenic, methylmercury, benzene, and toluene for the base-case (no interactions). Figure 6.17 (b) shows predicted liver benzene

concentration for the base-case scenario, and different interaction assumptions. The increase in benzene concentration beyond day 500 is due to increased metal exposure.

The precise relationships between toxic metal exposure and metabolic reaction rates of non-metals are not known. The reduction of CYP450 effectiveness due to exposure from metal mixtures requires tissue exposure-response models which do not yet exist, and a simplified noncompetitive inhibition model is probably insufficient. However, the developed framework can now be used to test different assumptions at varying levels of complexity. This will be essential in performing sensitivity analysis for the purpose of determining the most important interactions. Since it is impossible to model all metal compounds, volatile organics, and pharmaceuticals that simultaneously persist in the human body, it becomes necessary to limit the scope of the PBTK interaction models to only those that have significant impact on risk assessment.

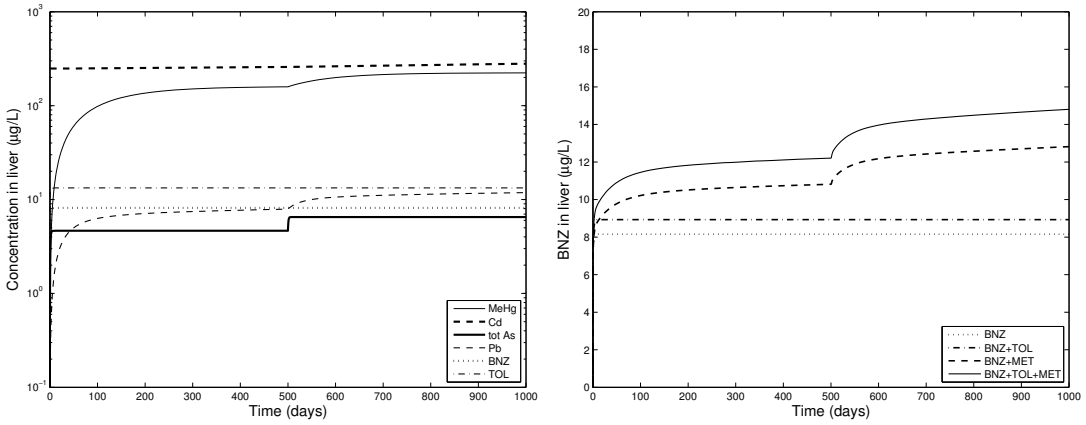

(a) Metal and VOC liver concentrations (b) Benzene liver concentrations

Figure 6.17: Effect of a hypothetical disruption by cadmium (Cd), lead (Pb), methylmercury (MeHg), and total arsenic (tot As) on benzene (BNZ) liver concentration, with competitive inhibition by toluene (TOL). Metal intakes were increased by 40% of the original intakes at day 500.

6.4 Population case study of methylmercury exposure

The generalized PBTK framework has been developed in such a way that it can act as a "black box" model and be utilized by larger exposure models developed in Matlab. For example, model inputs may only need to be physiology (age, gender, body weight, body height), exposure (duration and magnitude of exposure events), and physical exertion levels (higher exertion increases inhalation and cardiac rates). Outputs may be biomarkers (blood, urine, hair) or internal tissue concentration profiles. Together, these linked exposure, activity, and pharmacokinetic model make up a source-to-dose framework. Population source-to-dose modeling allows for a systematic analysis of the major causes and effects of exposure for either the general population, or populations which may be susceptible to toxic outcomes. For example, infants, young children, and women are particularly vulnerable to to metal toxicity [182, 285, 383, 384]. The following sections outline the methods and results of a population methylmercury simulation.

6.4.1 Sample demographics

Approximately 10000 "virtual individuals" were generated, with demographic characteristics matching that of Oswego County NY. The choice of a census tract for an exposure scenario helps risk assessors and policy makers gauge the proportion of susceptible individuals in a study population. Oswego County NY is relevant for methylmercury exposure due to its proximity to Lake Ontario, and the likelihood of there being more sports fish-consumers. Mercury levels in the lake could therefore become a health hazard to individuals consuming local fish, which is an issue that confronts both the U.S. and Canada.

Individuals most susceptible to methylmercury toxicity are young children (ages

1-5) and women of child-bearing age (ages 16-49). In order to get an estimate of the methylmercury intake of the "base" susceptible Oswego population (i.e. neglecting the sports fish-consumers and regional-specific mercury levels in local fish), it was assumed that the dietary patterns of the Oswego demographic group were similar to those of individuals the general U.S. population. This assumption allows for national U.S. dietary data (both food consumption patterns and measured mercury levels) to be applied to the Oswego demographic. As any additional regional-specific data becomes available, it can be applied to the virtual population, and the perturbations in mercury consumption (with respect to the base-case) can be evaluated.

6.4.2 Population exposure model

The method used to estimate longitudinal methylmercury intake in a population was adapted from [379]. The Continuing Survey of Food Intake by Individuals (CSFII) survey by the USFDA contains detailed information on food consumed by individuals in the U.S. over two non-consecutive 24-hour periods [115]. CSFII is highly detailed, with records of seafood intake for children and adults (normalized by body weight), sizes of portions for various seafood dishes (in g/eating occasion), and the fish species consumed with each dish. Additionally, CSFII has a large population sample size. However, it is only a snapshot in time of population fish consumption, and is insufficient for estimating chronic exposure. The National Health and Nutrition Examination Survey (NHANES) contains longitudinal fish consumption data for individuals (over 30-days), but with less detailed information on food portions and fish species. The method by [379] merges these two databases to produce a more detailed estimate of 30-day fish consumption patterns.

249 CSFII food codes are mapped to the 28 NHANES fish/shellfish categories,

allowing a single (general) NHANES category to be representative of multiple (detailed) CSFII definitions. Randomly sampled records of 30-day fish/shellfish intake frequencies are combined with randomly sampled CSFII records, while maintaining information about the food dishes (portion size and fish species). Results are in units of grams of food per kilogram of body weight per eating occasion. The resulting distribution of monthly seafood intake for the general U.S. population is merged with information on methylmercury levels of each fish species, producing a database of individuals and their corresponding average monthly methylmercury intakes. Fish methylmercury levels were based on national data from the USFDA and are provided in Tran et. al. (2004) [379].

To produce a "virtual population" based on a target population (i.e. individuals in Oswego, NY), individuals with demographic characteristics similar to those of the target census tract are randomly drawn from the general population database. This virtual population can be further specialized to reflect the target population by using local (as opposed to national) information on seafood intake and methylmercury levels.

6.4.3 Toxicokinetic assumptions

A pharmacokinetic model for methylmercury can be applied to the virtual population in order to make predictions of hair and blood biomarker levels, as well as internal tissue doses. An empirical model was implemented by Tran et. al. (2004) [379] to link intake rates with blood levels (using the average monthly methylmercury intake rate). For this example, the PBTK model based on the formulation of Shipp et. al. (2000) [338] was used, assuming that the average monthly methylmercury intake remained constant over a long period of time (until steady-state). Due to the long half-life of methylmercury in the body, daily or weekly fluctuations of intake have little impact on the quasi-steady-state biomarker estimate. However, the model neglects seasonal changes in fish

consumption which would significantly alter biomarker levels. Figure 6.18 outlines the overall methodology.

Estimates of whole-body physiology were obtained by [413] and [238], with remaining tissues not defined in the original methylmercury model lumped as slowly-perfused and rapidly-perfused. Tissue physiologies not defined by [413] (i.e. brain blood and hair) were obtained from Shipp et. al. (2000) [338]. Median values for physiochemical PBTK parameters were used for all individuals.

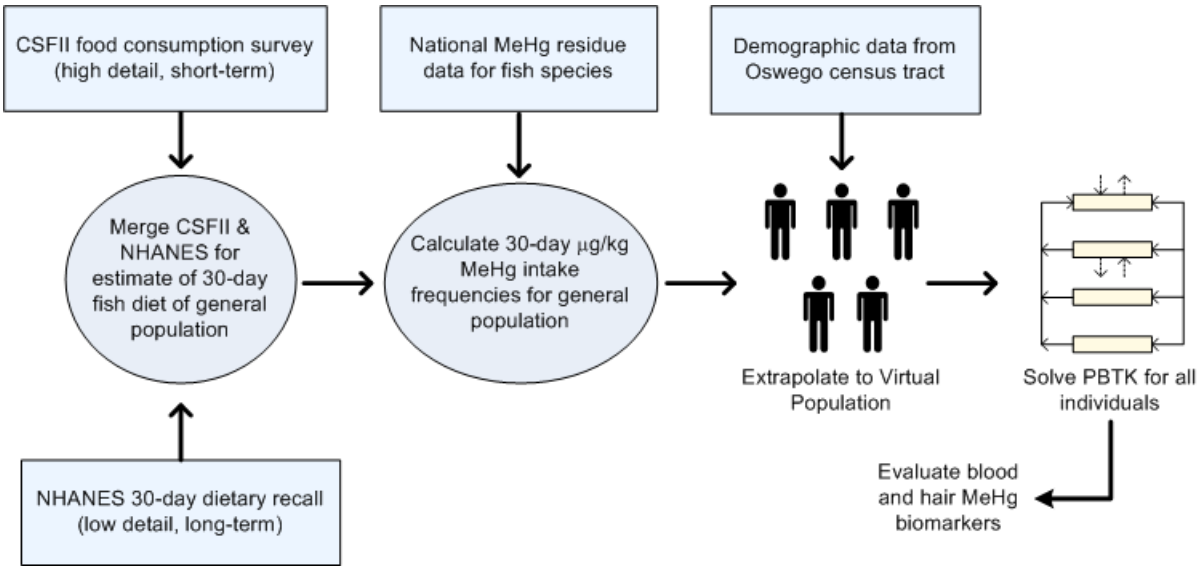

Figure 6.18: Schematic diagram of population methylmercury intake methodology based on Tran et. al. (2004) [379]. A base-case "virtual population" of individuals living in Oswego County NY is produced by merging national seafood consumption databases with the Oswego demographic profile. The PBTK model for methylmercury is then run to steady-state for each individual, assuming the average monthly seafood intake remains constant.

6.4.4 Results

Figure 6.19 compares the population results with observed national biomarker data. While the results for women of child-bearing age were very close to national measured results, the method over-predicted hair and blood methylmercury in children. Part of the problem could be due to the fact that the PBTK model was developed using adult data, and some absorption or elimination assumptions would need to be re-adjusted. Since children between 1 and 5 years old are rapidly growing, methylmercury pharmacokinetics might be significantly different. The results by Tran et. al. (2004) [379] had also over-estimated methylmercury levels in children, so it is likely that some of the error is due to the dietary model. An over-estimation in the amount of seafood children consume could occur by misinterpreting child survey data. It is also possible that children do not consume seafood as regularly or as often as adults, and extrapolating the 30-day survey results to a longer time frame is an incorrect assumption.

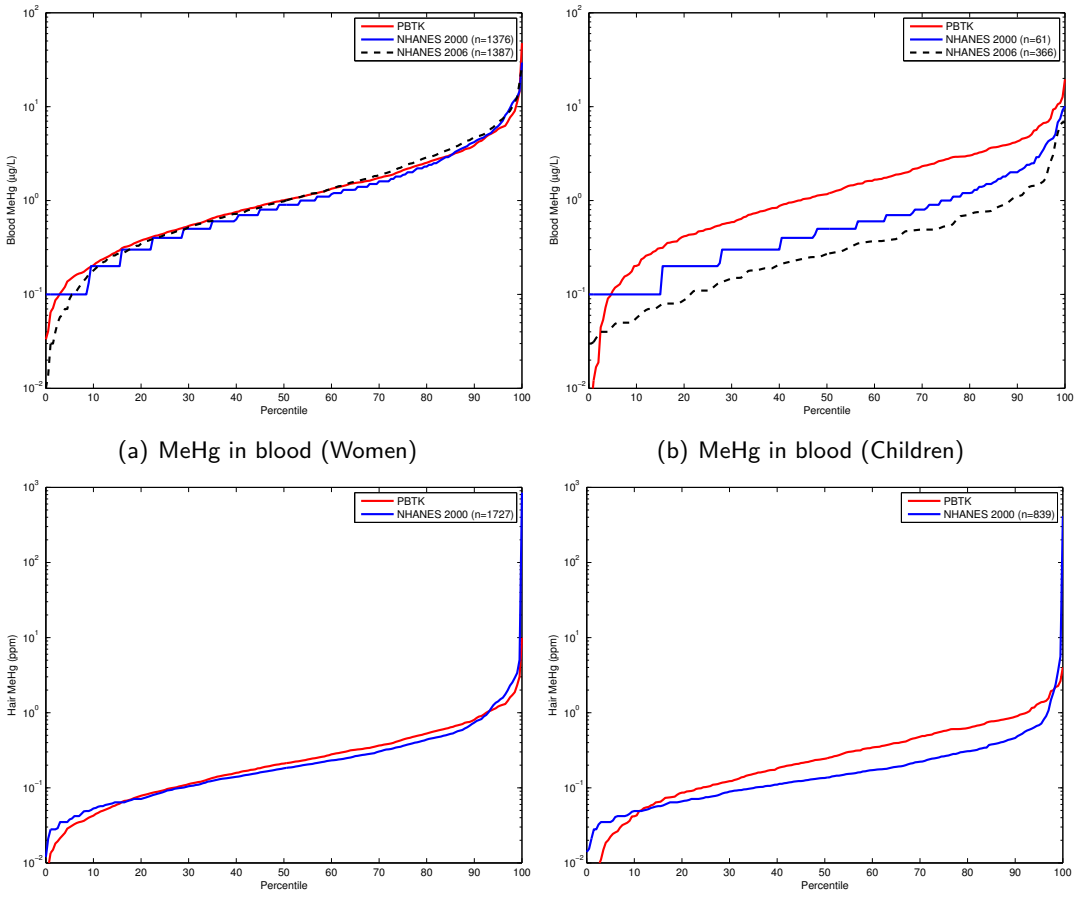

(a) MeHg in blood (Women)

(b) MeHg in blood (Children)

(c) MeHg in hair (Women)

(d) MeHg in hair (Children)

Figure 6.19: Percentiles of methylmercury biomarkers predicted for the Oswego County NY demographic, compared with national biomarker data (NHANES 2000 and NHANES 2006). Since only national seafood intake and methylmercury data were used, predicted biomarkers levels for Oswego should be similar to the general US population. The percentiles of NHANES 2000 data appear coarse due to lower analytical precision than NHANES 2006. Model predictions for women (aged 16-49) closely matches national data, while predictions for children (aged 1-5) overestimate methylmercury levels.

Chapter 7

Applications of the generalized model to mixtures of nonmetals

7.1 Bayesian Analysis of a PCB mixture using a lipid-based model

Lipid-based physiologically-based toxicokinetic (PBTK) models are a subset of traditional PBTK models that can simulate concentrations of highly lipophilic compounds in tissue lipids, without the need for numerous partition coefficient parameters [123]. The aim of this study was to apply a population Bayesian analysis to a lipid PBTK model for a mixture of six polychlorinated biphenyls (PCBs) in rats, incorporating a mechanistic model linking enzyme induction and metabolic rate. A hierarchical treatment of population metabolic parameters and a CYP450 induction model were incorporated into the fundamental lipid-based PBTK framework, and Markov-Chain Monte Carlo was applied using the previously published data. A mass balance of CYP1A and CYP2B in the liver was used to model PCB metabolism at high doses. The PBTK and CYP450 induction models both remained on a lipid basis, and were able to sufficiently model PCB concentrations in multiple tissues for varying dose levels and protocols.

7.1.1 Background

As with metals, PCBs have long half-lives in humans, and exist in the environment as mixtures. PCBs are also inducers of CYP450 enzymes, leading to an array of toxic

interactions. The ability to induce CYP450s is an important measure of toxicity for these and similar contaminants. In-vivo and in-vitro data for P450 induction of PCBs are used in determining the relative potency (REP) and toxic equivalency factor (TEF) metrics for risk assessment [179, 388].

Lipid-based PBTK models require no tissue/plasma partition coefficients, which drastically reduces the number of chemical-specific parameters needed for 209 PCB congeners and other highly lipophilic compounds. Residence time of chemical in each tissue depends only on lipid volumes, and the chemical-specific parameters are limited to absorption, metabolism, and elimination. Such models may lead to a more generalized treatment of large classes of chemicals, and more efficient simulations of large complex mixtures. Bayesian analysis has not yet been applied to these specific types of models. The lack of partition coefficients reduces the number of parameters, but also reduces model flexibility. Lipid-based models cannot be fit to data by individually adjusting parameters for every tissue-chemical combination. A hierarchical Bayesian framework can formerly incorporate these errors into the model.

7.1.2 Methods

Toxicokinetics

The fundamental PBTK model and primary data are outlined in [123]. The model consists of five compartments (blood/plasma, adipose tissue, liver, slowly and rapidly perfused), with metabolism occurring in the liver. Elimination primarily occurs via CYP450 metabolism, which is modeled as a first-order function of hepatic burden in the original model formulation. Under high PCB exposure, an increase in metabolic rate was observed, likely due to PCB induction [123].

Since PCBs are highly lipophilic, the PBTK model formulation assumes PCBs only

exist in the neutral lipid spaces of blood and tissues. Compartment volumes correspond to the lipid volumes in each tissue, and the total cardiac output is corrected for the fractional lipid content of blood. The lipid model assumptions eliminate the need for partition coefficients, thereby reducing the number of chemical-specific parameters. The PBTK model is based on chemical concentration in neutral lipid equivalent (NLE) components of blood and tissues, which can be converted to concentration in total lipids (a measurable quantity).

The lipid-based mass balances for tissues in the PBTK model are defined as: [122]

$$\frac{dA_{\mathrm{nlt}}}{dt} = Q_{\mathrm{nlt}}(C_{\mathrm{nla}} - C_{\mathrm{nlt}}) \tag{7.1}$$

$$C_{\mathrm{nlt}} = \frac{A_{\mathrm{nlt}}}{V_{\mathrm{nlt}}} \tag{7.2}$$

$$C_{\mathrm{tlt}} = C_{\mathrm{nlt}}\frac{V_{\mathrm{nlt}}}{V_{\mathrm{tlt}}} \tag{7.3}$$

Where A_{nlt} is the mass of chemical in the tissue NLEs (μg), Q_{nlt} is the flow rate of blood NLEs through the tissue (ml NLE/h), C_{nla} is the chemical concentration in the NLE fraction of arterial blood (μg/mL NLE), C_{nlt} is the chemical concentration in the tissue NLEs (μg/mL NLE), C_{tlt} is the chemical concentration expressed in terms of total lipids in tissue (μg/mL of total lipid), V_{nlt} is the volume of neutral lipid equivalents in tissue (mL NLE) and V_{tlt} is the volume of total lipids in tissue (mL total lipid). Volumes of total lipids in tissues are measurable quantities, while neutral lipid equivalents are quantities that are derived by assuming NLEs are composed of the all neutral lipids and 30% of the phospholipids in tissue [123, 296].

NLE-based volumes in Table 7.2 are obtained by multiplying conventional values with NLE ratios in Table 7.1. Flows are obtained by multiplying conventional values with the blood NLE ratio. The ratio of NLE/total lipid in Table 7.2 ($V_{\mathrm{nlt}}/V_{\mathrm{tlt}}$) is used

to convert concentrations from NLE basis to total lipid basis. To convert liver and fat NLE concentrations to a total lipid basis, the corresponding values in Table 7.1 (column 3) are used. For the conversion of whole-blood NLE concentration to plasma total lipid concentration, the whole-blood concentration is multiplied by the NLE/total lipid ratio for plasma. This is valid since it is assumed that chemical concentration in the NLEs of whole blood components (plasma and red blood cells) is uniform.

Table 7.1: Lipid content of rat tissues [123, 296]

Tissue	NLE[†]	NLE/total lipid
Blood	0.0019	0.576
Plasma	0.0009	0.748
Fat	0.8536	0.998
Liver	0.0425	0.710
Rapidly perfused	0.0425	0.710
Poorly perfused	0.0120	0.632

[†]Neutral Lipid Equivalent ratio (mL NLE/mL tissue)

Table 7.2: Physiological values for a standard 225-g rat (adapted from [123])

Tissue	Conventional model[†]	NLE-based model
Blood flow rates		
Fat	448 mL/h	0.85 mL lipid/h
Liver	1245 mL/h	2.36 mL lipid/h
Rapidly perfused	2540 mL/h	4.82 mL lipid/h
Poorly perfused	747 mL/h	1.42 mL lipid/h
Cardiac output	4980 mL/h	9.45 mL lipid/h
Volumes		
Blood	20.0 mL	0.038 mL lipid
Fat	17.5 mL	14.938 mL lipid
Liver	10.0 mL	0.425 mL lipid
Rapidly perfused	12.5 mL	0.531 mL lipid
Poorly perfused	167.5 mL	2.010 mL lipid

[†]Physiological parameter values obtained from [213, 221]

Data

The data consisted of rats receiving oral doses of a mixture of 6 PCB congeners: 118 (2,3',4,4',5-pentachlorobiphenyl), 138 (2,2',3',4,4',5-hexachlorobiphenyl), 153 (2,2',4,4',5,5'-hexachlorobiphenyl), 170 (2,2',3,3',4,4',5- heptachlorobiphenyl), 180 (2,2',3,4,4',5,5'-heptachlorobiphenyl), and 187 (2,2',3,4,5,5',6-heptachlorobiphenyl). The dosing experiments consisted of 3 dose levels (5, 50, and 500 μg/kg body weight of each PCB), and 4 dose protocols (one dose per day, one dose per week, consecutive daily doses for 13 days followed by no exposure, and 13 irregularly spaced doses). Rats were either sacrificed at 41 days or 90 days for data collection. PCB concentrations in total lipids of plasma, liver, and adipose tissue were measured (adipose tissue concentrations were measured for only those rats sacrificed at 90 days). Body weight and liver weight at time of sacrifice were also measured, allowing for improved estimates of physiological parameters. The final data consisted of approximately six rats for each dose level/dose protocol/sacrifice day combination (142 rats in total).

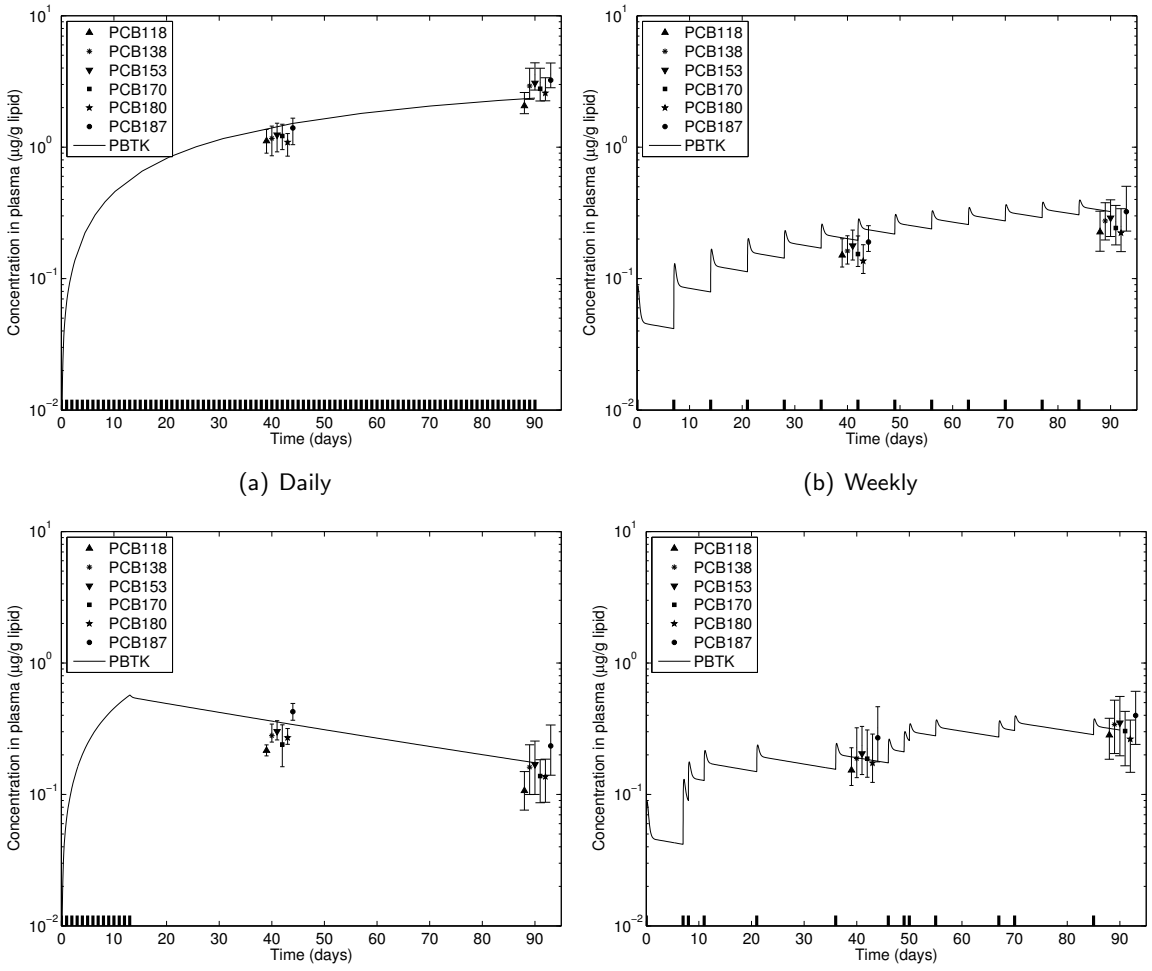

(a) Daily

(b) Weekly

(c) Daily (to day 13)

(d) Non periodic

Figure 7.1: The effects of the four different dosing scenarios on PBTK model predictions and biomarker data. The concentrations are of PCB in total plasma lipid for the low dose level (5 µg/kg). Points indicate the median measurement across the rats at time of sacrifice (either day 41 or 90). Error bars indicate the minimum and maximum measured values across rats.

Significant inter-individual variability is observed in many of the data sets. For much of the low-dose data, all PCBs were within 10% of each other in fat, liver, and plasma for each individual. Variation occurred between individuals, which can be attributed to differences in body and liver weights, as well as differences in metabolic rate in the population. Since the model assumes 100% oral absorption, it is unlikely that any significant variation is due to absorption rate (the absorption timescale is hours, while the data timescale is weeks). For low-dose data, the PCB concentrations for each rat were in a consistent order in some (but not all) data sets. At the high doses, PCB 118 was consistently lower than the other PCBs. Figure 7.2 illustrates some of the scatter and variability seen in the data. A population model may be used to account for these inter- and intra-individual differences in PCB concentrations.

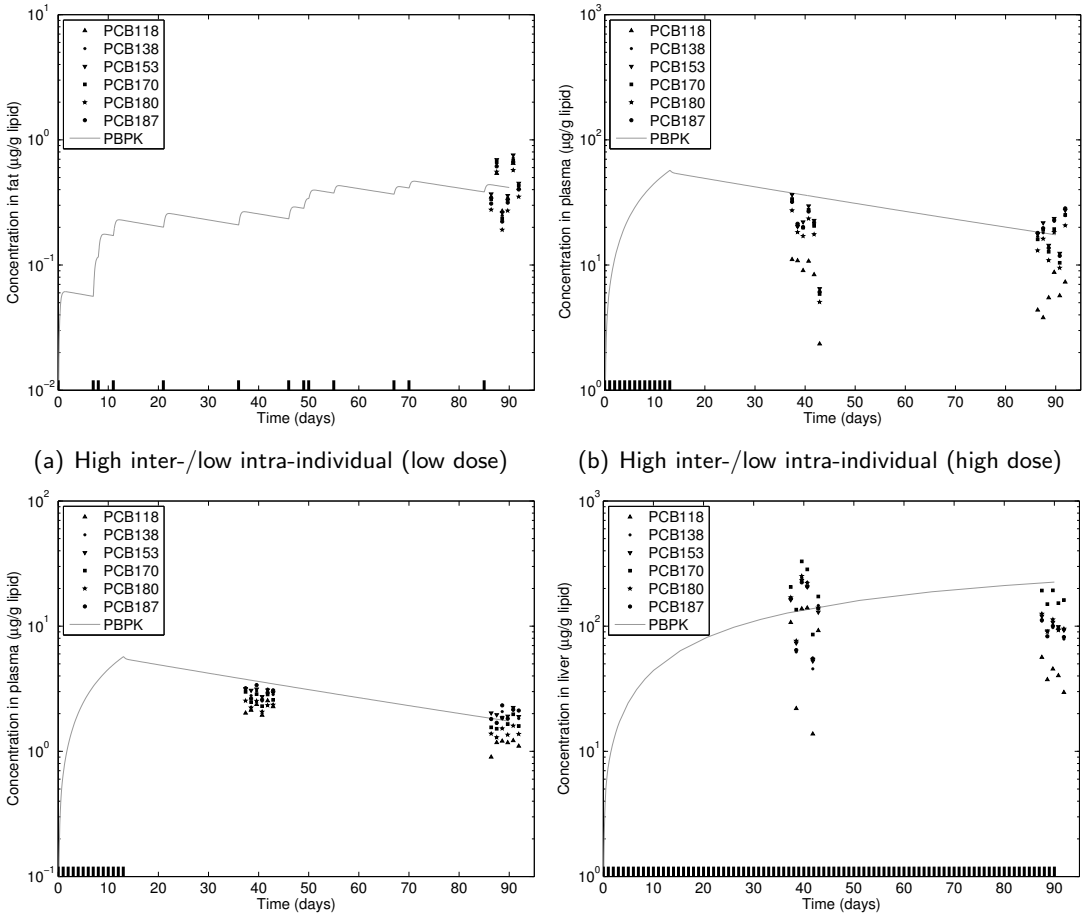

(a) High inter-/low intra-individual (low dose)

(b) High inter-/low intra-individual (high dose)

(c) Low inter-/low intra-individual

(d) High inter-/high intra-individual

Figure 7.2: An illustration of inter- and intra-individual variability observed in the data. Measured concentrations of each PCB for different rats are scattered along the x-axis. For some of the low-dose data (a), all PCB concentrations are within a small range for each rat, but differ greatly between rats. The same is shown at the higher doses (b), except with PCB 118 being significantly lower than the multi-ortho PCBs (which remain within a small range). However, some data sets showed very low data scatter (c), while others showed high scatter both between and within rats (d).

Induction model

Low, non-repetitive PCB doses have been shown to cause significant enzyme induction in rats [136, 184]. In the current dataset, high chronic doses of a PCB mixture led to a net increase in elimination rate, which is attributed to P450 induction [123]. PBTK models predicting P450 activities and directly relating them to metabolic rate have been previously implemented for various chemicals in rats [11, 122, 124, 324, 395]. A P450 balance on the liver can be defined as [11, 395]:

$$\frac{dA^{\mathrm{CYP}}}{dt} = k_0 - k_{\mathrm{e}} \times A^{\mathrm{CYP}} + S(t) \tag{7.4}$$

Where A^{CYP} is the amount of P450 in the liver (mass), k_0 is the basal P450 production rate (mass/time), k_{e} is the P450 degradation rate (time^{-1}), and $S(t)$ is the stimulation function for induction exposure response (mass/time). The initial condition for A^{CYP} is the baseline level A_0^{CYP}. In the presence of zero inducer, Equation 7.4 is at steady state, and $S(t) = 0$, therefore k_0 is equivalent to $k_{\mathrm{e}} A_0^{\mathrm{CYP}}$.

For simplicity, a linear function was adopted for $S(t)$. While a saturable Hill equation could have been implemented, it was found that optimizing Hill parameters with weak prior information was impractical using MCMC. The dose response parameters of this particular mixture at the three dose levels and four dose protocols is highly uncertain. Additionally, the lipid-based formulation of the PBTK model inherently requires different assumptions than traditional models. A common assumption for linked PBTK-induction models of lipophilic compounds is that only unbound chemical outside of the lipid space can initiate dose response (via DNA or Ah-receptor binding modeled using saturable equations). Since the current lipid-based PBTK formulation assumes

the concentration outside lipids is negligible, it follows that the external PCB concentration may never be high enough to cause receptor binding to approach saturation. Therefore, the model currently assumes that the dose response remains linear despite large differences in administered dose.

For simplicity, a linear function was adopted for $S(t)$. While a saturable Hill equation could have been implemented, it was found that optimizing Hill parameters with weak prior information was impractical using MCMC. The dose response parameters of this particular mixture at the three dose levels and four dose protocols is highly uncertain. Additionally, the lipid-based formulation of the PBTK model inherently requires different assumptions than traditional models. A common assumption for linked PBTK-induction models of lipophilic compounds is that only unbound chemical outside of the lipid space can initiate dose response (via DNA or Ah-receptor binding modeled using saturable equations). Since the current lipid-based PBTK formulation assumes the concentration outside lipids is negligible, it follows that the external PCB concentration may never be high enough to cause receptor binding to approach saturation. Therefore, the model currently assumes that the dose response remains linear despite large differences in administered dose.

It was assumed the initiation of P450 induction occurs proportionally to the inducing PCB concentration in the lipid space of the liver:

$$S(t) \quad = \quad k_0 F_{\mathrm{IND}}\, C_{\mathrm{IND}} \tag{7.5}$$

Where C_{IND} is a relative metric for inducer concentration, and F_{IND} (≥ 0) is the induction slope factor defining induction rate increase in CYP450 enzyme caused by C_{IND}. The total induction slope is defined with k_0 (which is known) in order to normalize F_{IND} (the unknown parameter to be optimized).

By trial-and-error, it was determined that the following relationship between P450 levels and metabolic reaction rate was flexible yet simple enough to adequately model the data:

$$v_{\mathrm{cl}} = v_0 \frac{A^{\mathrm{CYP}}}{A_0^{\mathrm{CYP}}} \tag{7.6}$$

Where v_{cl} is metabolic clearance (L/h), and v_0 is the basal metabolic clearance under low exposure and negligible induction (L/h). A_0^{CYP} is constant, while A^{CYP} is obtained from the solution of the P450 balance.

The rate of metabolism of each PCB was the product of the PCB concentration in the neutral lipid space of the liver ($A_{\mathrm{nlL}}/V_{\mathrm{nlL}}$), and the v_{cl} for the particular PCB.

$$\frac{dA_{\mathrm{nlL}}}{dt} = Q_{\mathrm{nlL}} \left(C_{\mathrm{nla}} - \frac{A_{\mathrm{nlL}}}{V_{\mathrm{nlL}}} \right) - v_{\mathrm{cl}} \cdot \frac{A_{\mathrm{nlL}}}{V_{\mathrm{nlL}}}$$

$$\frac{dA_{\mathrm{nlL}}}{dt} = Q_{\mathrm{nlL}} \left(C_{\mathrm{nla}} - \frac{A_{\mathrm{nlL}}}{V_{\mathrm{nlL}}} \right) - v_0 \frac{A^{\mathrm{CYP}}}{A_0^{\mathrm{CYP}}} \cdot \frac{A_{\mathrm{nlL}}}{V_{\mathrm{nlL}}}$$

$$\frac{dA^{\mathrm{CYP}}}{dt} = k_0 - k_{\mathrm{e}} \times A^{\mathrm{CYP}} + k_0 F_{\mathrm{IND}} C_{\mathrm{IND}}$$

For TCDD, the inducer concentration C_{IND} is defined to be the chemical concentration bound to the Ah-receptor [11], which is also a fair assumption for PCBs [322]. However, the TCDD models assumed that only "free" TCDD outside of the lipid space can bind to the Ah-receptor [395]. The PBTK model for PCBs assumes all chemical exist only within the lipid spaces of tissues, and neglects any PCB mass outside the lipids. Without a prediction of external PCB concentration, the previous Ah-receptor model assumptions are not applicable.

Optimizing all of the Ah-receptor binding model parameters, in addition to dose-response and metabolic parameters would be infeasible. The parameters would be

highly correlated and non-identifiable, since identical model results would be produced assuming either low Ah-binding with strong dose-response, or high Ah-binding with weak dose-response. To maintain the parsimony of the model and keep all concentrations lipid-based, C_{IND} was defined as the concentration of the inducing PCB congener(s) in the neutral-lipid space of the liver. Any additional resistance or barriers to induction were essentially lumped into the biological exposure-response parameters of $S(t)$.

PCB induction and metabolism are congener-specific, and are functions of structure and classification [20]. Non-ortho PCBs interact with (i.e. induce and are metabolized by) CYP1A, while multi-ortho substituted PCBs interact primarily with CYP2B. Mono-ortho PCBs interact with both CYP1A and CYP2B and are considered "mixed-type" inducers [88, 194, 322]. PCB congeners 138, 153, 170, and 180 are di-ortho; 187 is tri-ortho; 118 is mono-ortho. In the current dataset, PCB 118 had significantly increased clearance than the other congeners at the high dose level [123]. This difference is consistent with in-vitro induction and metabolic studies. A recent study in rat hepatocytes found that mono-ortho PCBs are primarily metabolized by CYP1A, and primarily induce CYP1A (with CYP2B being induced to a lesser extent) [405]. CYP1A induction by PCB 118 has also been shown to be orders of magnitude greater than induction by multi-ortho PCBs [389]. Meanwhile, CYP2B induction from both PCB 118 and multi-ortho PCBs was the same order of magnitude [88].

To explain the difference in PCB 118 metabolism at the high doses, the PBTK model assumes the multi-ortho PCBs are metabolized primarily through the CYP2B pathway, while PCB 118 is metabolized via CYP1A. It was also assumed both types

of PCBs induce CYP2B, but induction of CYP1A by multi-ortho PCBs was negligible (Figure 7.3).

Equations 7.4 and 7.5 were applied with parameters to describe both CYP1A and CYP2B kinetics. Parameters were obtained from literature and are summarized in Table 7.3. Induced clearance of PCB 118 was dependent on the CYP1A ratio, while the others were dependent on CYP2B ratio (Equation 7.6). For the induction of CYP1A, C_{IND} was assumed to be concentration of PCB 118 in the neutral lipid space of the liver. For CYP2B induction, C_{IND} was assumed to be the total PCB concentration (sum of all 6 PCBs) in the neutral lipid space of the liver. This assumes that dose response for CYP2B was additive for the mixture, with each PCB having equal weight. This is a simplifying assumption since the dose response is likely non-additive [378].

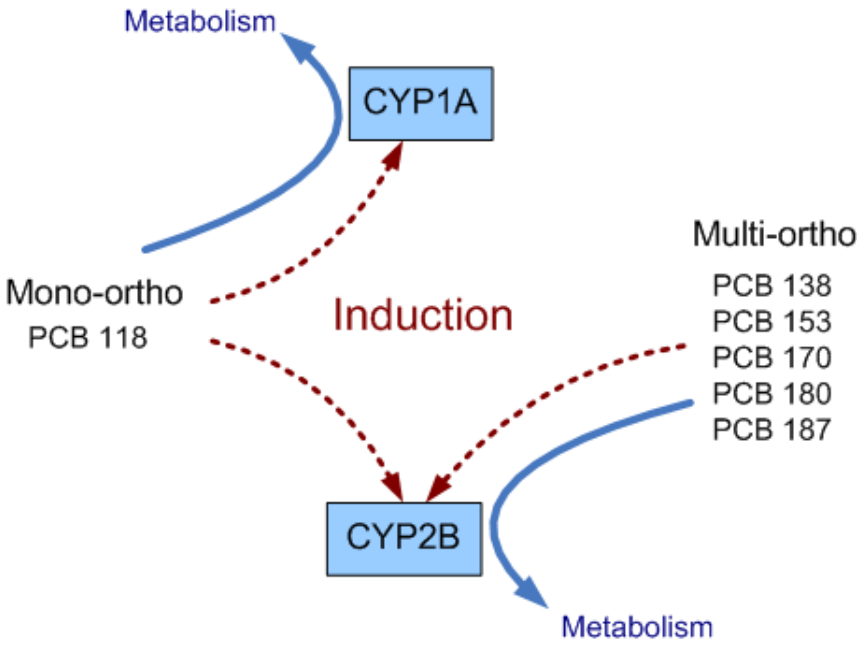

Figure 7.3: Schematic of CYP1A and CYP2B induction and metabolism for the two classes of PCBs.

Table 7.3: Basal CYP1A/2B parameters (adapted from [11, 324]):

Parameter	Symbol	Units	Value	Reference
Basal CYP2B level	A_0^{2B}	AUC†/µg protein	15.1	[251]
Basal CYP2B degradation	k_e^{2B}	h^{-1}	0.032	[339]
Basal CYP2B production	k_0^{2B}	AUC/h/µg protein	0.483	computed
Basal CYP1A level	A_0^{1A}	nmol/g protein	0.1	computed
Basal CYP1A degradation	k_e^{1A}	h^{-1}	0.04	[11]
Basal CYP1A production	k_0^{1A}	nmol/h/g protein	0.004	[11]

†Area under curve: cited reference used graphical techniques in deriving CYP2B levels

Hierarchical Bayesian Model

To model the inter-individual variation in metabolic parameters a hierarchical framework was constructed (Figure 7.1.2) to estimate these parameters at both the population and individual levels.

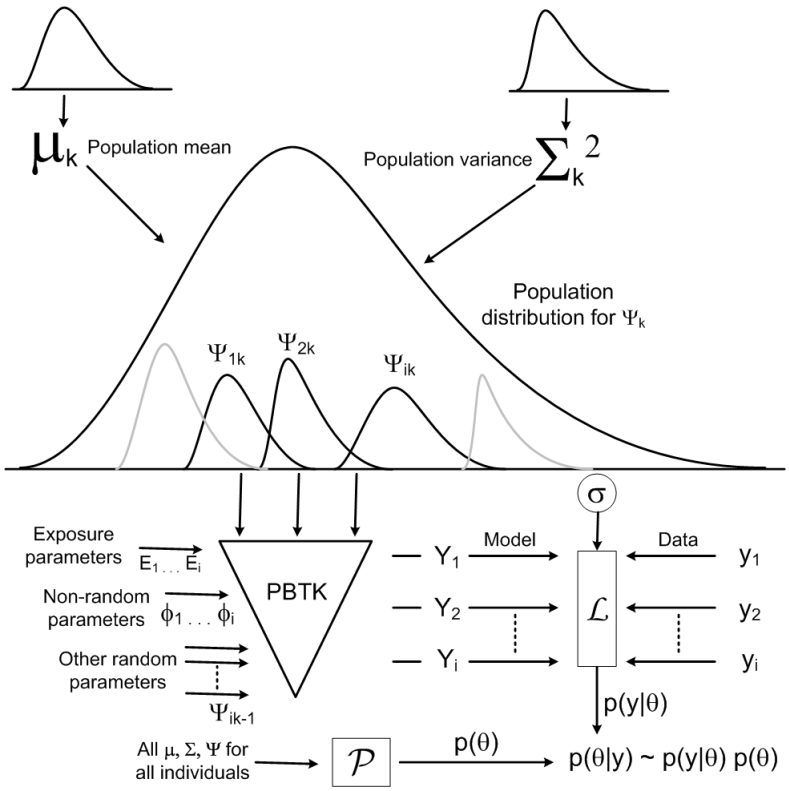

Figure 7.4: Schematic of a hierarchical Bayesian framework (adapted from [170]).

Each random parameter Ψ_{ik} is assumed to be derived from a population distribution defined by μ_k and Σ_k. Random and non-random parameters are used as inputs to the PBTK model to predict $\mathbf{Y_i}$. The likelihood function $\mathcal{L}$ calculates the probability of an adequate model prediction of data $\mathbf{y_i}$ given the set of random parameters. The prior function $\mathcal{P}$ calculates the probability of all random parameter values given the current set of assumptions of their distributions. The posterior probability is proportional to the product of the likelihood and prior.

A lognormal error function was used for the likelihood, assuming the log of the data measurements y_i are scattered in a normal distribution from the log of their corresponding model predictions Y_i:

$$\log(y_i) \quad = \quad \log(Y_i) + N(\mu = 0, \sigma) \tag{7.7}$$

The magnitude of the data scatter therefore scales proportionally with data and model predictions. Since there are three tissues measured (plasma, liver, and fat), three separate values for σ are necessary. This is to account for the potential that the PBTK model provides better (or worse) predictions for certain tissues.

The population and error parameters to be estimated are summarized in Table 7.5. Prior probabilities of the population-level parameters were typically wide and non-informative. The prior probabilities of individual-level parameters were calculated at every iteration using the updated values of population μ and Σ for each parameter. To reflect high uncertainty for the metabolic parameters, the prior for population variance Σ was assumed to be inverse-gamma distribution with a shape parameter of 1 (indicating large uncertainty), and a scale parameter of 0.8. The scale parameter value indicates that population parameters are expected to vary by less than an order of magnitude in the population (although the distribution is flexible enough to allow an optimized Σ to be greater or smaller than 0.8, depending on the strength of the data). Upper and lower limits for the uniform priors on mean population basal clearances μv_0^{PCBx} were arbitrarily set by observing model behavior at low and high v_0^{PCBx}, and comparing to data.

Table 7.4: Population-level parameters to be estimated by Bayesian analysis

Parameter	Unknowns	Prior
Basal metabolic rate[†]	μv_0^{PCBx}	Wide uniform
(L/h/kg$^{0.75}$)	Σv_0^{PCBx}	Inverse gamma
Induction factor	$F_{\text{IND}}^{\text{2B}}$	Wide uniform
	$F_{\text{IND}}^{\text{1A}}$	Wide uniform
Model/data error[‡]	σ	Wide uniform

[†]One each for PCBs 118, 138, 153, 170, 180, 187

[‡]One each for plasma, liver, and fat

Computational implementation

Markov-Chain Monte Carlo (MCMC) with Metropolis sampling was used to iteratively converge to the posterior distribution. The number of individual-level parameters per PBTK model, multiplied by the number of unique PBTK models (six PCBs), multiplied by 142 rats, and added with population and error parameters, leads to about 870 parameters. MCMC convergence issues arise with such high dimensions, especially since the data consists of spot-samples rather than full time-course data for each rat, and because population priors were non-informative. Additionally, each MCMC iteration requires the solution of $6 \times 142 = 852$ systems of differential equations, and multiple independent MCMC analyses (using different initial guesses) are required to confirm results. Since the problem might not converge for 100000 iterations, it was important to use simplifying assumptions to reduce model evaluations and improve convergence.

Because no (or minimal) induction effect was observed at the lowest dose [123], the parameter optimization can be decomposed into two steps. For the first step, induction is neglected and the model is optimized using only the low-dose data in order to obtain the basal metabolic rate (v_0) for each PCB. The resulting population distributions for the v_0s are then used as priors in the second step. For step 2, induction is incorporated,

and parameters are optimized using only data for the two high doses. This prevents the identifiability problem of being unable to separate basal metabolic rate and induced metabolic rate. While MCMC is still performed on the individual-level values for v_0 in step 2, they are defined by stronger population priors. Another simplifying assumption is that inter-individual variation of the induction factor F_{IND} is negligible. This is equivalent to stating that the prior probability on ΣF_{IND} is extremely small. Assuming negligible variation on F_{IND} eliminates the need to estimate individual-level F_{IND}s for each rat, and improves convergence. It was assumed that some rats may be fast or slow metabolizers (due to physiological or biochemical differences), and this variability would be accounted for by differences in v_0. Two induction factors (one each for 1B and 2A induction) would be optimized to fit the entire population.

The first step consisted of 249 parameters, since only the low-dose data (39 rats) were analyzed. The population distribution for the basal metabolic rate of each PCB was determined. The second step consisted of 479 random parameters, since 2 high dose datasets (79 rats) were analyzed. The data used for the optimization consisted of fewer rats than the total data, since an additional evaluation dataset was set aside to evaluate model performance. Parameters included population induction parameters for CYP1A and CYP2B induction, and individual-level parameters for basal metabolic rates. Population basal metabolic rate parameters were fixed and used as prior distributions (determined from step 1). Individual-level basal metabolic rates were free to explore the prior parameter space, and the priors were not updated.

For both step 1 and step 2 of the parameter optimization, three sets of independent Markov-chains were initiated using over-dispersed initial guesses. For the first 5000 iterations, relatively wide proposal distributions (for each proposed step in the

random walk) were used. This allowed for a rapid exploration of the parameter space, although acceptance rates became extremely low as parameters approached the convergence region. After these initial iterations, the proposal distributions were re-adjusted (by reducing the proposal distribution variances) to obtain higher acceptance rates. The chains were then run for an arbitrarily large number of iterations (i.e. 50000). If poor mixing or inadequate sampling rates were observed, proposal distributions were re-tuned, and the chains continued for another 50000 iterations. The chains were considered converged if the Gelman-Rubin convergence statistic was close to 1 for the parameters from all three independent sets of chains [153].

The PBTK models and Metropolis sampler were implemented in Matlab-Simulink, on a cluster of multicore machines. Since the computation for each rat is independent at each iteration, the problem is "embarrassingly parallel" and can be easily distributed across multiple machines. For example, since the likelihood is calculated by running the PBTK model for 79 independent rats, these 79 computations can be performed using a parallel for-loop over **n** machines. The computational time of each MCMC iteration is reduced by a factor of **n**. Convergence of the Markov-chains usually occurred after 80000 iterations and three days computational time.

7.1.3 Results

Posterior distributions

Despite the non-informative priors for basal metabolic clearances, results indicate these parameters will generally deviate from the mean by less than a factor of 2 in the population (Figure 7.5). The lognormal Σv_0 parameters were reduced by half. Because distributions for basal metabolic rate of all 6 PCBs were very similar, an additional MCMC analysis was performed for step 1 assuming a single population distribution for

all PCBs (parameter v_0^{all}). It allowed PCBs to have different basal clearances between and within individuals, but all were assumed to be drawn from the same population distribution. This reduced the number of population parameters, and improved convergence. The population distribution for v_0^{all} was in agreement with those determined for the individual PCBs, and is shown in Figure 7.6. Step 2 of the MCMC analysis (determination of induction parameters) was still performed using the original 6 separate PCB distributions.

Table 7.5: Posterior distributions of population metabolic parameters and modeling errors

Parameter	Unknowns	Posterior value	Uncertainty CV[†]
Basal metabolic rate (L/h/BW$^{0.75}$)	μv_0^{118}	0.038	0.06
	μv_0^{138}	0.026	0.09
	μv_0^{153}	0.024	0.09
	μv_0^{170}	0.028	0.1
	μv_0^{180}	0.034	0.1
	μv_0^{187}	0.017	0.15
	Σv_0^{118}	0.28	0.19
	Σv_0^{138}	0.39	0.20
	Σv_0^{153}	0.42	0.18
	Σv_0^{170}	0.44	0.15
	Σv_0^{180}	0.35	0.20
	Σv_0^{187}	0.55	0.19
Induction factor	$F_{\text{IND}}^{\text{2B}}$	0.0024	0.07
	$F_{\text{IND}}^{\text{1A}}$	0.048	0.09
Model/data error[‡]	σ_{fat}	0.30/0.22	0.10/0.06
	σ_{plasma}	0.21/0.23	0.06/0.05
	σ_{liver}	0.41/0.36	0.05/0.04

[†]Coefficient of variance of chain
[‡]Values for basal/induction optimization steps

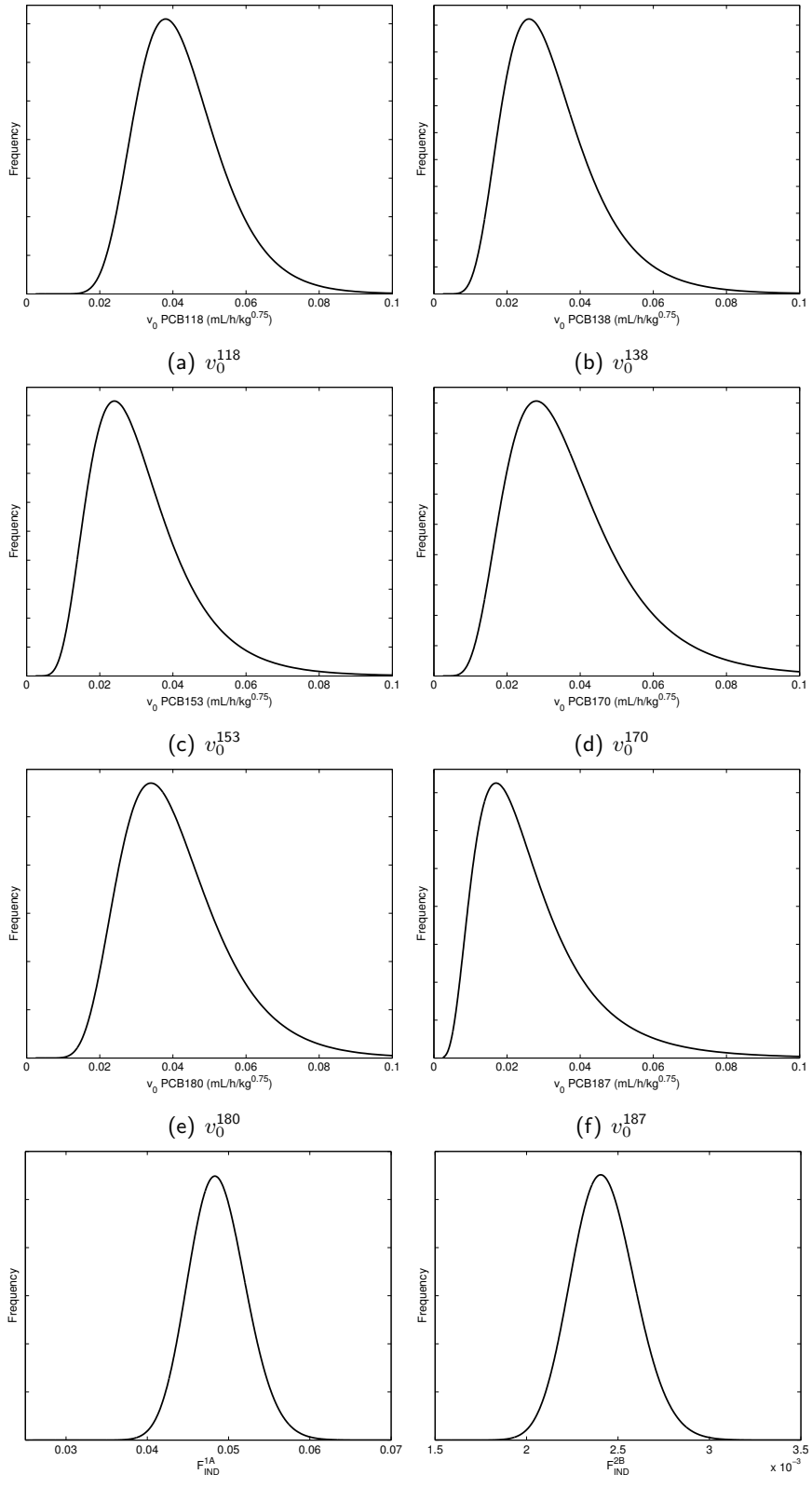

(a) v_0^{118} (b) v_0^{138}

(c) v_0^{153} (d) v_0^{170}

(e) v_0^{180} (f) v_0^{187}

(g) $F_{\mathsf{IND}}^{\mathsf{1A}}$ (h) $F_{\mathsf{IND}}^{\mathsf{2B}}$

Figure 7.5: Posterior distributions of population metabolic and induction parameters. Distributions are plotted from parameters in Table 7.5. Note that the induction factors are each on different scales, due to the difference in order of magnitude.

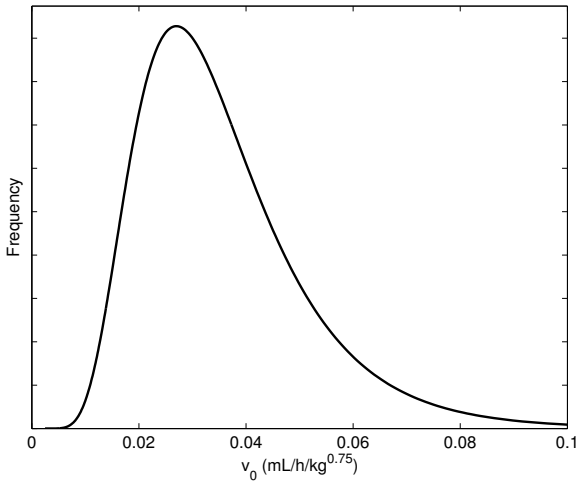

Figure 7.6: Posterior distributions of population metabolic parameter, assuming basal clearances of all PCBs are derived from a single common distribution.

Table 7.6: Posterior distributions of consolidated basal metabolic parameters and modeling errors

Parameter	Unknowns	Posterior value	Uncertainty CV†
Basal metabolic rate	μv_0^{all}	0.027	0.03
(L/h/BW$^{0.75}$)	Σv_0^{all}	0.43	0.08
Model/data error	σ_{fat}	0.30	0.08
	σ_{plasma}	0.23	0.08
	σ_{liver}	0.40	0.05

†Coefficient of variance of chain

Model evaluation

The model was evaluated by comparing predictions to the optimization data, and to data which were omitted during parameter estimation (a evaluation dataset consisting a rat randomly selected from each dose-level/dose-protocol/sacrifice-time). Figures 7.7(a-d) and 7.8(a-d) illustrate the variation in the population model predictions. These simulations consisted of 1000 model runs using parameters randomly sampled from the posterior distributions (Table 7.5), and body weights/liver weights randomly sampled from the data. Model/data error terms were excluded, and therefore the variations in model predictions are a direct result of the estimated parameter variation. These are compared with the data for all rats used in the optimization (the evaluation datasets were excluded). Figures 7.7(a-d) illustrate results for PCB 153 in plasma at the low dose (negligible induction), and Figs 7.8(a-d) show results for PCB 118 in plasma and liver at the high dose (large induction effect). The ranges of predictions are consistent with the variability and scatter observed in the data. It should be noted that due to simplifying assumptions in the model (i.e. neglecting NLE ratio variability and uncertainty, and assuming negligible variation of the induction factor), some model uncertainties are inherent in the estimated parameter variation.

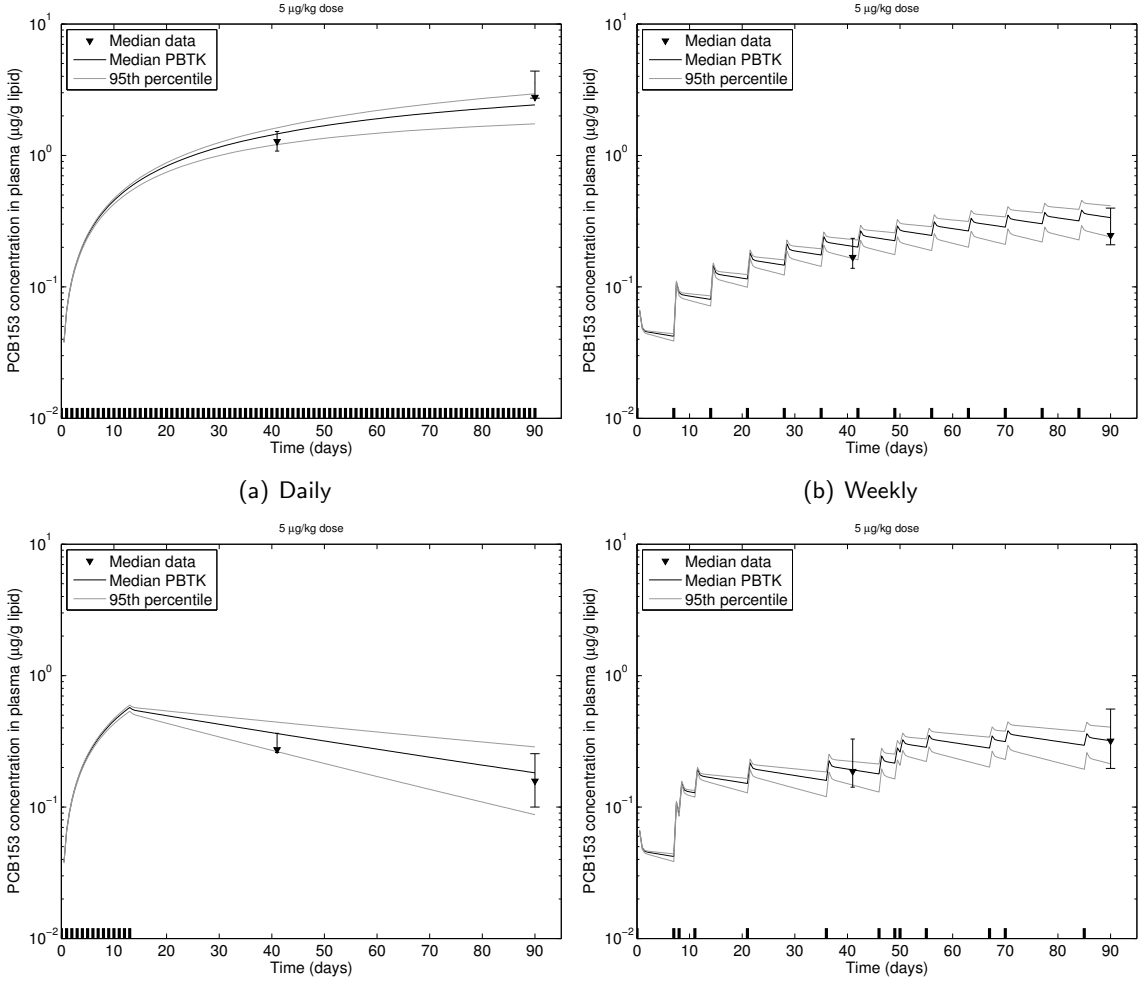

Figure 7.7: Model predictions and data for PCB 153 concentrations in total plasma lipid at 5 µg/kg exposure. Points indicate the median measurement across the rats at time of sacrifice, and error bars indicate the minimum and maximum data.

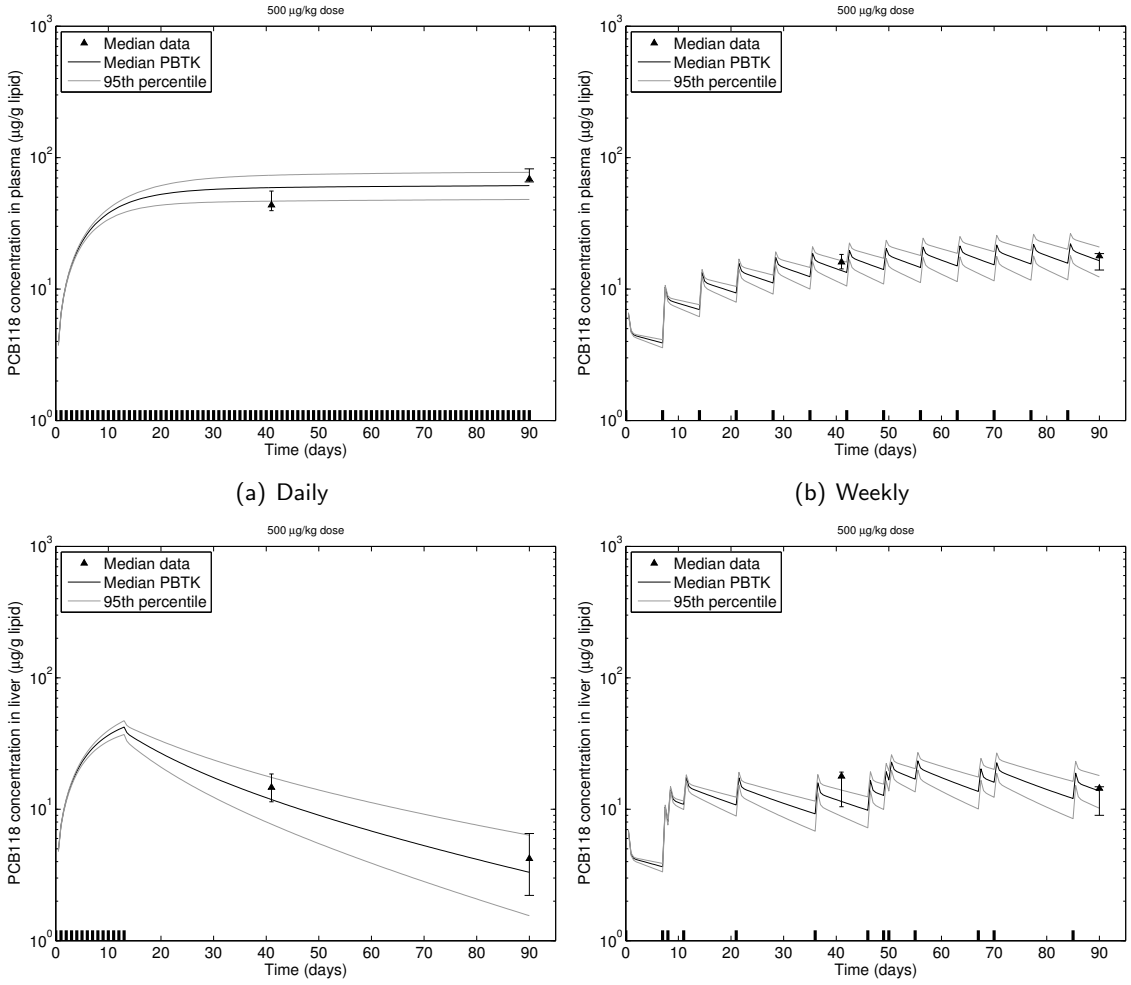

Figure 7.8: Model predictions and data for PCB 118 concentrations in total plasma (a,b) and liver (c,d) lipid at 500 µg/kg exposure. Points indicate the median measurement across the rats at time of sacrifice, and error bars indicate the minimum and maximum data.

One rat from each dose-level/dose-scenario/sacrifice-day had been omitted during the parameter optimization, in order to further evaluate model performance. Figures 7.9(a-d) illustrate results of the model (using median parameter values), compared to data for specific rats which were not used during the parameter optimization. Data for body and liver weights for each rat were incorporated in the model. Results were condensed into PCB 118 (non-ortho PCB) and the remaining PCBs (multi-ortho PCBs), since the multi-ortho PCBs followed the same induction model, with data and predictions typically within 10% of each other. A scatter plot comparing model predictions and measured data for the evaluation data set for all PCBs is presented in Figure 7.10.

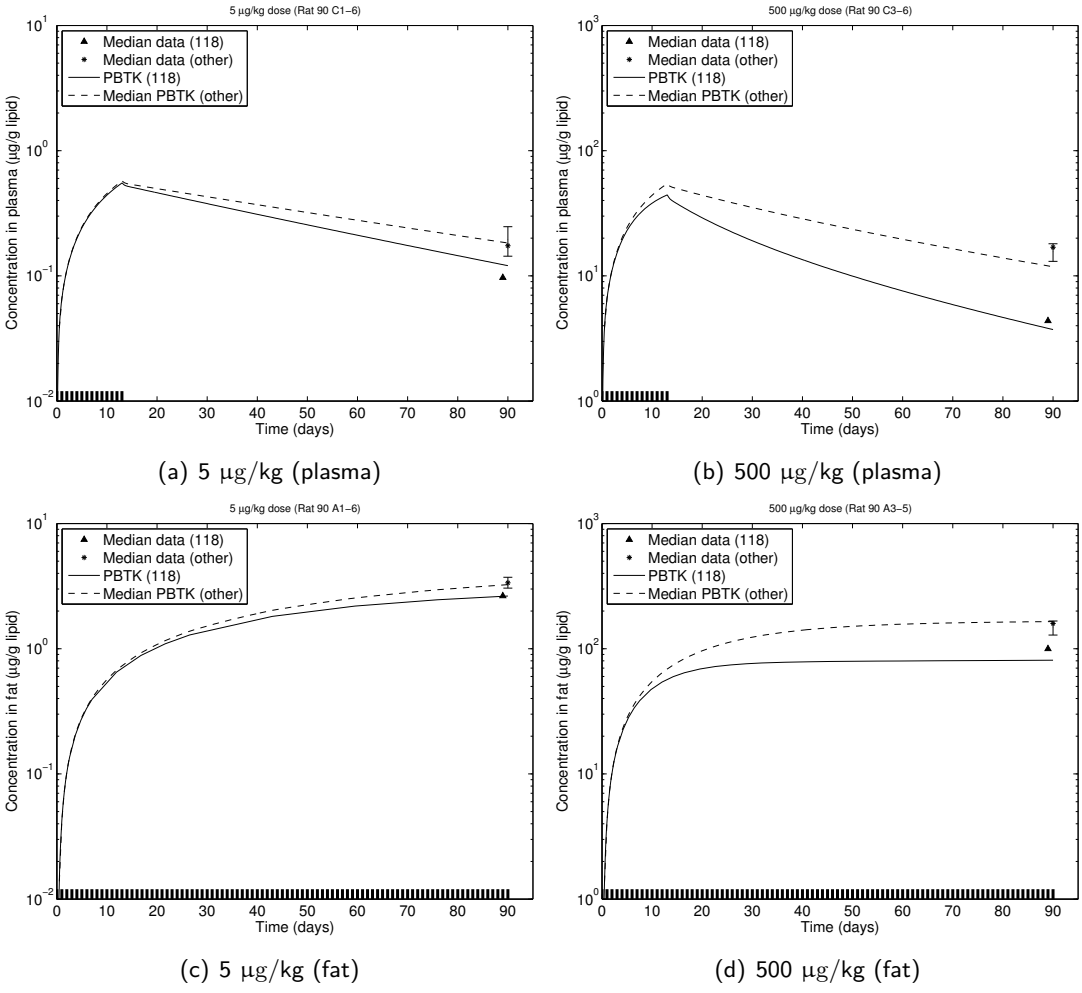

(a) 5 µg/kg (plasma)

(b) 500 µg/kg (plasma)

(c) 5 µg/kg (fat)

(d) 500 µg/kg (fat)

Figure 7.9: Model predictions for PCB concentrations for selected evaluation data. Results and data were condensed to show PCB 118 and the median result of all other PCBs. Points indicate the PCB measurements at time of sacrifice, and error bars indicate the minimum and maximum data for the multi-ortho PCBs.

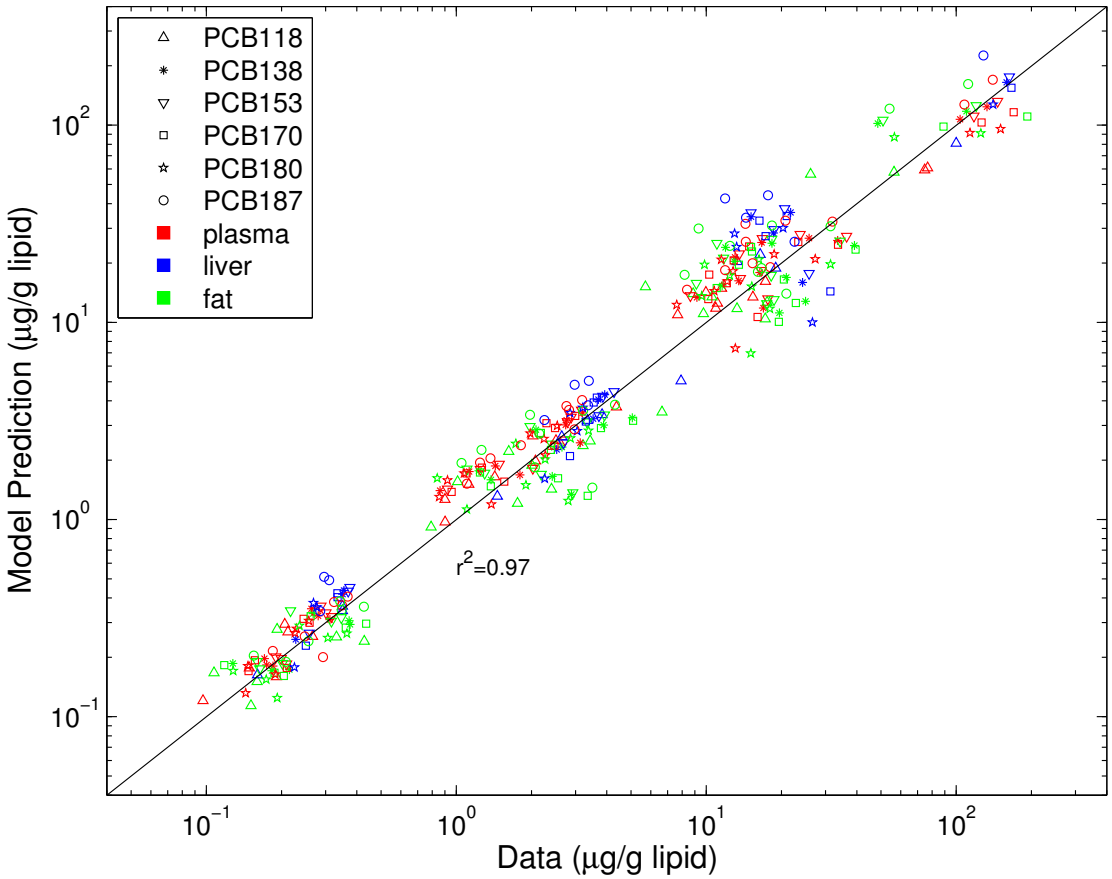

Figure 7.10: Scatterplot of PBTK model predictions vs. measured data for the evaluation dataset. One rat from each dose scenario, dose level, and sacrifice time was used to test the model behavior. Data from these rats were not used in the MCMC analysis. For each rat, data-specific body and liver weight were used to calculate physiological parameters, while median metabolic parameters were used. The model predictions at time of sacrifice were compared to the corresponding data. Data consisted of PCB concentration measurements in total lipid of plasma, liver and fat tissue.

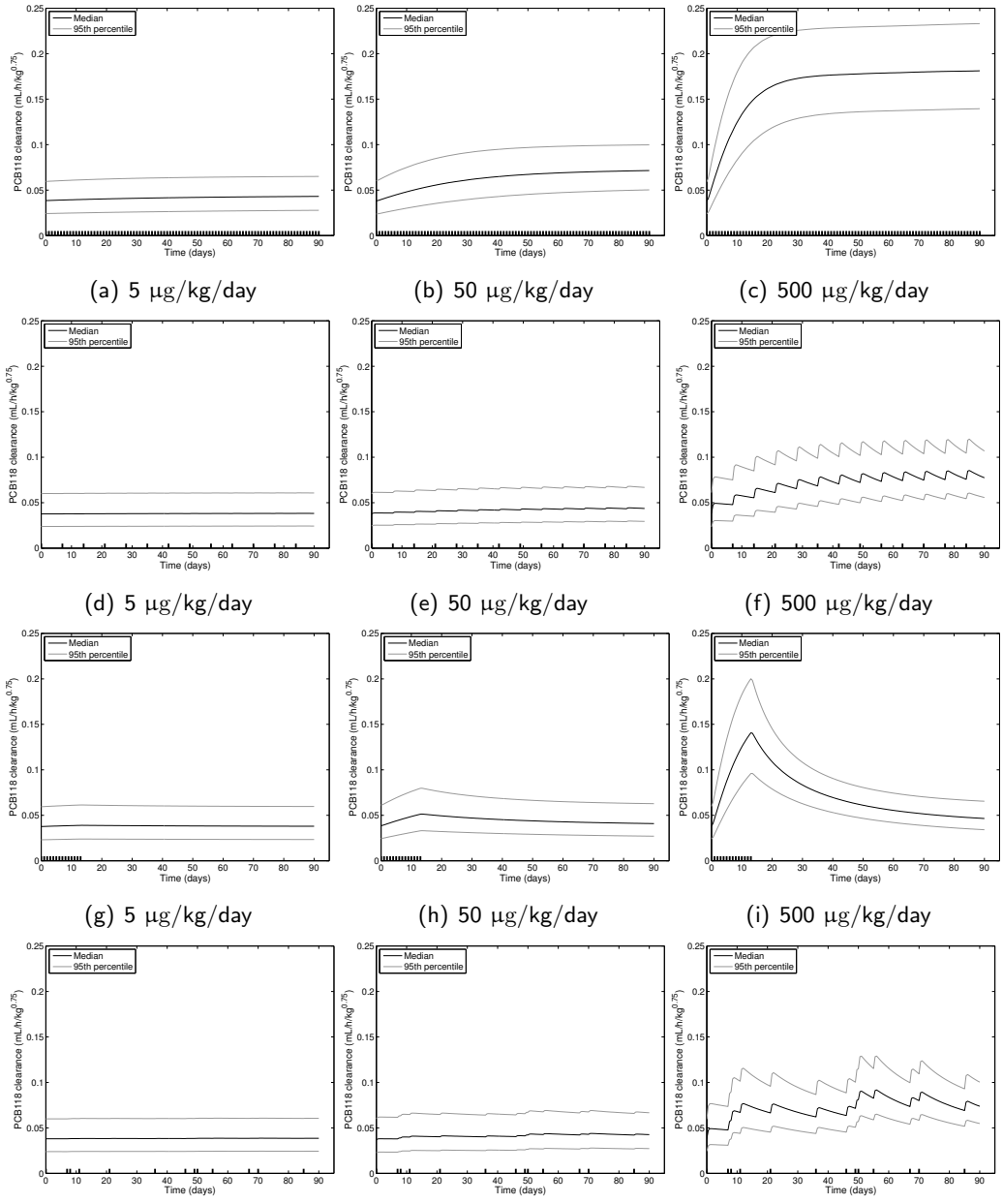

(a) 5 μg/kg/day (b) 50 μg/kg/day (c) 500 μg/kg/day

(d) 5 μg/kg/day (e) 50 μg/kg/day (f) 500 μg/kg/day

(g) 5 μg/kg/day (h) 50 μg/kg/day (i) 500 μg/kg/day

(j) 5 μg/kg/day (k) 50 μg/kg/day (l) 500 μg/kg/day

Figure 7.11: Predicted metabolic clearance of PCB 118 as a function of dose level and frequency using 500 random samples from the parameter posterior distributions. It was assumed the metabolic increase of clearance for PCB 118 was due only to CYP1A induction. Induction is negligible at the lowest dose. At the highest continuous dose level, metabolic clearance of PCB 118 may increase by a factor of 5; at other dose levels or dose patterns, the increase is lower (or occurs for a short time period). This remains consistent with previous observations by [123], but is now modeled as a continuous function across all dose levels and frequencies.

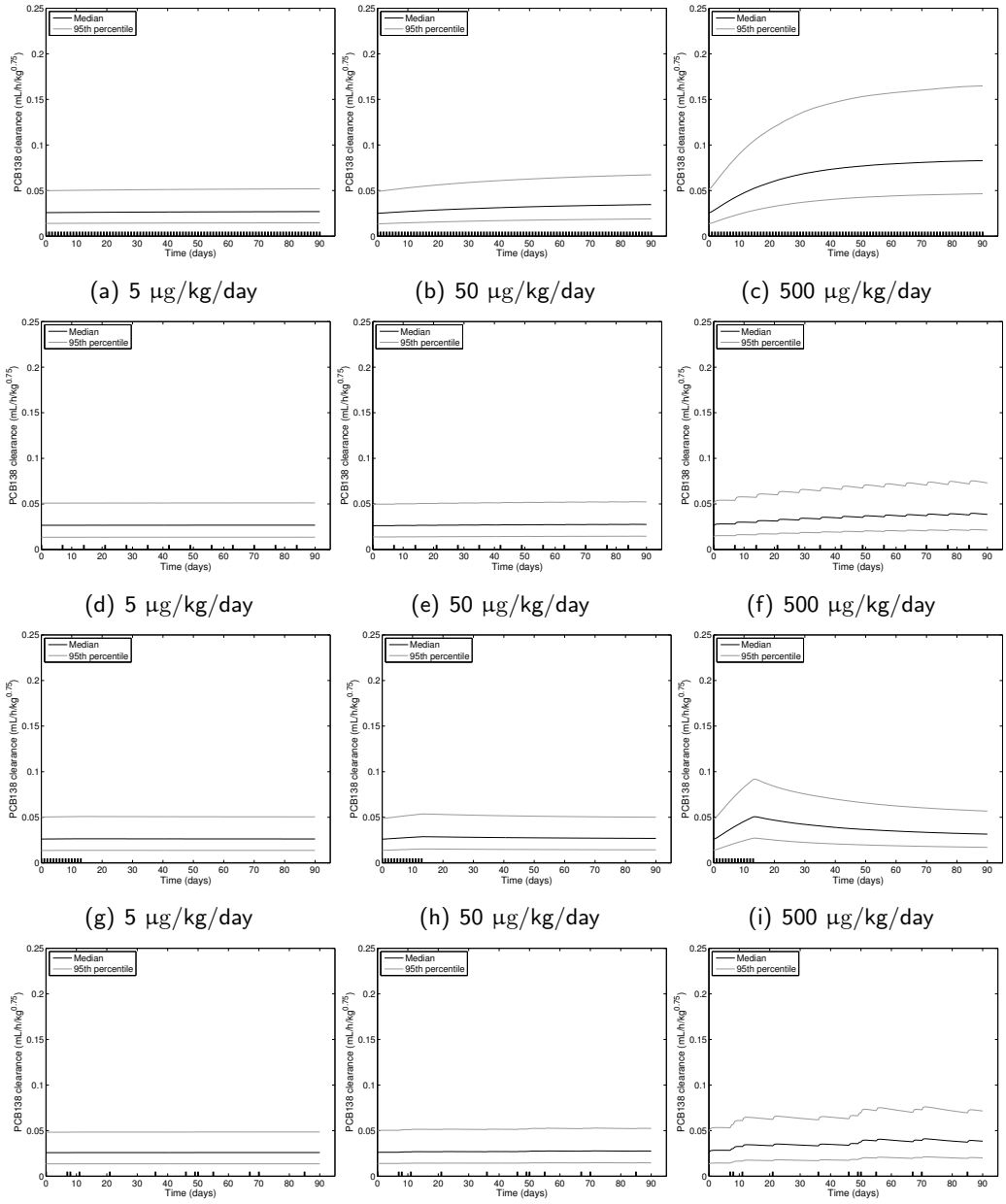

(a) 5 μg/kg/day (b) 50 μg/kg/day (c) 500 μg/kg/day

(d) 5 μg/kg/day (e) 50 μg/kg/day (f) 500 μg/kg/day

(g) 5 μg/kg/day (h) 50 μg/kg/day (i) 500 μg/kg/day

(j) 5 μg/kg/day (k) 50 μg/kg/day (l) 500 μg/kg/day

Figure 7.12: Predicted metabolic clearance of PCB 138 as a function of dose level and frequency using 500 random samples from the parameter posterior distributions. It was assumed the metabolic increase of clearance for all multi-ortho PCBs was due to CYP2B induction. Induction is negligible at the two low doses. At the highest continuous dose level, metabolic clearance of the multi-ortho PCBs (such as PCB 138) may increase by a factor of 3. The overall induction effect is much lower than for PCB 118. This remains consistent with previous observations by [123], but is now modeled as a continuous function across all dose levels and frequencies.

The performance of the induction model remained consistent with previous observations by [123]. At the highest continuous dose level, metabolic clearance of the multi-ortho PCBs may increase by a factor of 3, while clearance of PCB 118 may increase by a factor of 5. The increase in metabolic rates vary by dose protocol, due to differences in CYP450 induction dynamics. At the lowest dose, the model predicts negligible increase in metabolic clearance for both PCB groups. No additional re-parameterization was necessary to constrain the model to predict zero induction at the lowest dose. The model was able to simulate induction as a consistent function across all dose levels and protocols, while sufficiently reproducing observed data.

The lipid-based toxicokinetic model did have some inherent limitations. Because it does not include partition coefficients for each PCB/tissue combination, the model cannot capture differences in the ordering of PCB concentrations that are observed between different tissues of the same rat. Individual PCBs are predicted to have the same ordering of concentrations in all tissues, with the ordering dependent only on metabolic clearances. All PCBs follow identical mass balance equations, except for metabolism. The Bayesian framework implicitly incorporated these ordering discrepancies in the model/data error for each tissue. The error parameter σ for liver was highest, partially because liver data had many inconsistencies in PCB concentration order.

Figure 7.13 illustrates how frequently each PCB was measured at a particular order in concentration for each experiment (rat). For example, Figure 7.13c shows that for fat, PCB 187 was measured as having the highest concentration (over 50% of the time), while PCB 118 had the lowest (80% of the time). While PCB 118 is observed as having the lowest concentration in all tissue lipids for most of the rats, there is a tissue-dependency among the ordering of multi-ortho PCBs. For example, PCB 180

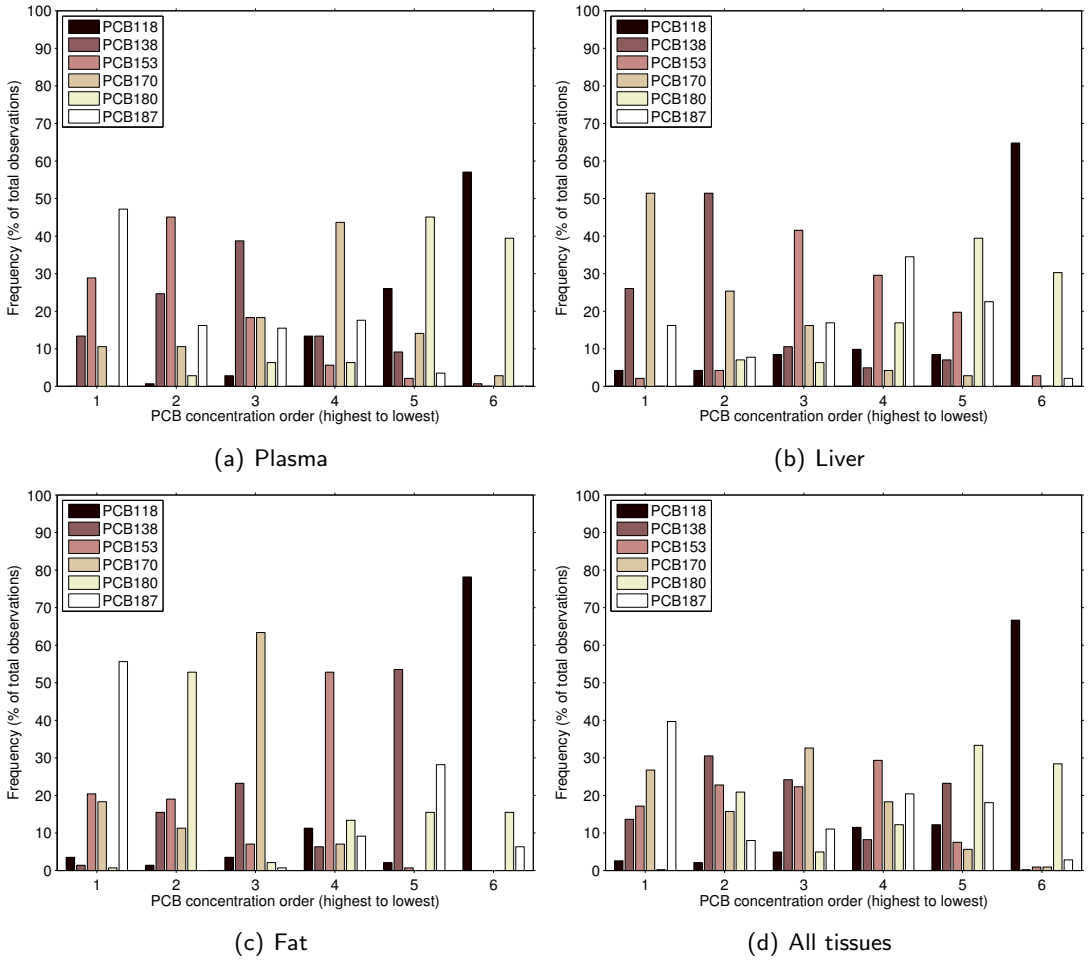

Figure 7.13: Measured PCB concentration order within rats. The ordering of the multi-ortho PCBs is not always consistent in all tissue lipids.

was observed as having the second highest PCB concentration in fat lipid (for over 50% of the observations), but usually had either the lowest or second-to-lowest concentration in plasma and liver lipids. PCB 187 usually had the highest concentrations in plasma and fat, but not liver. The model cannot account for these differences in PCB order between tissues of the same rat (it simply predicts the ordering in all tissues being equal to the ordering of clearance rates). However, the magnitude of the differences between non-ortho PCB concentrations are relatively small, and there is a benefit of not needing to estimate tissue/plasma partition coefficients for hundreds of highly-lipophilic compounds.

7.1.4 Discussion

This is the first application of a large-scale population Bayesian analysis to a lipid-based PBTK model for mixtures. Despite inflexibility inherent in these types of models (no partition coefficients to fit tissue data), the final model adequately reproduced experimental data in multiple tissue lipids, for varying dose levels and protocols. The incorporation of an induction dose response model using only neutral lipid based concentrations was also shown to be possible.

One of the main assumptions of the model is negligible induction at low doses. For low doses of PCB 126 (a potent dioxin-like non-ortho PCB) in rats, in-vivo studies have shown significant increases in EROD (7-ethoxyresorufin-O-deethylase) activity (which is indicative of CYP1A). A 10-fold increase in EROD activity has been observed after a single 7.5 μg/kg dose [136], and a 95-fold increase was observed for 1 μg/kg/day exposure [378]. Low-dose induction of CYP2B, indicated by PROD (7-pentoxyresorufin-o-dealkylase) activity, due to mixtures of mono-ortho and multi-ortho PCBs has also been observed [88]. The current model assumption of negligible induction for the low-dose data could have biased the results if low-dose PROD and EROD increases indicate significantly increased observable metabolic rate. However, the increase in PROD or EROD is less pronounced than the increase in in-vivo metabolic rate. In a study of rats exposed to octamethylcyclotetrasiloxane (D4), measured hepatic CYP2B concentration and PROD activity at maximum induction were 40 fold greater than the basal levels, and the maximum induced CYP2B production rate for the PBTK model was assumed to be 165 fold greater than the basal production rate. Meanwhile the maximum increase in the metabolic rate of D4 was only 2 fold [324]. Despite the over 100 fold increase in PROD or EROD activity which might have been caused by levels of PCBs in the

current data, there was at most a 6-fold increase in observed metabolic rate [123]. Since the increase in metabolic rate between the 5 and 50 μg/kg dose levels was very minor, the assumption of negligible rate increase between the "true" basal rate and the low dose rate is likely valid.

Other simplifying assumptions include linearization of biological exposure-response, neglecting Ah-receptor binding, and discretized the induction problem into only 2 PCB groups (multi-ortho and non-ortho) and 2 enzyme groups (CYP1A and CYP2B). Competitive inhibition for P450s [72], regional hepatic P450 induction [79], and induction of Phase-II metabolic enzymes [136] were also neglected. Such model complexities lie outside the scope of this work, and would have made a population Bayesian analysis infeasible.

A curvilinear dose-response cannot be derived since only three widely-spaced dose levels were analyzed. Additional data relating steady-state PCB levels in liver lipids with increase in metabolic rate might be used to extrapolate a Hill relationship from the current observations. For the current set of exposures, a CYP450 balance with a linear dose-response model was sufficient.

7.2 Application of toxicokinetic models to biomarker inversion

7.2.1 Background

Biomarker data can be used as early indicators of a biological effect for assessing health risks and in identifying contributors to exposures, thereby aiding health risk management planning. However, the use of biomonitoring data has primarily focused mainly on assessing the effectiveness of pollution controls for relatively straightforward exposure scenarios, such as those involving inert and persistent chemicals with relatively

long biological half-lives and well-defined sources of exposure (i.e. lead). For complex exposure scenarios, the use of biomonitoring data in designing and evaluating exposure reduction strategies may require significant amounts of supporting exposure information (e.g. variability in source activities and in background concentrations, and multimedia dynamics of the chemical.)

A computational framework that can address both the forward and inverse modeling aspects of exposures to multiple chemicals will enable enhanced interpretation of biomarkers through systematic reconstruction of human exposures. Physiologically Based ToxicoKinetic (PBTK) and Biologically Based Dose Response (BBDR) models in conjunction with numerical inversion techniques and optimization methods should form major components of such a framework. Eventually, a comprehensive exposure reconstruction framework should address reconstructions involving aggregate (i.e. from multiple exposure routes) and cumulative (i.e. for multiple chemicals) exposures.

Various computational techniques have been employed in the literature for numerical model inversion in general and for exposure reconstruction from biomarkers in particular. Georgopoulos et al. [155] used the Maximum Likelihood Estimation (MLE) method in conjunction with Physiologically Based Pharmacokinetic (PBPK) modeling for reconstructing short-term (30 minute) exposure to chloroform, and to resolve the total dose between two routes of uptake (i.e. inhalation and dermal absorption). Furthermore, Roy and Georgopoulos [318] used the combined MLE-PBPK modeling approach with synthetic biomarker data (simulated exhaled breath concentration) and demonstrated that it is mathematically feasible to reconstruct longer term exposures to VOCs. Rigas et al. [310] used urinary biomarker data and the inverse solution of a simple, two-compartment pharmacokinetic (PK) model for chlorpyrifos to estimate

the magnitude and timing of doses, based on the Minnesota Children's Pesticide Exposure Study (MNCPES) [302]. Some recent studies on population-level exposure reconstruction focused on data sampled from distributions of biomonitoring studies such as NHANES using direct deconvolution of biomarker distributions assuming a linear response [356], or a brute-force Monte Carlo sampling approach [343, 355].

Recognizing the limitations of existing methods for interpreting biomonitoring data is important, and the discussion that follows explores the issues and reveals priorities in conducting future work in this field of interpretation of biomonitoring data.

7.2.2 Methods for Exposure Reconstruction from Population Biomonitoring Studies

Computational inversion can be formulated as an optimization problem where the objective is to identify the specific input combinations or distributions that best explain the observed outputs while minimizing an "error metric". In case of exposure reconstruction, the inputs are the exposure and dose estimates, the outputs are observed biomarkers, and the error metric can be defined in terms of unknowns (i.e. population variation or random error).

Exposure Conversion Factor (ECF) Approach

This method, proposed by Tan et al. [356], assumes that the relationship between biomarker and dose can be approximated by a linear function for exposure reconstruction purposes. This approach involves three steps: (1) generating samples for forward model runs from distributions of possible exposure, physiological, and biochemical parameters, (2) running the forward model using a set of input samples from these distributions, and (3) inverting the distribution of output (i.e. simulated biomarker levels) to obtain an "exposure conversion factor" (ECF). Using the ECF and the distribution of

observed biomarkers, the possible exposures for that particular biomarker distribution can then be estimated through a straight-forward convolution.

For example, the PBPK model can be run using a unit dose or concentration value, and various samples from the possible distributions of variables such as activities, physiological parameters, biochemical parameters, biomarker sample times, etc., and a set of biomarker levels is generated. These levels then provide the distribution of biomarkers for a unit exposure metric, which can be inverted to obtain an ECF in units of the exposure metric divided by biomarker level units. The ECF can then be multiplied by available biomonitoring data (e.g. from biomarker databases such as NHEXAS or NHANES) to produce an estimate of dose distributions for the corresponding population. Though this method is conceptual simple and straightforward to use, the ECF can be highly sensitive to the assumptions of the prior distributions, while the linearization can sometimes produce very large tails in the distribution of reconstructed exposure metrics.

Discretized Bayesian Approach

This approach, used, for example, by Sohn et al. [343] and Tan et al. [355], employs a simplified, discrete Bayesian scheme to estimate the posterior probability of exposures from the biomarker data and prior exposure distributions. Posterior probabilities of exposures/doses are computed using biomarker data and forward model results at regularly spaced samples ("bins") or random samples, spanning the range described by prior probabilities. The posterior probability is estimated from the samples that agree most closely with the biomarker data (e.g. within a small percentage variation). This method, like the ECF method, requires strong informative prior probability distributions of exposure-related activities in order to produce a realistic reconstruction.

Furthermore, as the number of dimensions increases the sampling space becomes "vastly empty" [360]. This approach, therefore, necessitates trade-offs with respect to sample size, the resolution of the sampling, and the accuracy of the results.

Bayesian Markov-Chain Monte Carlo (MCMC)

The MCMC approach provides a means for sampling from the "posterior probability distribution" without having to sample the entire range of the prior distribution. The method requires defining the prior distributions, available biomarker data, and a likelihood function defining the likelihood of the data given a set of forward model parameters; then the MCMC approach involves marching in the sample space based on an acceptance criteria that consider the likelihood of the data given the parameters. Markov-Chain Monte Carlo (MCMC) techniques have been coupled with PBPK models for forward-modeling of population health risk assessment [92], and inverse modeling for parameter estimation [410]. In practice, with adequate data and prior information on exposure metrics and population toxicokinetic parameters, it is possible to directly apply MCMC techniques to estimate individual and population exposure parameters. The data requirements are typically demanding – including multiple biomarker measurements for each individual during each measurement period. However, when sufficient information is not available for estimating individual parameters, the estimation of population parameters using MCMC and PBPK models becomes impractical. This is often the case, as for example with studies such as NHEXAS and NHANES, which include relatively few biomarker measurements (often just one measurement) for different individual-chemical combinations.

7.2.3 Major Factors Influencing Exposure Reconstruction

Several major factors influence the feasibility and efficacy of exposure reconstruction from biomarkers. The specificity and the sensitivity of the biomarker with respect to the exposure metric of interest (e.g. concentration of the agent of concern) are two of the most important such factors. Lack of specificity can lead to the problem of identifiability, whereas the lack of sensitivity may result in large uncertainties in the reconstruction results. Biochemical properties of absorption, distribution, metabolism, and elimination (ADME) impact the types of exposures that can be estimated from the biomarker data [181]. Variability in ADME characteristics also results in a significant variation in the biological half-lives of different groups of environmental pollutants such as, e.g. volatile organics, organophosphate pesticides, and toxic metals. Some of these properties are also highly variable for a given contaminant within a population reflecting inter-individual physiological and biochemical variabilities, which may result in additional uncertainties in the use of biomarkers for exposure reconstruction.

Various exposure characteristics such as the frequency, magnitude, and duration of exposures, can provide supplemental information that can aid or is necessary for the reconstruction of exposures from biomarkers. Because exposures can occur through multiple pathways and mechanisms (e.g. direct exposure to a metabolite versus exposure to the parent compound), supplemental exposure data such as mouthing behavior, activities, source locations and personal monitoring, can also provide estimates of realistic constraints on possible exposures from specific pathways. Additionally, the adequacy of the biomarker data can be characterized in terms of the specificity of the available supplementary information such as the time of collection of biomarkers in relation to significant events (e.g. amount of urine collected, urinary void volume, last time of

urination, etc.) Other characteristics of the data sets such as the detection limits can also significantly impact the reconstruction process. In practice, two other factors impact the inversion process significantly: the applicability and adequacy of the forward model (e.g. toxicokinetic/toxicodynamic model) and the efficacy of the computational inversion technique used.

Impact of Biochemical Properties and Sampling Characteristics on Reconstruction

The "residence time" or "age" of an "observed" (i.e. measured) biomarker molecule can be defined as the time elapsed since it entered (or was generated in) the organ or organism studied. The observed exposure biomarker levels (molecules of either a chemical or its metabolites) represent an integration over molecules of different "ages", dependent on the time each molecule entered or was generated in the system, and elimination kinetics (i.e. potentially multiple exposures across multiple timescales). As an example, for chemicals and metabolites with short half-lives, only the exposure history of the previous days or weeks can be estimated. For those with longer half-lives, larger timescales of exposure history have to be considered, and the influence of confounding sources creates additional uncertainties.

In general, the age or residence time distribution can be defined as $R(t) = b(t)/\int_0^\infty b(t)dt$, where $b(t)$ is the concentration of a chemical in the system (i.e. a single biomarker concentration in blood, tissue, or urine concentration) at time t. Furthermore, $R(t)dt$ represents the fraction of the molecules that have spent a time between t and $t + dt$ in the system. The corresponding cumulative distribution function, $F(t)$ is the fraction of the molecules that have spent time t or less in the system, and is given by $F(t) = \int_0^t R(t)dt$.

In the simplest case of a steady, continuous exposure, and toxicokinetics that can be

described adequately by a single-compartment PK model, $b(t) = x'e^{-kt}$, $R(t) = ke^{-kt}$, and $F(t) = 1 - e^{-kt}$, where x' is a known exposure concentration, and the elimination rate k is related to half life $t_{1/2}$ as $k = \ln(2)/t_{1/2}$.

In the case of discrete "cyclical" exposures of time period Δt, assuming that the biomarkers are collected at a time $\lambda\Delta t$ after the end of the last exposure (where λ is an arbitrary fraction of total time between exposures, $0 < \lambda \leq 1$), and that all exposure concentrations are equal to x', the relative contribution of exposures that occurred at different times can be expressed in terms of "cycles" of exposure, as follows:

$$b(n) = \sum_{i=0}^{n} x'e^{-k(i+\gamma)\Delta t} \quad \text{and} \quad F(n) = \sum_{i=0}^{n} e^{-ik\Delta t} \Bigg/ \sum_{j=0}^{\infty} e^{-jk\Delta t} \tag{7.8}$$

Figure 7.14 shows, as a function of different half-lives, the relative contributions of different time-scales of continuous, steady exposures to observed chemical biomarker levels in a single-compartment system. These calculations are an extension of the approach presented in [275]. Figure 7.15 shows the relative contributions of prior exposures (discrete bolus doses) to observed chemical biomarker levels, as a function of different sampling times and exposure frequencies.

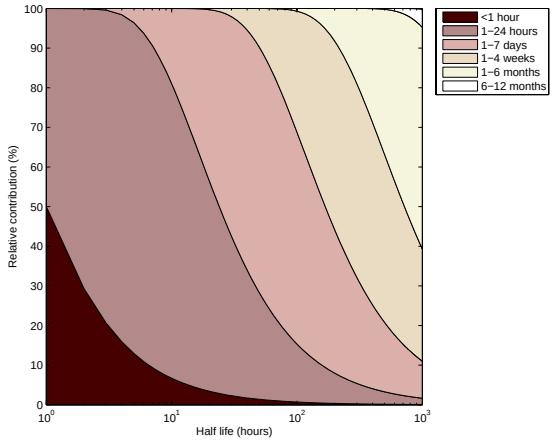

Figure 7.14: Impact of half-life on the relative contributions of different time-scales of exposures to observed chemical biomarker levels. The example shown above is based on a one-compartment PK model (linear decay); the biomarker represents the level of chemical in the compartment.

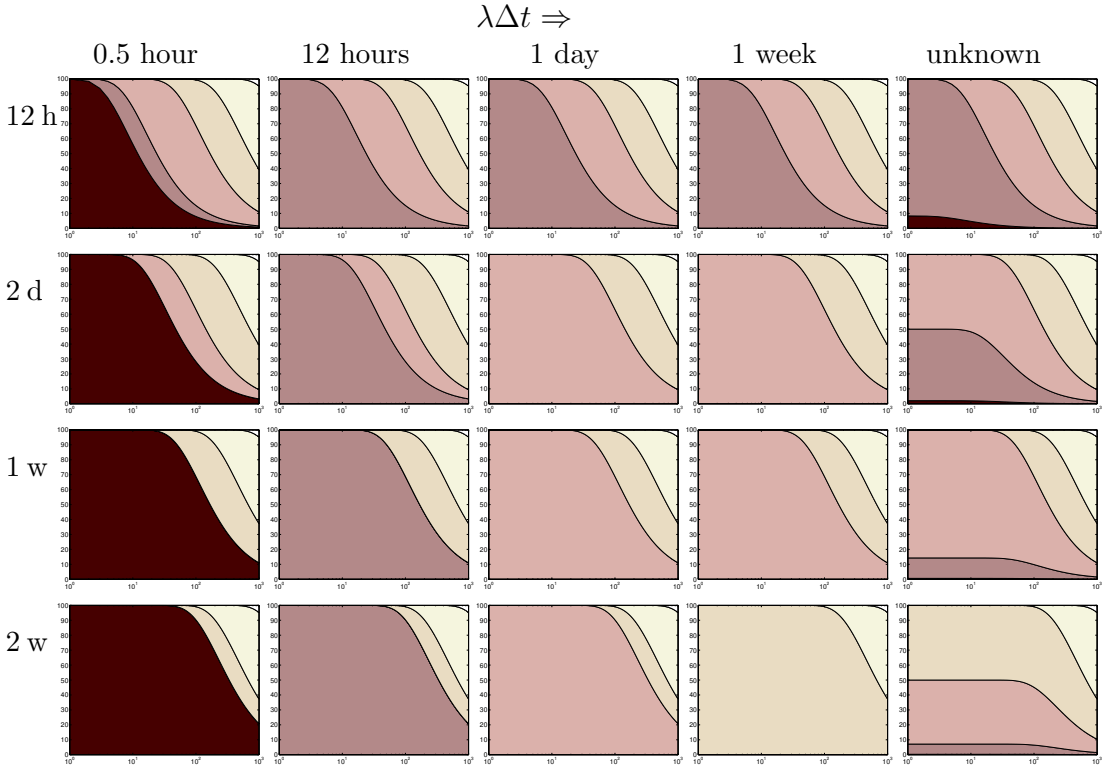

Figure 7.15: Contribution of prior exposures to observed biomarker levels as a function of intake frequency, sampling time, and biochemical properties. The rows represent the time period of exposure (e.g. every 12 hours, every 2 days, etc.), the columns represent the time of sampling after the last exposure. For cases when sampling time is unknown, the mean value of the contributions are shown, assuming a uniformly random sampling time. The legend for the colors is the same as in Figure 7.14.

When Δt is significantly larger than the exposure time scale of interest (β), $\lambda\Delta t$ becomes an important variable. When $\lambda\Delta t \leq \beta$, the biomarker captures exposures occurring within the past time period β. Otherwise, exposures occurring within β are not captured. It must be noted that the relative contributions are independent of the time of sampling within a cycle, whereas the relationship between the magnitude of the observed biomarker concentration and the exposure concentration are highly dependent on the time of sampling within a cycle.

As an example, consider a scenario where exposures occur once per month ($\Delta t =$ 1 month), and the biomarker contribution due to exposure within the past one day is known (β). If a sample is taken 12 hours after the last exposure ($\lambda\Delta t$), the biomarker will incorporate contributions which originate from exposure occurring within the past 24 hours. If the sample is taken 30 hours after the last exposure, there is zero mass contribution due to exposures within the past 24 hours. Figure 7.15 illustrates the effect of $\lambda\Delta t$ and Δt on the half-life and exposure time-scale relationship previously shown for the steady-state case in Figure 7.14.

As the length of time between biomarker sampling and the last exposure increases, contribution to biomarker from recent exposures diminishes. As cyclic exposure frequency decreases, relative contributions become more sensitive to biomarker sampling time. If exposures occur with high frequency, the system approaches steady-state and relative contributions are less sensitive to sampling time. In general, the residence time analysis approach can be readily expanded to include realistic PBPK models instead of half-life parameterizations, and estimates such as those shown in Figure 7.15, can be generated for different types of exposure and sampling profiles for different classes of compounds. The results from the residence time analysis can provide a screening

level estimate of the types of reconstruction that are feasible for a given chemical, biomonitoring characteristics, and possible exposure profiles.

7.2.4 Toxicokinetic model for chlorpyrifos exposure

The toxicokinetic model for chlorpyrifos (CPF) exposures is adapted from a 2-compartment PK model for CPF and the metabolite 3,5,6-trichloro-2-pyridinol (TCPy) used by Rigas et al. [310]. The rapid transformation 1 of CPF to TCPy, and the fact that currently available CPF PBTK models [374, 375] describe TCPy using 1-compartment kinetics, is the basis for this assumption. The toxicokinetic model is described by:

$$\begin{aligned} \frac{dC_a}{dt} &= -k_a\, C_a \\ \frac{dC_b}{dt} &= k_a\, C_a - k_e\, C_b \\ \frac{dU_{TCP}}{dt} &= k_e\, C_b\, V_d \\ C_a &= C_a(t_o) + \frac{S\,R\,F\,D_{\mathrm{CPF}}}{V_d} \quad \left(\frac{M_{\mathrm{TCP}}}{M_{\mathrm{CPF}}}\right) \end{aligned} \tag{7.9}$$

where, M_{TCP} is molecular weight of TCPy; M_{CPF}, molecular weight of CPF; D_{CPF}, bolus dose of CPF (μg); C_a, concentration of TCPy in absorption reservoir (μg/L); $C_a(t_o)$, concentration of TCPy in absorption reservoir before bolus event at time t_o (μg/L); C_b, concentration of TCPy in body (μg/L); F, absorption factor for ingested dose; R, stoichiometric ratio of CPF to TCPy; S, selectivity (molar amount that can be collected as metabolite); V_d, volume of distribution (L); k_e, elimination rate constant (/h); k_a, absorption rate constant (/h).

7.2.5 Case Study 1: Chlorpyrifos dose reconstruction from available NHEXAS-MD data

The NHEXAS Maryland (NHEXAS-MD) data set is longitudinal, and contains multiple biomarker and environmental measurements for households over a period of time. With respect to chlorpyrifos, the available biomarker data are urinary TCPy measurements

corresponding to the first void of the day. The concentrations of chlorpyrifos in food, air (at home), dust, etc., are also provided. The corresponding TCPy concentrations in food, however, were not measured. The food intake can be estimated through the four day duplicate plate, but the actual amount of food consumed is not easily available. The urinary void volume, the time of earlier urination, and the last food intake time, are also not available, thus introducing significant uncertainties into the exposure reconstruction process.

Here, two exposure scenarios are examined:

1. Steady-state, continuous exposure, which neglects potential issues in temporal variability in both exposure timing and biomarker sampling (referred to in the following as Scenario 1).

2. Time-varying dose and biomarker collection, assuming "reasonable" distributions for the frequency of intake and for the timing of the biomarker collection. An analysis on two separate time-varying exposure scenarios are performed, each assuming different constraints on the exposure profile (referred to in the following as Scenario 2):

   (a) Bolus dose frequency modeled as a complex time-activity profile. An individual may consume zero, one, two, or three meals containing CPF in a given day. An exposure may occur randomly on any, all, or none of the days in a week. More details of this scenario are given in Section 7.2.9.

   (b) Bolus dose frequency fixed at certain values (i.e. once per day, once per week).

   (c) Modifications and combinations of 2a and 2b. These include scenarios where

a background CPF inhalation dose occurs (sampled from summary distributions presented by Pang et al. [287]), and/or dietary exposure to the metabolite TCP occurs.

The NHEXAS-MD data set contains multiple samples per individual. However, for any given individual, the sampling intervals are separated by at least a month. Since the biomarker half-life is approximately one day [15], it is assumed that the measurements for the same individual at different sampling intervals are independent, and the correlations between them are assumed to be negligible.

There are significant differences in the uncertainties associated with cases 1 and 2. For Scenario 1, the average daily dose (ADD) is distributed evenly throughout the day, and therefore dynamic uncertainties do not exist. For case 2, the ADD is apportioned differently throughout time. The ADD is not known, the apportionment may not be known, and the modeled "biomarker collection time" is randomly assigned to a time before the first meal of the day. Since the half-life of TCPy is one day, there is the potential that a sampled individual receives a high ADD which occurs infrequently. Depending on the sampling time, the biomarker level can vary between extremely high, to non-detectable levels. The less frequent the exposure, the more likely the biomarker measurement will be a non-detect, regardless of the exposure magnitude. Other simulated individuals may receive a moderate dose once per day, and the biomarker profile approaches the steady-state condition. A more detailed discussion on exposure frequency, average daily dose, and biomonitoring can be found in Hays et al. [181].

In this case study, uncertainties on PK parameters are assumed to be negligible and are set to the mean values based on an original pharmacokinetics study by Nolan et al. [266]. For both the steady-state and time-variant biomarker dose reconstructions,

only the total dose absorbed is considered because the absorption fraction and intake amount are coupled, and hence, individually unidentifiable. There is also a factor of two difference in the fraction absorbed that has been found across different studies (e.g. [266] and [374]).

The toxicokinetic model is used to predict cumulative amount of TCPy excreted in urine. The biomarker is estimated from the model calculations of cumulative TCPy excreted over a over a 6-10 hour period (uniform random), resulting in an average TCPy excretion rate. NHEXAS biomarkers are assumed to represent morning void samples, with overnight bladder TCPy accumulation occurring over approximately 8 hours. Converting model output (in mass TCPy/day) to biomarker measurement units (mass TCPy/volume urine, and mass TCPy/mass creatinine) introduces additional uncertainties, since urinary liquid or creatinine excretion rates must be known. The NRC Biomonitoring report [275] notes that inter- and intra-individual variation in urinary water and creatinine content can be a source of biomarker misinterpretation (specific discussion on chlorpyrifos exposure and TCPy biomarkers is also contained in the report). The following three methods for converting the units are evaluated:

- For data from the Minnesota study, Rigas et al. [310] converted measured urinary TCPy concentrations to urinary TCPy excretion rates. TCPy concentration in urine is multiplied by urine void volume, and divided by the length of time urine accumulated in the bladder (estimated from the Minnesota study questionnaire). However, the NHEXAS-MD study does not provide urine void volume amounts, so this approach has not been used here.

- An assumption of a mean daily liquid urine output of 22 mL/kg body weight can

be used to convert TCPy rates to mass TCPy/volume urine [261, 400].

- Age, gender, body weight, and body height relationships can be used to estimate creatinine excretion rates [244]. This converts TCPy rate to mass TCPy/mass creatinine (which is reported in NHEXAS). Advantages of this method over the above two methods in population exposure assessment have been previously discussed in Barr et al. [30].

7.2.6 Preliminary analysis of the linked PK-biomarker approach using forward modeling

A CPF exposure/dose model for the NHEXAS Maryland population is coded based on the approach of [287] is evaluated for its use as a "prior" estimate of CPF dose. It has been found that by using the exposure estimates from Pang et al. [287] as inputs to the PK model (using both steady state and time-variant assumptions) the TCPy biomarker is significantly under-predicted (Figure 7.16). This leads to the conclusion that the NHEXAS-derived exposure estimates are inadequate for use as "prior" exposure information in this particular case. This limitation can be attributed to one or more of the following possibilities:

- the exposure model is not appropriate, as the available environmental and biomarker measurements correspond to spot-samples,
- food and air concentrations change with time, and more of an exposure history is needed to reduce exposure/dose uncertainty,
- the NHEXAS Maryland population also experiences TCPy exposure, and
- a combination of both TCPy exposure, and uncertainties in CPF exposure/dose modeling exists.

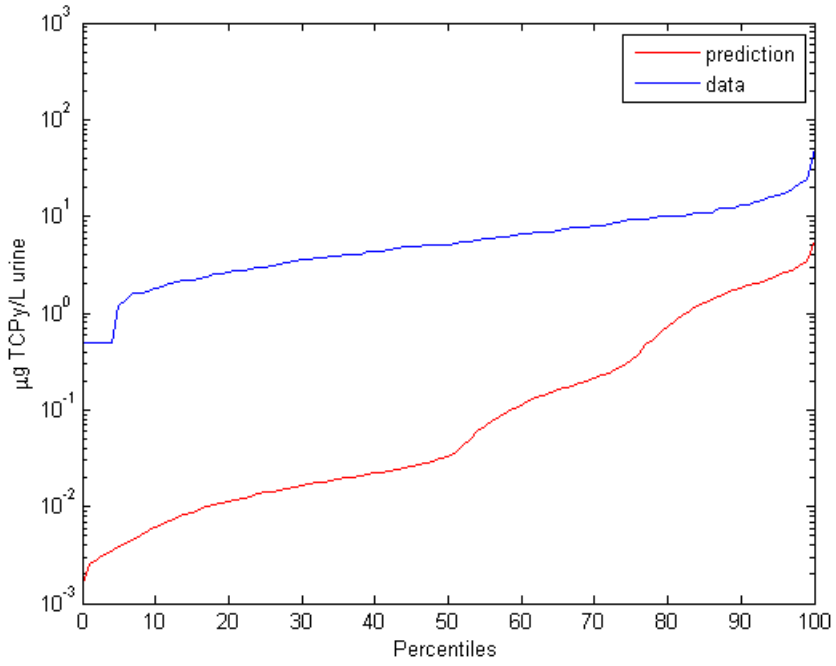

Figure 7.16: Comparison of urinary TCPy biomarker levels predicted using exposure estimates of (Pang et al., 2002) for the NHEXAS-MD population with the toxicokinetic model assuming steady-state exposure, and actual NHEXAS-MD biomarker measurements

Previous studies noted in the NRC biomarkers report have found that levels of TCPy in multimedia are generally comparable to CPF, and TCPy levels in solid food are an order of magnitude higher than CPF [261, 275, 400]. It has also been noted that only a small percentage of dietary CPF exposure correlates with the TCPy levels seen in urine for the NHEXAS Maryland dataset [119, 241], further supporting the possibility that neglecting TCPy exposure in dose-reconstruction over-predicts CPF exposure [29].

For a majority of the inversion test cases, it is assumed that the CPF exposure is the primary source of the TCPy biomarker. However, given the apparent inconsistency of NHEXAS exposure and biomarkers data, an additional biomarker inversion is performed to estimate population CPF exposure that considers direct TCPy exposures (see Case Study 2). This inversion also used the estimates of NHEXAS-MD population

CPF exposures developed by Pang et al. [287]. The PK model has been modified to allow for both CPF and TCPy exposure contributions to urinary TCPy biomarkers, and is used in subsequent exposure reconstruction. Without CPF exposure data, the decoupling of TCPy and CPF exposure contributions to biomarker levels will not be possible.

7.2.7 Computational Inversion Techniques used for Evaluation

Steady-state approximation

Assuming intake and excretion rates are equal, the following equations relate TCPy biomarker and CPF dose:

$$D_{\text{CPF}} = C_{\text{tcp-adj}} E_{\text{cre}} \left(M_{\text{cpf}}/M_{\text{tcp}}\right) \tag{7.10}$$

$$D_{\text{CPF}} = C_{\text{tcp-liq}} E_{\text{liq}} \left(M_{\text{cpf}}/M_{\text{tcp}}\right) \tag{7.11}$$

where

D_{CPF} Bolus dose of CPF (μg)

E_{liq} Urinary excretion rate in (L/day)

E_{cre} Creatinine excretion rate in (g/day)

$C_{\text{tcp-liq}}$ Urinary TCPy biomarker in (μ/g/L urine)

$C_{\text{tcp-adj}}$ Urinary TCPy biomarker adjusted for creatinine concentration (μg/g creatinine)

M_{TCP} Molecular weight of TCPy

M_{CPF} Molecular weight of CPF

Equation 7.10 is used if TCPy urinary biomarker measurements are specified in terms of mass TCPy/mass creatinine, and equation 7.11 is used if biomarker measurements are specified is terms of mass TCPy/volume urine. An estimation of either liquid urinary

production or urinary creatinine elimination is needed (which is the source of potential biomarker misinterpretation stated earlier [275]). Both approaches have been previously used in the context of CPF exposure: Mage et al. [244] used creatinine-adjusted biomarkers to estimate CPF exposure of the NHANES population; and Morgan et al. [261] used absolute liquid concentrations and excretion rates in assessing CPF and TCPy exposures.

Time-varying approaches

When incorporating temporal uncertainties in dose and biomarker collection, an algebraic solution is usually not possible. Dose and sample time uncertainties, and uncertainties in PK model parameters effecting dynamics and TCPy half life need to be accounted for. The discretized Bayesian approach, and the exposure conversion factor (ECF) approach are used in this study, since they have been recently developed and applied for population dose-reconstruction of short half-life chemicals ([356]). The Bayesian approach used 40,000 model simulations, while the ECF used 5,000 simulations.

7.2.8 Results for Case Study 1

Figure 7.17 compares CPF exposure estimated via the steady-state assumption, using either liquid urinary biomarkers, or creatinine-adjusted urinary biomarkers. Both methods appear to agree, with creatinine-adjusted predictions of daily CPF doses being slightly lower than the absolute liquid concentration predictions. At the tails of the distribution, however, there is about a factor of 5 difference in the lower tail of the distribution and about a factor of 2.5 in the higher tail, with the urinary-concentration

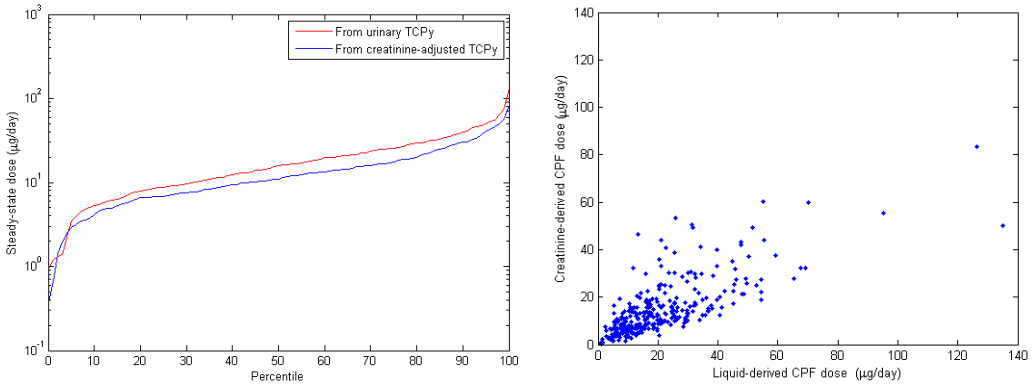

Figure 7.17: Comparison of predicted steady-state doses using creatinine-adjusted urinary TCPy biomarkers, and using liquid urinary concentration TCPy biomarkers: (a) cumulative distributions, and (b) scatter plot

based method predicting systematically higher intake doses.

The inversion results appear to be sensitive to the dose profile assumption, as shown in Figures 7.18 and 7.19. The results also indicate that apportioning "average daily dose" randomly to once a week resulted in greater uncertainty (evident in the upper tails), when compared to constraining doses to once per day. Incorporating the more complex time-activity assumption (Scenario 2a) resulted in estimated doses similar to the once per day case (results not shown). This may be due to the fact that both scenarios approach steady-state conditions, due to the high frequency of exposures. As the exposures become less frequent, there are more cases of low simulated biomarker levels implying a high exposure, since the biomarkers from any magnitude exposure have likely reduced to low levels by the time a hypothetical sample is taken. As previously noted, inversion becomes more sensitive to uncertainties in biomarker sampling time for less frequent exposures.

Additionally, there was only a slight difference between the results from the ECF and the discretized Bayesian methods. Due to the uncertainties involved, neither of these three methods can conclusively be considered superior when examining a short

half-life biomarker such as TCPy. Theoretically, the simple Bayesian method should produce more realistic results than the ECF method, since a linear relationship of biomarker to dose is not assumed. The Bayesian method would be further improved by including better prior information of population doses or activities. However, this was not possible for the NHEXAS-MD data due to the apparent non-specificity of the TCPy biomarker to low-dose CPF exposure, and difficulty in adequately characterizing exposure-time profile and biomarker collection times.

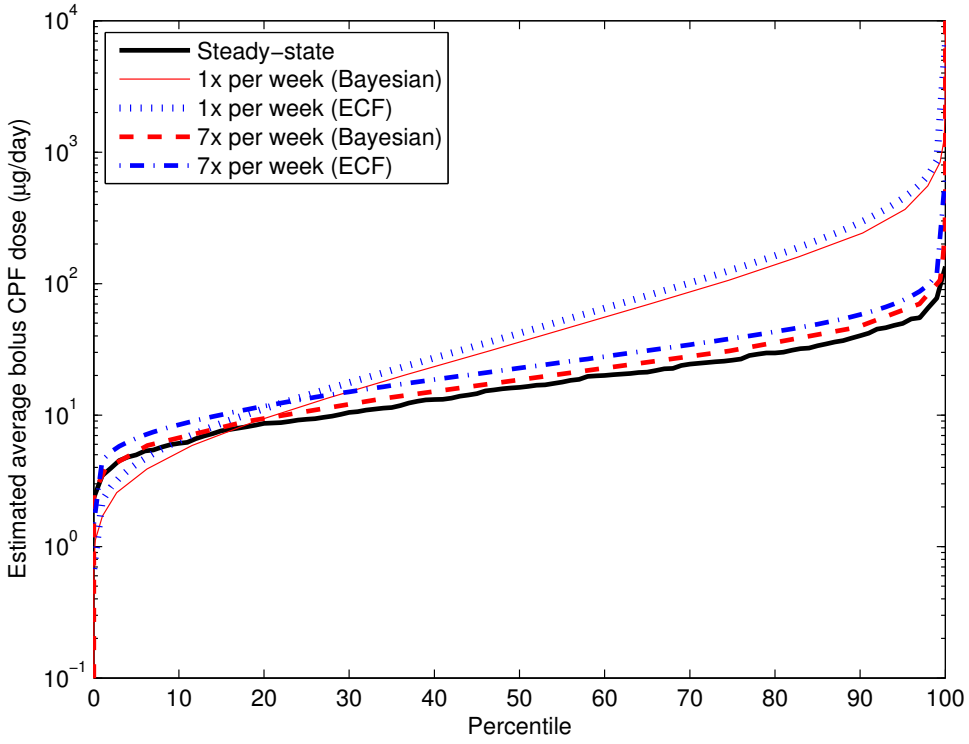

Figure 7.18: Cumulative distribution functions of dietary CPF uptakes for the NHEXAS-MD population estimated by the ECF and Bayesian methods, using three different dose assumptions. Results only show population for which the biomarkers were above the detection limit (which comprised of 95% of the samples).

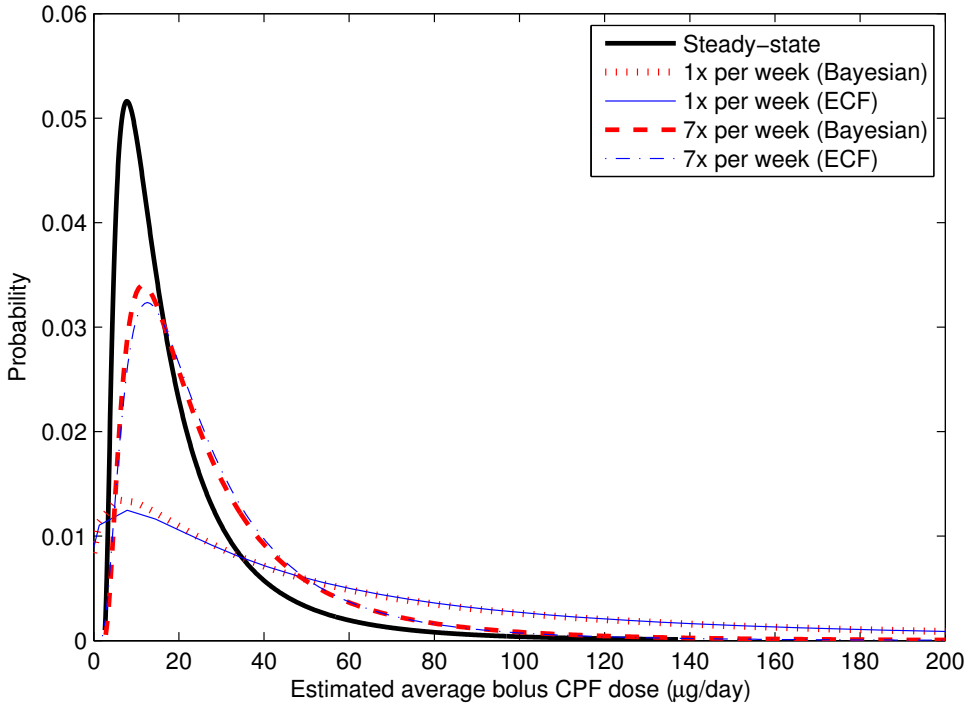

Figure 7.19: Probability density functions of dietary CPF uptakes for the NHEXAS-MD population estimated by the ECF and Bayesian methods, corresponding to results in Figure 7.18.

Value of additional information

More detailed information on potential exposure reduces uncertainty in back-calculating doses from biomarkers. Many "idealized" methods to collect more data are relatively impractical for large-scale studies (i.e. urine collection through an entire day, blood collection, longitudinal dietary and multimedia measurements). While more detailed dietary-recall and exposure information has previously been shown to aid in exposure assessment and biomarker interpretation for chemicals such as CPF [252, 261, 400], it is likely that the short biomarker half-life prohibits feasible biomarker estimates via toxicokinetic modeling inversion for large population studies. For a long half-life chemical such as methylmercury, however, it has been illustrated that by merging fish consumption surveys, dietary intake models and national fish methylmercury data, reasonable agreement between biomarkers and data can be reached [67].

7.2.9 Case Study 2: Chlorpyrifos dose reconstruction from a "synthetically-augmented" NHEXAS-MD data

This case study presents an evaluation of inversion methods using "augmented" biomarker data, because of the uncertainties associated with the reconstruction of actual data. The data set is a "synthetically augmented" version of the NHEXAS-MD database that was developed by filling in missing information via randomly sampling using estimates from sources such as Pang et al. [287]. This data set is then used to evaluate approaches for estimating population parameters. Furthermore, since all the relevant parameter values are known for the new data set, the performance of various methods can be directly assessed.

It was assumed there are only two routes of CPF exposure: (a) continuous background inhalation exposure, and (b) bolus doses due to dietary ingestion. It was

also assumed that dietary CPF exposure was directly correlated with dietary TCP exposure, due to studies showing that TCP may exist in food at levels higher than CPF [261, 275, 400]. For simplicity, a 10:1 ratio of TCP:CPF dietary exposure was initially assumed for the generation of synthetic data.

While the synthetic dietary and background exposures are based on the summary exposure distributions from Pang et al. [287], they are not re-assigned to the specific individuals, on which the exposure estimates are based, as the corresponding data on intake amounts are not available. In this case study, the impact of this assignment is not significant, as the aim is obtain augmented data that are similar to NHEXAS-MD, but with the ability to specify all exposure-relevant parameters for each individual. Only the total doses absorbed are considered because the absorption fraction and intake amount are coupled, and hence, individually unidentifiable.

The assignment of synthetic data for each of the 339 entries in the NHEXAS-MD database was performed through the following procedure:

- Individuals are randomly drawn from the NHEXAS-MD population (relevant physiological parameters were age, gender, body weight, and body height).
- Miscellaneous parameters such as daily liquid urination rate, daily creatinine elimination rate, and inhalation rate, are calculated based on physiology using population distributions from available sources such as NHANES.[1]
- An average daily background CPF dose, average daily dietary CPF dose, and average daily TCP dose (10 times the CPF dose) are drawn randomly from distributions in Pang et al. [287], and randomly assigned to individuals of the population.

[1]Other sources such as the International Commission on Radiological Protection (ICRP) [197], the Physiological Parameters for PBPK Modeling (P3M) [232], etc., are also used

- A week-long exposure profile was generated, randomly assigning bolus doses to 3 meals per day. Each day was a separate random assignment of both meal times, and distribution of CPF dose among the 3 meals (consumption of CPF during one, two, or 3 meals was possible, with uneven distribution). The problem was constrained such that the total bolus weekly dose was consistent with the individual's assigned average daily dose.

- In this study, uncertainties on PK parameters are assumed to be lognormally distributed, with means and standard deviations based on an original pharmacokinetics study by Nolan et al. [266].

- The week-long exposure profile was used as an input to the CPF/TCP PK model, and repeated until a quasi-steady state was reached (a little over a month).

- A biomarker collection day was randomly chosen within the quasi-steady state region. A biomarker collection time was simulated to occur some time in the morning before the first meal of the day.

- A TCP biomarker was simulated as being the total amount of TCP which had accumulated in the bladder since the previous urinary excretion time (dependent on the sample time and prior urination time).

7.2.10 Results for Case Study 2

Different inversion approaches are applied to the synthetic data, with varying degrees of augmentation being introduced. It is assumed that the population-level exposure parameters are known to the same degree as the initial biomarker generation (i.e., the inversion method utilized the same probability distributions for meal times and

Table 7.7: Ranges of supporting exposure parameters used in augmenting the NHEXAS-MD data

Parameter (and distribution)	Values/ranges	Description
Meal time ranges (U)	7-9 (breakfast); 11-14 (lunch); 17.5-20.5 (dinner)	hours of the day a meal may be consumed
Sample time ranges (U)	6.5-8	hour of the day a sample is collected
Prior urination time (U)	21-24	hour of previous day the bladder is emptied, before biomarker collection
Meal probabilities (C)	0.3 (breakfast); 0.3 (lunch); 0.4 (dinner)	probability of CPF being in a given meal
Background CPF concentrations (CDF)	From Pang et al. [287]	Percentiles of background CPF concentrations
Daily ingested CPF (dietary) (CDF)	From Pang et al. [287]	Percentiles of daily CPF intake dose
Ratio of TCPy to CPF in diet (CDF)	*10:1 assumed for simplicity*	Amount of TCPy ingested (synthetic)
Biomarker	PBPK model output	PBPK model run with corresponding sampled inputs

sample times for the population). The physiological parameters are drawn from the adult NHANES population. The inversion has been done using different assumptions: (a) assuming no TCP exposure; (b) assuming a 10:1 TCP:CPF bolus dose exposure ratio (consistent with the approach used in the generation scenario), (c) assuming no background CPF exposure, (d) assuming increased randomness/uncertainty in PK parameters (i.e., PK parameters, and meal time parameters). As in Case Study 1, the Bayesian approach used 40,000 model simulations, while the ECF used 5,000 simulations. Neglecting background CPF exposure, or increasing PK parameter or exposure uncertainty resulted in only minor differences in predicted doses (not shown). This is likely due to the fact that there is an overall high frequency bolus doses, and a quasi-steady state is reached in biomarker measurement.

Analyzing the synthetic biomarkers with different constraints on bolus dose effected

the results in a way similar to Case Study 1. Constraining doses to once per day gave results nearly identical to the steady-state and "base-case" assumptions, and constraining doses to once per week gave a wider distribution (results are not shown).

As shown in Figure 7.20, the ECF and the Bayesian techniques do not adequately reconstruct the exposures, despite using the same sampling time assumptions. This limitation arises from the fact that these methods as used currently cannot utilize the correlations between the exposure and supporting biomarker data (i.e. the individual-level exposure-biomarker relationships). While population-level probability distributions in exposure, sampling, and TCP exposure remained the same for both forward and inverse modeling, the inability of these current methods to match individual-level exposure information prevents a more accurate analysis of the biomarker data.

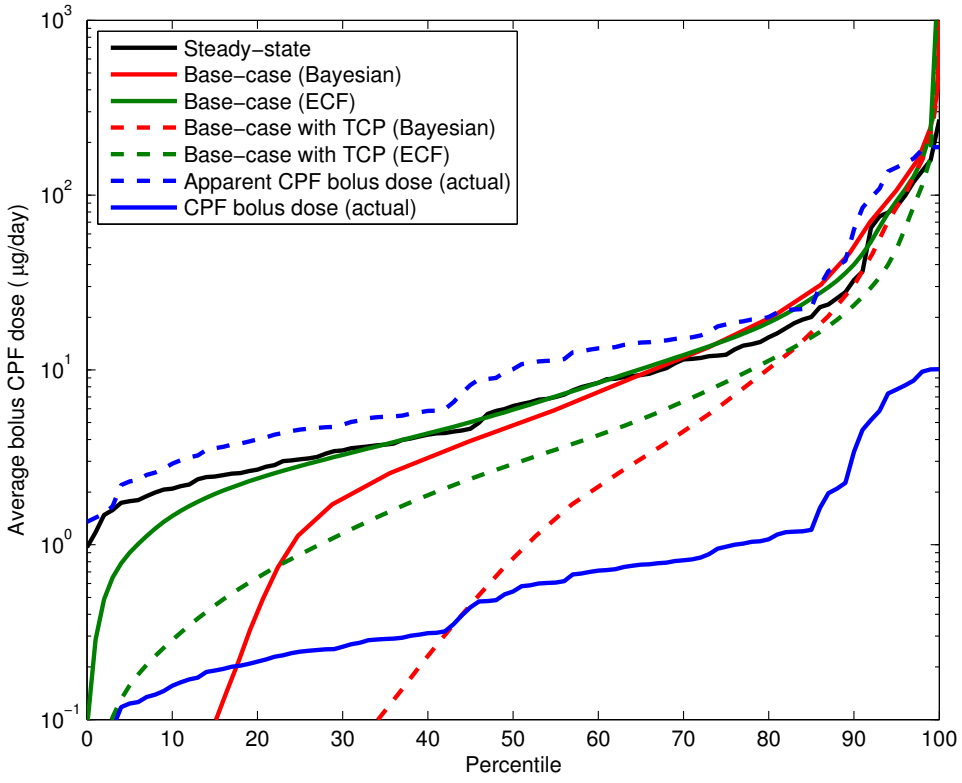

Figure 7.20: Cumulative distribution functions of dietary CPF uptakes for the synthetic population estimated by the ECF and Bayesian methods, using different dose assumptions. Results only show the synthetic individuals with detectable biomarker levels (which comprised of 42% of the samples). "Apparent" CPF dose denotes the sum of the actual CPF and TCP bolus doses (corrected for molecular weight), which may be misinterpreted as a CPF dose if TCP exposure is neglected. "Base-case" results denote those results obtained using the random time-activity assumption with 3 potential CPF doses per day, 0-7 days per week.

7.2.11 Discussion and Conclusion

A comparison of general characteristics of the NHEXAS and NHANES databases with regard to exposure and dose reconstruction is shown in Table 7.8. Although the NHEXAS data set provides significant amount of supporting exposure-related information, when compared to NHANES, this information is still not adequate for detailed reconstruction of exposures under several conditions, as shown in the case studies.

The analysis here identifies specific limitations in existing exposure reconstruction methods that can be applied to population biomarker data, and suggests potential approaches for addressing exposure reconstruction from population biomarker data based on the supporting exposure data available.

The problem of reconstructing exposures from biomarkers can also be addressed through the development or use of sophisticated numerical inversion techniques. The techniques used in the evaluation in this study (the ECF and the discrete Bayesian approach) are not fully equipped to utilize all available biomarker and supporting exposure-related data (e.g. the individual level supporting exposure data). For example, when partial individual level exposure information are available, the data can be potentially used in reconstructing population exposures. However, such data cannot be used in reconstructing exposures at an individual level. This implies that when sparse, individual level exposure data are available, the traditional techniques such as MLE cannot be applied (as the data are too sparse), whereas the methods such as ECF and the discrete Bayesian approached cannot utilize all the available information. There is a scope for improvement in the inversion approaches.

Two other areas for potential improvement in exposure reconstruction involve reconstruction of route- or pathway- specific exposures (i.e. simultaneous reconstruction/estimation of multiple inputs/parameters). There is also a need for "optimal" exposure reconstruction using PBPK models, based on the rationale that incorporating optimization approaches in the inverse modeling process can result in faster convergence and more robust solutions. Though typical PBPK/PK models can be run quickly on modern computers (of the order of seconds per simulation), the computational demands can become challenging when hundreds of thousands of simulations are used in the inverse modeling on desktop computers. Likewise, complex PBPK modeling scenarios (e.g. mixtures of metals or pesticides with large half lives) may need significantly more computational time for a single simulation. Thus use of Fast Equivalent Operating Models (FEOMs) (e.g. see [25, 231, 394]) may be necessary in order to achieve reasonable computational performance.

One of the uncertainties that was not considered in this study is the uncertainty associated with genetic polymorphism. A genetic polymorphism effecting the metabolism of an intermediate metabolite (CPF-oxon) exists in the population, and has been previously incorporated into a chlorpyrifos PBTK model [374]. However, the metabolism of CPF-oxon to TCP is rapid in relation to overall TCP formation and elimination. The polymorphism alters toxicodynamics, but does not significantly alter the TCP biomarker. For other chemicals besides chlorpyrifos, genetic polymorphisms may alter population biomarker measurements (e.g., arsenic metabolites and the AS3MT polymorphism [368]). For short half-life chemicals, the uncertainty in exposure and biomarker assumptions overshadow any effect that polymorphisms may have. For long half-life chemicals, where the biomarker levels are at a quasi-steady state, it may be

more practical to analyze the effect of polymorphisms in the context of dose reconstruction. Table 7.9 lists examples of major underlying biochemical and genetic factors that can contribute to the variability in the metabolism and transport of organophosphates, VOCs, and metals in humans and animals. While these factors may only effect small subsets of the population, they may shed light on potential extreme cases.

In conclusion, the case studies presented here highlight the gaps in existing biomonitoring studies, which need to be considered when developing improved designs for future biomonitoring studies. Furthermore, the analysis here identifies specific limitations in existing exposure reconstruction methods that can be applied to population biomarker data, and suggests potential approaches for addressing exposure reconstruction from population biomarker data based on the supporting exposure data available.

Table 7.8: Comparison of NHEXAS and NHANES datasets *vis a vis* needs for detailed exposure reconstruction

Attribute	NHANES	NHEXAS	Requirement[2]
Baseline Parameters (individual characteristics)			
Smoking and tobacco use	X	X	Chemical dependent
Dietary recall	X	X	Required
Pesticide use	X	X	Chemical dependent
Demographic background/occupation	X	X	Dependent on model complexity
Recent activity diary	-	X	Dependent on model complexity
Housing characteristics	X	X	Dependent on model complexity
Physiological Characteristics (at individual level)			
Age	X	X	Required
Gender	X	X	Required
Body weight	X	X	Required
Body height	X	X	Required
Cardiac output	-	-	Required (population distributions)
Urinary excretion rate	-	-	Required for urinary biomarkers
Urinary creatinine excretion rate	-	-	Required
Environmental Concentrations			
Food residues	-	X	Required
Personal air	o (VOCs)	X	Required
Indoor/outdoor air	-	X	Required
Dust	o (Lead)	X	Required
Soil	-	X	Required
Tap water	-	X	Required
Dermal residue	-	X	Required
Behavioral/Health			
Diet behavior and nutrition	X	X	Possibly required for toxic metals
Baseline health condition	X	-	Rarely required
Biochemical parameters	-	-	Required (from other studies)
Biomarker Data Characteristics			
Actual sampling time	-	-	For short-half-life chemicals
Time of last void	-	-	Required for urinary biomarkers
Time of last meal before void	-	-	Urinary biomarkers
Multiple biomarkers	o	o	Chemical and pathway dependent

Table 7.9: Selected information available on underlying mechanisms for inter-individual variability due to genetic factors that affect the transport and transformation of pesticides (organophosphates, pyrethroids), fungicides (conazoles), VOCs, and metals in humans and animals.

Species class	Metabolism and transport	Notes
Organophosphates	Liver microsomes, CYP-1A2, 2B6, 2C8, 2C9, 2C19, 2D6, 2E1, 3A4, 3A5 [189]	Organophosphates share P450s for metabolism [316, 358]. Paraoxonase (PON1) polymorphism [374] model.
Pyrethroids	Liver microsomes, alcohol and aldehyde dehydrogenases [189, 259, 292]	Induce various P450s. [1, 183, 382]. PON1 genotype effects metabolism. [169]
Metals/metalloids	Glutathione and cysteine [288, 303], arsenic methyltransferase (arsenic) [114, 256, 368, 401], metallothionein [274], divalent metal transporter-1 (DMT1) [49, 151], bone mineral exchange (lead)	Interactions with essential elements [26, 164]. Arsenic metabolism affected by CYT19, hNP, and hGSTO1-1 genotypes [114, 256]. Cadmium and lead can alter P450 levels and activities [23, 260]. Metal speciation significantly alters toxicity [409]
Conazoles	Human CYP-2C18, 2C19, 3A4, 3A5, 2B6; Rat CYP-2C6, 2C11, 3A1, 3A2, 2B1 [32, 312]	Significantly alters levels/activities of P450s [212, 349, 380]
VOCs	Glutathione, Glutathione-S-transferase, CYP-2E1, 2C6, 2C11, 1A1, 1A2 [307]	GST genotypes effect metabolism and toxicity [111, 169, 301, 307, 340]

Chapter 8

Discussion and Conclusions

Development of the multi-metals PBTK model

This was the first work to present an interactive multi-metals PBTK modeling framework. The generalized toxicokinetic model is capable of simulating binary and higher order interactions between metals and nonmetals. The need for such a model was outlined using extensive literature reviews of the toxicology and toxicokinetics of the contaminants most relevant to regulatory risk assessments.

Incorporation into exposure frameworks

Construction of the model in the Matlab/Simulink environment allowed for integration with both long-term and short-term models for exposure.

The generalized model was linked with the O'Flaherty lead multi-route exposure model, in order to both validate the equations and to estimate long-timescale lead and cadmium exposure. Due to the nature of lead kinetics in bone, such a long-term exposure model is necessary to create the baseline initial conditions for lead exposure studies. Lifetime background lead exposure accumulates in bone and effects observed blood lead levels. Similarly, assumptions for lifetime background cadmium exposure is needed due to the extremely high half-life in liver and kidneys.

The generalized model was also linked with a population dietary model for methylmercury exposure. The model fetches demographic data, merges it with survey data of monthly consumption of fish and shellfish, and can be used to model the levels of methylmercury that might be seen in the population. Adjustments on the assumptions of methylmercury content in the different fish and shellfish can allow for quick sensitivity analysis. As illustrated in this work, combining multiple dietary surveys and demographic data could be used to estimate methylmercury exposure, despite having data that spans only 30 days. Since the generalized model can be used to model other chemical simultaneously, data for other chemicals found in fish (i.e. arsenic and PCBs) could also be incorporated into the analysis. However, such an approach cannot capture long-term changes in contaminant levels in the body that may be due to seasonal changes in diet or pollution, without additional information.

Evaluation and use of Bayesian methods

The Bayesian approach to both estimate PBTK parameters and exposure levels based on measured biomarker data has been getting much attention in the literature recently. A Bayesian framework using both freely available and proprietary Metropolis samplers was developed and linked with the generalized toxicokinetic model. Alternative sampling methods were evaluated for convergence efficiency by using synthetic data. This also served as a verification that the Bayesian implementation functioned correctly.

A large-scale population Bayesian analysis was used to derive the parameters for a PBTK model of a mixture of six PCBs. A proposed induction model was used to describe the behavior of the mixture, which consisted of PCBs with different structures and metabolic pathways. This was the first time such an analysis was done on the

class of lipid-based PBTK models, and it was illustrated that a CYP450 balance with a linear dose response model was adequate in simulating data for wide-ranging dose levels and dose protocols.

Future work

Essential element interactions

PBTK models for essential elements in humans (once they become available) may be readily incorporated into the metal mixtures framework. While there currently are no models for metal interactions, there are some generalizations that can be made (i.e. correlations between health, elemental status and metal absorption). Assuming that susceptible individuals exposed to metals will experience higher absorption of the entire mixture, it follows that toxic endpoints (either due to additive or synergistic interactions) may occur with a greater likelihood. This is particularly important since some metals exhibit the same toxic effects (such as hepatic and renal toxicity). Essential element interactions may also be very important when considering population biomarker inversion. Individuals with a high toxic metal absorption fraction due to low blood iron may show higher biomarker levels than those with higher exposure and low absorption.

Dose response models

The development of biologically-based dose-response (BBDR) models for metals (or any chemical for that matter) are still in the early stages. For metal mixtures, there is a particular need for dose response models of the renal and hepatic effects. Impacts of arsenic, cadmium, and lead on the kidneys has been shown to cause renal dysfunction, and the molecular biomarkers indicating early renal effects (low molecular weight proteins found in the urine) have indicated toxic interactions [393]. Renal dysfunction

strongly impacts the elimination and recycle of essential and toxic metals in the plasma, effecting toxicokinetics. Additionally, induction or inhibition of CYP450 enzymes leads to potential interactions with organics, drugs, PCBs and pesticides. The magnitude of these interactions in-vivo are not fully known, however it is now possible to evaluate hypotheses in a framework capable of modeling multiple metals and nonmetals.

Improvement of biomarker inversion methods

The estimation of exposure based on biomarker data using PBTK models is both computationally- and data-expensive. Government population studies of biomarkers and exposure (such as NHANES and NHEXAS) provide much of the data necessary, however current inversion methods have not yet been able to maximize data utility. Inversion methods that focus too heavily on biomarkers will not provide an accurate assessment, since the lack of exposure context (i.e. time passed since exposure occurred) makes analysis difficult. Methods that focus on exposure may neglect physiological and biochemical differences in the population that effect both absorbed dose and toxic outcomes.

Obviously, an exposure data-rich situation in which all pathways are assessed and all time-varying exposure concentrations (food, water, dermal, air, dust) are known for a large sample population, would not require biomarkers to assess exposure. Similarly, biomarker data-rich situations where all possible excretions are continuously measured for a population would require minimal exposure data for the inversion. Since these scenarios are unrealistic, biomarkers and toxicokinetic models are necessary to bridge the gap between biological and environmental surveillance.

Appendix A

Toxic metals in dust

Indoor dust is a significant pathway for toxic metal exposure [58, 89]. Dust may be inhaled by adults and ingested by children via hand-to-mouth activity. In an effort to obtain the most relevant information on the metal composition of dust (particularly for future source-to-dose modeling of metal exposure), literature reviews were conducted for select toxic metals frequently found in house dust. The tables below summarize many articles on the subject, and it should be noted that this is only a partial review. Studies are continuously being performed throughout the world.

Table A.1: Mean lead concentration in house dust (mg/kg).

Location	Date	Mean or median	Range	Comments	Reference
England	1979	3366	276-8619	Near smelter	[132, 263]
	1979	1540	368-3057	Control houses	[263]
	1979	716	510-970	Lancaster	[176]
	1982	440-3110		Shipham	[207]
	1984	398-608*	94-146000	SW England, mining	[95]
	1984	177-259	36-1075	Range of sites	[121]
	1985		349-2364	Leeds	[350]
	1987	1007	5-36900	London boroughs	[96, 175, 372]
	1987	578	111-3110	Birmingham	[101, 102, 369]
	1987	1436	79-15000	Under door mats	[101, 102, 369]
	1987	1846	51-26755	London	[226]
	1987	808	22-26620	Suffolk	[348]
	1988	756*	132-26760	Shipham	[372]
	1988	411*	50-19320	North Petherton	[372]
Netherlands	1981	1144	457-8097	Near lead smelter	[53]
	1981	1054	463-4741	Fine floor dust	[110]
New Zealand	1981	5580		Home of battery workers	[144]
	1981	1620		Along busy road	[144]
	1985	615		City survey	[133]
	1985	457		Brick homes	[133]
	1985	727		Wooden homes	[133]
	1986	734	287-1408	City wide	[134]
	1988	573*	101-3510	Christchurch survey	[216]
Scotland	1987	308*		Edinburgh	[304]
UK	1983	346-1163*	47-30060	Nation-wide survey	[97, 98]
	1987	507	13-34530	Nation-wide survey	[175, 372]
	1990	561		Indoor dust	[373]
	2005	178*	56.8-358	Indoor dust	[381]
USA	1975	4022		Close to smelter (El Paso)	[225]
	1975	816		Further away (El Paso)	[225]
	1975	11000	4900-17000	High blood lead	[230]
	1976	600	170-1400	Homes in good condition	[344]
	1984		76-5571	Omaha, battery plant	[14]
	1984		18-485	Omaha, suburbs	[14]
	1986	900	82-13820	Cincinnati	[46]
	1994		100-25000	Near smelter	[38]
	1999	463	70-700	NHEXAS region-5 survey	[82, 284]
	1990-2001	1200 (1990), 400 (2001)*		Bunker Hill superfund, ID	[337, 391]
	2000	613		Seasonal study, NJ	[406]
	2004	1641		Lead paint hazard control	[81]
Wales	1985	346	8-2943	Old mining area	[100]

References prior to 1990 are adapted from Fergusson and Kim, 1991 [132].

Table A.1: (Continued)

Location	Date	Mean or median	Range	Comments	Reference
	1985	169	28-813	Old mining area	[100]
	1987	634	164-3984	Swansea	[175]
Canada	1993	619		Pre-1950 home, Ottawa	[306, 359]
	1993	266		Post-1950 home, Ottawa	[306, 359]
	1993	462		Electric heat home, Ottawa	[306, 359]
	1993	389		Gas heated home, Ottawa	[306, 359]
	1993	409		Oil heated home, Ottawa	[306, 359]
	2001	406	50-3226	Residential home, Ottawa	[306]
Philippines	2005	50*	8-1046	Near closed air base	[309]
Finland	2004	75	43-199	Near smelter	[236]
	2004	27	18-35	Near smelter	[236]
Jordan	2004	60*	48-66	Jordanian petroleum refinery complex	[204]
Germany	1999	127	0.9-1947	Smelter town	[255]
	1990	5.9		National survey	[333]
Australia	2003	85.2	18.2-16600	Sydney	[71]
China	2000	47-308*		Hong Kong districts	[376]

References prior to 1990 are adapted from Fergusson and Kim, 1991 [132].

Table A.2: Mean cadmium concentration in house dust (mg/kg) . References prior to 1990 are adapted from Fergusson and Kim, 1991 [132].

Location	Date	Mean or median	Range	Comments	Reference
England	1979	193	12-387	Near smelter	[263]
	1979	15.7	9-26	Controls	[263]
	1979	10.7	1-21	Indoor dust	[176]
	1982		2-93	Shipham village	[207]
	1983	7-10	1-450	Various sites	[97, 98]
	1984	5-10	1-62	Various sites	[95]
	1985	7.7	<1-336	London boroughs	[372]
	1987	6.8	<1-840	Survey	[96, 175, 371, 372]
	1988	22*	1-279	Shipham village	[371]
	1988	8*	0.8-150	North Petherton village	[371]
	2005	1.1*	0.6-4.9	Four U.K. regions	[381]
US	1976	18	7-48	Residential homes	[344]
	1999	4.6*	3.6-16.6	NHEXAS	[284]
	2001	10		Indoor dust	[416]
Canada	2001	6.46	1.12-34.94	Ottawa	[306]
	2001	0.33	0.08-1.12	Ottawa	[306]
Germany	1999	2.6	0.3-52.7	Smelter town	[255]
	1990	0.9		Nationwide survey	[333]
Australia	2003	4.4	0.3-109	Sydney	[71]
China	2000	4.3	0.2-2340	Hong Kong districts	[376]
Jordan	2004	6.36	4.46-12.24	Various locations	[204]
New Zealand	1988	4.3*	0.6-21	Christchurch	[216]

Table A.3: Paired indoor and outdoor metal concentrations

Location and metal	Date	Outdoor metric mean or median	Indoor metric mean or median	Comments	Reference
US					
Pb	1999	Air: 8.5* Soil: 41.9*	Air: 6.6* Dust: 129*	NHEXAS region 5	[82, 284, 320]
As	1999	Air: 0.73* Soil : 1.6	Air: 0.51* Dust: 0.26*		
Pb	2004	Soil: 345 Soil: 55	Dust: 75 Dust: 27	Near lead smelter	[236]
Pb	1990 1998 1990 2001	Soil: 700 Soil: 180 Soil: 750 Soil: 100	Dust: 1200 Dust: 630 Dust: 1800 Dust: 300	Superfund (pre-cleanup) Superfund (post-cleanup) Superfund (pre-cleanup) Superfund (post-cleanup)	[337]
Pb	1999	Soil: 245	Vacuum dust: 468 Floor dust: 1026	Northern Idaho	[345]
Canada					
As	2001	Road dust: 1.3 Soil: 3.0	Dust: 7.3	Ottawa	[306]
Cd	2001	Road dust: 0.37 Soil: 0.3	Dust: 6.46		
Mn	2001	Road dust: 432 Soil: 5.23	Dust: 269.3		
Pb	2001	Road dust: 39 Soil: 65	Dust: 405.56		
Hg	2001	Road dust: 0.029 Soil:0.107	Dust:3.633		
Philippines					
Pb	2005	Soil : 19*	Dust: 50*	Near air base	[309]
Jordan					
Cd	2004	Soil: 1.24	Dust: 6.36	Various locations	[204]
Pb	2004	Soil: 21	Dust:74		

Table A.4: Metal composition of household dust (μg/g) sampled in the U.K., adapted from Turner and Simmonds (2006)

Region	Parameter	Al	Cd	Cu	Fe	Mn	Ni	Pb	Sn	Zn
Birmingham	AM ± S.D.	6720 ± 1930	1.5 ± 0.9	373 ± 176	5970 ± 1170	493 ± 345	49.4 ± 25.0	109 ± 87.0	37.9 ± 32.1	803 ± 227
(n =7)	GM	6470	1.3	344	5880	416	44.8	90.5	29.4	774
	Median	6890	1	297	6060	323	42.7	62.5	19.4	690
	Range	3850-9850	0.7-3.0	228-724	4980-8230	240-1150	27.2-97.1	57.0-298	17.2-95.7	496-1065
W. Midlands	AM ± S.D.	8800 ± 3150	1.3 ± 1.3	320 ± 137	9140 ± 3590	520 ± 179	53.7 ± 20.6	194 ± 124	20.4 ± 10.2	733 ± 243
(n = 10)	GM	8380	1	284	8620	494	50.5	154	18.3	700
	Median	7460	0.8	340	8240	485	51.7	177	17.4	680
	Range	5790-14800	0.6-4.9	71-537	4990-18000	286-852	31.5-89.9	56.8-352	9.0-40.9	368-1300
Plymouth	AM ± S.D.	11,900 ± 9240	1.5 ± 0.9	395 ± 237	9930 ± 3700	531 ± 182	63.6 ± 17.3	251 ± 71.2	30.7 ± 9.6	661 ± 215
(n =6)	GM	9420	1.3	343	9350	509	61.7	243	29.5	630
	Median	6120	1.2	326	9280	492	61	243	28.3	668
	Range	5630-23800	0.7-3.1	173-799	5550-14300	368-867	49.0-89.1	174-358	18.8-46.4	363-987
W. Devon	AM ± S.D.	8120 ± 2080	1.1 ± 0.3	297 ± 132	12,200 ± 3730	868 ± 280	60.4 ± 17.5	174 ± 82.7	28.5 ± 22.7	489 ± 177
(n =9)	GM	7870	1.1	265	11500	681	58.1	157	24	455
	Median	7670	1.2	320	14500	776	60.1	183	22.3	515
	Range	4320-12100	0.7-1.8	110-441	5530-16,200	286-1190	37.6-89.6	73.1-335	12.9-87.0	213-693
All results	AM ± S.D.	8740 ± 4630	1.3 ± 0.9	339 ± 163	9450 ± 3840	578 ± 262	56.5 ± 20.0	181 ± 104	28.4 ± 20.5	666 ± 240
(n = 32)	GM	7950	1.2	301	8740	524	53.1	150	23.9	622
	Median	7410	1.1	326	8280	501	53.3	178	21	665
	Range	3850-23800	0.6-4.9	71-799	4980-18000	286-1190	27.2-97.1	56.8-358	9.0-95.7	213-1300

Table A.5: Literature summary of studies focusing on microenvironmental concentrations of metals

Ref.	Type	Micro-environment	Location	Al	As	Cd	Cr	Cu	Fe	Pb	Mn	Hg	Ni	Zn
[89]	comprehensive review	indoor, outdoor	NA		X	X			X			X		
[58]	comprehensive review	indoor	NA	X	X	X	X	X	X	X	X	X	X	X
[229]	indoor dust	indoor	US (LA)		X	X	X	X	X	X		X	X	
[71]	Indoor dust	indoor	Australia			X	X	X	X	X	X		X	X
[82, 83, 284, 320]	NEXAS	indoor, outdoor	US	X	X	X	X	X	X	X	X	X	X	X
[290]	waste site	indoor, outdoor	Armenia		X		X	X	X	X	X	X	X	X
[408]	WTC	indoor, outdoor	US (NY)											
[359]	WTC	indoor, outdoor	US (NY)							X				
[235]	WTC	outdoor	US (NY)	X		X	X	X		X	X	X	X	
[323]	roadways	outdoor	Greece			X	X	X	X	X	X		X	
[376]	homes	indoor, outdoor	Hong Kong			X		X		X	X			X
[309]	waste site, air base	indoor	Philippines							X		X		
[237]	roadways	outdoor	US (WI)	X					X	X				X
[161]	atmosphere	outdoor	Naples		X		X	X		X			X	X
[80]	soil	outdoor	India							X				
[73]	subways	indoor, outdoor	US (NY)				X		X		X			
[22]	urban	outdoor	Paris	X				X						
[336]	power plant	outdoor	India	X		X	X	X	X	X	X	X	X	X
[282]	aerosols	outdoor	Beijing	X	X	X	X	X		X	X		X	X
[262]	emissions	outdoor	Great Lakes									X		
[236]	waste site		Finland							X				
[204]	industrial area	indoor, outdoor	Jordan	X		X	X	X	X	X				X
[147]	air monitoring	outdoor	India			X	X		X	X			X	X
[137]	multimedia	indoor, outdoor	Mexico							X				

Table A.5: (Continued)

Ref.	Type	Micro-environment	Location	Al	As	Cd	Cr	Cu	Fe	Pb	Mn	Hg	Ni	Zn
[81]	remediation	indoor, outdoor	US (OH)							X				
[34]	smelters	outdoor	France			X				X				X
[6]	atmosphere	outdoor	Egypt							X				
[2]	tire dust	outdoor	Japan	X			X	X	X	X				X
[112]	remediation	indoor	US (MD)							X				
[407]	remediation	indoor	US (NJ)							X				
[391]	remediation, waste site	indoor	US (ID)							X				
[366]	atmosphere	outdoor	Greece		X	X				X			X	
[337]	remediation, waste site	indoor	US (ID)							X				
[162]	various	indoor, outdoor	NA									X		
[62]	remediation	indoor	US (PA)							X				
[283]	industrial area	outdoor	Spain			X				X		X		X
[130]	air monitoring	outdoor	China									X		
[127]	demolitions	indoor, outdoor	US (MD)							X				
[126]	roadways	outdoor	Taiwan					X	X	X	X			X
[265]	playground	outdoor	Hong Kong			X	X	X	X	X	X			X
[27]	air monitoring	outdoor	Canada								X			
[402]	industrial area	indoor, outdoor	China							X				
[308]	remediation	indoor	US (NY)							X				
[192]	service stations	outdoor	Jordan				X	X	X	X			X	X
[163]	smelters	outdoor	Canada							X				X
[135]	atmosphere	outdoor	Spain	X	X		X	X	X	X		X	X	X
[125]	remediation	indoor	US							X				
[248]	roadways	outdoor	UK			X				X				
[45]	mining town	indoor, outdoor	US (ID)							X				
[354]	air monitoring	outdoor	Poland			X	X	X	X	X			X	X

Table A.5: (Continued)

Ref.	Type	Micro-environment	Location	Al	As	Cd	Cr	Cu	Fe	Pb	Mn	Hg	Ni	Zn
[306]	multimedia	indoor, outdoor	Canada	X		X				X				
[293]	atmosphere	outdoor	US (VT)		X					X	X			X
[258]	power sanding	indoor	US (LA)			X	X	X		X	X		X	X
[178]	air monitoring	outdoor	Egypt			X				X				
[65]	indoor air	indoor	US									X		
[40]	air monitoring	outdoor	Argentina			X	X	X	X	X	X		X	X
[174]	indoor release	indoor	US (OH)							X				
[139]	remediation	indoor	US (NJ)				X							
[406]	seasonal	indoor, outdoor	US (NJ)							X				
[131]	incinerator	outdoor				X				X				
[254]	industrial area	indoor	Germany			X				X				
[255]	smelter	indoor	Germany		X	X				X				
[36]	smelters	outdoor	Mexico		X	X				X				
[346]	waste site	indoor, outdoor	US (MO)							X				
[234]	remediation	indoor	US (NJ)							X				
[3]	exposure metrics	indoor	US (NJ)							X				
[381]	homes	indoor	UK	X		X		X	X	X	X		X	X
[345]	homes	indoor, outdoor	US (ID)							X				
[191]	homes	indoor, outdoor	Belgium			X				X				
[199]	homes	outdoor	Turkey			X								
[191]	homes	indoor	US (AL)		X		X	X						
[63, 64]	urban	outdoor	US (NYC)							X				
[44]	remediation	indoor	Australia							X				
[399]	homes	indoor, outdoor	US (MI)							X				
[68]	waste site	outdoor	Mexico		X					X				

Appendix B

Complete PCB evaluation runs

In the interest of making the main body of the document concise, results were omitted from Section 7.1. The following pages show the model/data comparisons for the full evaluation data set, which were used to generate the scatterplot of Figure 7.10. To reiterate Section 7.1, these figures are the results of running the PBTK model of the six PCB mixture for individual rats which had been omitted from the optimization. Data-specific body and liver weights for each rat where used in the model. Median values of the optimized parameters were used, which explains why not all model predictions match the data perfectly. These model/data differences are relatively minor, since the data are still within the upper and lower limits of the population model if parameter variabilities were included.

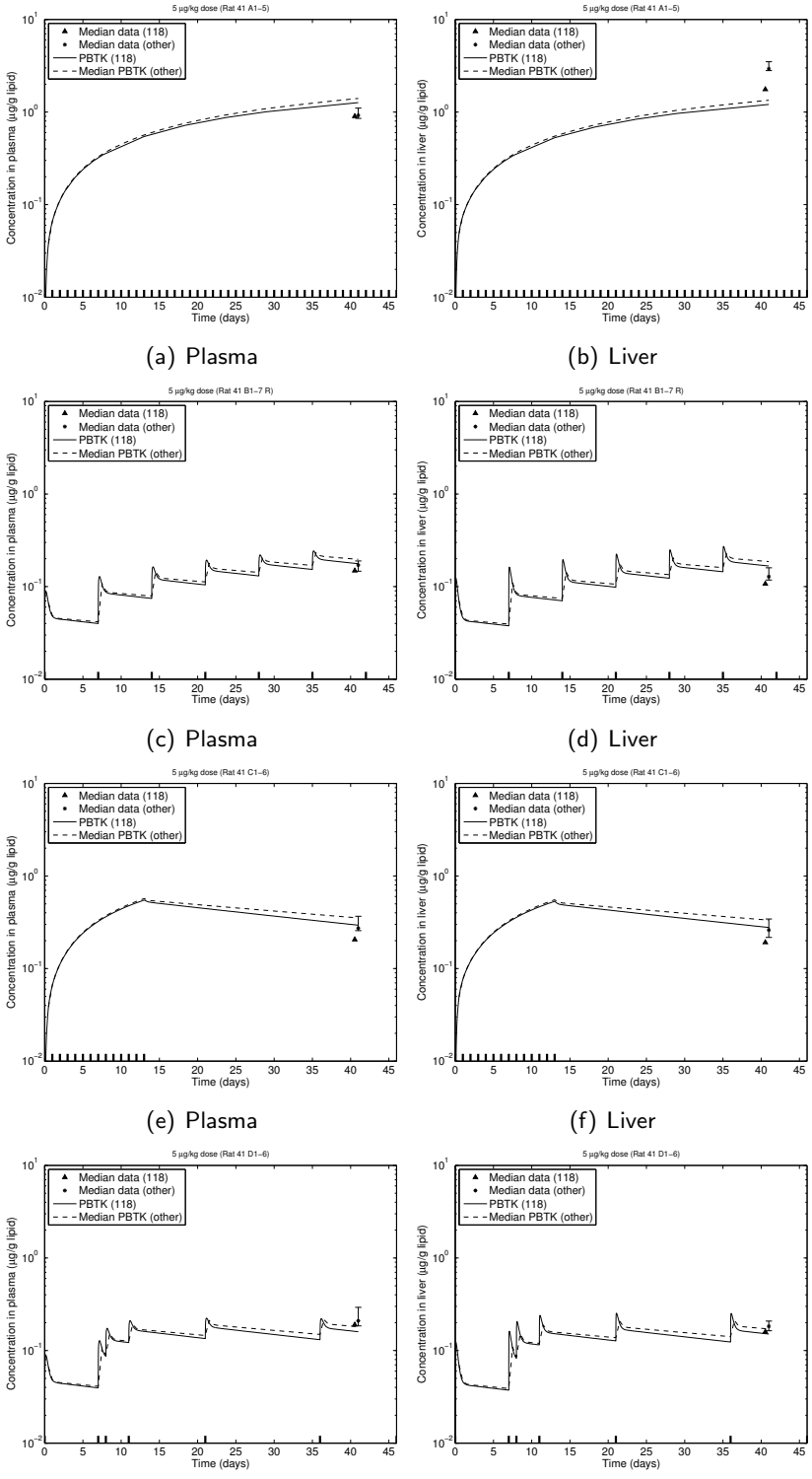

Figure B.1: Model predictions for PCB concentrations at 5 µg/kg exposure for the evaluation data set of rats sacrificed at day 41. Data-specific body measurements were used for each rat. Results and data were condensed to show the results for PCB 118 (the non-ortho PCB) and the median result of all other PCBs (multi-ortho PCBs). Points indicate the PCB measurements at time of sacrifice, and error bars indicate the minimum and maximum measured values of multi-ortho PCBs.

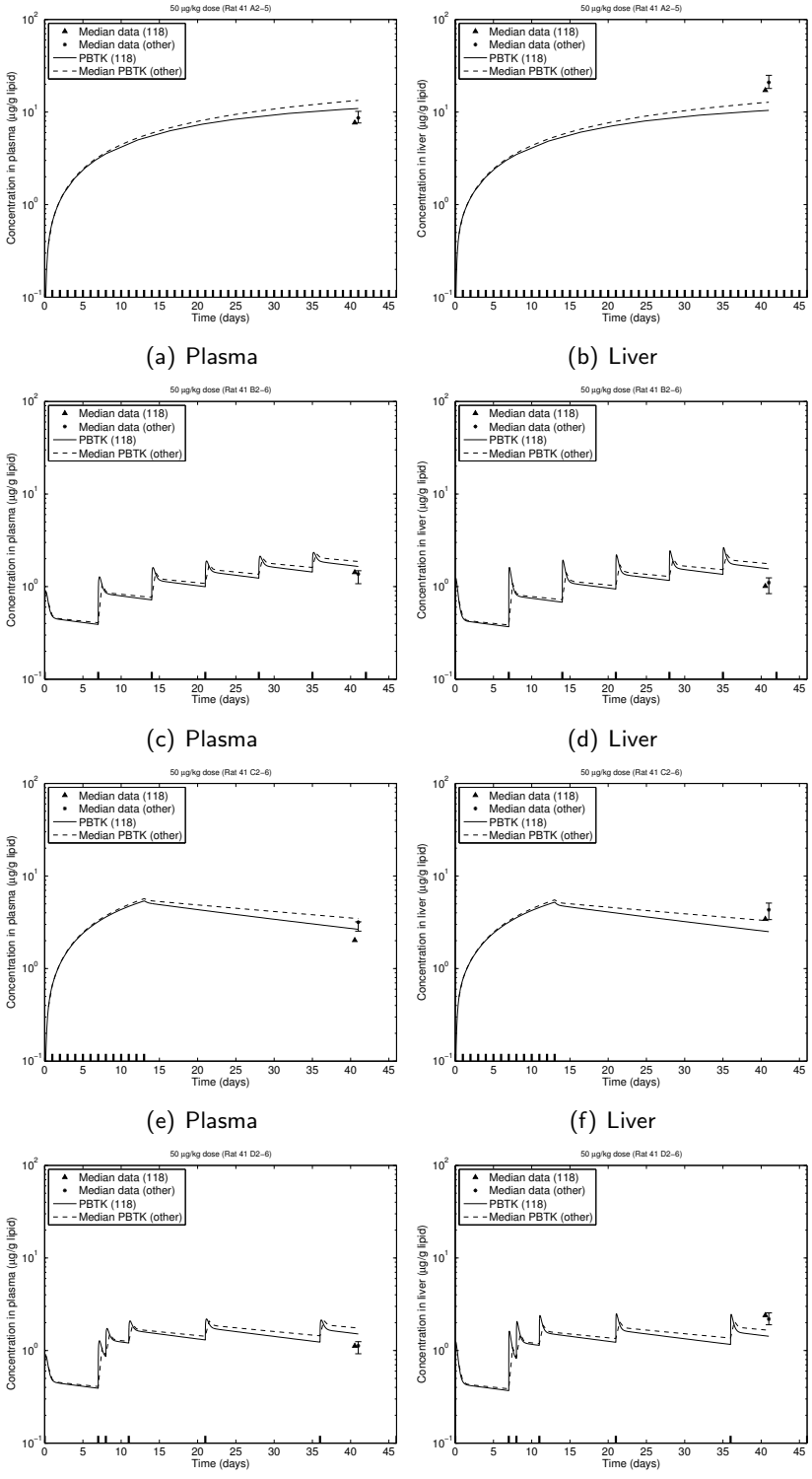

Figure B.2: Model predictions for PCB concentrations at 50 µg/kg exposure for the evaluation data set of rats sacrificed at day 41. Data-specific body measurements were used for each rat. Results and data were condensed to show the results for PCB 118 (the non-ortho PCB) and the median result of all other PCBs (multi-ortho PCBs). Points indicate the PCB measurements at time of sacrifice, and error bars indicate the minimum and maximum measured values of multi-ortho PCBs.

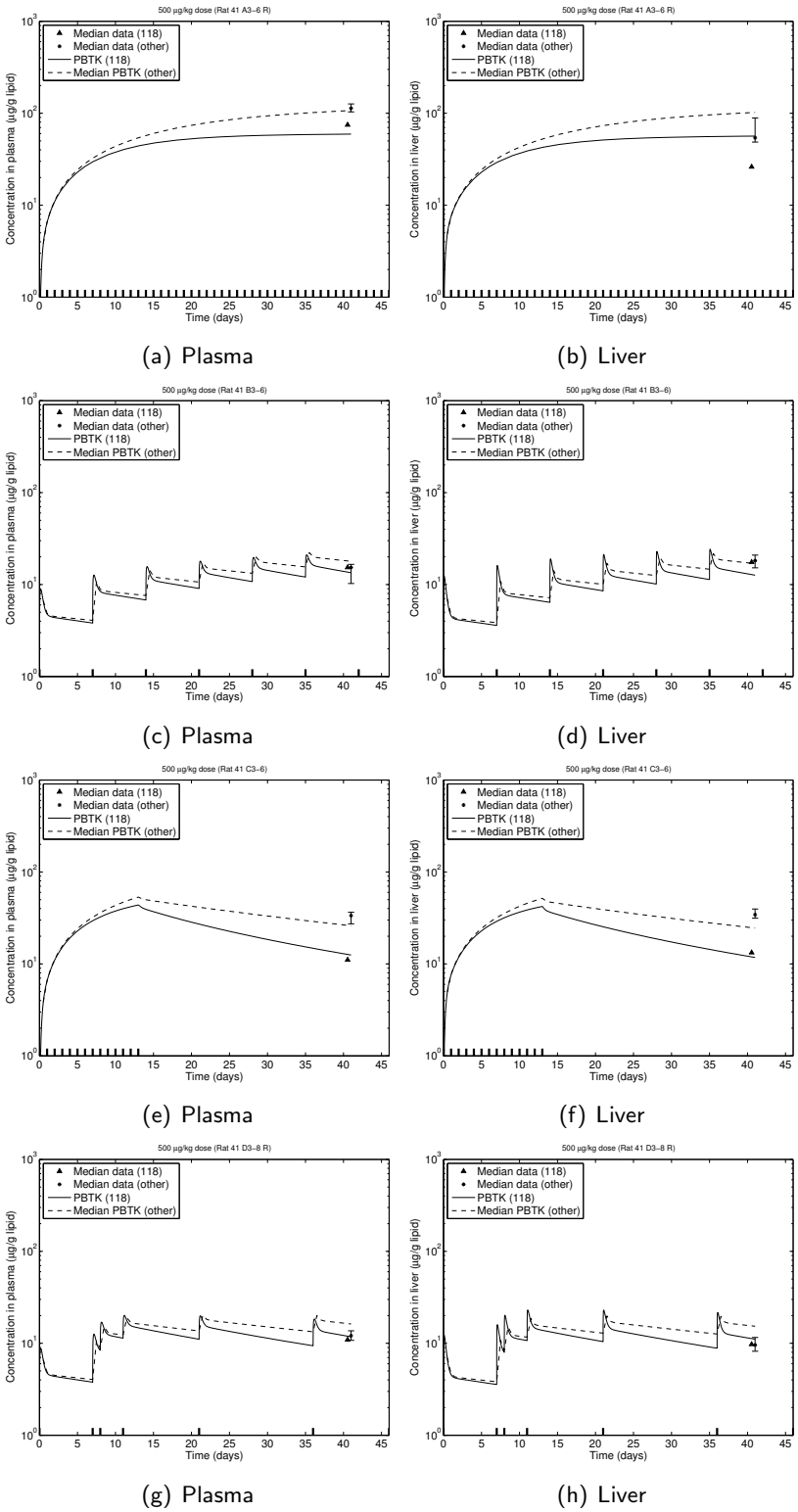

Figure B.3: Model predictions for PCB concentrations at 500 µg/kg exposure for the evaluation data set of rats sacrificed at day 41. Data-specific body measurements were used for each rat. Results and data were condensed to show the results for PCB 118 (the non-ortho PCB) and the median result of all other PCBs (multi-ortho PCBs). Points indicate the PCB measurements at time of sacrifice, and error bars indicate the minimum and maximum measured values of multi-ortho PCBs.

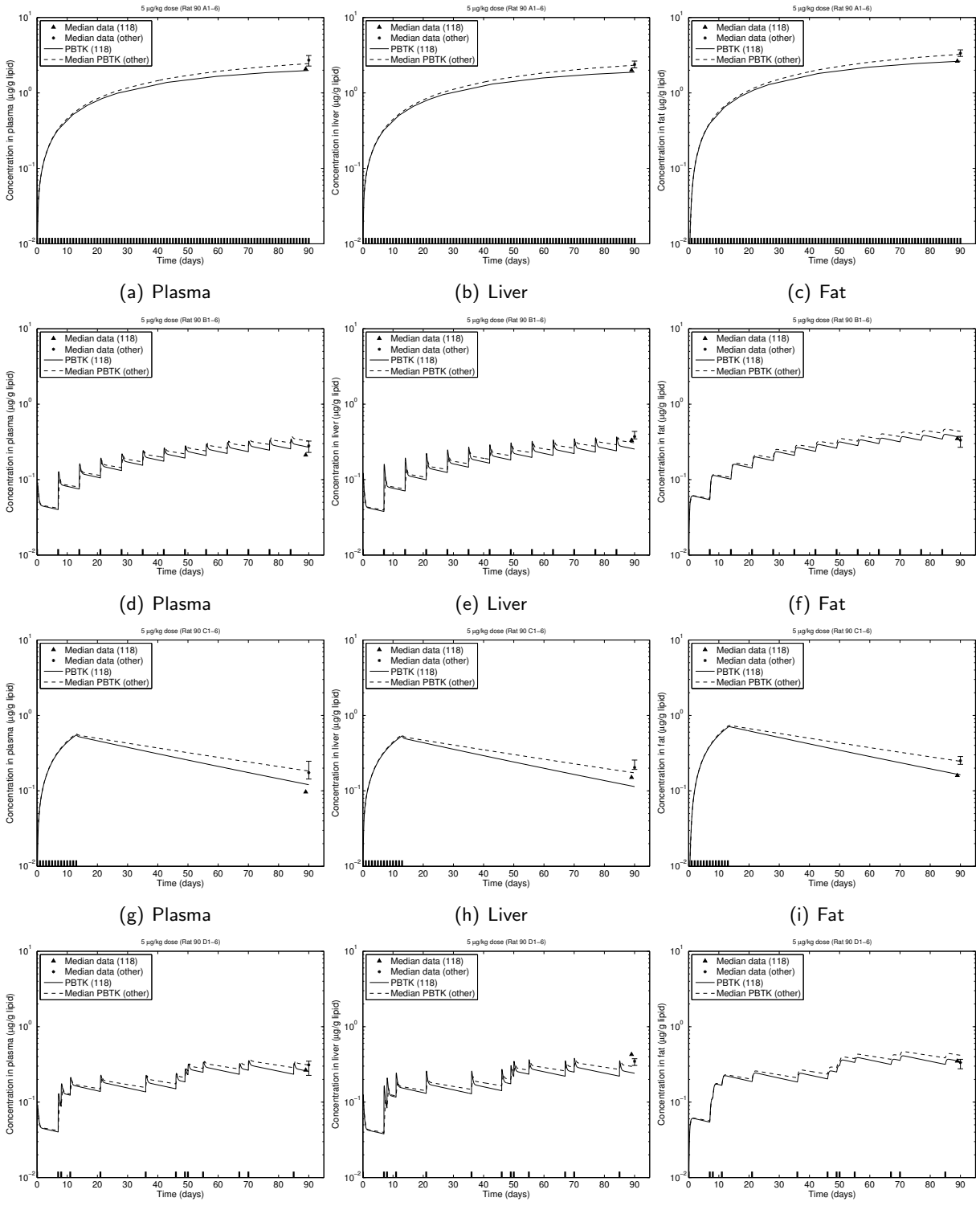

Figure B.4: Model predictions for PCB concentrations at 5 µg/kg exposure for the evaluation data set of rats sacrificed at day 90. Data-specific body measurements were used for each rat. Results and data were condensed to show the results for PCB 118 (the non-ortho PCB) and the median result of all other PCBs (multi-ortho PCBs). Points indicate the PCB measurements at time of sacrifice, and error bars indicate the minimum and maximum measured values of multi-ortho PCBs.

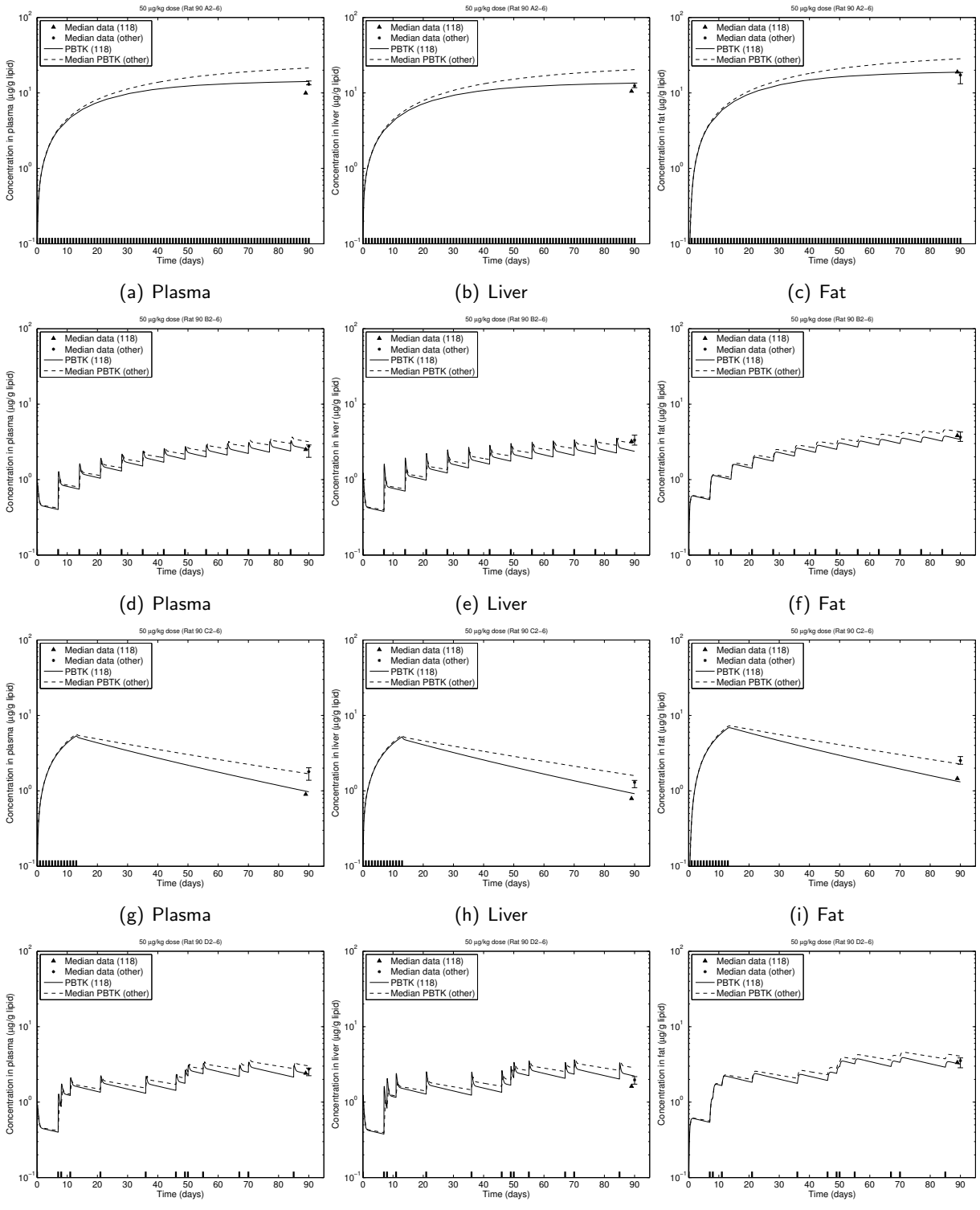

Figure B.5: Model predictions for PCB concentrations at 50 µg/kg exposure for the evaluation data set of rats sacrificed at day 90. Data-specific body measurements were used for each rat. Results and data were condensed to show the results for PCB 118 (the non-ortho PCB) and the median result of all other PCBs (multi-ortho PCBs). Points indicate the PCB measurements at time of sacrifice, and error bars indicate the minimum and maximum measured values of multi-ortho PCBs.

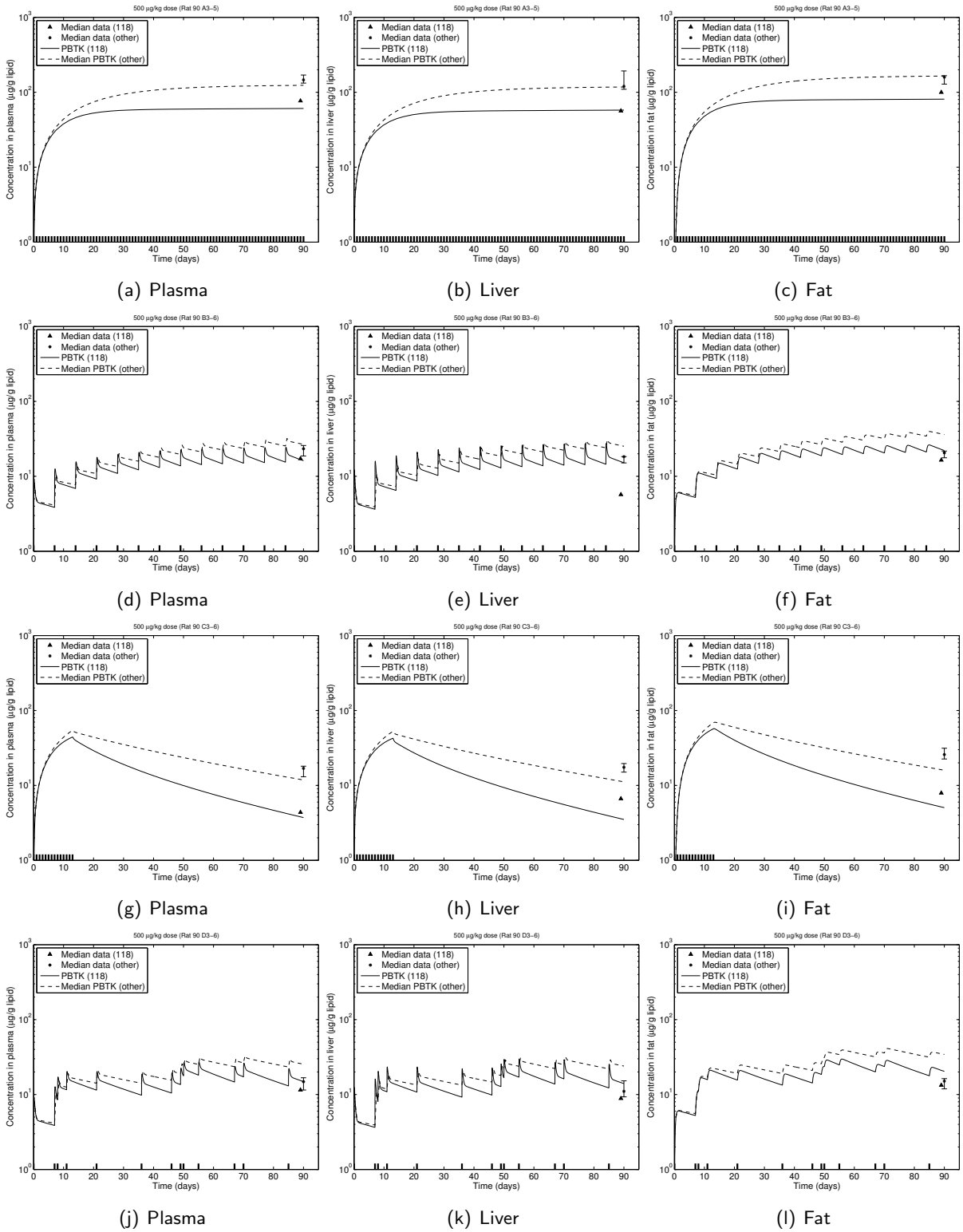

Figure B.6: Model predictions for PCB concentrations at 500 µg/kg exposure for the evaluation data set of rats sacrificed at day 90. Data-specific body measurements were used for each rat. Results and data were condensed to show the results for PCB 118 (the non-ortho PCB) and the median result of all other PCBs (multi-ortho PCBs). Points indicate the PCB measurements at time of sacrifice, and error bars indicate the minimum and maximum measured values of multi-ortho PCBs.

Bibliography

[1] A. W. Abu-Qare and M. B. Abou-Donia. Combined exposure to DEET (N,N-diethyl-m-toluamide) and permethrin-induced release of rat brain mitochondrial cytochrome c. *Journal of Toxicology and Environmental Health, Part A*, 63(4):243–52, Jun 22 2001.

[2] K. Adachi and Y. Tainosho. Characterization of heavy metal particles embedded in tire dust. *Environ Int*, 30(8):1009–17, Oct 2004.

[3] J. L. Adgate, C. Weisel, Y. Wang, G. G. Rhoads, and P. J. Lioy. Lead in house dust: relationships between exposure metrics. *Environ Res*, 70(2):134–47, Aug 1995.

[4] S. Agatonovic-Kustrin and R. Beresford. Basic concepts of artificial neural network (ANN) modeling and its application in pharmaceutical research. *Journal of Pharmaceutical and Biomedical Analysis*, 22(5):717–727, JUN 2000.

[5] P. S. Agutter and D. N. Wheatley. Metabolic scaling: consensus or controversy? *Theor Biol Med Model*, 1(1):13, Nov 16 2004.

[6] A. A. Ahmed, A. Mohamed, A. E. Ali, A. Barakat, M. Abd El-Hady, and A. El-Hussein. Seasonal variations of aerosol residence time in the lower atmospheric boundary layer. *J Environ Radioact*, 77(3):275–83, 2004.

[7] A. Albores, C. J. Sinal, M. G. Cherian, and J. R. Bend. Selective increase of rat lung cytochrome P450 1A1 dependent monooxygenase activity after acute sodium arsenite administration. *Can J Physiol Pharmacol*, 73(1):153–8, Jan 1995.

[8] L. Amin-Zaki, S. Elhassani, M. A. Majeed, T. W. Clarkson, R. A. Doherty, M. R. Greenwood, and T. Giovanoli-Jakubczak. Perinatal methylmercury poisoning in Iraq. *Am J Dis Child*, 130(10):1070–6, Oct 1976.

[9] B. Amzal, B. Julin, M. Vahter, A. Wolk, G. Johanson, and A. Akesson. Population Toxicokinetic Modeling of Cadmium for Health Risk Assessment. *Environmental Health Perspectives*, (in press), 2009.

[10] M. E. Andersen. Toxicokinetic modeling and its applications in chemical risk assessment. *Toxicol Lett*, 138(1-2):9–27, Feb 18 2003.

[11] M. E. Andersen, L. S. Birnbaum, H. A. Barton, and C. R. Eklund. Regional hepatic CYP1A1 and CYP1A2 induction with 2,3,7,8-tetrachlorodibenzo-p-dioxin evaluated with a multicompartment geometric model of hepatic zonation. *Toxicology and Applied Pharmacology*, 144(1):145–155, May 1997. ISSN 0041-008X.

[12] M. E. Andersen, R. W. Lutz, K. H. Liao, and W. K. Lutz. Dose-incidence modeling: consequences of linking quantal measures of response to depletion of critical tissue targets. *Toxicol Sci*, 89(1):331–7, Jan 2006.

[13] O. Andersen, J. B. Nielsen, and G. F. Nordberg. Nutritional interactions in intestinal cadmium uptake–possibilities for risk reduction. *Biometals*, 17(5):543–7, Oct 2004.

[14] C. R. Angle, A. Marcus, I. H. Cheng, and M. S. McIntire. Omaha childhood blood lead and environmental lead: a linear total exposure model. *Environ Res*, 35(1):160–70, Oct 1984.

[15] ATSDR. Toxicological Profile for Chlorpyrifos. Technical report, US Department of Health and Human Services, 1997.

[16] ATSDR. Toxicological Profile for Cadmium. Technical report, US Department of Health and Human Services, Atlanta, GA, 1999.

[17] ATSDR. Toxicological Profile for Lead. Technical report, US Department of Health and Human Services, Atlanta, GA, 1999.

[18] ATSDR. Toxicological Profile for Arsenic. Technical report, US Department of Health and Human Services, Atlanta, GA, 2000.

[19] ATSDR. Toxicological Profile for Chromium. Technical report, US Department of Health and Human Services, Atlanta, GA, 2000.

[20] ATSDR. Toxicological Profile for Polychlorinated Biphenyls (PCBs). Technical report, US Department of Health and Human Services, Atlanta, GA, 2000.

[21] ATSDR. Interaction profile for arsenic, cadmium, chromium, and lead. Technical report, US Department of Health and Human Services, 2004.

[22] S. Azimi, V. Rocher, M. Muller, R. Moilleron, and D. R. Thevenot. Sources, distribution and variability of hydrocarbons and metals in atmospheric deposition in an urban area (Paris, France). *Sci Total Environ*, 337(1-3):223–39, Jan 20 2005.

[23] J. R. Baker, R. J. Edwards, J. M. Lasker, M. R. Moore, and S. Satarug. Renal and hepatic accumulation of cadmium and lead in the expression of CYP4F2 and CYP2E1. *Toxicol Lett*, 159(2):182–91, Nov 15 2005.

[24] F. Bakir, S. F. Damluji, L. Amin-Zaki, M. Murtadha, A. Khalidi, N. Y. al Rawi, S. Tikriti, H. I. Dahahir, T. W. Clarkson, J. C. Smith, and R. A. Doherty. Methylmercury poisoning in Iraq. *Science*, 181(96):230–41, Jul 20 1973.

[25] S. Balakrishnan, A. Roy, M. G. Ierapetritou, G. P. Flach, and P. G. Georgopoulos. Uncertainty reduction and characterization for complex environmental fate and transport models: An empirical Bayesian framework incorporating the stochastic response surface method. *Water Resources Research*, 39(12):–, Dec 17 2003. ISSN 0043-1397.

[26] N. Ballatori. Transport of toxic metals by molecular mimicry. *Environ Health Perspect*, 110 Suppl 5:689–94, Oct 2002.

[27] V. Bankovitch, G. Carrier, C. Gagnon, L. Normandin, G. Kennedy, and J. Zayed. Total suspended particulate manganese in ambient air in Montreal 1981-2000. *Sci Total Environ*, 308(1-3):185–93, Jun 1 2003.

[28] O. Barbier, G. Jacquillet, M. Tauc, M. Cougnon, and P. Poujeol. Effect of heavy metals on, and handling by, the kidney. *Nephron Physiol*, 99(4):p105–10, 2005.

[29] D. B. Barr and J. Angerer. Potential uses of biomonitoring data: a case study using the organophosphorus pesticides chlorpyrifos and malathion. *Environ Health Perspect*, 114 (11):1763–9, Nov 2006.

[30] D. B. Barr, L. C. Wilder, S. P. Caudill, A. J. Gonzalez, L. L. Needham, and J. L. Pirkle. Urinary creatinine concentrations in the U.S. population: implications for urinary biologic monitoring measurements. *Environ Health Perspect*, 113(2):192–200, Feb 2005.

[31] L. M. Barraj and J. S. Tsuji. A probabilistic arsenic exposure assessment for children who contact CCA-treated playsets and decks. *Risk Anal*, 27(1):1–3; author reply 5–6, Feb 2007.

[32] H. A. Barton, J. Tang, Y. M. Sey, J. P. Stanko, R. N. Murrell, J. C. Rockett, and D. J. Dix. Metabolism of myclobutanil and triadimefon by human and rat cytochrome P450 enzymes and liver microsomes. *Xenobiotica*, 36(9):793–806, Sep 2006.

[33] F. Baruthio. Toxic effects of chromium and its compounds. *Biol Trace Elem Res*, 32: 145–53, Jan-Mar 1992.

[34] Y. Batonneau, C. Bremard, L. Gengembre, J. Laureyns, A. Le Maguer, D. Le Maguer, E. Perdrix, and S. Sobanska. Speciation of PM10 sources of airborne nonferrous metals within the 3-km zone of lead/zinc smelters. *Environ Sci Technol*, 38(20):5281–9, Oct 15 2004.

[35] J. L. Benedetti, O. Samuel, E. Dewailly, S. Gingras, and M. A. Lefebvre. Levels of cadmium in kidney and liver tissues among a Canadian population (province of Quebec). *J Toxicol Environ Health A*, 56(3):145–63, Feb 12 1999.

[36] A. L. Benin, J. D. Sargent, M. Dalton, and S. Roda. High concentrations of heavy metals in neighborhoods near ore smelters in northern Mexico. *Environ Health Perspect*, 107(4): 279–84, Apr 1999.

[37] P. Bernillon and F. Y. Bois. Statistical issues in toxicokinetic modeling: a bayesian perspective. *Environ Health Perspect*, 108 Suppl 5:883–93, Oct 2000.

[38] P. J. Berny, L. M. Cote, and W. B. Buck. Relationship between soil lead, dust lead, and blood lead concentrations in pets and their owners: evaluation of soil lead threshold values. *Environ Res*, 67(1):84–97, Oct 1994.

[39] J. L. Bert, L. J. van Dusen, and J. R. Grace. A generalized model for the prediction of lead body burdens. *Environ Res*, 48(1):117–27, Feb 1989.

[40] C. Bilos, J. C. Colombo, C. N. Skorupka, and M. J. Rodriguez Presa. Sources, distribution and variability of airborne trace metals in La Plata City area, Argentina. *Environ Pollut*, 111(1):149–58, 2001.

[41] K. B. Bischoff and R. L. Dedrick. Thiopental pharmacokinetics. *J Pharm Sci*, 57(8): 1346–51, Aug 1968.

[42] Blancato, J. N. and Power, F. and Brown, R.N. and Dary, C. Exposure Related Dose Estimating Model (ERDEM): A Physiologically-Based Pharmacokinetic and Pharmacodynamic (PBPK/PD) Model for Assessing Human Exposure and Risk. Technical report, USEPA Office of Research and Development, Las Vegas, NV, 2006.

[43] K. T. Bogen. Pharmacokinetics for regulatory risk analysis: the case of trichloroethylene. *Regul Toxicol Pharmacol*, 8(4):447–66, Dec 1988.

[44] F. Boreland and D. M. Lyle. Lead dust in Broken Hill homes: effect of remediation on indoor lead levels. *Environ Res*, 100(2):276–83, Feb 2006.

[45] F. Boreland, D. M. Lyle, J. Wlodarczyk, W. A. Balding, and S. Reddan. Lead dust in broken hill homes–a potential hazard for young children? *Aust N Z J Public Health*, 26 (3):203–7, 2002.

[46] R. Bornschein, P. Succop, K.M. Krafft, C. S. Clark, B. Peace, and P.B. Hammond. Exterior surface dust lead, interior house dust lead and childhood exposure in an urban environment. *Trace Subst. Environ. Health*, 20:322–332, 1986.

[47] R. L. Bornschein, P. B. Hammond, K. N. Dietrich, P. Succop, K. Krafft, S. Clark, O. Berger, D. Pearson, and S. Que Hee. The Cincinnati prospective study of low-level lead exposure and its effects on child development: protocol and status report. *Environ Res*, 38(1):4–18, Oct 1985.

[48] I. Bremner. Interactions between metallothionein and trace elements. *Prog Food Nutr Sci*, 11(1):1–37, 1987.

[49] J. P. Bressler, L. Olivi, J. H. Cheong, Y. Kim, and D. Bannona. Divalent metal transporter 1 in lead and cadmium transport. *Ann N Y Acad Sci*, 1012:142–52, Mar 2004.

[50] J. P. Bressler, L. Olivi, J. H. Cheong, Y. Kim, A. Maerten, and D. Bannon. Metal transporters in intestine and brain: their involvement in metal-associated neurotoxicities. *Human & Experimental Toxicology*, 26(3):221–229, Mar 2007. ISSN 0960-3271.

[51] C. C. Bridges and R. K. Zalups. Molecular and ionic mimicry and the transport of toxic metals. *Toxicol Appl Pharmacol*, 204(3):274–308, May 1 2005.

[52] R. R. Briefel. Assessment of the US diet in national nutrition surveys: national collaborative efforts and NHANES. *Am J Clin Nutr*, 59(1 Suppl):164S–167S, Jan 1994.

[53] B. Brunekreef, S. J. Veenstra, K. Biersteker, and J. S. Boleij. The Arnhem Lead Study. I. Lead uptake by 1- to 3-year-old children living in the vicinity of a secondary lead smelter in Arnhem, The Netherlands. *Environ Res*, 25(2):441–8, Aug 1981.

[54] M. M. Brzoska and J. Moniuszko-Jakoniuk. Interactions between cadmium and zinc in the organism. *Food Chem Toxicol*, 39(10):967–80, Oct 2001.

[55] J. P. Buchet, R. Lauwerys, and H. Roels. Comparison of the urinary excretion of arsenic metabolites after a single oral dose of sodium arsenite, monomethylarsonate, or dimethylarsinate in man. *Int Arch Occup Environ Health*, 48(1):71–9, 1981.

[56] J. P. Buchet, R. Lauwerys, and H. Roels. Urinary excretion of inorganic arsenic and its metabolites after repeated ingestion of sodium metaarsenite by volunteers. *Int Arch Occup Environ Health*, 48(2):111–8, 1981.

[57] J. P. Buchet, J. F. Heilier, A. Bernard, D. Lison, T. Jin, X. Wu, Q. Kong, and G. Nordberg. Urinary protein excretion in humans exposed to arsenic and cadmium. *Int Arch Occup Environ Health*, 76(2):111–20, Mar 2003.

[58] W. Butte and B. Heinzow. Pollutants in house dust as indicators of indoor contamination. *Rev Environ Contam Toxicol*, 175:1–46, 2002.

[59] J. Z. Byczkowski and J. C. Lipscomb. Physiologically based pharmacokinetic modeling of the lactational transfer of methylmercury. *Risk Anal*, 21(5):869–82, Oct 2001.

[60] Edward J. Calabrese. *Principles of animal extrapolation.* Environmental science and technology,. Wiley, New York, 1983. ISBN 0471087629.

[61] J. Campain. Metals and Inorganic Compounds (Chapter 9). In M. B. Reddy, R. S. H. Yang, H. J. Clewell, and M. E. Andersen, editors, *Physiologically based pharmacokinetic modeling : science and applications*, pages 239–270. Wiley-Interscience, Hoboken, N.J., 2005.

[62] C. Campbell, D. F. Schwarz, D. Rich, and D. W. Dockery. Effect of a follow-up professional home cleaning on serial dust and blood lead levels of urban children. *Arch Environ Health*, 58(12):771–80, Dec 2003.

[63] J. Caravanos, A. L. Weiss, M. J. Blaise, and R. J. Jaeger. A survey of spatially distributed exterior dust lead loadings in New York City. *Environ Res*, 100(2):165–72, Feb 2006.

[64] J. Caravanos, A. L. Weiss, and R. J. Jaeger. An exterior and interior leaded dust deposition survey in New York City: results of a 2-year study. *Environ Res*, 100(2):159–64, Feb 2006.

[65] A. Carpi and Y. F. Chen. Gaseous elemental mercury as an indoor air pollutant. *Environ Sci Technol*, 35(21):4170–3, Nov 1 2001.

[66] G. Carrier, M. Bouchard, R. C. Brunet, and M. Caza. A toxicokinetic model for predicting the tissue distribution and elimination of organic and inorganic mercury following exposure to methyl mercury in animals and humans. II. Application and validation of the model in humans. *Toxicology and Applied Pharmacology*, 171(1):50–60, Feb 15 2001.

[67] C. D. Carrington and M. P. Bolger. An exposure assessment for methylmercury from seafood for consumers in the United States. *Risk Anal*, 22(4):689–99, Aug 2002.

[68] L. Carrizales, I. Razo, J. I. Tellez-Hernandez, R. Torres-Nerio, A. Torres, L. E. Batres, A. C. Cubillas, and F. Diaz-Barriga. Exposure to arsenic and lead of children living near a copper-smelter in San Luis Potosi, Mexico: Importance of soil contamination for exposure of children. *Environ Res*, 101(1):1–10, May 2006.

[69] I. Cascorbi. Genetic basis of toxic reactions to drugs and chemicals. *Toxicol Lett*, 162(1): 16–28, Mar 15 2006.

[70] H. Cember. A model for the kinetics of mercury elimination. *American Industrial Hygiene Association Journal*, 30(4):367–71, Jul-Aug 1969.

[71] G. Chattopadhyay, K. C. Lin, and A. J. Feitz. Household dust metal levels in the Sydney metropolitan area. *Environ Res*, 93(3):301–7, Nov 2003.

[72] J. J. Chen, G. S. Chen, and N. J. Bunce. Inhibition of CYP 1A2-dependent MROD activity in rat liver microsomes: an explanation of the hepatic sequestration of a limited subset of halogenated aromatic hydrocarbons. *Environ Toxicol*, 18(2):115–9, Apr 2003.

[73] S. N. Chillrud, D. Grass, J. M. Ross, D. Coulibaly, V. Slavkovich, D. Epstein, S. N. Sax, D. Pederson, D. Johnson, J. D. Spengler, P. L. Kinney, H. J. Simpson, and P. Brandt-Rauf. Steel dust in the New York City subway system as a source of manganese, chromium, and iron exposures for transit workers. *J Urban Health*, 82(1):33–42, Mar 2005.

[74] W. A. Chiu and P. White. Steady-state solutions to PBPK models and their applications to risk assessment I: Route-to-route extrapolation of volatile chemicals. *Risk Anal*, 26(3): 769–80, Jun 2006. ISSN 0272-4332 (Print).

[75] A. L. Choi, E. Budtz-Jorgensen, P. J. Jorgensen, U. Steuerwald, F. Debes, P. Weihe, and P. Grandjean. Selenium as a potential protective factor against mercury developmental neurotoxicity. *Environ Res*, 107(1):45–52, May 2008.

[76] S. Chou, J. Colman, C. Tylenda, and C. De Rosa. Chemical-specific health consultation for chromated copper arsenate chemical mixture: port of Djibouti. *Toxicol Ind Health*, 23 (4):183–208, May 2007.

[77] H. Choudhury, T. Harvey, W. C. Thayer, T. F. Lockwood, W. M. Stiteler, P. E. Goodrum, J. M. Hassett, and G. L. Diamond. Urinary cadmium elimination as a biomarker of exposure for evaluating a cadmium dietary exposure–biokinetics model. *Journal of Toxicology and Environmental Health-Part A*, 63(5):321–50, Jul 6 2001.

[78] B. A. Chowdhury and R. K. Chandra. Biological and health implications of toxic heavy metal and essential trace element interactions. *Prog Food Nutr Sci*, 11(1):55–113, 1987.

[79] L. S. Chubb, M. E. Andersen, C. J. Broccardo, M. E. Legare, R. E. Billings, C. E. Dean, and W. H. Hanneman. Regional induction of CYP1A1 in rat liver following treatment with mixtures of PCB 126 and PCB 153. *Toxicol Pathol*, 32(4):467–73, Jul-Aug 2004.

[80] C. S. Clark, V. Thuppil, R. Clark, S. Sinha, G. Menezes, H. D'Souza, N. Nayak, A. Kuruvilla, T. Law, P. Dave, and S. Shah. Lead in paint and soil in Karnataka and Gujarat, India. *J Occup Environ Hyg*, 2(1):38–44, Jan 2005.

[81] S. Clark, W. Menrath, M. Chen, P. Succop, R. Bornschein, W. Galke, and J. Wilson. The influence of exterior dust and soil lead on interior dust lead levels in housing that had undergone lead-based paint hazard control. *J Occup Environ Hyg*, 1(5):273–82, May 2004.

[82] C. A. Clayton, E. D. Pellizzari, R. W. Whitmore, R. L. Perritt, and J. J. Quackenboss. National Human Exposure Assessment Survey (NHEXAS): distributions and associations of lead, arsenic and volatile organic compounds in EPA region 5. *J Expo Anal Environ Epidemiol*, 9(5):381–92, Sep-Oct 1999.

[83] C. A. Clayton, E. D. Pellizzari, and J. J. Quackenboss. National Human Exposure Assessment Survey: analysis of exposure pathways and routes for arsenic and lead in EPA Region 5. *J Expo Anal Environ Epidemiol*, 12(1):29–43, Jan-Feb 2002.

[84] H. J. Clewell, J. M. Gearhart, P. R. Gentry, T. R. Covington, C. B. VanLandingham, K. S. Crump, and A. M. Shipp. Evaluation of the uncertainty in an oral reference dose for methylmercury due to interindividual variability in pharmacokinetics. *Risk Anal*, 19 (4):547–58, Aug 1999.

[85] H. J. Clewell, P. R. Gentry, J. M. Gearhart, B. C. Allen, and M. E. Andersen. Comparison of cancer risk estimates for vinyl chloride using animal and human data with a PBPK model. *Sci Total Environ*, 274(1-3):37–66, Jul 2 2001.

[86] H. J. Clewell, J. Teeguarden, T. McDonald, R. Sarangapani, G. Lawrence, T. Covington, R. Gentry, and A. Shipp. Review and evaluation of the potential impact of age- and gender-specific pharmacokinetic differences on tissue dosimetry. *Crit Rev Toxicol*, 32(5): 329–89, Sep 2002.

[87] H. J. Clewell, R. S. Thomas, P. R. Gentry, K. S. Crump, E. M. Kenyon, H. A. El-Masri, and J. W. Yager. Research toward the development of a biologically based dose response assessment for inorganic arsenic carcinogenicity: A progress report. *Toxicol Appl Pharmacol*, Mar 30 2007.

[88] K. Connor, S. Safe, C. R. Jefcoate, and M. Larsen. Structure-dependent induction of CYP2B by polychlorinated biphenyl congeners in female Sprague-Dawley rats. *Biochem Pharmacol*, 50(11):1913–20, Nov 27 1995.

[89] A. G. Cook, P. Weinstein, and J. A. Centeno. Health effects of natural dust: role of trace elements and compounds. *Biol Trace Elem Res*, 103(1):1–15, Jan 2005.

[90] R. A. Corley, T. J. Mast, E. W. Carney, J. M. Rogers, and G. P. Daston. Evaluation of physiologically based models of pregnancy and lactation for their application in children's health risk assessments. *Crit Rev Toxicol*, 33(2):137–211, 2003.

[91] R. A. Corley, M. J. Bartels, E. W. Carney, K. K. Weitz, J. J. Soelberg, R. A. Gies, and K. D. Thrall. Development of a Physiologically Based Pharmacokinetic Model for Ethylene Glycol and Its Metabolite, Glycolic Acid, in Rats and Humans. *Toxicol Sci*, Feb 16 2005.

[92] T. R. Covington, P. Robinan Gentry, C. B. Van Landingham, M. E. Andersen, J. E. Kester, and H. J. Clewell. The use of Markov chain Monte Carlo uncertainty analysis to support a Public Health Goal for perchloroethylene. *Regul Toxicol Pharmacol*, 47(1): 1–18, Feb 2007.

[93] D. M. Cowan, Q. Fan, Y. Zou, X. Shi, J. Chen, M. Aschner, F. S. Rosenthal, and W. Zheng. Manganese exposure among smelting workers: blood manganese-iron ratio as a novel tool for manganese exposure assessment. *Biomarkers*, 14(1):3–16, Feb 2009.

[94] Y. Cui, Y. G. Zhu, R. Zhai, Y. Huang, Y. Qiu, and J. Liang. Exposure to metal mixtures and human health impacts in a contaminated area in Nanning, China. *Environ Int*, 31 (6):784–90, Aug 2005.

[95] E.B. Culbard and L.R. Johnson. Elevated arsenic concentrations in house dusts located in a mineralized area of Southwest England: implication for human health. *Trace Subst. Environ. Health*, 18:311–319, 1984.

[96] E.B. Culbard and I. Thornton. Metal contamination in British urban streets. *J. Environ. Qual*, 17:226–234, 1988.

[97] E.B. Culbard, S. Moorcroft, J. M. Watt, I. Thornton, and J.F.A Thomas. A nationwide reconnaisance survey of metals in urban dusts and soils. *Min. Environ.*, 5:82–84, 1983.

[98] E.B. Culbard, I. Thornton, J. M. Watt, S. Moorcroft, K. Brooks, and M. Thompson. A nation wide reconnaisance survey of the United Kingdom to determine metal concentrations in urban dusts and soils. *Trace Subst. Environ. Health*, XVII:236–241, 1983.

[99] R. Danzeisen and H. J. McArdle. Copper and iron interactions in a placental cell line (BeWo). *Biochem Soc Trans*, 26(2):S99, May 1998.

[100] B. Davies, P. C. Elwood, J. E. Gallacher, and R.C. Ginnever. The relationship between heavy metals in garden soils and housedusts in an old mining area of North Wales, Great Britain. *Environ Pollut*, B9:225–266, 1985.

[101] D. J. Davies, J. M. Watt, and I. Thornton. Lead levels in Birmingham dusts and soils. *Sci Total Environ*, 67(2-3):177–85, Dec 1987.

[102] D.J.A Davies, I. Thornton, J. M. Watt, and E.B. Culbard. Lead levels in and around the homes of inner-city children. In I. Thornton and E.B. Culbard, editors, *Lead in the Home Environment*, pages 102–122. Science Reviews Ltd., Northwood, England, 1987.

[103] M. Degawa, H. Arai, M. Kubota, and Y. Hashimoto. Ionic lead, a unique metal ion as an inhibitor for cytochrome P450IA2 (CYP1A2) expression in the rat liver. *Biochem Biophys Res Commun*, 200(2):1086–92, Apr 29 1994.

[104] T. Degim, J. Hadgraft, S. Ilbasmis, and Y. Ozkan. Prediction of skin penetration using artificial neural network (ANN) modeling. *J Pharm Sci*, 92(3):656–64, Mar 2003.

[105] J. I. Delic, P. D. Lilly, A. J. MacDonald, and G. D. Loizou. The utility of PBPK in the safety assessment of chloroform and carbon tetrachloride. *Regul Toxicol Pharmacol*, 32 (2):144–55, Oct 2000. ISSN 0273-2300 (Print).

[106] J. E. Dennison, P. L. Bigelow, and M. E. Andersen. Occupational exposure limits in the context of solvent mixtures, consumption of ethanol, and target tissue dose. *Toxicol Ind Health*, 20(6-10):165–75, Sep 2004.

[107] J. E. Dennison, P. L. Bigelow, M. M. Mumtaz, M. E. Andersen, I. D. Dobrev, and R. S. Yang. Evaluation of potential toxicity from co-exposure to three cns depressants (toluene, ethylbenzene, and xylene) under resting and working conditions using PBPK modeling. *J Occup Environ Hyg*, 2(3):127–35, Mar 2005.

[108] R. S. DeWoskin, S. Barone, H. J. Clewell, and R. W. Setzer. Improving the development and use of biologically based dose response models (BBDR) in risk assessment. *Human and Ecological Risk Assessment*, 7(5):1091–1120, Oct 2001. ISSN 1080-7039.

[109] G. L. Diamond, W. C. Thayer, and H. Choudhury. Pharmacokinetics/pharmacodynamics (PK/PD) modeling of risks of kidney toxicity from exposure to cadmium: estimates of dietary risks in the U.S. population. *J Toxicol Environ Health A*, 66(22):2141–64, Nov 28 2003.

[110] J. A. Diemel, B. Brunekreef, J. S. Boleij, K. Biersteker, and S. J. Veenstra. The Arnhem Lead Study. II. Indoor pollution, and indoor/outdoor relationships. *Environ Res*, 25(2): 449–56, Aug 1981.

[111] U. Dirksen, K. A. Moghadam, C. Mambetova, C. Esser, M. Fuhrer, and S. Burdach. Glutathione S transferase theta 1 gene (GSTT1) null genotype is associated with an increased risk for acquired aplastic anemia in children. *Pediatr Res*, 55(3):466–71, Mar 2004.

[112] S. L. Dixon, J. W. Wilson, P. A. Succop, M. Chen, W. A. Galke, W. Menrath, and C. S. Clark. Residential dust lead loading immediately after intervention in the HUD lead hazard control grant program. *J Occup Environ Hyg*, 1(11):716–24, Nov 2004.

[113] M. L. Dourson, M. E. Andersen, L. S. Erdreich, and J. A. MacGregor. Using human data to protect the public's health. *Regul Toxicol Pharmacol*, 33(2):234–56, Apr 2001.

[114] Z. Drobna, S. B. Waters, F. S. Walton, E. L. LeCluyse, D. J. Thomas, and M. Styblo. Interindividual variation in the metabolism of arsenic in cultured primary human hepatocytes. *Toxicol Appl Pharmacol*, 201(2):166–77, Dec 1 2004.

[115] J. Dwyer, M. F. Picciano, and D. J. Raiten. Future directions for the integrated CSFII-NHANES: What We Eat in America-NHANES. *J Nutr*, 133(2):576S–81S, Feb 2003.

[116] M. R. Easterling, M. V. Evans, and E. M. Kenyon. Comparative analysis of software for physiologically based pharmacokinetic modeling: Simulation, optimization, and sensitivity analysis. *Toxicology Methods*, 10(3):203–229, Jul-Sep 2000. ISSN 1051-7235.

[117] A. N. Edginton, W. Schmitt, and S. Willmann. Development and evaluation of a generic physiologically based pharmacokinetic model for children. *Clinical Pharmacokinetics*, 45 (10):1013–1034, 2006. ISSN 0312-5963.

[118] R. F. Edlich, K. L. Winters, and 3rd Long, W. B. Treated wood preservatives linked to aquatic damage, human illness, and death–a societal problem. *J Long Term Eff Med Implants*, 15(2):209–23, 2005.

[119] P. P. Egeghy, J. J. Quackenboss, S. Catlin, and P. B. Ryan. Determinants of temporal variability in NHEXAS-Maryland environmental concentrations, exposures, and biomarkers. *J Expo Anal Environ Epidemiol*, 15(5):388–97, Sep 2005.

[120] H. A. El-Masri and E. M. Kenyon. Development of a human physiologically based pharmacokinetic (PBPK) model for inorganic arsenic and its mono- and di-methylated metabolites. *J Pharmacokinet Pharmacodyn*, Oct 18 2007.

[121] P. C. Elwood, J. E. Gallacher, K. M. Phillips, B. E. Davies, and C. Toothill. Greater contribution to blood lead from water than from air. *Nature*, 310(5973):138–40, Jul 12-18 1984.

[122] C. Emond, L. S. Birnbaum, and M. J. DeVito. Physiologically based pharmacokinetic model for developmental exposures to TCDD in the rat. *Toxicol Sci*, 80(1):115–33, Jul 2004.

[123] C. Emond, M. Charbonneau, and K. Krishnan. Physiologically based modeling of the accumulation in plasma and tissue lipids of a mixture of PCB congeners in female Sprague-Dawley rats. *Journal of Toxicology and Environmental Health-Part a-Current Issues*, 68 (16):1393–1412, Aug 27 2005. ISSN 1528-7394.

[124] C. Emond, L. S. Birnbaum, and M. J. DeVito. Use of a physiologically based pharmacokinetic model for rats to study the influence of body fat mass and induction of CYP1A2 on the pharmacokinetics of TCDD. *Environ Health Perspect*, 114(9):1394–400, Sep 2006.

[125] A. S. Ettinger, R. L. Bornschein, M. Farfel, C. Campbell, N. B. Ragan, G. G. Rhoads, M. Brophy, S. Wilkens, and D. W. Dockery. Assessment of cleaning to control lead dust in homes of children with moderate lead poisoning: treatment of lead-exposed children trial. *Environ Health Perspect*, 110(12):A773–9, Dec 2002.

[126] G. C. Fang, Y. S. Wu, C. C. Chu, S. H. Huang, and J. Y. Rau. The concentration, dry deposition, composition study of ambient air particulate and metallic pollutants at a traffic sampling site. *Toxicol Ind Health*, 19(1):25–35, Feb 2003.

[127] M. R. Farfel, A. O. Orlova, P. S. Lees, C. Rohde, P. J. Ashley, and Jr. Chisolm, J. J. A study of urban housing demolitions as sources of lead in ambient dust: demolition practices and exterior dust fall. *Environ Health Perspect*, 111(9):1228–34, Jul 2003.

[128] E. M. Faustman, T. A. Lewandowski, R. A. Ponce, and S. M. Bartell. Biologically based dose-response models for developmental toxicants: lessons from methylmercury. *Inhal Toxicol*, 11(6-7):559–72, Jun-Jul 1999.

[129] E. M. Faustman, R. A. Ponce, Y. C. Ou, M. A. Mendoza, T. Lewandowski, and T. Kavanagh. Investigations of methylmercury-induced alterations in neurogenesis. *Environ Health Perspect*, 110 Suppl 5:859–64, Oct 2002.

[130] X. Feng, S. Tang, L. Shang, H. Yan, J. Sommar, and O. Lindqvist. Total gaseous mercury in the atmosphere of Guiyang, PR China. *Sci Total Environ*, 304(1-3):61–72, Mar 20 2003.

[131] Y. Feng and R. Barratt. Distributions of lead and cadmium in dust in the vicinity of a sewage sludge incinerator. *J Environ Monit*, 1(2):169–76, Apr 1999.

[132] J. E. Fergusson and N. D. Kim. Trace elements in street and house dusts: sources and speciation. *Sci Total Environ*, 100 Spec No:125–50, Mar 1991.

[133] J. E. Fergusson and R. J. Schroeder. Lead in house dust of Christchurch, New Zealand: sampling, levels and sources. *Sci Total Environ*, 46:61–72, Nov 1985.

[134] J. E. Fergusson, E.A. Forbes, R. J. Schroeder, and D.E. Ryan. The elemental composition and sources of house dust and street dust. *Sci Total Environ*, 50:217–221, 1986.

[135] J. A. Fernandez, A. Ederra, E. Nunez, J. Martinez-Abaigar, M. Infante, P. Heras, M. J. Elias, V. Mazimpaka, and A. Carballeira. Biomonitoring of metal deposition in northern Spain by moss analysis. *Sci Total Environ*, 300(1-3):115–27, Dec 2 2002.

[136] J. W. Fisher, J. Campbell, S. Muralidhara, J. V. Bruckner, D. Ferguson, M. Mumtaz, B. Harmon, J. M. Hedge, K. M. Crofton, H. Kim, and T. L. Almekinder. Effect of PCB 126 on hepatic metabolism of thyroxine and perturbations in the hypothalamic-pituitary-thyroid axis in the rat. *Toxicol Sci*, 90(1):87–95, Mar 2006.

[137] J. Flores and L. A. Albert. Environmental lead in Mexico, 1990-2002. *Rev Environ Contam Toxicol*, 181:37–109, 2004.

[138] C. A. Franklin, M. J. Inskip, C. L. Baccanale, C. M. Edwards, W. I. Manton, E. Edwards, and J. O'Flaherty E. Use of sequentially administered stable lead isotopes to investigate changes in blood lead during pregnancy in a nonhuman primate (Macaca fascicularis). *Fundam Appl Toxicol*, 39(2):109–19, Oct 1997.

[139] N. C. Freeman, P. J. Lioy, and A. H. Stern. Reduction in residential chromium following site remediation. *J Air Waste Manag Assoc*, 50(6):948–53, Jun 2000.

[140] L. Friberg, C.G. Elinder, and T. Kjellstrom. *Cadmium*. Environmental health criteria 134. World Health Organization, Geneva, 1992. ISBN 9241571349.

[141] L. Friis, L. Petersson, and C. Edling. Reduced cadmium levels in human kidney cortex in sweden. *Environ Health Perspect*, 106(4):175–8, Apr 1998.

[142] Gilbert F. Froment and Kenneth B. Bischoff. *Chemical reactor analysis and design*. Wiley series in chemical engineering. Wiley, New York, 2nd edition, 1990. ISBN 0471510440.

[143] Howard Frumkin. *Environmental health : from global to local*. Jossey-Bass, San Francisco, CA, 2005. ISBN 0787973831 (alk. paper).

[144] J.E. Furgusson, K.A. Hibbard, and R. Lau Hie Ting. Lead in human hair: general survey - battery factory employees and thier families. *Environ. Pollut.*, B2:235–248, 1981.

[145] Jr. Furtaw, E. J. An overview of human exposure modeling activities at the USEPA's National Exposure Research Laboratory. *Toxicol Ind Health*, 17(5-10):302–14, Jun 2001.

[146] J. Gailer. Arsenic-selenium and mercury-selenium bonds in biology. *Coordination Chemistry Reviews*, 251(1-2):234–254, Jan 2007. ISSN 0010-8545.

[147] D. G. Gajghate and A. D. Bhanarkar. Tracking toxic metals in the ambient air of Agra City, India. *Bull Environ Contam Toxicol*, 72(4):806–12, Apr 2004.

[148] M. Gamo, K. Ono, and J. Nakanishi. Meta-analysis for deriving age- and gender-specific dose-response relationships between urinary cadmium concentration and beta2-microglobulinuria under environmental exposure. *Environ Res*, 101(1):104–12, May 2006.

[149] M. L. Gargas, T. R. Tyler, L. M. Sweeney, R. A. Corley, K. K. Weitz, T. J. Mast, D. J. Paustenbach, and S. M. Hays. A toxicokinetic study of inhaled ethylene glycol monomethyl ether (2-ME) and validation of a physiologically based pharmacokinetic model for the pregnant rat and human. *Toxicol Appl Pharmacol*, 165(1):53–62, May 15 2000.

[150] M. L. Gargas, T. R. Tyler, L. M. Sweeney, R. A. Corley, K. K. Weitz, T. J. Mast, D. J. Paustenbach, and S. M. Hays. A toxicokinetic study of inhaled ethylene glycol ethyl ether acetate and validation of a physiologically based pharmacokinetic model for rat and human. *Toxicol Appl Pharmacol*, 165(1):63–73, May 15 2000.

[151] M. D. Garrick, K. G. Dolan, C. Horbinski, A. J. Ghio, D. Higgins, M. Porubcin, E. G. Moore, L. N. Hainsworth, J. N. Umbreit, M. E. Conrad, L. Feng, A. Lis, J. A. Roth, S. Singleton, and L. M. Garrick. DMT1: a mammalian transporter for multiple metals. *Biometals*, 16(1):41–54, Mar 2003.

[152] A. E. Gaweda, A. A. Jacobs, M. E. Brier, and J. M. Zurada. Pharmacodynamic population analysis in chronic renal failure using artificial neural networks–a comparative study. *Neural Netw*, 16(5-6):841–5, Jun-Jul 2003.

[153] Andrew Gelman. *Bayesian data analysis*. Texts in statistical science. Chapman & Hall/CRC, Boca Raton, Fla., 2nd edition, 2004. ISBN 158488388X (alk. paper).

[154] P. R. Gentry, T. R. Covington, M. E. Andersen, and 3rd Clewell, H. J. Application of a physiologically based pharmacokinetic model for isopropanol in the derivation of a reference dose and reference concentration. *Regul Toxicol Pharmacol*, 36(1):51–68, Aug 2002.

[155] P. G. Georgopoulos, A. Roy, and M. A. Gallo. Reconstruction of Short-Term Multiroute Exposure to Volatile Organic-Compounds Using Physiologically-Based Pharmacokinetic Models. *Journal of Exposure Analysis and Environmental Epidemiology*, 4(3):309–328, Jul-Sep 1994. ISSN 1053-4245.

[156] P. G. Georgopoulos, S. W. Wang, Y. C. Yang, J. Xue, V. G. Zartarian, T. McCurdy, and H. Ozkaynak. Biologically based modeling of multimedia, multipathway, multiroute population exposures to arsenic. *J Expo Sci Environ Epidemiol*, 18(5):462–76, Sep 2008.

[157] P.G. Georgopoulos, A. Roy, and M.A. Gallo. Reconstruction of Short-Term Multi-Route Exposure to Volatile Organic Compounds Using Physiologically Based Pharmacokinetic Models. *Journal of Exposure Analysis and Environmental Epidemiology*, 4(309-328), 1994.

[158] L. Gerhardsson and S. Skerfving. Concepts on biological markers and biomonitoring for metal toxicity. In L.W. Chang, editor, *Toxicology of Metals*, pages 81–107. Lewish Publishers, Boca Raton, FL, 1996.

[159] L. E. Gerlowski and R. K. Jain. Physiologically based pharmacokinetic modeling: principles and applications. *J Pharm Sci*, 72(10):1103–27, Oct 1983.

[160] Milo Gibaldi and Donald Perrier. *Pharmacokinetics*. Drugs and the pharmaceutical sciences ; v. 1. M. Dekker, New York, 1975. ISBN 0824762649.

[161] S. Giordano, P. Adamo, S. Sorbo, and S. Vingiani. Atmospheric trace metal pollution in the Naples urban area based on results from moss and lichen bags. *Environ Pollut*, 136 (3):431–42, Aug 2005.

[162] M. Gochfeld. Cases of mercury exposure, bioavailability, and absorption. *Ecotoxicol Environ Saf*, 56(1):174–9, Sep 2003.

[163] F. Goodarzi, H. Sanei, M. Labonte, and W. F. Duncan. Sources of lead and zinc associated with metal smelting activities in the Trail area, British Columbia, Canada. *J Environ Monit*, 4(3):400–7, Jun 2002.

[164] R. A. Goyer. Toxic and essential metal interactions. *Annu Rev Nutr*, 17:37–50, 1997.

[165] Peter J. Green and Antonietta Mira. Delayed rejection in reversible jump metropolis-hastings. *Biometrika*, 88:1035–1053, 2001.

[166] I. Gueorguieva, I. A. Nestorov, and M. Rowland. Reducing whole body physiologically based pharmacokinetic models using global sensitivity analysis: diazepam case study. *J Pharmacokinet Pharmacodyn*, 33(1):1–27, Feb 2006.

[167] H. Haario, E. Saksman, and J. Tamminen. An adaptive Metropolis algorithm. *Bernoulli*, 7(2):223–242, Apr 2001. ISSN 1350-7265.

[168] H. Haario, M. Laine, A. Mira, and E. Saksman. DRAM: Efficient adaptive MCMC. *Statistics and Computing*, 16(4):339–354, Dec 2006. ISSN 0960-3174.

[169] L. T. Haber, A. Maier, P. R. Gentry, H. J. Clewell, and M. L. Dourson. Genetic polymorphisms in assessing interindividual variability in delivered dose. *Regul Toxicol Pharmacol*, 35(2 Pt 1):177–97, Apr 2002.

[170] C. E. Hack. Bayesian analysis of physiologically based toxicokinetic and toxicodynamic models. *Toxicology*, 221(2-3):241–8, Apr 17 2006.

[171] S. Haddad, G. Charest-Tardif, and K. Krishnan. Physiologically based modeling of the maximal effect of metabolic interactions on the kinetics of components of complex chemical mixtures. *J Toxicol Environ Health A*, 61(3):209–23, Oct 13 2000.

[172] S. Haddad, G. Charest-Tardif, R. Tardif, and K. Krishnan. Validation of a physiological modeling framework for simulating the toxicokinetics of chemicals in mixtures. *Toxicol Appl Pharmacol*, 167(3):199–209, Sep 15 2000.

[173] S. Haddad, C. Restieri, and K. Krishnan. Characterization of age-related changes in body weight and organ weights from birth to adolescence in humans. *J Toxicol Environ Health A*, 64(6):453–64, Nov 23 2001.

[174] J. Harney, M. Trunov, S. Grinshpun, K. Willeke, K. Choe, S. Trakumas, and W. Friedman. Release of lead-containing particles from a wall enclosure. *Aihaj*, 61(5):743–52, Sep-Oct 2000.

[175] M. Harper, K.R. Sullivan, and M.J Quinn. Wind dispersal of metals from smelter waste tips and thier contribution to environmental contamination. *Environ. Sci. Technol.*, 21: 319–333, 1987.

[176] R. M. Harrison. Toxic metals in street and household dusts. *Sci Total Environ*, 11(1): 89–97, Jan 1979.

[177] R. R. Hashemi and J. F. Young. The prediction of methylmercury elimination half-life in humans using animal data: a neural network/rough sets analysis. *J Toxicol Environ Health A*, 66(23):2227–52, Dec 12 2003.

[178] M. A. Hassanien, J. Rieuwerts, A. A. Shakour, and A. Bitto. Seasonal and annual variations in air concentrations of Pb, Cd and PAHs in Cairo, Egypt. *Int J Environ Health Res*, 11(1):13–27, Mar 2001.

[179] L. C. Haws, S. H. Su, M. Harris, M. J. Devito, N. J. Walker, W. H. Farland, B. Finley, and L. S. Birnbaum. Development of a refined database of mammalian relative potency estimates for dioxin-like compounds. *Toxicol Sci*, 89(1):4–30, Jan 2006.

[180] S. M. Hays, B. A. Elswick, G. M. Blumenthal, F. Welsch, R. B. Conolly, and M. L. Gargas. Development of a physiologically based pharmacokinetic model of 2-methoxyethanol and 2-methoxyacetic acid disposition in pregnant rats. *Toxicol Appl Pharmacol*, 163(1):67–74, Feb 15 2000.

[181] S. M. Hays, R. A. Becker, H. W. Leung, L. L. Aylward, and D. W. Pyatt. Biomonitoring equivalents: A screening approach for interpreting biomonitoring results from a public health risk perspective. *Regulatory Toxicology and Pharmacology*, 47(1):96–109, Feb 2007. ISSN 0273-2300.

[182] L. M. Heath, K. L. Soole, M. L. McLaughlin, G. T. McEwan, and J. W. Edwards. Toxicity of environmental lead and the influence of intestinal absorption in children. *Rev Environ Health*, 18(4):231–50, Oct-Dec 2003.

[183] A. F. Heder, K. I. Hirsch-Ernst, D. Bauer, G. F. Kahl, and H. Desel. Induction of cytochrome P450 2B1 by pyrethroids in primary rat hepatocyte cultures. *Biochemical Pharmacology*, 62(1):71–9, Jul 1 2001.

[184] B. Heinrich-Hirsch, H. Beck, I. Chahoud, K. Grote, J. Hartmann, and W. Mathar. Tissue distribution, toxicokinetics and induction of hepatic drug metabolizing enzymes in male rats after a single s.c. dose of 3,4,3',4'-tetrachlorobiphenyl (PCB-77). *Chemosphere*, 34 (5-7):1523–34, Mar-Apr 1997.

[185] H. F. Hemond and H. M. Solo-Gabriele. Children's exposure to arsenic from CCA-treated wooden decks and playground structures. *Risk Anal*, 24(1):51–64, Feb 2004.

[186] A. R. Hensley, A. Scott, P. E. Rosenfeld, and J. J. Clark. Attic dust and human blood samples collected near a former wood treatment facility. *Environ Res*, 105(2):194–9, Oct 2007.

[187] P. H. Hinderling. Red blood cells: a neglected compartment in pharmacokinetics and pharmacodynamics. *Pharmacol Rev*, 49(3):279–95, Sep 1997.

[188] J. T. Hislop, T. Collier, G. White, Khathing D., and French E. The use of keratinized tissues to monitor the detailed exposure of man to methyl mercury from fish. In Brown S. and Savory J., editors, *Chemical Toxicology and Clinical Chemistry of Metals*, pages 145–148. IUPAC, London, 1983.

[189] E. Hodgson. In vitro human phase I metabolism of xenobiotics I: Pesticides and related compounds used in agriculture and public health, May 2003. *Journal of Biochemical and Molecular Toxicology*, 17(4):201–206, 2003. ISSN 1095-6670.

[190] K. Hogan, A. Marcus, R. Smith, and P. White. Integrated exposure uptake biokinetic model for lead in children: empirical comparisons with epidemiologic data. *Environmental Health Perspectives*, 106 Suppl 6:1557–67, Dec 1998.

[191] J. Hogervorst, M. Plusquin, J. Vangronsveld, T. Nawrot, A. Cuypers, E. Van Hecke, H. A. Roels, R. Carleer, and J. A. Staessen. House dust as possible route of environmental exposure to cadmium and lead in the adult general population. *Environ Res*, 103(1): 30–7, Jan 2007.

[192] M. Homady, H. Hussein, A. Jiries, A. Mahasneh, F. Al-Nasir, and K. Khleifat. Survey of some heavy metals in sediments from vehicular service stations in Jordan and their effects on social aggression in prepubertal male mice. *Environ Res*, 89(1):43–9, May 2002.

[193] F. Hong, T. Jin, and A. Zhang. Risk assessment on renal dysfunction caused by co-exposure to arsenic and cadmium using benchmark dose calculation in a Chinese population. *Biometals*, 17(5):573–80, Oct 2004.

[194] K. Hu and N. J. Bunce. Metabolism of polychlorinated dibenzo-p-dioxins and related dioxin-like compounds. *J Toxicol Environ Health B Crit Rev*, 2(2):183–210, Apr-Jun 1999.

[195] Z. Huang, Q. Pei, G. Sun, S. Zhang, J. Liang, Y. Gao, and X. Zhang. Low selenium status affects arsenic metabolites in an arsenic exposed population with skin lesions. *Clinica Chimica Acta*, 387(1-2):139–144, Jan 2008. ISSN 0009-8981.

[196] ICRP. Basic anatomical and physiological data for use in radiological protection: reference values. A report of age- and gender-related differences in the anatomical and physiological characteristics of reference individuals. ICRP Publication 89. *Ann ICRP*, 32(3-4):5–265, 2002.

[197] ICRP. International commission od radiological protection, 2003. URL `http://www.icrp.org/`.

[198] N. G. Ilback, P. Frisk, J. Tallkvist, I. L. Gadhasson, J. Blomberg, and G. Friman. Gastrointestinal uptake of trace elements are changed during the course of a common human viral (Coxsackievirus B3) infection in mice. *J Trace Elem Med Biol*, 22(2):120–30, 2008.

[199] B. Isikli, T. A. Demir, T. Akar, A. Berber, S. M. Urer, C. Kalyoncu, and M. Canbek. Cadmium exposure from the cement dust emissions: a field study in a rural residence. *Chemosphere*, 63(9):1546–52, Jun 2006.

[200] S.S. Isukapalli. *Uncertainty Analysis of Transport-Transformation Models*. PhD thesis, Rutgers University, 1999.

[201] S.S. Isukapalli and A. Roy. General principles of programming (computer and statistical) (Chapter 2). In Ene I. Ette and Paul J. Williams, editors, *Pharmacometrics: the Science of Quantitative Pharmacology (in press)*. Wiley, 2007. ISBN 0471677833.

[202] S.S. Isukapalli, A. Sasso, P. G. Georgopoulos, and K. Krishnan. An interaction-based algorithm for predicting internal dose of chemicals in mixtures during chronic exposures. *Regulatory Toxicology and Pharmacology (in preparation)*, 2010.

[203] M. Jamei, S. Marciniak, K. Feng, A. Barnett, G. Tucker, and A. Rostami-Hodjegan. The Simcyp((R)) Population-based ADME Simulator. *Expert Opin Drug Metab Toxicol*, Feb 6 2009.

[204] Q. M. Jaradat, K. A. Momani, A. A. Jbarah, and A. Massadeh. Inorganic analysis of dust fall and office dust in an industrial area of Jordan. *Environ Res*, 96(2):139–44, Oct 2004.

[205] L. Jarup. Hazards of heavy metal contamination. *Br Med Bull*, 68:167–82, 2003.

[206] T. Jin, J. Lu, and M. Nordberg. Toxicokinetics and biochemistry of cadmium with special emphasis on the role of metallothionein. *Neurotoxicology*, 19(4-5):529–35, Aug-Oct 1998.

[207] D.L. Johnson, R. Fortmann, and I. Thornton. Individual particle characterization of heavy metal rich household dusts. *Trace Subst. Environ. Health*, 16:116–123, 1982.

[208] F. Jonsson, G. Sandborgh-Englund, and G. Johanson. A compartmental model for the kinetics of mercury vapor in humans. *Toxicology and Applied Pharmacology*, 155(2):161–8, Mar 1 1999.

[209] F. Jonsson, E. N. Jonsson, F. Y. Bois, and S. Marshall. The application of a Bayesian approach to the analysis of a complex, mechanistically based model. *Journal of Biopharmaceutical Statistics*, 17(1):65–92, Jan-Feb 2007. ISSN 1054-3406.

[210] P. Kakkar and F. N. Jaffery. Biological markers for metal toxicity. *Environmental Toxicology and Pharmacology*, 19(2):335–349, Feb 2005. ISSN 1382-6689.

[211] M. Kantola, R. Purkunen, P. Kroger, A. Tooming, J. Juravskaja, M. Pasanen, S. Saarikoski, and T. Vartiainen. Accumulation of cadmium, zinc, and copper in maternal blood and developmental placental tissue: differences between Finland, Estonia, and St. Petersburg. *Environ Res*, 83(1):54–66, May 2000.

[212] W. A. Kappers, R. J. Edwards, S. Murray, and A. R. Boobis. Diazinon is activated by cyp2c19 in human liver. *Toxicol Appl Pharmacol*, 177(1):68–76, Nov 15 2001. ISSN 0041-008X (Print).

[213] L. B. Kedderis, J. J. Mills, M. E. Andersen, and L. S. Birnbaum. A physiologically based pharmacokinetic model for 2,3,7,8-tetrabromodibenzo-p-dioxin (TBDD) in the rat: tissue distribution and CYP1A induction. *Toxicol Appl Pharmacol*, 121(1):87–98, Jul 1993.

[214] B. I. Khan, J. Jambeck, H. M. Solo-Gabriele, T. G. Townsend, and Y. Cai. Release of arsenic to the environment from CCA-treated wood. 2. Leaching and speciation during disposal. *Environ Sci Technol*, 40(3):994–9, Feb 1 2006.

[215] B. I. Khan, H. M. Solo-Gabriele, T. G. Townsend, and Y. Cai. Release of arsenic to the environment from CCA-treated wood. 1. Leaching and speciation during service. *Environ Sci Technol*, 40(3):988–93, Feb 1 2006.

[216] N. D. Kim and J. E. Fergusson. Cadmium, copper, lead and zinc in housedust of Christchurch, New Zealand: levels and sources. In R.G. McLaren, R.J. Haynes, and G.P. Savage, editors, *New Zeland Trace Elem. Gp. Conf*, Trace Elements in New Zealand Environment, Human and Animal, pages 193–200, New Zealand, 1988.

[217] T. Kjellstrom and G. F. Nordberg. A kinetic model of cadmium metabolism in the human being. *Environ Res*, 16(1-3):248–69, Jul 1978.

[218] R. L. Kodell, J. J. Chen, R. R. Delongchamp, and J. F. Young. Hierarchical models for probabilistic dose-response assessment. *Regulatory Toxicology and Pharmacology*, 45(3): 265–272, Aug 2006. ISSN 0273-2300.

[219] M. Korbas, A. J. Percy, J. Gailer, and G. N. George. A possible molecular link between the toxicological effects of arsenic, selenium and methylmercury: methylmercury(II) seleno bis(S-glutathionyl) arsenic(III). *J Biol Inorg Chem*, 13(3):461–70, Mar 2008.

[220] C. D. Kozul, H. K. Ely, R. I. Enelow, and J. W. Hamilton. Low-Dose Arsenic Compromises the Immune Response to Influenza A Infection in Vivo. *Environ Health Perspect*, 119(9): 1441–47, May 2009.

[221] K. Krishnan and M. E. Andersen. Physiologically based pharmacokinetic modeling in toxicology. In A. W. Hayes, editor, *Principles and methods of toxicology*, pages 1931–1241. Raven Press, New York, 2001.

[222] K. Krishnan, S. Haddad, M. Beliveau, and R. Tardif. Physiological modeling and extrapolation of pharmacokinetic interactions from binary to more complex chemical mixtures. *Environ Health Perspect*, 110 Suppl 6:989–94, Dec 2002.

[223] B. R. Kuhnert, P. M. Kuhnert, N. Lazebnik, and P. Erhard. The relationship between placental cadmium, zinc, and copper. *J Am Coll Nutr*, 12(1):31–5, Feb 1993.

[224] W. T. Kwong, P. Friello, and R. D. Semba. Interactions between iron deficiency and lead poisoning: epidemiology and pathogenesis. *Sci Total Environ*, 330(1-3):21–37, Sep 1 2004.

[225] P. J. Landrigan, S. H. Gehlbach, B. F. Rosenblum, J. M. Shoults, R. M. Candelaria, W. F. Barthel, J. A. Liddle, A. L. Smrek, N. W. Staehling, and J. F. Sanders. Epidemic lead absorption near an ore smelter. The role of particulate lead. *N Engl J Med*, 292(3): 123–9, Jan 16 1975.

[226] D.P.H Laxen, F. Lindsay, G.M. Raab, R. Hunter, G.S. Fell, and M. Fulton. The variability of lead in dusts within homes of young children. In I. Thornton and E.B. Culbard, editors, *Lead in the Home Environment*, pages 113–125. Science Reviews Ltd., Northwood, England, 1987.

[227] R. W. Leggett. An age-specific kinetic model of lead metabolism in humans. *Environmental Health Perspectives*, 101(7):598–616, Dec 1993.

[228] R. W. Leggett, N. B. Munro, and K. F. Eckerman. Proposed revision of the ICRP model for inhaled mercury vapor. *Health Physics*, 81(4):450–5, Oct 2001.

[229] R. Lemus, A. A. Abdelghani, T. G. Akers, and W. E. Horner. Health risks from exposure to metals in household dusts. *Rev Environ Health*, 11(4):179–89, Oct-Dec 1996.

[230] M. L. Lepow, L. Bruckman, M. Gillette, S. Markowitz, R. Robino, and J. Kapish. Investigations into sources of lead in the environment of urban children. *Environ Res*, 10(3): 415–26, Dec 1975.

[231] G. Y. Li, S. W. Wang, H. Rabitz, S. Y. Wang, and P. Jaffe. Global uncertainty assessments by high dimensional model representations (HDMR). *Chemical Engineering Science*, 57 (21):4445–4460, Nov 2002. ISSN 0009-2509.

[232] Lifeline Group. Physiological parameters for pbpk modeling version 1.2 (p3m), 2004. URL `http://www.thelifelinegroup.org/P3M/`.

[233] Y. S. Lin, P. P. Egeghy, and S. M. Rappaport. Relationships between levels of volatile organic compounds in air and blood from the general population. *J Expo Sci Environ Epidemiol*, Dec 5 2007.

[234] P. J. Lioy, L. M. Yiin, J. Adgate, C. Weisel, and G. G. Rhoads. The effectiveness of a home cleaning intervention strategy in reducing potential dust and lead exposures. *J Expo Anal Environ Epidemiol*, 8(1):17–35, Jan-Mar 1998.

[235] P. J. Lioy, C. P. Weisel, J. R. Millette, S. Eisenreich, D. Vallero, J. Offenberg, B. Buckley, B. Turpin, M. Zhong, M. D. Cohen, C. Prophete, I. Yang, R. Stiles, G. Chee, W. Johnson, R. Porcja, S. Alimokhtari, R. C. Hale, C. Weschler, and L. C. Chen. Characterization of the dust/smoke aerosol that settled east of the World Trade Center (WTC) in lower Manhattan after the collapse of the WTC 11 September 2001. *Environ Health Perspect*, 110(7):703–14, Jul 2002.

[236] K. Louekari, U. M. Mroueh, L. Maidell-Munster, S. Valkonen, T. Tuomi, and K. Savolainen. Reducing the risks of children living near the site of a former lead smeltery. *Sci Total Environ*, 319(1-3):65–75, Feb 5 2004.

[237] G. C. Lough, J. J. Schauer, J. S. Park, M. M. Shafer, J. T. Deminter, and J. P. Weinstein. Emissions of metals associated with motor vehicle roadways. *Environ Sci Technol*, 39(3): 826–36, Feb 1 2005.

[238] R. H. Luecke, B. A. Pearce, W. D. Wosilait, Jr. Slikker, W., and J. F. Young. Postnatal growth considerations for PBPK modeling. *J Toxicol Environ Health A*, 70(12):1027–37, Jun 2007.

[239] R. H. Luecke, B. A. Pearce, W. D. Wosilait, D. R. Doerge, Jr. Slikker, W., and J. F. Young. Windows((R)) based general PBPK/PD modeling software. *Comput Biol Med*, Jul 25 2008.

[240] T. D. Lyon, E. Aughey, R. Scott, and G. S. Fell. Cadmium concentrations in human kidney in the UK: 1978-1993. *J Environ Monit*, 1(3):227–31, Jun 1999.

[241] D. L. MacIntosh, C. Kabiru, S. L. Echols, and P. B. Ryan. Dietary exposure to chlorpyrifos and levels of 3,5,6-trichloro-2-pyridinol in urine. *J Expo Anal Environ Epidemiol*, 11(4): 279–85, Jul-Aug 2001.

[242] E. F. Madden. The role of combined metal interactions in metal carcinogenesis: a review. *Rev Environ Health*, 18(2):91–109, Apr-Jun 2003.

[243] E. F. Madden and B. A. Fowler. Mechanisms of nephrotoxicity from metal combinations: a review. *Drug Chem Toxicol*, 23(1):1–12, Feb 2000.

[244] D. T. Mage, R. H. Allen, G. Gondy, W. Smith, D. B. Barr, and L. L. Needham. Estimating pesticide dose from urinary pesticide concentration data by creatinine correction in the Third National Health and Nutrition Examination Survey (NHANES-III). *J Expo Anal Environ Epidemiol*, 14(6):457–65, Nov 2004.

[245] A. Maier, T. P. Dalton, and A. Puga. Disruption of dioxin-inducible phase I and phase II gene expression patterns by cadmium, chromium, and arsenic. *Mol Carcinog*, 28(4): 225–35, Aug 2000.

[246] A. Maier, B. L. Schumann, X. Chang, G. Talaska, and A. Puga. Arsenic co-exposure potentiates benzo[a]pyrene genotoxicity. *Mutat Res*, 517(1-2):101–11, May 27 2002.

[247] S. Mann, P. O. Droz, and M. Vahter. A physiologically based pharmacokinetic model for arsenic exposure. II. Validation and application in humans. *Toxicol Appl Pharmacol*, 140 (2):471–86, Oct 1996.

[248] A. M. Massadeh and R. D. Snook. Determination of Pb and Cd in road dusts over the period in which Pb was removed from petrol in the UK. *J Environ Monit*, 4(4):567–72, Aug 2002.

[249] Mathworks. Matlab Simbiology Toolbox, 2007. URL `http://www.mathworks.com/products/simbiology/`.

[250] T. McCurdy, G. Glen, L. Smith, and Y. Lakkadi. The national exposure research laboratory's consolidated human activity database. *J Expo Anal Environ Epidemiol*, 10(6 Pt 1):566–78, Nov-Dec 2000.

[251] McKim, J. M., Jr. Effects of Repeated Whole Body Inhalation Exposure to Octamethylcyclotetrasiloxane (D4) Vapors on Hepatic Microsomal CYP2B1/2 Induction in Female Fischer 344 Rats: A Dose-Response Study. Technical report, Dow Corning Corporation, Midland, MI, 1998.

[252] J. D. Meeker, D. B. Barr, L. Ryan, R. F. Herrick, D. H. Bennett, R. Bravo, and R. Hauser. Temporal variability of urinary levels of nonpersistent insecticides in adult men. *J Expo Anal Environ Epidemiol*, 15(3):271–81, May 2005.

[253] H. M. Meltzer, A. Maage, T. A. Ydersbond, E. Haug, E. Glattre, and H. Holm. Fish arsenic may influence human blood arsenic, selenium, and T4:T3 ratio. *Biol Trace Elem Res*, 90(1-3):83–98, Winter 2002.

[254] I. Meyer, J. Heinrich, and U. Lippold. Factors affecting lead and cadmium levels in house dust in industrial areas of eastern Germany. *Sci Total Environ*, 234(1-3):25–36, Aug 30 1999.

[255] I. Meyer, J. Heinrich, and U. Lippold. Factors affecting lead, cadmium, and arsenic levels in house dust in a smelter town in eastern Germany. *Environ Res*, 81(1):32–44, Jul 1999.

[256] M. M. Meza, L. Yu, Y. Y. Rodriguez, M. Guild, D. Thompson, A. J. Gandolfi, and W. T. Klimecki. Developmentally restricted genetic determinants of human arsenic metabolism: association between urinary methylated arsenic and CYT19 polymorphisms in children. *Environ Health Perspect*, 113(6):775–81, Jun 2005.

[257] M. H. Mickle. Structure, use, and validation of the IEUBK model. *Environ Health Perspect*, 106 Suppl 6:1531–4, Dec 1998.

[258] H. W. Mielke, E. T. Powell, A. Shah, C. R. Gonzales, and P. W. Mielke. Multiple metal contamination from house paints: consequences of power sanding and paint scraping in New Orleans. *Environ Health Perspect*, 109(9):973–8, Sep 2001.

[259] A. Mirfazaelian, K. B. Kim, S. S. Anand, H. J. Kim, R. Tornero-Velez, J. V. Bruckner, and J. W. Fisher. Development of a Physiologically Based Pharmacokinetic Model for Deltamethrin in the Adult Male Sprague-Dawley Rat. *Toxicological Sciences*, Jul 10 2006.

[260] M. R. Moore. A commentary on the impacts of metals and metalloids in the environment upon the metabolism of drugs and chemicals. *Toxicol Lett*, 148(3):153–8, Mar 21 2004.

[261] M. K. Morgan, L. S. Sheldon, C. W. Croghan, P. A. Jones, G. L. Robertson, J. C. Chuang, N. K. Wilson, and C. W. Lyu. Exposures of preschool children to chlorpyrifos and its degradation product 3,5,6-trichloro-2-pyridinol in their everyday environments. *J Expo Anal Environ Epidemiol*, 15(4):297–309, Jul 2005.

[262] M. Murray and S. A. Holmes. Assessment of mercury emissions inventories for the Great Lakes states. *Environ Res*, 95(3):282–97, Jul 2004.

[263] C. J. Muskett, L. H. Roberts, and B. J. Page. Cadmium and lead pollution from secondary metal refinery operations. *Sci Total Environ*, 11(1):73–87, Jan 1979.

[264] I. Nestorov. Whole-body physiologically based pharmacokinetic models. *Expert Opin Drug Metab Toxicol*, 3(2):235–249, Apr 2007.

[265] S. L. Ng, L. S. Chan, K. C. Lam, and W. K. Chan. Heavy metal contents and magnetic properties of playground dust in Hong Kong. *Environ Monit Assess*, 89(3):221–32, Dec 2003.

[266] R. J. Nolan, D. L. Rick, N. L. Freshour, and J. H. Saunders. Chlorpyrifos: pharmacokinetics in human volunteers. *Toxicol Appl Pharmacol*, 73(1):8–15, Mar 30 1984.

[267] A. Nong, M. D. Taylor, 3rd Clewell, H. J., D. C. Dorman, and M. E. Andersen. Manganese tissue dosimetry in rats and monkeys: accounting for dietary and inhaled Mn with physiologically-based pharmacokinetic modeling. *Toxicol Sci*, Dec 19 2008.

[268] A. Nong, J. G. Teeguarden, 3rd Clewell, H. J., D. C. Dorman, and M. E. Andersen. Pharmacokinetic modeling of manganese in the rat IV: Assessing factors that contribute to brain accumulation during inhalation exposure. *J Toxicol Environ Health A*, 71(7): 413–26, 2008.

[269] A. Nong, M. D. Taylor, 3rd Clewell, H. J., D. C. Dorman, and M. E. Andersen. Manganese tissue dosimetry in rats and monkeys: accounting for dietary and inhaled Mn with physiologically based pharmacokinetic modeling. *Toxicol Sci*, 108(1):22–34, Mar 2009.

[270] G. F. Nordberg. Cadmium and health in the 21st Century - historical remarks and trends for the future. *Biometals*, 17(5):485–489, Oct 2004. ISSN 0966-0844.

[271] G. F. Nordberg. Biomarkers of exposure, effects and susceptibility in humans and their application in studies of interactions among metals in China. *Toxicol Lett*, Jun 21 2009.

[272] G. F. Nordberg and T. Kjellstrom. Metabolic model for cadmium in man. *Environ Health Perspect*, 28:211–7, Feb 1979.

[273] G. F. Nordberg, T. Jin, F. Hong, A. Zhang, J. P. Buchet, and A. Bernard. Biomarkers of cadmium and arsenic interactions. *Toxicology and Applied Pharmacology*, 206(2):191–197, Aug 7 2005. ISSN 0041-008X.

[274] M. Nordberg and G. F. Nordberg. Toxicological aspects of metallothionein. *Cell Mol Biol (Noisy-le-grand)*, 46(2):451–63, Mar 2000.

[275] NRC. Human Biomonitoring for Environmental Chemicals. Technical report, Committee on Human Biomonitoring for Environmental Toxicants, Board on Environmental Studies and Toxicology, Division on Earth and Life Studies, National Research Council, Washington DC, 2006.

[276] E. J. O'Flaherty. Physiologically based models for bone-seeking elements. II. Kinetics of lead disposition in rats. *Toxicol Appl Pharmacol*, 111(2):313–31, Nov 1991.

[277] E. J. O'Flaherty. Physiologically based models for bone-seeking elements. IV. Kinetics of lead disposition in humans. *Toxicol Appl Pharmacol*, 118(1):16–29, Jan 1993.

[278] E. J. O'Flaherty. Physiologically based models for bone-seeking elements. V. Lead absorption and disposition in childhood. *Toxicol Appl Pharmacol*, 131(2):297–308, Apr 1995.

[279] E. J. O'Flaherty. Physiologically based models of metal kinetics. *Crit Rev Toxicol*, 28(3): 271–317, May 1998.

[280] E. J. O'Flaherty. Modeling normal aging bone loss, with consideration of bone loss in osteoporosis. *Toxicol Sci*, 55(1):171–88, May 2000.

[281] E. J. O'Flaherty, B. D. Kerger, S. M. Hays, and D. J. Paustenbach. A physiologically based model for the ingestion of chromium(iii) and chromium(vi) by humans. *Toxicol Sci*, 60(2):196–213, Apr 2001.

[282] T. Okuda, J. Kato, J. Mori, M. Tenmoku, Y. Suda, S. Tanaka, K. He, Y. Ma, F. Yang, X. Yu, F. Duan, and Y. Lei. Daily concentrations of trace metals in aerosols in Beijing, China, determined by using inductively coupled plasma mass spectrometry equipped with laser ablation analysis, and source identification of aerosols. *Sci Total Environ*, 330(1-3): 145–58, Sep 1 2004.

[283] A. Ordonez, J. Loredo, E. De Miguel, and S. Charlesworth. Distribution of heavy metals in the street dusts and soils of an industrial city in northern Spain. *Arch Environ Contam Toxicol*, 44(2):160–70, Feb 2003.

[284] M. K. O'Rourke, P. K. Van de Water, S. Jin, S. P. Rogan, A. D. Weiss, S. M. Gordon, D. M. Moschandreas, and M. D. Lebowitz. Evaluations of primary metals from NHEXAS Arizona: distributions and preliminary exposures. National Human Exposure Assessment Survey. *J Expo Anal Environ Epidemiol*, 9(5):435–45, Sep-Oct 1999.

[285] A. Oskarsson, I. Palminger Hallen, J. Sundberg, and K. Petersson Grawe. Risk assessment in relation to neonatal metal exposure. *Analyst*, 123(1):19–23, Jan 1998.

[286] C. D. Pandya, P. P. Pillai, and S. S. Gupta. Lead and Cadmium Co-exposure Mediated Toxic Insults on Hepatic Steroid Metabolism and Antioxidant System of Adult Male Rats. *Biol Trace Elem Res*, Aug 4 2009.

[287] Y. Pang, D. L. MacIntosh, D. E. Camann, and P. B. Ryan. Analysis of aggregate exposure to chlorpyrifos in the NHEXAS-Maryland investigation. *Environ Health Perspect*, 110(3): 235–40, Mar 2002.

[288] L. Patrick. Toxic metals and antioxidants: Part II. The role of antioxidants in arsenic and cadmium toxicity. *Altern Med Rev*, 8(2):106–28, May 2003.

[289] M. A. Peraza, F. Ayala-Fierro, D. S. Barber, E. Casarez, and L. T. Rael. Effects of micronutrients on metal toxicity. *Environmental Health Perspectives*, 106:203–216, FEB 1998.

[290] V. Petrosyan, A. Orlova, C. E. Dunlap, E. Babayan, M. Farfel, and M. Von Braun. Lead in residential soil and dust in a mining and smelting district in northern Armenia: a pilot study. *Environ Res*, 94(3):297–308, Mar 2004.

[291] G. Pierrehumbert, P. O. Droz, R. Tardif, G. Charest-Tardif, and G. Truchon. Impact of human variability on the biological monitoring of exposure to toluene, phenol, lead, and mercury: II. Compartmental based toxicokinetic modelling. *Toxicology Letters*, 134(1-3): 165–75, Aug 5 2002.

[292] T. S. Poet, H. Wu, A. A. Kousba, and C. Timchalk. In vitro rat hepatic and intestinal metabolism of the organophosphate pesticides chlorpyrifos and diazinon. *Toxicological Sciences*, 72(2):193–200, Apr 2003.

[293] A. V. Polissar, P. K. Hopke, and R. L. Poirot. Atmospheric aerosol over Vermont: chemical composition and sources. *Environ Sci Technol*, 35(23):4604–21, Dec 1 2001.

[294] P. Poulin and K. Krishnan. A Biologically-Based Algorithm for Predicting Human Tissue - Blood Partition Coefficients of Organic Chemicals. *Human & Experimental Toxicology*, 14(3):273–280, Mar 1995. ISSN 0144-5952.

[295] P. Poulin and K. Krishnan. An Algorithm for Predicting Tissue-Blood Partition-Coefficients of Organic-Chemicals from N-Octanol-Water Partition-Coefficient Data. *Journal of Toxicology and Environmental Health*, 46(1):117–129, Sep 1995. ISSN 0098-4108.

[296] P. Poulin and K. Krishnan. Molecular structure-based prediction of the partition coefficients of organic chemicals for physiological pharmacokinetic models. *Toxicology Methods*, 6(3):117–137, Jul-Sep 1996. ISSN 1051-7235.

[297] P. Poulin and K. Krishnan. A tissue composition-based algorithm for predicting tissue:air partition coefficients of organic chemicals. *Toxicol Appl Pharmacol*, 136(1):126–30, Jan 1996.

[298] J. G. Pounds and R. W. Leggett. The ICRP age-specific biokinetic model for lead: validations, empirical comparisons, and explorations. *Environ Health Perspect*, 106 Suppl 6:1505–11, Dec 1998.

[299] K. Price, S. Haddad, and K. Krishnan. Physiological modeling of age-specific changes in the pharmacokinetics of organic chemicals in children. *J Toxicol Environ Health A*, 66(5): 417–33, Mar 14 2003.

[300] P. S. Price, R. B. Conolly, C. F. Chaisson, E. A. Gross, J. S. Young, E. T. Mathis, and D. R. Tedder. Modeling interindividual variation in physiological factors used in PBPK models of humans. *Crit Rev Toxicol*, 33(5):469–503, 2003.

[301] Q. Qu, R. Shore, G. Li, L. Su, X. Jin, A. A. Melikian, N. Roy, L. C. Chen, I. Wirgin, B. Cohen, S. Yin, Y. Li, and R. Mu. Biomarkers of benzene: urinary metabolites in relation to individual genotype and personal exposure. *Chem Biol Interact*, 153-154: 85–95, May 30 2005.

[302] J. J. Quackenboss, E. D. Pellizzari, P. Shubat, R. W. Whitmore, J. L. Adgate, K. W. Thomas, N. C. Freeman, C. Stroebel, P. J. Lioy, A. C. Clayton, and K. Sexton. Design strategy for assessing multi-pathway exposure for children: the Minnesota Children's Pesticide Exposure Study (MNCPES). *Journal of Exposure Analysis and Environmental Epidemiology*, 10(2):145–58, Mar-Apr 2000.

[303] D. Quig. Cysteine metabolism and metal toxicity. *Alternative Medicine Review*, 3(4): 262–70, Aug 1998.

[304] G.M. Raab, D.P.H Laxen, and M. Fulton. Lead from dust and water and exposure sources for children. *Environ Geochem Health*, 9:80–85, 1987.

[305] M. B. Rabinowitz, G. W. Wetherill, and J. D. Kopple. Kinetic analysis of lead metabolism in healthy humans. *J Clin Invest*, 58(2):260–70, Aug 1976.

[306] P. E. Rasmussen, K. S. Subramanian, and B. J. Jessiman. A multi-element profile of housedust in relation to exterior dust and soils in the city of Ottawa, Canada. *Sci Total Environ*, 267(1-3):125–40, Feb 21 2001.

[307] M. B. Reddy, R. S. H. Yang, H. J. Clewell, and M. E. Andersen. *Physiologically based pharmacokinetic modeling : science and applications*. Wiley-Interscience, Hoboken, N.J., 2005. ISBN 0471478148 (cloth).

[308] D. B. Reissman, T. D. Matte, K. L. Gurnitz, R. B. Kaufmann, and J. Leighton. Is home renovation or repair a risk factor for exposure to lead among children residing in New York City? *J Urban Health*, 79(4):502–11, Dec 2002.

[309] A. M. Riederer, J. P. Shine, L. M. Danan, and T. E. Ford. Concentrations of lead and mercury in multimedia samples from homes near the former Clark Air Base, Philippines. *Sci Total Environ*, 341(1-3):53–69, Apr 1 2005.

[310] M. L. Rigas, M. S. Okino, and J. J. Quackenboss. Use of a pharmacokinetic model to assess chlorpyrifos exposure and dose in children, based on urinary biomarker measurements. *Toxicological Sciences*, 61(2):374–81, Jun 2001.

[311] G. O. Roberts and J. S. Rosenthal. Optimal scaling for various Metropolis-Hastings algorithms. *Statistical Science*, 16(4):351–367, Nov 2001. ISSN 0883-4237.

[312] J. C. Rockett, M. G. Narotsky, K. E. Thompson, I. Thillainadarajah, C. R. Blystone, A. K. Goetz, H. Ren, D. S. Best, R. N. Murrell, H. P. Nichols, J. E. Schmid, D. C. Wolf, and D. J. Dix. Effect of conazole fungicides on reproductive development in the female rat. *Reproductive Toxicology*, Jun 12 2006.

[313] C. E. Rodriguez, D. A. Mahle, J. M. Gearhart, D. R. Mattie, J. C. Lipscomb, R. S. Cook, and H. A. Barton. Predicting age-appropriate pharmacokinetics of six volatile organic compounds in the rat utilizing physiologically based pharmacokinetic modeling. *Toxicol Sci*, 98(1):43–56, Jul 2007.

[314] V. M. Rodriguez, L. Carrizales, M. S. Mendoza, O. R. Fajardo, and M. Giordano. Effects of sodium arsenite exposure on development and behavior in the rat. *Neurotoxicol Teratol*, 24(6):743–50, Nov-Dec 2002.

[315] A. Rolfs and M. A. Hediger. Intestinal metal ion absorption: an update. *Curr Opin Gastroenterol*, 17(2):177–183, Mar 2001.

[316] R. L. Rose and E. Hodgson. Pesticide metabolism and potential for metabolic interactions. *Journal of Biochemical and Molecular Toxicology*, 19(4):276–7, 2005.

[317] J. A. Roth and M. D. Garrick. Iron interactions and other biological reactions mediating the physiological and toxic actions of manganese. *Biochem Pharmacol*, 66(1):1–13, Jul 1 2003.

[318] A. Roy and P. G. Georgopoulos. Reconstructing week-long exposures to volatile organic compounds using physiologically based pharmacokinetic models. *J Expo Anal Environ Epidemiol*, 8(3):407–22, Jul-Sep 1998. ISSN 1053-4245 (Print).

[319] A. Roy, C. P. Weisel, P. J. Lioy, and P. G. Georgopoulos. A distributed parameter physiologically-based pharmacokinetic model for dermal and inhalation exposure to volatile organic compounds. *Risk Anal*, 16(2):147–60, Apr 1996.

[320] A. Roy, P. G. Georgopoulos, M. Ouyang, N. Freeman, and P. J. Lioy. Environmental, dietary, demographic, and activity variables associated with biomarkers of exposure for benzene and lead. *Journal of Exposure Analysis and Environmental Epidemiology*, 13(6): 417–26, Nov 2003.

[321] P. B. Ryan, K. A. Scanlon, and D. L. MacIntosh. Analysis of dietary intake of selected metals in the NHEXAS-Maryland investigation. *Environ Health Perspect*, 109(2):121–8, Feb 2001.

[322] S. H. Safe. Polychlorinated biphenyls (PCBs): environmental impact, biochemical and toxic responses, and implications for risk assessment. *Crit Rev Toxicol*, 24(2):87–149, 1994.

[323] C. Samara and D. Voutsa. Size distribution of airborne particulate matter and associated heavy metals in the roadside environment. *Chemosphere*, 59(8):1197–206, May 2005.

[324] R. Sarangapani, J. Teeguarden, K. P. Plotzke, Jr. McKim, J. M., and M. E. Andersen. Dose-response modeling of cytochrome p450 induction in rats by octamethylcyclotetrasiloxane. *Toxicol Sci*, 67(2):159–72, Jun 2002.

[325] S. Satarug, M. Nishijo, P. Ujjin, Y. Vanavanitkun, J. R. Baker, and M. R. Moore. Evidence for concurrent effects of exposure to environmental cadmium and lead on hepatic CYP2A6 phenotype and renal function biomarkers in nonsmokers. *Environ Health Perspect*, 112 (15):1512–8, Nov 2004.

[326] S. Satarug, P. Ujjin, Y. Vanavanitkun, J. R. Baker, and M. R. Moore. Influence of body iron store status and cigarette smoking on cadmium body burden of healthy Thai women and men. *Toxicol Lett*, 148(3):177–85, Mar 21 2004.

[327] S. Satarug, P. Ujjin, Y. Vanavanitkun, M. Nishijo, J. R. Baker, and M. R. Moore. Effects of cigarette smoking and exposure to cadmium and lead on phenotypic variability of hepatic CYP2A6 and renal function biomarkers in men. *Toxicology*, 204(2-3):161–73, Nov 15 2004.

[328] S. Satarug, M. Nishijo, J. M. Lasker, R. J. Edwards, and M. R. Moore. Kidney dysfunction and hypertension: role for cadmium, p450 and heme oxygenases? *Tohoku J Exp Med*, 208(3):179–202, Mar 2006.

[329] B. Scharf and L. D. Trombetta. Toxicity and bioaccumulation of the wood preservative copper dimethyldithiocarbamate in tissues of Long-Evans rats. *J Toxicol Environ Health A*, 71(19):1300–6, 2008.

[330] K. Schlawicke Engstrom, K. Broberg, G. Concha, B. Nermell, M. Warholm, and M. Vahter. Genetic polymorphisms influencing arsenic metabolism: evidence from Argentina. *Environ Health Perspect*, 115(4):599–605, Apr 2007.

[331] H. Schmidt. SBaddon: High Performance Simulation for the Systems Biology Toolbox for MATLAB. *Bioinformatics*, Jan 18 2007.

[332] K. Schumann and B. Elsenhans. The impact of food contaminants on the bioavailability of trace metals. *J Trace Elem Med Biol*, 16(3):139–44, 2002.

[333] B. Seifert, K. Becker, D. Helm, C. Krause, C. Schulz, and M. Seiwert. The German Environmental Survey 1990/1992 (GerES II): reference concentrations of selected environmental pollutants in blood, urine, hair, house dust, drinking water and indoor air. *J Expo Anal Environ Epidemiol*, 10(6 Pt 1):552–65, Nov-Dec 2000.

[334] J. M. Seubert, C. J. Sinal, and J. R. Bend. Acute sodium arsenite administration induces pulmonary CYP1A1 mRNA, protein and activity in the rat. *J Biochem Mol Toxicol*, 16 (2):84–95, 2002.

[335] K. Sexton, D. E. Kleffman, and M. A. Callahan. An introduction to the National Human Exposure Assessment Survey (NHEXAS) and related phase I field studies. *J Expo Anal Environ Epidemiol*, 5(3):229–32, Jul-Sep 1995.

[336] R. Sharma and S. Pervez. A case study of spatial variation and enrichment of selected elements in ambient particulate matter around a large coal-fired power station in central India. *Environ Geochem Health*, 26(4):373–81, Dec 2004.

[337] S. Sheldrake and M. Stifelman. A case study of lead contamination cleanup effectiveness at Bunker Hill. *Sci Total Environ*, 303(1-2):105–23, Feb 15 2003.

[338] A. M. Shipp, P. R. Gentry, G. Lawrence, C. Van Landingham, T. Covington, H. J. Clewell, K. Gribben, and K. Crump. Determination of a site-specific reference dose for methylmercury for fish-eating populations. *Toxicol Ind Health*, 16(9-10):335–438, Nov 2000.

[339] H. Shiraki and F. P. Guengerich. Turnover of Membrane-Proteins - Kinetics of Induction and Degradation of 7 Forms of Rat-Liver Microsomal Cytochrome-P-450, Nadph-Cytochrome-P-450 Reductase, and Epoxide Hydrolase. *Archives of Biochemistry and Biophysics*, 235(1):86–96, 1984. ISSN 0003-9861.

[340] C. Silva Mdo, J. Gaspar, I. Duarte Silva, A. Faber, and J. Rueff. Gstm1, GSTT1, and GSTP1 genotypes and the genotoxicity of hydroquinone in human lymphocytes. *Environ Mol Mutagen*, 43(4):258–64, 2004.

[341] J. C. Smith and F. F. Farris. Methyl mercury pharmacokinetics in man: a reevaluation. *Toxicology and Applied Pharmacology*, 137(2):245–52, Apr 1996.

[342] E. Smolders. Cadmium uptake by plants. *Int J Occup Med Environ Health*, 14(2):177–83, 2001.

[343] M. D. Sohn, T. E. McKone, and J. N. Blancato. Reconstructing population exposures from dose biomarkers: inhalation of trichloroethylene (TCE) as a case study. *Journal of Exposure Analysis and Environmental Epidemiology*, 14(3):204–13, May 2004.

[344] R.L. Solomon and J.W. Hartford. Lead and cadmium in dust and soils in a small urban community. *Environ Sci Technol*, 10:773–777, 1976.

[345] S. M. Spalinger, M. C. von Braun, V. Petrosyan, and I. H. von Lindern. Northern Idaho house dust and soil lead levels compared to the Bunker Hill Superfund Site. *Environ Monit Assess*, 130(1-3):57–72, Jul 2007.

[346] D. A. Sterling, D. L. Johnson, A. M. Murgueytio, and R. G. Evans. Source contribution of lead in house dust from a lead mining waste superfund site. *J Expo Anal Environ Epidemiol*, 8(3):359–73, Jul-Sep 1998.

[347] D. Stilwell, M. Toner, and B. Sawhney. Dislodgeable copper, chromium and arsenic from CCA-treated wood surfaces. *Sci Total Environ*, 312(1-3):123–31, Aug 1 2003.

[348] C.D. Strehlow and D. Barltrop. Lead in the home environment. In I. Thornton and E.B. Culbard, editors, *Lead in the Home Environment*, pages 167–178. Science Reviews Ltd., Northwood, England, 1987.

[349] M. Strolin-Benedetti and M. Bani. Metabolism-based drug interactions involving oral azole antifungals in humans. *Drug Metab Rev*, 31(3):665–717, Aug 1999. ISSN 0360-2532 (Print).

[350] W. T. Sturges and R. M. Harrison. An assessment of the contribution from paint flakes to the lead content of some street and household dusts. *Sci Total Environ*, 44(3):225–34, Sep 1985.

[351] M. Styblo and D. J. Thomas. Selenium modifies the metabolism and toxicity of arsenic in primary rat hepatocytes. *Toxicol Appl Pharmacol*, 172(1):52–61, Apr 1 2001.

[352] K. D. Sugden, K. M. Rigby, and B. D. Martin. Oxidative activation of the human carcinogen chromate by arsenite: a model for synergistic metal activation leading to oxidative DNA damage. *Toxicol In Vitro*, 18(6):741–8, Dec 2004.

[353] Y. Suwazono, S. Sand, M. Vahter, A. F. Filipsson, S. Skerfving, J. Lidfeldt, and A. Akesson. Benchmark dose for cadmium-induced renal effects in humans. *Environ Health Perspect*, 114(7):1072–6, Jul 2006.

[354] K. Szafraniec and W. Jedrychowski. Spatial variability and trends in ambient air concentrations of metals in Cracow, Poland. *Int J Occup Med Environ Health*, 14(3):261–5, 2001.

[355] Y. M. Tan, K. H. Liao, and H. J. Clewell. Reverse dosimetry: interpreting trihalomethanes biomonitoring data using physiologically based pharmacokinetic modeling. *J Expo Sci Environ Epidemiol*, Nov 15 2006. Advanced online publication.

[356] Y. M. Tan, K. H. Liao, R. B. Conolly, B. C. Blount, A. M. Mason, and H. J. Clewell. Use of a physiologically based pharmacokinetic model to identify exposures consistent with human biomonitoring data for chloroform. *Journal of Toxicology and Environmental Health, Part A*, 69(18):1727–56, Sep 2006.

[357] E. Tanaka, M. Terada, and S. Misawa. Cytochrome P450 2E1: its clinical and toxicological role. *J Clin Pharm Ther*, 25(3):165–75, Jun 2000.

[358] J. Tang, Y. Cao, R. L. Rose, A. A. Brimfield, D. Dai, J. A. Goldstein, and E. Hodgson. Metabolism of chlorpyrifos by human cytochrome P450 isoforms and human, mouse, and rat liver microsomes. *Drug Metabolism and Disposition*, 29(9):1201–1204, Sep 2001. ISSN 0090-9556.

[359] K. M. Tang, Jr. Nace, C. G., C. L. Lynes, M. A. Maddaloni, D. LaPosta, and K. C. Callahan. Characterization of background concentrations in upper Manhattan, New York apartments for select contaminants identified in World Trade Center dust. *Environ Sci Technol*, 38(24):6482–90, Dec 15 2004.

[360] Albert Tarantola. *Inverse Problem Theory and Methods for Model Parameter Estimation*. Society for Industrial and Applied Mathematics, Philadelphia, PA, 2005.

[361] J. G. Teeguarden, D. C. Dorman, T. R. Covington, 3rd Clewell, H. J., and M. E. Andersen. Pharmacokinetic modeling of manganese. I. Dose dependencies of uptake and elimination. *J Toxicol Environ Health A*, 70(18):1493–504, Sep 2007.

[362] J. G. Teeguarden, D. C. Dorman, A. Nong, T. R. Covington, 3rd Clewell, H. J., and M. E. Andersen. Pharmacokinetic modeling of manganese. II. Hepatic processing after ingestion and inhalation. *J Toxicol Environ Health A*, 70(18):1505–14, Sep 2007.

[363] J. G. Teeguarden, J. Gearhart, 3rd Clewell, H. J., T. R. Covington, A. Nong, and M. E. Andersen. Pharmacokinetic modeling of manganese. III. Physiological approaches accounting for background and tracer kinetics. *J Toxicol Environ Health A*, 70(18):1515–26, Sep 2007.

[364] S. Telisman. Interactions of essential and/or toxic metals and metalloid regarding interindividual differences in susceptibility to various toxicants and chronic diseases in man. *Arh Hig Rada Toksikol*, 46(4):459–76, Dec 1995.

[365] L. K. Teuschler, G. E. Rice, C. R. Wilkes, J. C. Lipscomb, and F. W. Power. A feasibility study of cumulative risk assessment methods for drinking water disinfection by-product mixtures. *J Toxicol Environ Health A*, 67(8-10):755–77, Apr 23-May 28 2004.

[366] N. S. Thomaidis, E. B. Bakeas, and P. A. Siskos. Characterization of lead, cadmium, arsenic and nickel in PM(2.5) particles in the Athens atmosphere, Greece. *Chemosphere*, 52(6):959–66, Aug 2003.

[367] D. J. Thomas, S. B. Waters, and M. Styblo. Elucidating the pathway for arsenic methylation. *Toxicol Appl Pharmacol*, 198(3):319–26, Aug 1 2004.

[368] D. J. Thomas, J. Li, S. B. Waters, W. Xing, B. M. Adair, Z. Drobna, V. Devesa, and M. Styblo. Arsenic (+3 oxidation state) methyltransferase and the methylation of arsenicals. *Exp Biol Med (Maywood)*, 232(1):3–13, Jan 2007.

[369] J.F.A Thomas, E.B. Culbard, T. Delves, P.G. Harvey, J. Sherlock, A. Davies, M. J. Quinn, J. Morgan, G. Smart, A. Spurgeon, I. Thornton, and J. M. Watt. Lead intakes of young children from dust and other sources. In *Heavy Metals in the Environment*, volume 1, pages 317–320, Athens, 1985. CEP Consultants.

[370] C. M. Thompson, D. O. Johns, B. Sonawane, H. A. Barton, D. Hattis, R. Tardif, and K. Krishnan. Database for physiologically based pharmacokinetic (PBPK) modeling: physiological data for healthy and health-impaired elderly. *J Toxicol Environ Health B Crit Rev*, 12(1):1–24, Jan 2009.

[371] I. Thornton. Metal content of soils and dust. *Sci Total Environ*, 75:21–39, 1988.

[372] I. Thornton, E.B. Culbard, S. Moorcroft, J. M. Watt, M. Wheatley, M. Thompson, and J.F.A Thomas. Metals in urban dusts and soils. *Environ. Technol. Lett.*, 6:137–144, 1985.

[373] I. Thornton, D. J. Davies, J. M. Watt, and M. J. Quinn. Lead exposure in young children from dust and soil in the United Kingdom. *Environ Health Perspect*, 89:55–60, Nov 1990.

[374] C. Timchalk, A. Kousba, and T. S. Poet. Monte Carlo analysis of the human chlorpyrifos-oxonase (PON1) polymorphism using a physiologically based pharmacokinetic and pharmacodynamic (PBPK/PD) model. *Toxicol Lett*, 135(1-2):51–9, Sep 5 2002.

[375] C. Timchalk, R. J. Nolan, A. L. Mendrala, D. A. Dittenber, K. A. Brzak, and J. L. Mattsson. A Physiologically based pharmacokinetic and pharmacodynamic (PBPK/PD) model for the organophosphate insecticide chlorpyrifos in rats and humans. *Toxicol Sci*, 66(1):34–53, Mar 2002.

[376] S. T. Tong and K. C. Lam. Home sweet home? A case study of household dust contamination in Hong Kong. *Sci Total Environ*, 256(2-3):115–23, Jul 10 2000.

[377] A. Tossavainen, M. Nurminen, P. Mutanen, and S. Tola. Application of mathematical modelling for assessing the biological half-times of chromium and nickel in field studies. *British Journal of Industrial Medicine*, 37(3):285–91, Aug 1980.

[378] H. Toyoshiba, N. J. Walker, A. J. Bailer, and C. J. Portier. Evaluation of toxic equivalency factors for induction of cytochromes P450 CYP1A1 and CYP1A2 enzyme activity by dioxin-like compounds. *Toxicol Appl Pharmacol*, 194(2):156–68, Jan 15 2004.

[379] N. L. Tran, L. Barraj, K. Smith, A. Javier, and T. A. Burke. Combining food frequency and survey data to quantify long-term dietary exposure: a methyl mercury case study. *Risk Anal*, 24(1):19–30, Feb 2004.

[380] E. R. Trosken, K. Scholz, R. W. Lutz, W. Volkel, J. A. Zarn, and W. K. Lutz. Comparative assessment of the inhibition of recombinant human cyp19 (aromatase) by azoles used in agriculture and as drugs for humans. *Endocrine Research*, 30(3):387–94, Aug 2004.

[381] A. Turner and L. Simmonds. Elemental concentrations and metal bioaccessibility in UK household dust. *Sci Total Environ*, 371(1-3):74–81, Dec 1 2006.

[382] K. A. Usmani, R. L. Rose, J. A. Goldstein, W. G. Taylor, A. A. Brimfield, and E. Hodgson. In vitro human metabolism and interactions of repellent N,N-diethyl-m-toluamide. *Drug Metab Dispos*, 30(3):289–94, Mar 2002.

[383] M. Vahter, M. Berglund, A. Akesson, and C. Liden. Metals and women's health. *Environ Res*, 88(3):145–55, Mar 2002.

[384] M. Vahter, A. Akesson, C. Liden, S. Ceccatelli, and M. Berglund. Gender differences in the disposition and toxicity of metals. *Environ Res*, Sep 20 2006.

[385] M. E. Vahter. Interactions between arsenic-induced toxicity and nutrition in early life. *Journal of Nutrition*, 137(12):2798–2804, Dec 2007. ISSN 0022-3166.

[386] D. D. Vakharia, N. Liu, R. Pause, M. Fasco, E. Bessette, Q. Y. Zhang, and L. S. Kaminsky. Effect of metals on polycyclic aromatic hydrocarbon induction of CYP1A1 and CYP1A2 in human hepatocyte cultures. *Toxicol Appl Pharmacol*, 170(2):93–103, Jan 15 2001. 0041-008X (Print) Journal Article Research Support, Non-U.S. Gov't Research Support, U.S. Gov't, Non-P.H.S.

[387] D. D. Vakharia, N. Liu, R. Pause, M. Fasco, E. Bessette, Q. Y. Zhang, and L. S. Kaminsky. Polycyclic aromatic hydrocarbon/metal mixtures: effect on PAH induction of CYP1A1 in human HEPG2 cells. *Drug Metab Dispos*, 29(7):999–1006, Jul 2001.

[388] M. Van den Berg, L. Birnbaum, A. T. Bosveld, B. Brunstrom, P. Cook, M. Feeley, J. P. Giesy, A. Hanberg, R. Hasegawa, S. W. Kennedy, T. Kubiak, J. C. Larsen, F. X. van Leeuwen, A. K. Liem, C. Nolt, R. E. Peterson, L. Poellinger, S. Safe, D. Schrenk, D. Tillitt, M. Tysklind, M. Younes, F. Waern, and T. Zacharewski. Toxic equivalency factors (TEFs) for PCBs, PCDDs, PCDFs for humans and wildlife. *Environ Health Perspect*, 106(12): 775–92, Dec 1998.

[389] A. S. van der Burght, P. J. Clijsters, G. J. Horbach, P. L. Andersson, M. Tysklind, and M. van den Berg. Structure-dependent induction of CYP1A by polychlorinated biphenyls in hepatocytes of cynomolgus monkeys (Macaca fascicularis). *Toxicol Appl Pharmacol*, 155(1):13–23, Feb 15 1999.

[390] A. Vivante, N. Hirshoren, T. Shochat, and D. Merkel. Association between acute lead exposure in indoor firing ranges and iron metabolism. *Isr Med Assoc J*, 10(4):292–5, Apr 2008.

[391] I. H. von Lindern, S. M. Spalinger, B. N. Bero, V. Petrosyan, and M. C. von Braun. The influence of soil remediation on lead in house dust. *Sci Total Environ*, 303(1-2):59–78, Feb 15 2003.

[392] F. S. Walton, S. B. Waters, S. L. Jolley, E. L. LeCluyse, D. J. Thomas, and M. Styblo. Selenium compounds modulate the activity of recombinant rat AsIII-methyltransferase and the methylation of arsenite by rat and human hepatocytes. *Chem Res Toxicol*, 16(3): 261–5, Mar 2003.

[393] G. Wang and B. A. Fowler. Roles of biomarkers in evaluating interactions among mixtures of lead, cadmium and arsenic. *Toxicol Appl Pharmacol*, Jan 31 2008.

[394] S.W. Wang, P.G. Georgopoulos, G. Li, and H. Rabitz. Characterizing uncertainties in human exposure modeling through the Random Sampling-High Dimensional Model Representation (RS-HDMR) methodology. *International Journal of Risk Assessment and Management*, 5:387–406, 2005.

[395] X. Wang, M. J. Santostefano, M. V. Evans, V. M. Richardson, J. J. Diliberto, and L. S. Birnbaum. Determination of parameters responsible for pharmacokinetic behavior of TCDD in female Sprague-Dawley rats. *Toxicol Appl Pharmacol*, 147(1):151–68, Nov 1997.

[396] S. J. Wasson, W. P. Linak, B. K. Gullett, C. J. King, A. Touati, F. E. Huggins, Y. Chen, N. Shah, and G. P. Huffman. Emissions of chromium, copper, arsenic, and PCDDs/Fs from open burning of CCA-treated wood. *Environ Sci Technol*, 39(22):8865–76, Nov 15 2005.

[397] S. Willmann, W. Schmitt, J. Keldenich, J. Lippert, and J. B. Dressman. PK-Sim: a physiologically based pharmacokinetic 'whole-body' model. *Biosilico*, 1:121–124, 2003.

[398] S. Willmann, K. Hohn, A. Edginton, M. Sevestre, J. Solodenko, W. Weiss, J. Lippert, and W. Schmitt. Development of a Physiology-Based Whole-Body Population Model for Assessing the Influence of Individual Variability on the Pharmacokinetics of Drugs. *J Pharmacokinet Pharmacodyn*, Mar 13 2007.

[399] J. Wilson, S. Dixon, W. Galke, and P. McLaine. An investigation of dust lead sampling locations and children's blood lead levels. *J Expo Sci Environ Epidemiol*, 17(1):2–12, Jan 2007.

[400] N. K. Wilson, J. C. Chuang, C. Lyu, R. Menton, and M. K. Morgan. Aggregate exposures of nine preschool children to persistent organic pollutants at day care and at home. *J Expo Anal Environ Epidemiol*, 13(3):187–202, May 2003.

[401] T. C. Wood, O. E. Salavagionne, B. Mukherjee, L. W. Wang, A. F. Klumpp, B. A. Thomae, B. W. Eckloff, D. J. Schaid, E. D. Wieben, and R. M. Weinshilboum. Human arsenic methyltransferase (AS3MT) pharmacogenetics - Gene resequencing and functional genomics studies. *Journal of Biological Chemistry*, 281(11):7364–7373, Mar 17 2006. ISSN 0021-9258.

[402] Y. Wu, Q. Huang, X. Zhou, G. Hu, Z. Wang, H. Li, R. Bao, H. Yan, C. Li, L. Wu, and F. He. Study on the effects of lead from small industry of battery recycling on environment and children's health. *Zhonghua Liu Xing Bing Xue Za Zhi*, 23(3):167–71, Jun 2002.

[403] J. Xue, V. G. Zartarian, H. Ozkaynak, W. Dang, G. Glen, L. Smith, and C. Stallings. A probabilistic arsenic exposure assessment for children who contact chromated copper arsenate (CCA)-treated playsets and decks, Part 2: Sensitivity and uncertainty analyses. *Risk Anal*, 26(2):533–41, Apr 2006.

[404] S. Yamamura. Clinical application of artificial neural network (ANN) modeling to predict pharmacokinetic parameters of severely ill patients. *Adv Drug Deliv Rev*, 55(9):1233–51, Sep 12 2003.

[405] F. Yang, Y. Xu, H. Pan, and D. Wu. Induction of hepatic cytochrome P4501A1/2B activity and disruption of thyroglobulin synthesis/secretion by mono-ortho polychlorinated biphenyl and its hydroxylated metabolites in rat cell lines. *Environ Toxicol Chem*, 27(1): 220–5, Jan 2008.

[406] L. M. Yiin, G. G. Rhoads, and P. J. Lioy. Seasonal influences on childhood lead exposure. *Environ Health Perspect*, 108(2):177–82, Feb 2000.

[407] L. M. Yiin, P. J. Lioy, and G. G. Rhoads. Impact of home carpets on childhood lead intervention study. *Environ Res*, 92(2):161–5, Jun 2003.

[408] L. M. Yiin, J. R. Millette, A. Vette, V. Ilacqua, C. Quan, J. Gorczynski, M. Kendall, L. C. Chen, C. P. Weisel, B. Buckley, I. Yang, and P. J. Lioy. Comparisons of the dust/smoke particulate that settled inside the surrounding buildings and outside on the streets of southern New York City after the collapse of the World Trade Center, September 11, 2001. *J Air Waste Manag Assoc*, 54(5):515–28, May 2004.

[409] R. A. Yokel, S. M. Lasley, and D. C. Dorman. The speciation of metals in mammals influences their toxicokinetics and toxicodynamics and therefore human health risk assessment. *Journal of Toxicology and Environmental Health-Part B-Critical Reviews*, 9(1): 63–85, Jan-Feb 2006. ISSN 1093-7404.

[410] K. Yokley, H. T. Tran, K. Pekari, S. Rappaport, V. Riihimaki, N. Rothman, S. Waidyanatha, and P. M. Schlosser. Physiologically-based pharmacokinetic modeling of benzene in humans: a Bayesian approach. *Risk Analysis*, 26(4):925–43, Aug 2006.

[411] J. F. Young, W. S. Branham, D. M. Sheehan, M. E. Baker, W. D. Wosilait, and R. H. Luecke. Physiological "constants" for PBPK models for pregnancy. *J Toxicol Environ Health*, 52(5):385–401, Dec 12 1997.

[412] J. F. Young, W. D. Wosilait, and R. H. Luecke. Analysis of methylmercury disposition in humans utilizing a PBPK model and animal pharmacokinetic data. *Journal of Toxicology and Environmental Health, Part A*, 63(1):19–52, May 11 2001.

[413] J. F. Young, R. H. Luecke, B. A. Pearce, T. Lee, H. Ahn, S. Baek, H. Moon, D. W. Dye, T. M. Davis, and S. J. Taylor. Human organ/tissue growth algorithms that include obese individuals and black/white population organ weight similarities from autopsy data. *J Toxicol Environ Health A*, 72(8):527–40, 2009.

[414] D. Yu. A physiologically based pharmacokinetic model of inorganic arsenic. *Regul Toxicol Pharmacol*, 29(2 Pt 1):128–41, Apr 1999.

[415] D. Yu. A pharmacokinetic modeling of inorganic arsenic: a short-term oral exposure model for humans. *Chemosphere*, 39(15):2737–47, Dec 1999.

[416] L. L. Yu, R. D. Vocke, K. E. Murphy, and 2nd Beck, C. M. Determination of As, Cd, Cr, and Hg in SRM 2584 (trace elements in indoor dust) by high-resolution inductively coupled plasma mass spectrometry. *Fresenius J Anal Chem*, 370(7):834–7, Aug 2001.

[417] L. Zaragoza and K. Hogan. The integrated exposure uptake biokinetic model for lead in children: independent validation and verification. *Environ Health Perspect*, 106 Suppl 6: 1551–6, Dec 1998.

[418] V. G. Zartarian, J. Xue, H. Ozkaynak, W. Dang, G. Glen, L. Smith, and C. Stallings. A probabilistic arsenic exposure assessment for children who contact CCA-treated playsets and decks, Part 1: Model methodology, variability results, and model evaluation. *Risk Anal*, 26(2):515–31, Apr 2006.

[419] H. Zeng, E. O. Uthus, and Jr. Combs, G. F. Mechanistic aspects of the interaction between selenium and arsenic. *J Inorg Biochem*, 99(6):1269–74, Jun 2005.

[420] W. Zheng, M. Aschner, and J. F. Ghersi-Egea. Brain barrier systems: a new frontier in metal neurotoxicological research. *Toxicol Appl Pharmacol*, 192(1):1–11, Oct 1 2003.

Vita

Alan F. Sasso

1999-2003	B.Sc. in Chemical Engineering from Villanova University
2004-2005	Teaching assistant, Department of Chemical and Biochemical Engineering, Rutgers University
2004-2009	Research Assistant, Environmental and Occupational Health Sciences Institute, a Joint Project of UMDNJ and Rutgers University
2010	Ph.D. in Chemical Engineering, Rutgers University